RICE UNIVERSITY

Diluted Bitumen Emulsion Characterization and Separation

by

Tianmin Jiang

A THESIS SUBMITTED

IN PARTIAL FULFILLMENT OF THE
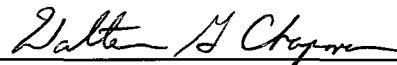
REQUIREMENTS FOR THE DEGREE

Doctor of Philosophy

APPROVED, THESIS COMMITTEE:

Clarence A. Miller

Dr. Clarence A. Miller, Louis Calder
Professor of Chemical Engineering, Co-
chair

George J. Hirasaki

Dr. George J. Hirasaki, A. J. Hartsook
Professor of Chemical Engineering, Co-
chair

Walter G Chapman

Dr. Walter G. Chapman, William W. Akers
Professor of Chemical Engineering

Mason Tomson

Dr. Mason B. Tomson, Professor of Civil
and Environmental Engineering

HOUSTON, TEXAS

DECEMBER, 2009

UMI Number: 3421153

UMI®

Dissertation Publishing

ProQuest®

ABSTRACT

Diluted Bitumen Emulsion Characterization and Separation

by

Tianmin Jiang

Stable water-in-oil emulsions persist in bitumen froth from surface mining process of Athabasca oil sands because of asphaltenes and clay solids. This dissertation focuses on the characterization and separation of water in diluted bitumen emulsions.

A novel approach to process experimental data from classic NMR experiments for the characterization of water in diluted bitumen emulsions has been proposed and tested. NMR PGSE restricted diffusion measurement can characterize emulsion drop size distribution. Experiments show that drop size of emulsion does not change much with time, which indicates that water in diluted bitumen emulsion is very stable without demulsifier. Water fraction profile and water droplet sedimentation velocity can be obtained from MRI 1-D T_1 weighted profile measurement. Emulsion flocculation can be deduced by comparing the sedimentation velocity from experiment data and Stokes Law prediction.

PR$_5$ (a polyoxyethylene (EO)/ polyoxypropylene (PO) alkylphenol formaldehyde resin) is an appropriate demulsifier for water in diluted bitumen emulsion. Almost complete separation can be obtained in the absence of clay solids. For the sample with solids, a rag layer containing solids with moderate density forms

between the clean oil and free water layers. Partially oil-wet clay solids prevent complete separation of the emulsion.

Experiments reveal that wettability of clay solids has significant effect on emulsion stability. Kaolinite with 100 ppm sodium naphthenate in toluene-brine mixture is chosen as model system for wettability test. Wettability of kaolinite can be altered by pH control, silicate and surfactant. Adding 3×10^{-3} M Na_2SiO_3 at pH 10 can get 80% of kaolinite water-wet. Over 90% of kaolinite becomes water-wet adding C_8TAB, betaine 13 and amine oxide DO with optimal dosages. In diluted bitumen emulsion, about 10^{-4} M sodium meta-silicate can change the wettability of solids from partially oil-wet to more water-wet. Hereby the clay solids can settle down to the aqueous phase and the separation is almost complete.

Wettability of kaolinite can be characterized via zeta potential measurement and modeling. Simplified Gouy-Stern-Grahame model and oxide site-binding model can be used to correlate zeta potential of kaolinite in brine with different additives. Sodium silicates have the greatest effect per unit addition on changing zeta potential of kaolinite and can be used to change the wettability of clay solids.

Almost complete separation be obtained by the three-step procedure: (a) adding 10^{-4} M Na_2SiO_3 during initial emulsion formation to make the solids less oil wet; (b) removing the clean oil formed following subsequent treatment with demulsifier and adding NaOH or Na_2SiO_3 with shaking to destroy the rag layer and form a relatively concentrated oil-in-water emulsion nearly free of solids; and (c) adding hydrochloric acid to break the oil-in-water emulsion.

Acknowledgements

I am very grateful as a graduate student at Rice University. I would like to express my sincere appreciation to my two advisors, Professor Clarence A. Miller and Professor George J. Hirasaki for their guidance, inspiration, and assistance. Their wisdom and authoritative knowledge have helped me a lot throughout these years.

I appreciate Professor Walter G. Chapman and Professor Mason B. Tomson for serving on my thesis committee.

Many research staffs, graduates and undergraduates have contributed with their experimental work and/or valuable ideas to this thesis. I wish to express my sincere thankfulness and appreciation to them:

Maura Puerto, Olina Raney and Shunhua Liu for their assistance and suggestions to my research work.

Marc Fleury, Arjun Kurup, Michael Rauschhuber, Vivek Anand, Mark Flaum, Clint Aichele and Zheng Yang for their help with NMR measurement, and for useful suggestions to my research on NMR characterization of emulsion.

Dr. Matteo Pasquali, Nikta Fakhri and Arjun Prakash for their help of microscopy observation of emulsion.

Dr. Kyriacos Zygourakis, Dr. Michael Wong, Jie Yu, Yu-lun Fang and Xuan Guo for their help of emulsion centrifugation.

Yu Bian and Feng Li for the BET analysis and acid number titration.

Jose Lopez-Salinas, Leyu Cui and Kun Ma for all their help with the laboratory experiments.

Many other students and research staff in Dr. Miller's and Dr. Hirasaki's laboratories have offered me help and their friendships too. I am grateful to this group of people.

At the end, I would like to thank my family for their support and encouragement.

Table of Contents

List of Tables

List of Figures

Chapter 1

1. Introduction

This chapter briefly introduces the basic industrial background and motivations, project objectives and thesis outline.

1.1. Background and motivations

Canadian oil sands represent a huge amount of oil reserves. The estimated amount of bitumen is 600 billion barrels, which is four times the oil reserves in Saudi Arabia [1], [2]. However, oil sands are unconsolidated deposits of very heavy hydrocarbon bitumen and require multiple stages before refining, which increase production costs.

About 60 billion barrels of oil sands can be recovered by surface mining process [1], [2]. Figure 1.1 shows general scheme for oil sands processing using water-based extraction processes [3]. Each box in the figure identifies a unit plant operation. First oil sands from surface mining are transported to the extraction plant. Oil sands are mixed with hot water to form slurry. In flotation process, the corresponding slurry containing water, bitumen, sands and air bubbles, is left for separation. Tailing slurry from extraction plant enters water management unit. Recovered bitumen and recycled water are injected back to extraction plant. Bitumen rises to the surface to form a froth, which contains 30% water (as a stable w/o emulsion) and fine solids up to 10%. In froth treatment unit, froth is

diluted with light solvents (e.g. naphtha) together with a demulsifier for further separation.
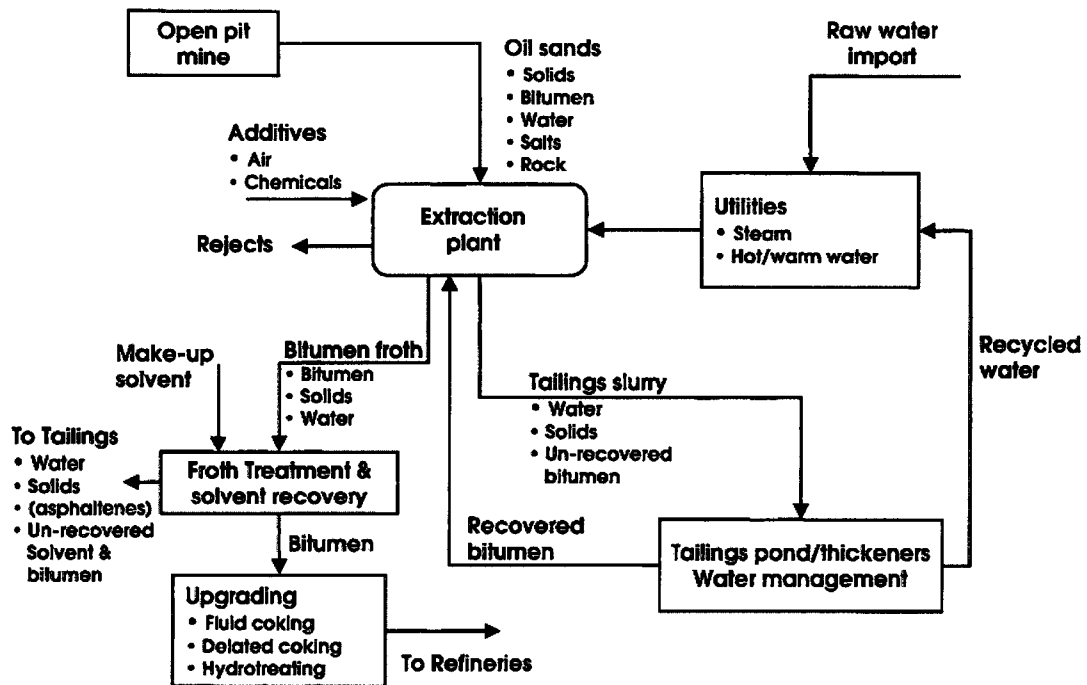
Figure 1.1 Scheme of oil sands processing using water-based extraction [3]

Figure 1.2 shows general scheme of froth treatment process [4]. Diluted bitumen containing bitumen, naphtha, water, sand and clay is fed into *splitter* and temporarily retained to produce a bottom layer of tailings comprising sand and middling, a *rag layer* comprising hydrocarbons in a skin of fine, and a top layer of hydrocarbons with small droplets of water and fines (raw diluted bitumen). Demulsifier is mixed with raw diluted bitumen, which enters a *polisher* tank to produce polished diluted bitumen containing less than 2.0 w.% water and 0.9 w.%

solids. The splitter underflow tails and polisher sludge are mixed with additional

naphtha to raise naphtha/ bitumen (N/B) ratio to 4.0 -10.0. This mixture enters

scrubber. Scrubber overflow containing residual bitumen and polisher sludge are

recycled to splitter. Polished diluted bitumen is sent for solvent recovery and

finally transported to refinery.
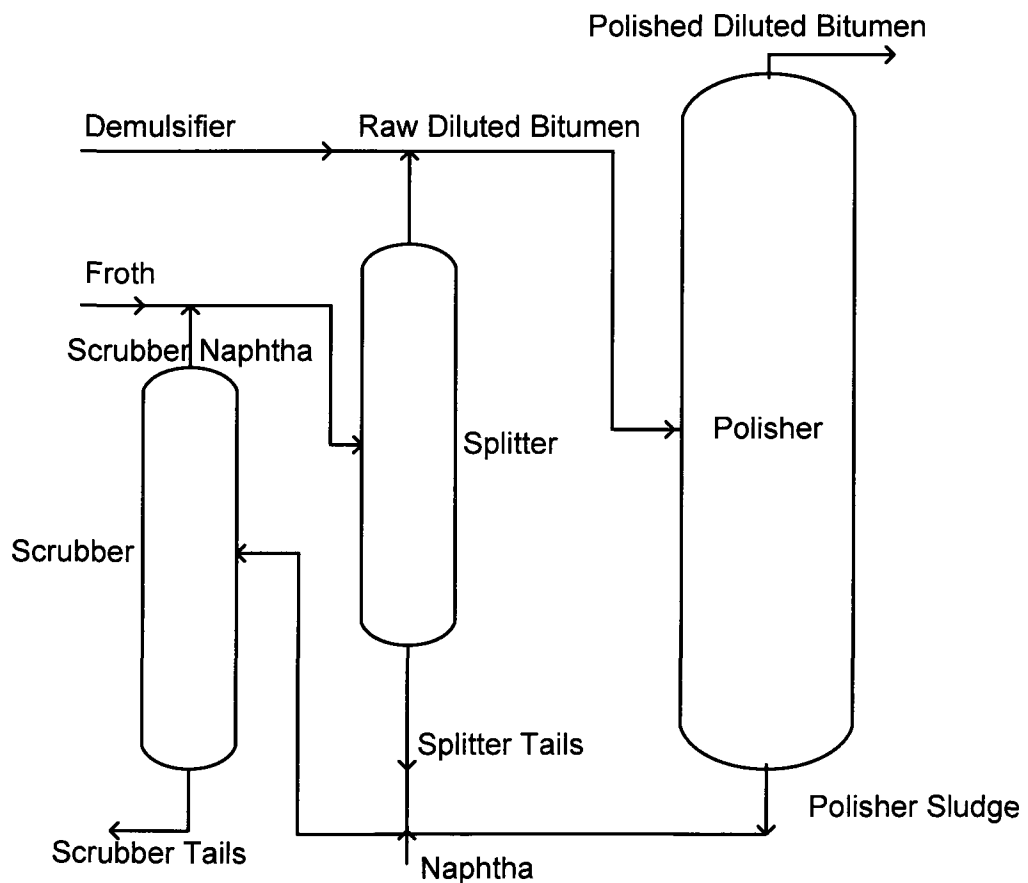
Figure 1.2 General scheme of froth treatment process [4]

During this continuous process, a rag layer contains oil, water and solid forms

in the middle of scrubber, which prevents complete separation. The accumulation

of rag layer eventually occupies the whole container and stops the separation process. Our study is related to this final stage separation of bitumen froth treatment.

1.2. Project objectives

During bitumen froth treatment process of Athabasca oil sands, stable water-in-oil emulsions are problematic because of clay solids. The objectives of this study are to characterize the time evolution of the properties of emulsions and to reach complete separation of water, oil and solids using appropriate demulsifier with proper separation procedure.

Detailed objectives are:

1) Quantify the amount of water and oil in the emulsions made from diluted bitumen containing clay solids.

2) Characterize the rag layer which develops during emulsion separation.

3) Reduce or eliminate rag layer with proper emulsion separation procedure.

In the thesis, Chapter 2 presents extensive background information. Emulsions and emulsion stability are reviewed, especially literature on the separation of water in diluted bitumen emulsions.

Chapter 3 focuses on NMR techniques applied in the characterization of water-in-oil emulsions.

Chapter 1

Chapter 4 discusses clay wettability, zeta potential characterization and effects of clay on emulsion stability.

Chapter 5 presents the methods and procedures that are focused on the brine in diluted bitumen emulsions with demulsifier, silicate and pH control.

Chapter 6 is devoted to the conclusions of current work and some recommendations for future work.

1.3. Reference

[1]   G. J. Demaison, D. A. Redford, A. G. Winestock, *The oil sands of Canada- Venezuela* **1977**, CIM Special, Vol. 17.

[2]   Canadian Institute of Mining, Metallurgy, and Petroleum: Calgary, Canada, **1977**; 9-16.

[3]   J. Masliyah, Z. J. Zhou, Z. Xu, J. Czarnecki, H. Hamza, Understanding water-based bitumen extraction from Athabasca oil sands, *Can. J. Chem. Eng.*, **2004**, *82* (8), 628-654.

[4]   G. Cymerman, P. Dougan, T. Tran, J. Lorenz, C. Mayr, Staged settling process for removing water solids from oils and extraction froth, US Patent, Patent No. US 6746599B2, June 8, **2004**.

Chapter 2

2. Emulsion and emulsion stability

This chapter briefly introduces the basic definitions and concepts of emulsion, summarizes the conventional knowledge on emulsion stability.

2.1. Basic definitions

Emulsion is a relatively stable dispersion of a liquid within another liquid with which it exhibits limited miscibility (IUPAC, 1972). The dispersed phase is commonly present in an emulsion in the form of spherical drops. Due to the large surface area per droplet, the excess Gibbs energy per droplet is high to make the emulsion thermodynamically unstable. The stability of emulsion is characterized by a time evolution of its basic parameters, for instance, the volume fraction and drop size distribution of the dispersed phase in the medium [1]. Notwithstanding their thermodynamic instability, many emulsions are kinetically stable and do not change appreciably for a prolonged period. The surface active agents at the interfaces can delay the separation tendency of emulsion. Such agents are molecules with polar and non-polar chemical groups in their structure, usually referred to as surfactants, or finely divided solids [2].

In general, emulsions contain an organic liquid (oil phase) and an aqueous solution (water phase). Emulsions of droplets of an oil phase in an aqueous solution are indicated by the symbol O/W and emulsions of aqueous droplets in

an organic liquid as W/O. For W/O emulsions, water is considered the dispersed

or internal phase, and oil is the continuous or external phase, and conversely for

the O/W type. Multiple emulsions such as O/W/O or W/O/W emulsions are also

present in some cases.

2.2. Properties of emulsions

2.2.1. Drop size distribution

A population of emulsions is described by emulsion drop size distribution.

The corresponding drop size distribution is a statistical inventory of the

disaggregation of the dispersed phase. Drop size distribution can be expressed

as frequency distribution curves or cumulative curves.

Among various drop size distributions, log-normal distribution function

describes well drop sizes in emulsions [3]. Studies on solid grinding [4] and

emulsification with turbulent stirring [5] show that breakup sequences of drops lead

to such distribution.

$$p(d) = \frac{1}{\sqrt{2\pi}d\sigma_g}e^{-\frac{[\ln(d)-\ln(d_g)]^2}{2\sigma_g^2}}$$ [2.1]

Here d is the drop diameter, d_g is the geometric mean drop size and σ_g is the

geometric standard deviation of the distribution.

In some other cases, lognormal distribution is not observed. The drop size

may be described by other distributions, as shown in Figure 2.1 [2]. In these cases,

the mean drop size is the most commonly used to characterize an emulsion [6].
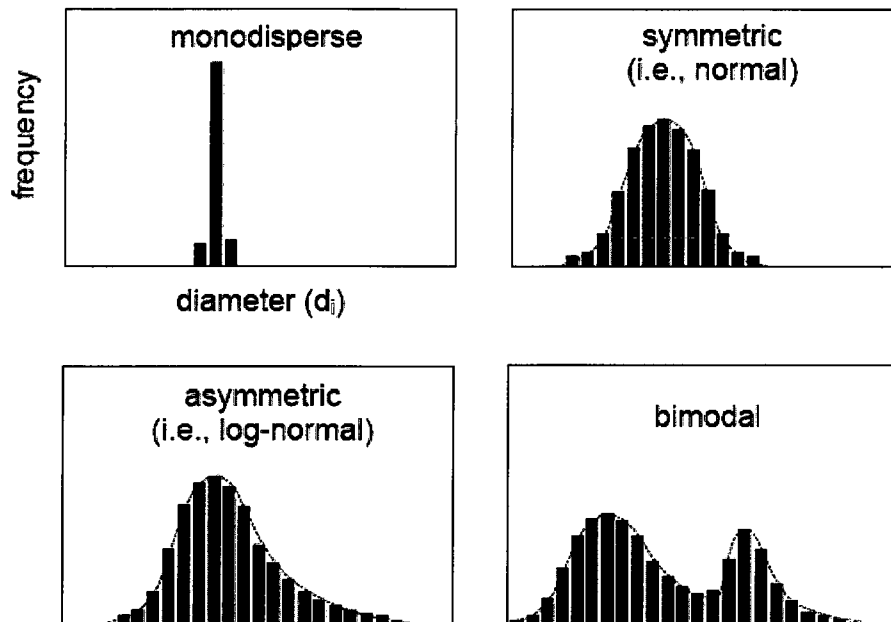
Figure 2.1 Different drop size distributions [2]

Several experimental methods have been used to determine drop sizes in

emulsions, including microscopy, photomicrography, video microscopy, light

scattering, sedimentation, coulter counting, turbidimetry, nuclear magnetic

resonance (NMR) and acoustics among others [7].

2.2.2. Emulsion morphology

The morphology is the most basic characteristic of an emulsion.

Morphologies of different type of emulsions are shown in Figure2.2 [2].

Some qualitative procedures can be used to discern emulsion type. One simple method is contacting a drop of the emulsion with water or oil and observing whether the external phase is miscible or not with it. However, this method can't distinguish simple and multiple emulsions.
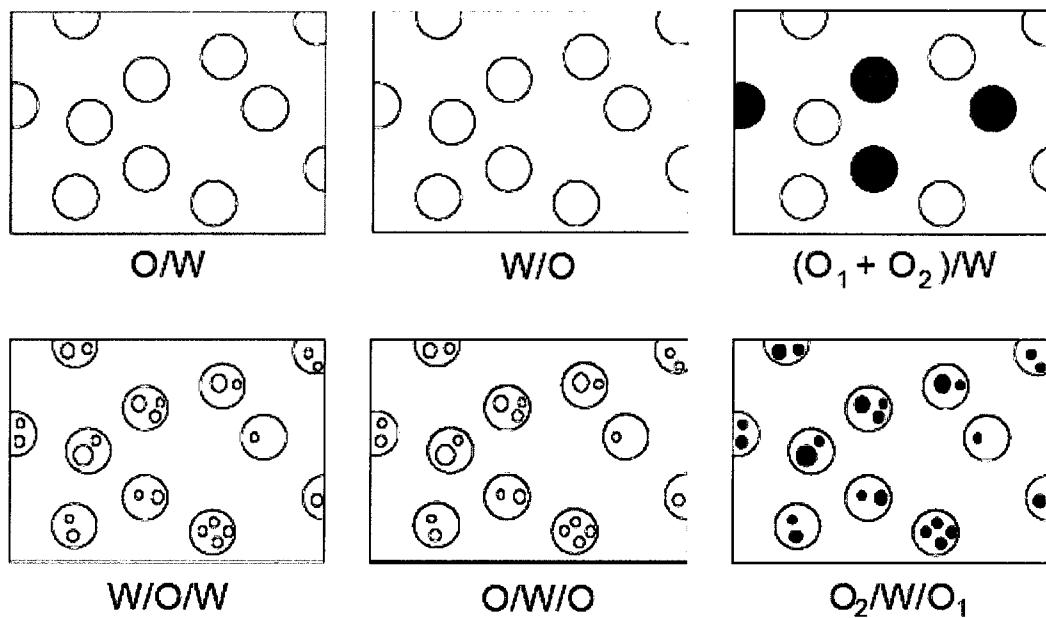
Figure 2.2 Morphologies of different type of emulsions [2]

The type of emulsion can also be determined by measuring its electrical conductivity. The aqueous phase in an emulsion usually contains electrolytes and therefore a relatively high conductivity should be observed (of order mS/cm) for O/W emulsion with water as external phase. On the contrary, in most cases non-polar liquids exhibit very low electrical conductivity (of order μS/cm), and so would W/O emulsions with oil as external phase.

To distinguish simple and multiple emulsions, optical microscopy method is also used. If the optical property difference between the water and oil phase is significant enough, it is easy to find the type the emulsions under microscopy observation. This method is often used in complicated water/oil systems and will be mentioned later.

2.2.3. Shear viscosity

Rheology properties of emulsion are obviously important physical attributes. In qualitative terms, emulsions range from low viscosity milk-like Newtonian liquids through thicker shear-thinning liquids, right up to thick, cream-like materials with apparent yield stresses [8].

As shear-thinning liquids, emulsions can be described by apparent shear viscosity η, which is analogous to that of pure fluids as given by Newton's law. η is the proportionality coefficient between stress (τ_{ji}) and rate of strain (also shear rate, γ_{ij}), $\eta = \tau_{ji}/\gamma_{ij}$.

Factors affecting the shear viscosity of an emulsion are, in order of relevance, the viscosity of the continuous phase (η_C), the dispersed phase content (φ), and the mean size and size distribution of droplets [2].

The viscosity increases with the dispersed phase content due to interactions among droplets. For diluted colloidal dispersions ($\varphi<0.02$) the correction

proposed by Einstein from hydrodynamic considerations on suspensions of hard spheres [9], [10]:

$$\eta = \eta_C (1 + K\varphi)$$
[2.2]

Here K = 1-2.5 is a constant and φ is the dispersed phase content.

For emulsions with higher dispersed phase content, one corrected equation is [11]:

$$\eta = \eta_C \left(1 + \frac{\varphi / \varphi_{100}}{1.187 - \varphi / \varphi_{100}} \right)^{2.49}$$
[2.3]

Here φ_{100} is the dispersed phase content at η / η_C = 100 which is measured experimentally.

Another important factor is the mean drop size. Friction between droplets is related to the interfacial area and therefore increases viscosity when the surface-to-volume ratio of the dispersed phase increases [12]. Thus an emulsion with smaller mean drop size should exhibit higher apparent viscosity than another with higher mean drop size.

2.3. Emulsion stability

2.3.1. Interaction forces

The most often referred to mechanism in emulsion literature to explain emulsion interaction is the so-called DLVO theory, developed independently by

Chapter 2

Derjaguin, Landau [13], Verwey and Overbeek [14], based on the long range London-van der Waals attractive forces and repulsive electrostatic forces between two close spheres.

The universal attractive forces, known as van der Waals forces, arise from spontaneous electric and magnetic polarizations, giving a fluctuating electromagnetic field within the media in the gap between them [1].

For two spheres with radii R_1 and R_2 and center-center separation distance H, the interaction energy is:

$$U_A = -\frac{A}{6}\left[\frac{2R_1R_2}{h^2+2(R_1+R_2)h} + \frac{2R_1R_2}{h^2+2(R_1+R_2)h+4R_1R_2} + \ln\frac{h^2+2(R_1+R_2)h}{h^2+2(R_1+R_2)h+4R_1R_2}\right] \qquad [2.4]$$

Here $h = H - R_1 - R_2$ is the minimum distance between the two approaching surfaces. If $R_1 = R_2 = R$, Eq. [2.4] becomes:

$$U_A = -\frac{A}{6}\left[\frac{2R^2}{h^2+4Rh} + \frac{2R^2}{h^2+4Rh+4R_1R_2}R^2 + \ln\frac{H^2+4Rh}{H^2+4Rh+4R^2}\right] \qquad [2.5]$$

If $h<<R$, Eq. [2.5] can be simplified as:

$$U_A = -\frac{AR}{12h} \qquad [2.6]$$

In these expressions, A is the so-called Hamaker constant. Eq. [2.4] was derived for spheres in vacuum. For similar materials, spheres of material 1 suspended in another medium of material 2, A is now the effective Hamaker constant, usually calculated as:

$$A = (A_{11}^2 - A_{22}^2)^{1/2}$$
[2.7]

Here A_{11} and A_{22} correspond to the constants of the two materials.

From Eq. [2.7], Hamaker constants are always positive, which means the van der Waals interaction between similar materials in a liquid would be always be attractive.

Most emulsions in aqueous media are charged due to various reasons, such as the ionization of surface groups, specific adsorption of ions, and so forth [1]. In an electrolyte solution, the distribution of ions around a charged sphere is not uniform and gives an *electrical double layer*.

When two charged spheres approach each other in an electrolyte solution, their diffuse layers will overlap and repulsion develops between them. For two identical spheres, the repulsion energy is [15]:

$$U_E = \frac{64\pi R c_0 N_A kT \aleph_0^2}{\kappa^2} \exp(-\kappa h)$$
[2.8]

Here c_0 is the bulk concentration of the ionic specie, N_A is the Avogadro's number (6.02 ×10^{23} mol^{-1}), $\aleph$ = *tanh (ze$_0$ψ$_0$/4kt)* with z being the magnitude of the ion valence, e_0 the electronic charge (1.60 × 10^{-19} C), κ^{-1} the so-called Debye length, which is used to characterize electrical double layer thickness, and ψ_0 the electrical potential at the interfaces.

Chapter 2

2.3.2. Emulsion evolution

Due to the high interfacial area and surface free energy, oil and water in emulsions will separate to form two continuous phases. Thus the properties of the emulsion (drop size distribution, mean drop size and other properties) will change with time. The stability of emulsion is characterized by the time-dependent behavior of its basic parameters.

Emulsions may degrade via a number of different mechanisms. Figure 2.3 schematically illustrates several physical instabilities that lead to phase separation in emulsions. Sedimentation or creaming takes place when the two liquids exhibit different densities due to the gravity. Aggregation occurs when droplets stay very close to one another and form flocs. Coalescence takes place when the thin film of continuous phase between two drops breaks and they fuse rapidly to form a single droplet. Ostwald ripening occurs due to the difference of solubility of drops with different drop size, which does not require the droplets to be close each other.

In the following discussion, theory on sedimentation and creaming, aggregation and coalescence is presented. The effect of surfactants and solids on the emulsions will also be mentioned in next section.
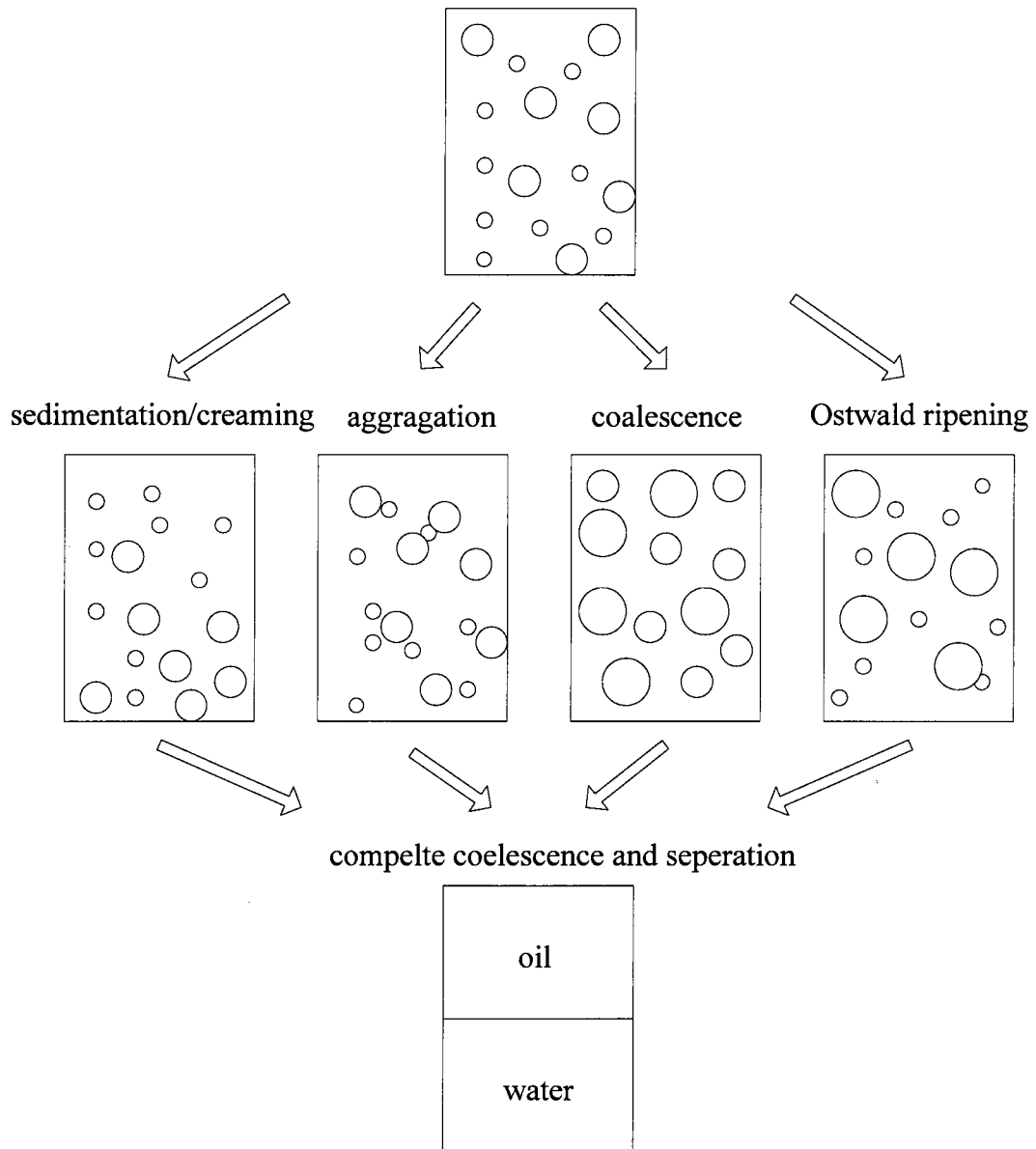
Figure 2.3 Scheme of destabilizing mechanisms in emulsions

2.3.3. Sedimentation and creaming

Sedimentation or creaming takes place when the two liquids exhibit different densities due to gravity. Stokes equation can describe the terminal sedimentation velocity of spheres in Newtonian fluids.

$$v_s = \frac{\Delta\rho g d^2}{18\eta_C}$$

[2.9]

Here v_s is the terminal sedimentation velocity, $\Delta\rho$ is the density difference of dispersed and continuous phase, d is the diameter of droplet, η_C is the viscosity of continuous phase, g is the acceleration either due to gravity (g = 9.81 m/s^2) or to centrifugation ($g = L\omega^2$, with L being the effective radius of the centrifuge and ω the angular velocity). If $\Delta\rho$ > 0, emulsions sediment; otherwise, the process is referred to as creaming. Sedimentation applies to most W/O emulsions and solid dispersions; creaming applies to most O/W emulsions and bubbles dispersed in liquids.

Eq. [2.9] is only satisfied for very dilute dispersions. If the volume fraction of the dispersed phase φ is significant (say φ > 0.01), so-called hindered sedimentation takes place. In general, the effect of φ is to reduce the sedimentation rate due to hydrodynamic interactions among droplets. The expression is as follows [16]:

$$\frac{v_{eff}}{v_s} = (1-\varphi)^n \qquad\qquad [2.10]$$

Here φ is the volume fraction of the dispersed phase, v_{eff} is the effective terminal sedimentation velocity, n is an empirical constant, which ranges from 6.5 to 8.6. [17].

If the emulsion is poly-dispersed, the average diameter square should replace d^2 in Eq. [2.9]. The increase in polydispersity will decrease the sedimentation rate [2].

$$d_{53}^2 = \frac{\sum N_I d_I^5}{\sum N_I d_I^3} \qquad\qquad [2.11]$$

When repulsive forces dominate, sedimentation is slower, probably because group sedimentation is not favored. On the other hand, if attractive forces dominate and aggregation takes place, sedimentation rate will increase with larger size aggregates.

2.3.4. Aggregation

From DLVO theory discussed in section 2.3.1, aggregation of emulsions depends on the van der Waals attractive interaction and electrical repulsion interaction. The overall interaction energy U is given by the sum of U_A and U_E, which is the combination of Eq. [2.4] and [2.8].

$$U = U_A + U_E \qquad\qquad [2.12]$$

Figure 2.4 shows a typical profile for U [2]. When two droplets are very close ($h \rightarrow 0$), attractive forces dominate and droplets are expected to aggregate irreversibly, which is referred to as *coagulation*. When h reaches secondary energy minimum, droplets may form aggregates reversibly that can be re-dispersed which is usually termed *flocculation*. Generally aggregation is used to describe either coagulation or flocculation.
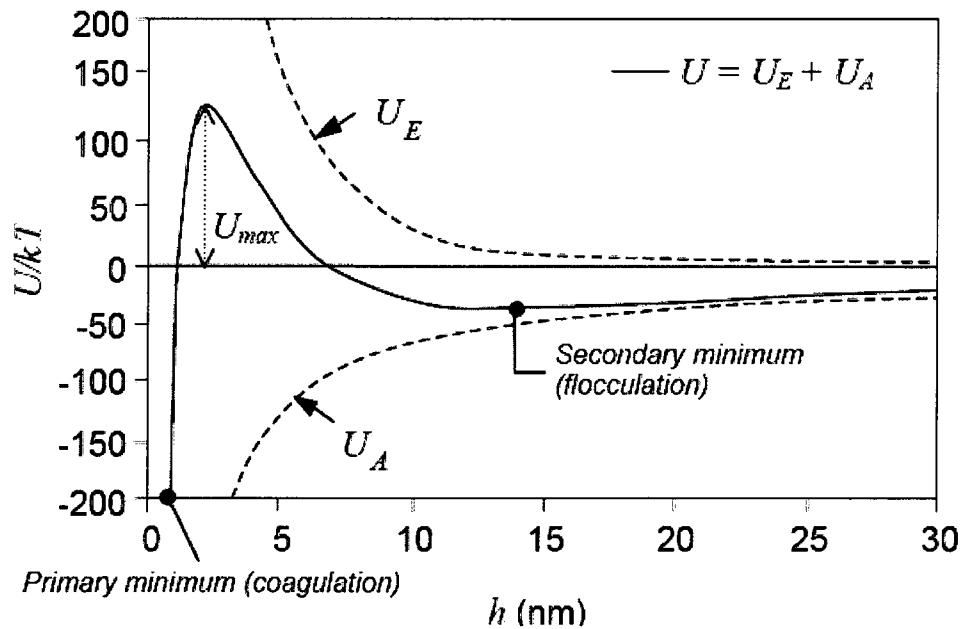
Figure 2.4 Energy of interaction between two spherical droplets [2]

If $U_{max} \leq 0$, there is no energy barrier to prevent the two surfaces from approaching each other. In this case, so-called fast aggregation takes place. On the other hand, if $U_{max} > 0$, an energy barrier must be overcome to achieve

aggregation. This process is usually referred to as slow aggregation.

For fast aggregation, if it is Brownian diffusion dominated, the process is referred to as *perikinetic* aggregation and the rate of change of the number of droplets per unit volume N is given by [18]:

$$-\frac{dN}{dt} = k_P N^2 = (8\pi DR)N^2 = (\frac{4kT}{3\eta})N^2, \quad N(t) = \frac{N_0}{1 + k_P N_0 t} \quad [2.13]$$

Here D is the diffusion coefficient of the droplets, η is the viscosity of the continuous phase and N_0 is the initial number concentration of droplets in solution.

If non-Brownian forces dominant the displacement of the droplets, aggregation is termed as *orthokinetic* [18]. In this case, the rate is:

$$-\frac{dN}{dt} = k_O N^2 = (\frac{8}{3}R^3 G)N^2, \quad N(t) = \frac{N_0}{1 + k_0 N_0 t} \quad [2.14]$$

Here G is the velocity gradient. k_O is the orthokinetic rate constant. At room temperature, perikinetic aggregation would be more significant for smaller particles ($R < 2$ μm) and orthokinetic aggregation would dominate otherwise ($R > 5$ μm).

For slow aggregation, the rate is [19]:

$$-\frac{dN}{dt} = \frac{k_P}{W}N^2 \quad [2.15]$$

Here k_P is the perikinetic rate and W is the so-called stability ratio.

$$W = 2R \int_{2R}^{\infty} \exp(\frac{U}{kT}) \frac{dH}{H^2} \approx \frac{2\pi^{1/2} R}{H_{max}^2 p} \exp(\frac{U_{max}}{kT}), \quad p^2 = -\frac{(\partial^2 U / \partial H^2)_{H=H max}}{2kT} \quad [2.16]$$

From Eq. [2.15] and [2.16], the increase in U_{max} causes a reduction of the aggregation rate.

2.3.5. Coalescence

Coalescence is the rupture of the thin film of continuous phase that separates two nearby droplets. Coalescence is usually characterized by the film-drainage model [20]. Coalescence process of droplets can be divided into three steps: approach, film drainage and rupture.

The stages of film thinning for a simple emulsion system can be described as follows [21]: 1) When two droplets are approaching, film thickness δ decreases rapidly with time, and dimpling (also corrugations and oscillations) precedes the formation of a plane parallel film; 2) as interfacial resistance increases the film is slowly thinned to a critical thickness δ_{cr} for rupture; 3) rupture occurs when a hole formed.

Many efforts have been devoted to the understanding of the formation and thinning of a flat film between drops. Weber number is imported here, which refers the internal Laplace pressure P_L and external stress τ_{ext} exerted upon the doublet of drops.

$$W_e = \frac{\tau_{ext}}{P_L}$$

[2.17]

If $We \ll 1$, the stability criterion is suggested as [18], [19]:

$$\frac{d^2U(h)}{dh^2} - \frac{dU(h)}{hdh} > -C\frac{\sigma}{R^2}$$

[2.18]

Here $U(h)$ is the energy in DLVO theory, $C > 0$ is a constant, σ is interfacial tension. From Eq. [2.18], coalescence would only take place if the drops get close enough as to reach the primary minimum (in Figure2.4).

When $We \gg 1$, large flat films will form. Deformation is favored by large drop sizes and low interfacial tensions. In this case, coalescence is preceded by the drainage of the liquid present in the film. For the symmetrical drainage of a film of Newtonian liquid with viscosity η between two flat disks of radii r and separated by a distance h ($h/r \ll 1$) with the pressure difference ΔP, the rate of thinning of the film $-dh/dt$ is [22]:

$$-\frac{dh}{dt} = \frac{2}{3}\frac{r\Delta P}{\eta}(\frac{h}{r})^3$$

[2.19]

If the electrostatic repulsion is strong enough as to balance van der Waals attraction and the capillary pressure, the film is referred to as *common black film* ($h \sim$ 20-30 nm) [2]. If the electrostatic repulsion is weak and short range repulsive forces dominate instead, the film is very thin ($h \sim$ 5-10 nm) and is referred to as *Newton black film.*

Chapter 2

2.4. Emulsion of water in diluted bitumen

Chapter 1 briefly discussed the formation of water in diluted bitumen emulsions during bitumen froth treatment. Crude oils are complex mixtures of a number of species that differ significantly in molecular weight, structure and elementary composition. Therefore water in diluted bitumen exhibits different characteristics from other water-in-oil emulsions, especially its stability due to the surface-active components and fine clay solids.

Most often used way to classify species in crude oil is in solubility classes. Asphaltenes are defined as the components of crude oil that are insoluble in paraffinic hydrocarbons such as n-pentane or n-heptane, but that are soluble in aromatic solvents like toluene. The elemental analysis of asphaltenes shows that carbon (~ 80 wt.%) and hydrogen (~ 8 wt.%) are the main components of their structure, and that heteroatoms (S, O, N, Ni, V) are commonly present in amounts that vary considerably for asphaltenes from different sources [23].

Several tentative chemical structures have been proposed for asphaltenes. Figure 2.5 shows the proposed structure of asphaltenes present in Athabasca bitumen [24]. It contains small groups of aromatic rings interconnected by alkyl chains and naphthenic and aliphatic rings, in a fashion that has been termed the *archipelago* model [24].

Chapter 2

The molecule size of asphaltenes ranges from 2 to 10 nm. Aggregates can reach up to 100 μm. The critical concentration of aggregation is about 0.1 %, so asphaltenes will aggregate even at very low concentration. Aggregation is thought to take place by stacking of the planar polynuclear aromatic parts of the molecules, probably due to π-π interactions or hydrogen bonding of the polar groups [2], as shown in Figure 2.6.
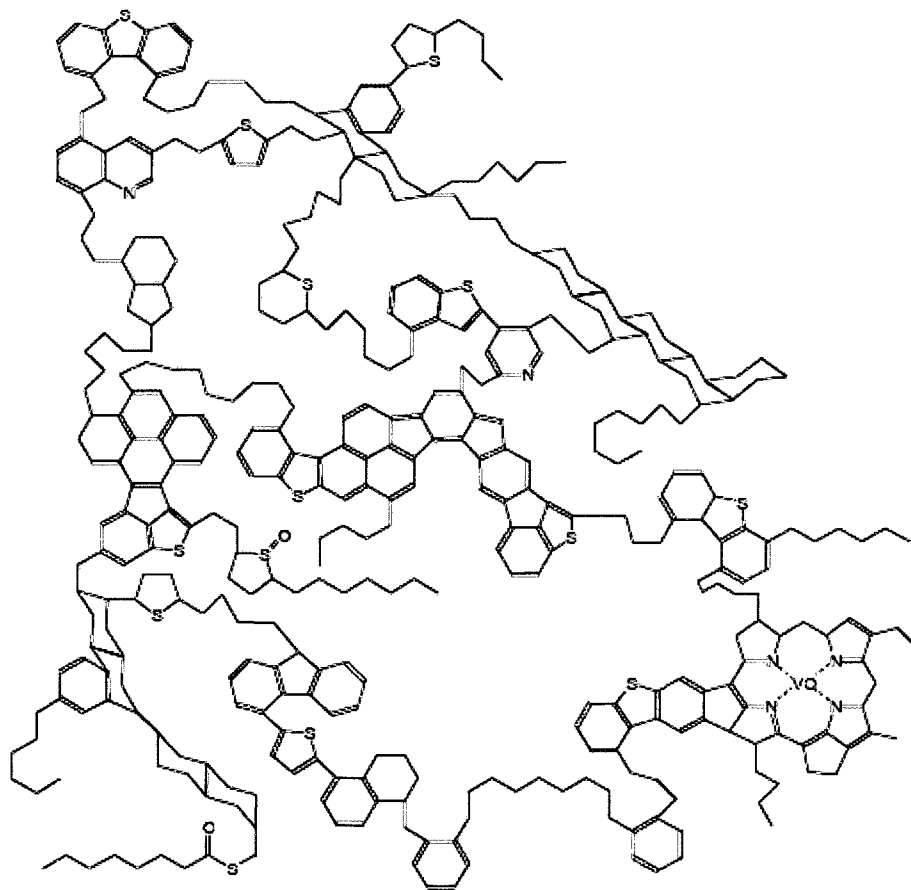
Figure 2.5 Proposed structure of asphaltenes in Athabasca bitumen [24]

The components of a crude oil soluble in paraffinic hydrocarbons such as n-pentane or n-heptane are referred to as the maltenes. They contain three different types of compounds: saturates, aromatics and resins (SAR). Resins can be separated from saturates and aromatics through chromatographic methods. Resins and asphaltenes have similarities in chemical structure and resins play a key role in the solubilization of asphaltene aggregates in crude oil. They are thought to solvate the edges of the aromatic clusters of asphaltene colloids [25].
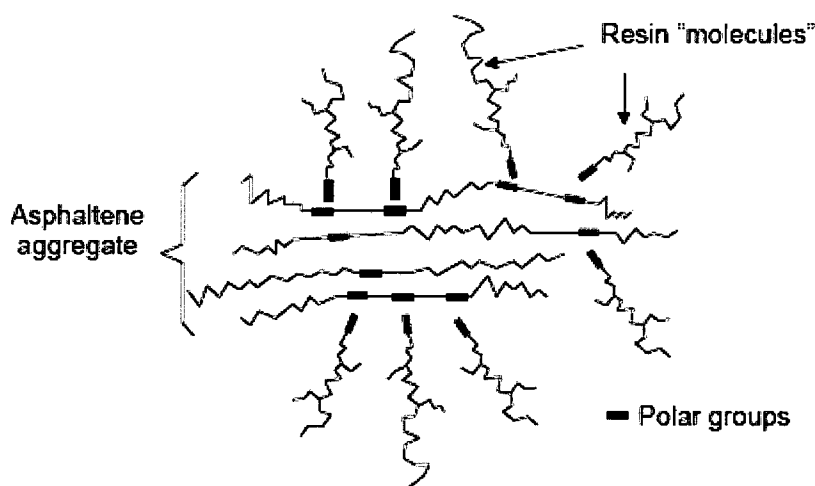
Figure 2.6 Schematic of asphaltenes aggregation [2]

Naphthenic acids are carboxylic acids exhibiting aliphatic rings of 5-6 carbon atoms. They are surface-active when the corresponding salt (naphthenate) is formed after the ionization of the carboxylic group. Naphthenates can be considered as a sub-class of resins and may play a role in the stabilization of asphaltene aggregates [26].

Figure 2.7 shows the scheme of water-in-crude oil or bitumen emulsions [21].

Asphaltenes, together with resins and solids, form a mechanical interfacial skin

which is described as structurally rigid film and barrier to coalescence.

In the emulsion formation during surface mining process, the degree of

emulsification depends on several factors: the energy of the mixing step in the

processes, the amounts of surface-active components in the crude oil, the

physicochemical properties of crudes, water and surfactant, the residual time and

emulsion age. The quantity of water in the emulsions varies from 30 % for regular

emulsions up to 80 % ~ 90 % in the form of extremely concentrated emulsions [21].

Water-in-oil emulsion

Salts, surfactants, pH, soluble organic solvents →Water

continuous phase
Crude oil or bitumen
(Aromatics, satrurates, resins, asphaltenes, waxes)

Interfacial layer
skin

Asphaltenes, resins, waxes, solids, metalloporphyrins, surfactants
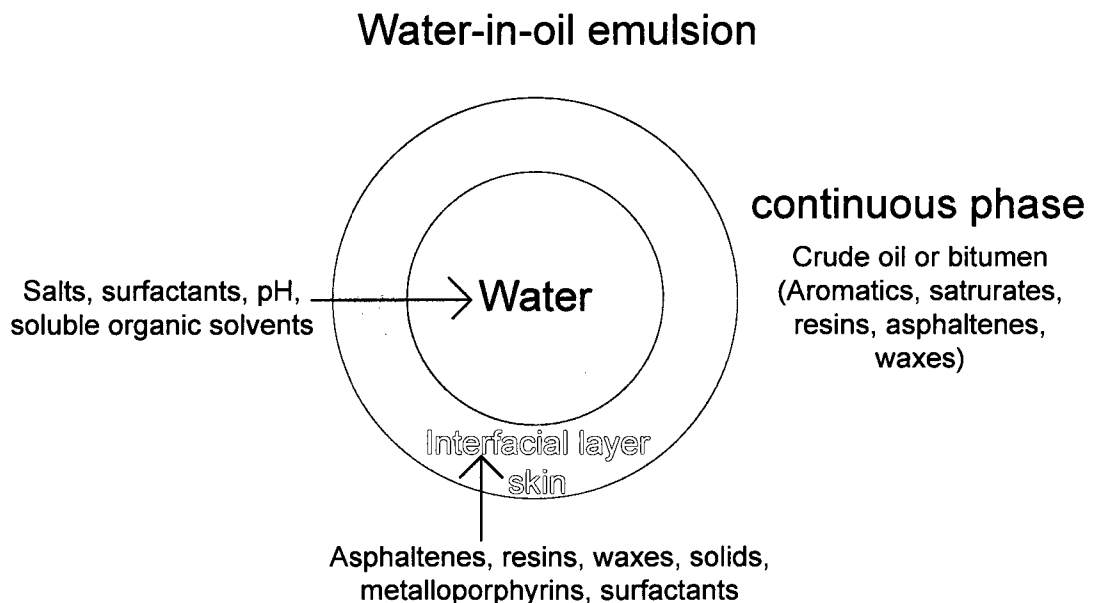
Figure 2.7 Schematic of water-in-crude oil or bitumen emulsion

Chapter 2

2.5. Effects of asphaltenes and demulsifier selection

For water in crude oil emulsion, several mechanisms have been suggested for the stability [27], [28]: (a) steric repulsion due to the adsorption of asphaltenes and resins, followed by formation of rigid films at the water/oil interfaces; (b) formation of long-range particle structure inside the film between two approaching drops; (c) steric repulsion due to the adsorption of naphthenates at high pH.

For mechanism a), the thickness of such films can be several hundred nanometers and the solubility of asphaltenes will affect the formation of rigid film. For Athabasca bitumen, the solvencies of the solvents are as follows [21]: paraffins < olefins < napthenes < cycloolefins < condensed napthenes < aromatics < condensed aromantics. By increasing the aromaticity of the oil phase and the resin/ asphaltene ratio, the average number of asphaltene molecules present in the colloid diminishes and therefore their solubilization in the oil phase will increase. Conversely, decreasing the aromaticity of the oil and/or the resin/asphaltene ratio leads to an increase in the asphaltene aggregation number and therefore to precipitation. If asphaltenes are less soluble in the solvents, they will precipitate and adsorb at the water/ oil interface forming the film structure. The thickness and concentration of these surfactant-active materials around the droplet's periphery build over time until the layer becomes a structural barrier

against coalescence with other droplets [21].

Methods to separate water-in-crude oil emulsions can be classified as mechanical, electrical and chemical [29]. Mechanical methods focus on breaking the physical barrier and/or on the difference in density between the aqueous and oil phases to achieve separation. Electrical demulsification is based on the application of an electric field to deform the droplets and generate a force of attraction between drops, thus leading to coalescence. Chemical demulsification refers to using chemicals to promote flocculation and/or modify the properties of the interfacial films so as to cause coalescence.

For chemical demulsification, in order to demulsify the emulsion, the requirements for the demulsifiers are [21]: 1) strong attraction to the oil/water interface with the ability to destabilize the protective film around the droplet and/ or to change the wettability of solids; 2) ability to flocculate the droplets; 3) ability to promote coalescence by opening pathways for water's natural attraction to water; 4) promotion of film drainage and thinning of the inter-droplet lamella by inducing the changes of the interfacial rheology such as decreased interfacial tension and increased compressibility of the interfacial film.

Each demulsifier plays a specific role in the demulsfication. Amphiphilic molecules with molecular weight 3,000-10,000 Da, such as polyalkoxylated

alkylphenolformaldehyde resins and complex block copolymers, are usually used for the separation of a large fraction of the dispersed aqueous phase [2]. They are often termed *coalescers*. These molecules penetrate the stabilizing film at the water/oil interfaces and modify its compressibility and rheological properties by disrupting the tight conformation of adsorbed asphaltenes, which leads to coalescence.

Molecules with molecular weight above 10,000 Da such as ethoxylated/ propoxylated amine polyols act as *flocculators* by adsorbing at the water/oil interfaces and interacting with molecules also adsorbed at the interfaces of nearby drops [30]. These molecules are effective in removing remaining small water drops and tight, fine emulsions once most of the dispersed phase has been removed.

Low molecular weight compounds (typically below 3,000 Da), such as common surfactants, exhibit high interfacial activity. Thus they can suppress interfacial tension gradients that occur in deforming interfaces of approaching drops that precedes film rupture and coalescence. They can alter the wettability (from hydrophobic to hydrophilic) of solid particles that are often adsorbed at the interface and that also contribute to the stability of the film.

Solvents are used as carriers of the active components. In the solvents the

demulsifiers do not aggregate to a significant extent and remain surface active. Aromatic hydrocarbons such as toluene and xylene and water-miscible hydroxycompounds such as n-butanol, isopropanol and monoethylene glycols are often used as solvents for demulsifiers [21].

All the demulsifiers should be surface active to aggregate at water/oil interface. Thus the demulsifier needs to participate in both oil and water phase. HLB (hydrophilic-lipophilic balance) values are used to characterize such properties [31]. For nonionic surfactant, HLB ranges from 0 (completely lipophilic) to 20 (completely hydrophilic) [31]. Abdel-Azim *et al*. [32] found demulsification was favored by an increase in the number of polar groups and in aromaticity with HLB values from 6 to 14. The authors claimed that such changes in the structure of the demulsifiers favor their adsorption at the water-oil interfaces and therefore the displacement/ solubilization of asphaltenes clustered in this region.

For the emulsions of water in diluted bitumen from Athabasca, the flocculation of water droplets is significant, which will be discussed in chapter 3. But the emulsion is very stable due to the asphaltenes and clay solids. Thus the first step is to choose an appropriate coalescer with solvents for the coalescence and chemicals to change the wettability of the clay solids.

Chapter 2

2.6. Effects of clay solid wettability and rag layer formation

Wettability of clay solid can also affect emulsion stability. Wettability is the preference of one fluid to spread on or adhere to a solid surface in the presence of other immiscible fluids [33]. For water-oil-clay system, wettability of clay depends on the structure and surface property of clay, the composition of oil and water, and temperature. Wettability can be characterized by measuring the *contact angle θ* of oil and water on clay surface, which is shown in Figure 2.8 [34].

The equilibrium contact angle is defined by Eq. 2.20.

$$\sigma_{ow} \cos\theta = \sigma_{os} - \sigma_{ws} \qquad [2.20]$$

θ: equilibrium contact angle.

σ_{ow}: interfacial tension between oil and water phases.

σ_{ws}: surface energy between water and substrate.

σ_{os}: surface energy between phase oil and substrate.
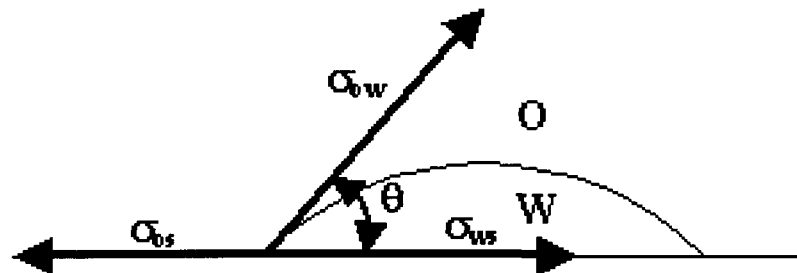
Figure 2.8 Force balance at three phase contact line

Clay has very small particle size (about 1-10 μm), thus it is hard to measure contact angle directly as shown in Figure 2.8. Other methods need to be used to

characterize clay wettability.

Solids which are partially hydrophobic with contact angle $\theta > 90°$ (measured through the water) can also act as emulsifiers to make water-in-oil emulsions more stable. Figure 2.9 [35] shows the wettability of solids and the types of emulsions formed by the effect of solids wettability.

water-wet   amphiphilic   oil-wet

Wettability of solids

oil-in-water emulsions   water-in-oil emulsions
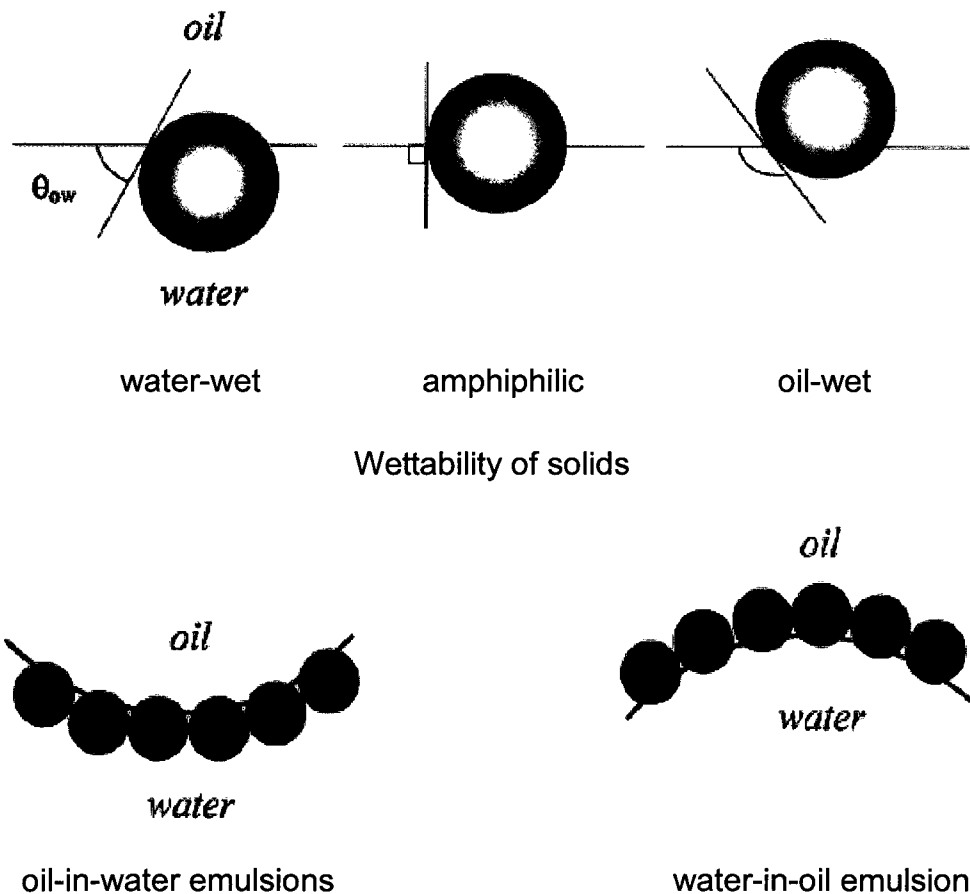
Figure 2.9 Wettability of solids and the types of emulsions

For hydrophilic solids, the contact angle is smaller than 90°. The surface of solids is water-wet and the solids tend to stay in water phase. On the contrary, for

hydrophobic solids, the contact angle is greater than 90°. The surface of solids is oil-wet and the solids tend to stay in oil phase. If the solids are amphiphilic, they will stay at the interface of oil and water. According to the Bancroft rule [36], the phase in which the emulsifiers are most soluble is the continuous phase. So the amphiphilic solids which are somewhat hydrophobic can act as the emulsifier to form the water-in-oil emulsions.

If the particle is small enough (typically less than a micron in diameter) so that the effect of gravity is negligible, the energy $(-\Delta_{int}G)$ required to remove a particle of radius r from an oil-water interface of tension γ_{ow} is [35]:

$$-\Delta_{int}G = \pi r^2 \gamma_{ow}(1 \pm \cos\theta_{ow})^2 \qquad [2.21]$$

Here the sign inside the bracket is negative for removal into the water phase, and positive for removal into oil. Compared with surfactant molecules, clay solids have much larger radii, thus the energy to remove a solid particle from oil-water interface is much larger than that to remove a typical surfactant molecule. The clay solids will stay at the water/oil interface to make the film more rigid acting as the barrier of coalescence.

The pH in bitumen froth treatment process is around 8.5. During bitumen froth treatment process, clay solids in diluted bitumen adsorb some of the oil components and become partially oil-wet. The partially oil-wet clay solids can

retard water-in-oil emulsion coalescence. They also entrap oil drops and form aggregates, which results in a *rag layer* in the middle of the sample. Figure 2.10 shows a partially separated emulsion sample (details can be found in section 4.1) of water in diluted bitumen with a rag layer in the middle. Photomicrographs show the structure of rag layer. The upper part of the rag layer is water in oil emulsion. The lower part of the rag layer contains aggregates (*skins*) of partially oil-wet clay solid with adsorbed oil and entrapped oil droplets in continuous water phase.

If clay solid becomes more water-wet, it will prefer to stay in water phase instead of water/oil interface. Adsorbed oil will be displaced by water and separated clay solids enter water phase. Thereby the loss of more water wet solids from the interface will destabilize the emulsion.
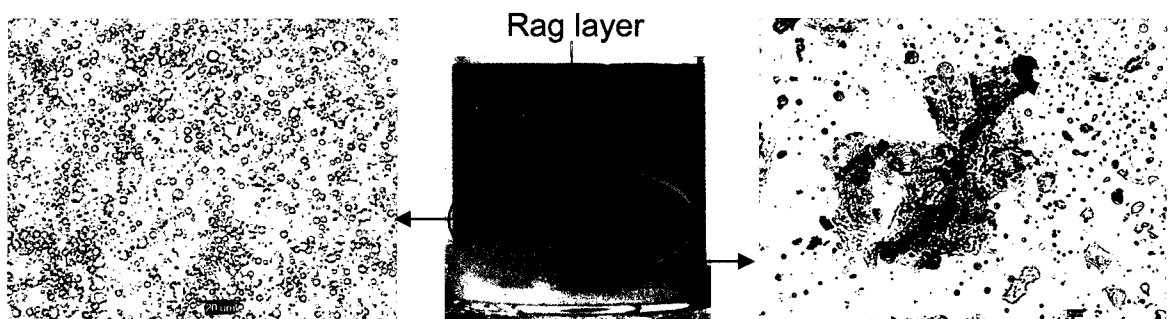
Figure 2.10 Rag layer in diluted bitumen emulsion sample

2.7. Reference

[1]   J. Sjöblom, Emulsions and emulsion stability, Surfactant science series, CRC Press, **2006**.

Chapter 2

[2] A. Pena, Dynamic aspects of emulsion stability, PhD thesis, Rice University, **2004**.

[3] P. Sherman, *Emulsion Science*, Academic Press, London, **1968**.

[4] B. Epstein, Logarithmico-normal distribution in breakage of solids, *Ind. Eng. Chem.*, **1948**, 40, 2289-2290.

[5] J. Lachaise, B. Mendiboure, C. Dicharry, G. Marion, M. Bourrel, P. Cheneviere, J.L. Salager, A simulation of emulsification by turbulent stirring, *Colloids Surf. A: Phys. Chem. Eng. Aspects*, **1995**, 94, 189-195.

[6] C. Orr, Emulsion droplet size data, *Encyclopedia of Emulsion Technology*, P. Becher, Editor. Vol. 1. Ch. 6. Marcel Dekker, New York, **1983**.

[7] Ø. Sæther, Video-enhanced microscopy investigation of emulsion droplets and size distributions, *Encyclopedic Handbook of Emulsion Technology*, J. Sjöblom, Editor. Marcel Dekker, Inc., New York, **2001**.

[8] Howard A. Barnes, Reology of emulsions-a review, *Colloids Surf. A: Phys. Chem. Eng. Aspects*, **1994**, 91, 89-95.

[9] A. Einstein, Eine neue bestimmung der moleküldimensionen, *Ann. Physik*, **1906**, 19, 289-306.

[10] A. Einstein, Berichtigung zu meiner arbeit: Eine neue bestimmung der moleküldimensionen, *Ann. Physik*, **1911**, 34, 591-592.

[11] R. Pal, E. Rhodes, Viscosity-concentration relationships for emulsions, *J. Rheol.*, **1989**, 33,1021-1045.

[12] R. Pal, Effect of droplet size on the rheology of emulsions, *AIChE J.*, **1996**, 42, 3181-3190.

[13] B.V. Derjaguin, L. Landau, Acta Physicochem. URSS, **1941**, 14.

[14] E.J.W. Verwey, J.T.G. Overbeek, Theory of the Stability of Lyophobic Colloids, Elsevier, Amsterdam, **1948**.

[15] C.A. Miller, P. Neogi, Interfacial Phenomena: Equilibrium and Dynamic Effects, Marcel Dekker, Inc., New York, **1985**.

[16] J.F. Richardson, W.N. Zaki, Sedimentation and fluidisation: Part I, *Trans. Inst. Chem. Eng.*, **1954**, 32, 35-53.

[17] G..K. Batchelor, Sedimentation in a dilute dispersion of spheres, *J. Fluid Mech.*,**1972**, 52, 245-268.

[18] M.V. Smoluchowski, Versuch einer mathematischen theorie der koagulation-skinetik kolloider lösungen, *Z. Phys. Chem.*, **1918**, 92, 129-168.

[19] P. Walstra, Emulsion stability, *Encyclopedia of Emulsion Technology*, P. Becher, Editor. Vol. 4. Marcel Dekker, Inc., New York, **1990**.

[20] J. A. Kitchener, P. R. Musselwhite, I. P. Sherman, Emulsion science, New York: Academic Press, **1968**.

[21] C.W. Angle, Chemical demulsification of stable crude oil and bitumen emulsions in petroleum recovery - a review, in *Encyclopedic handbook of emulsion technology*, J. Sjöblom, Editor. Marcel Dekker, Inc., New York, **2001**

[22] O. Reynolds, On the theory of lubrication and its application to Mr. Beauchamp Tower's experiments, including an experimental determination of the viscosity of olive oil, *Philos. Trans. R. Soc.*, London, **1886**, 177, 157-234.

[23] D. Espinat, E. Rosemberg, M. Scarsella, L. Barre, D. Fenistein, D. Broseta, Colloidal structural evolution from stable to flocculated state of asphaltene solutions and heavy crudes, *Structure and dynamics of asphaltenes*, O. Mullins and E. Sheu, Editors, Plenum Press, New York, **1998**.

[24] K.L. Gawrys, P.M. Spiecker, P.K. Kilpatrick, The role of asphaltene solubility and chemical composition on asphaltene aggregation, *Petr. Sci. Technol.*, **2003**, 21, 461-489.

[25] J. McLean, P. M. Spiecker, A. Sullivan, P. K. Kilpatrick, The role of petroleum asphaltenes in the stabilization of water-in-oil emulsions, *Structure and dynamics of asphaltenes*, O. Mullins and E. Sheu, Editors, Plenum Press, New York, **1998**.

[26] J. Czarnecki, J. Masliyah, Emulsion studies associated with bitumen recovery from Canadian oil sands: Part II., Proceedings of the 3rd International Conference on Petroleum Phase Behavior and Fouling, New Orleans, USA, **2002**, 323-328.

[27] A. Goldszal, M. Bourrel, C. Hurtevent, J-L. Volle, Stability of water in acidic crude oil emulsions, Proceedings of the 3rd International Conference on Petroleum Phase Behavior and Fouling, New Orleans, USA, **2002**, 386-400.

[28] Y. H. Kim, A. D. Nikolov, D. Wasan, H. Díaz-Arauzo, C. S. Shetty, Demulsification of water-in-crude oil emulsions: effects of film tension, elasticity, diffusivity and interfacial activity of demulsifier individual components and their blends, *J. Disp. Sci. Technol.*, **1996**, 17, 33-53.

[29] K. Lissant, Demulsification, Surfactant Science Series, Vol. 13. Marcel Dekker, Inc., New York, **1983**.

[30] P. J. Breen, A. Yen, and J. Tapp, Demulsification of asphaltene-stabilized emulsions- correlation of demulsifier performance with crude oil composition, Proceedings of the 3rd International Conference on Petroleum Phase Behavior and Fouling, New Orleans, USA, **2002**, 359-366.

[31] W. C. Griffin, Classification of Surface-Active Agents by 'HLB', *Soc. of Cosmetic Chemists* 1, **1949**, 31, 1-326.

[32] A. A. Abdel-Azim, N.N. Zaki, and N.E.S. Maysour, Polyalkoxylated amines for breaking water-in-oil emulsions: effect of structural variations on the demulsification efficiency, *Polym. Adv. Technol.*, **1998**, 9, 159-166.

[33] F. F. Craig, The reservoir engineering aspects of water flooding, Monograph V. 3 of Henry L. Doherty series, Society of Petroleum Engineers of AIME, Dallas, **1971**.

[34] N. R., Morrow, Interfacial Phenomena in Petroleum Recovery, Marcel Dekker, Inc., New York, **1991**.

[35] R. Aveyard, B. P. Binks, J. H. Clint, Emulsions stabilized solely by colloidal particles, *Adv. Colloid Interface Sci.*, **2003**, 503–546.

[36] WD. Bancroft. The Theory of Emulsification, *J. Phys. Chem.*, **1913**, 17, 501-519.

Chapter 3

3. Characterization of emulsions by NMR

This chapter focuses on the characterization of diluted bitumen emulsion properties from nuclear magnetic resonance (NMR) measurements. Sections 3.1 - 3.4 first introduce MNR techniques; then show how to characterize diluted bitumen emulsion using these methods. The rest part of the chapter discusses experimental procedures and results.

3.1. Introduction

NMR spectroscopy is based on the fact that some nuclei process a permanent nuclear magnetic moment. Some nuclei, such as protons, have a permanent magnetic moment p. When a steady uniform magnetic field B_0 is applied on these nuclei, they take certain stated which correspond to distinct energy levels. The magnetic moment p precesses around the direction of B_0 at the *Larmor frequency* $\omega_0 = \gamma B_0$, where γ is a constant. The nuclei exhibit net magnetization M in the direction of B_0. If a radio frequency (*rf*) pulse of a second magnetic field B_1 orthogonal to B_0 is applied, the net magnetization is rotated to an extent (typically 90° or 180°) that depends on the duration of the pulse. After the *rf* pulse, M will relax and finally reach equilibrium state. Relaxation of M can be measured from the *spins* (precessing protons), either in the direction of B_0 (longitude magnetization), or transverse plane (transverse magnetization).

Transitions between neighboring energy levels take place due to the adsorption of electromagnetic radiation of characteristic wave lengths at *Larmor frequency*. The precession of spins at the same Larmor frequency is referred as *coherent* or *in-phase*.

NMR is a versatile method because [1]: 1) It is not a destructive technique. The system can be studied without any perturbation that will affect the outcomes of the measurement. The system can be characterized repeatedly with no time-consuming sample preparation in between runs. 2) A large number of spectroscopic parameters can be determined by NMR relating to both static and dynamic aspects of a wide variety of systems.

For water-in-diluted bitumen emulsions, several characteristics, such as water content and drop size can be estimated by different NMR protocols.

3.2. T_2 distribution from CPMG measurement

3.2.1. Introduction

Relaxation of spins net magnetization M in longitudinal direction and in transverse plane can be expressed as [2]:

$$\frac{dM_z}{dt} = -\frac{M_z - M_z^0}{T_1}, \quad \frac{dM_{xy}}{dt} = -\frac{M_{xy}}{T_2} \qquad [3.1]$$

Here M_z^0 is equilibrium magnetization in longitudinal direction. M_z and M_{xy} are

Chapter 3

magnetization in longitudinal direction and transverse plane at time t. T_1 and T_2 are time constants, which are referred as *longitude relaxation time* and *transverse relaxation time*.

T_2 can be measured by CPMG (developed by Carr and Purcell [3] and refined by Meiboom and Gill [4]) measurement. For CPMG measurement, the spin echoes are produced by the a series of 180° *rf* pulses following the preparative 90° pulse, as shown in Figure 3.1 [5]. As time proceeds, relaxation of the magnetization takes place and the amplitude of the spin-echo is generated after 180° re-phasing decay. In the experiment, decay of echo magnitude in the transverse plane is measured and the equation for the relaxation is [5]:

$$\frac{M_{xy}(2n\tau)}{M_{xy}(0)} = \sum_{i=1}^{m} f_i \exp(-\frac{2n\tau}{T_{2,i}}); \quad 0 \le n \le N; \quad m < N; \quad \sum_{i=1}^{m} f_i = 1; \quad f_i \ge 0 \qquad [3.2]$$
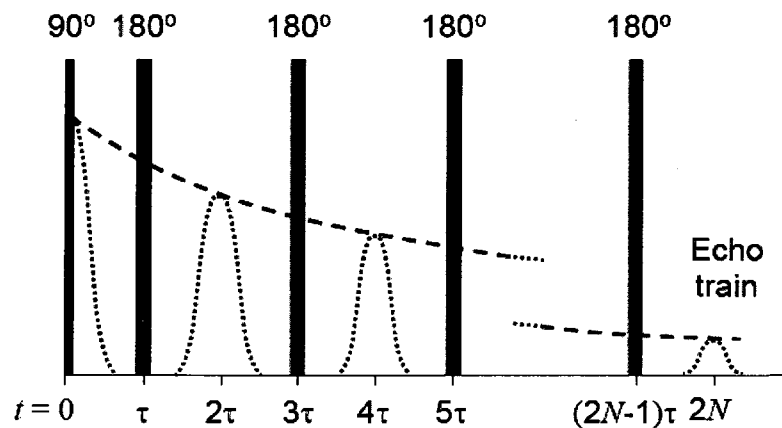
Figure 3.1 Sequence of CPMG measurement

Here N is number of 180° *rf* pulses, $M_{xy}(0)$ is the amplitude corresponding to

Chapter 3

the initial transverse magnetization, f_i is the fraction of protons with relaxation time $T_{2,i}$. T_2 distribution of the sample can be obtained using multi-exponential fitting to the raw data of spin echoes, which was developed by Huang [6]. Fitting data to a multi-exponential sum is an illposed problem [7]. For this reason, a regularization method is used to calculate the most representative T_2 distribution [8].

3.2.2. Characterization of emulsions with CPMG measurement

In Eq. [3.2], f_i is proportional to the spin density of the fluids. Thus the volume fraction φ_k of phase k is related to the T_2 distribution [9]:

$$\varphi_k \propto \frac{\sum (f_i)_k}{HI_k}$$ [3.3]

HI is the hydrogen index, which is the ratio of proton density in the fluid and that in water. In general, HI is about 1 for aqueous solutions, and 0.9 - 1.0 for most crude oils, except aromatic oils, which is 0.6-0.8. From Eq. [3.3], for water in oil emulsion, the water fraction can be calculated as:

$$\varphi_{DP} = \frac{[\sum (f_i)_{DP} / HI_{DP}]}{[\sum (f_i)_{CP} / HI_{CP}] + [\sum (f_i)_{DP} / HI_{DP}]}$$ [3.4]

Here subscript DP is the dispersed water phase, subscript CP is the continuous oil phase.

NMR CPMG measurement has been regarded as superior to all other available techniques for the determination of water content in heavy oil, bitumen

and oilfield emulsions [10]. This application is an extension of the usage of NMR

relaxation measurements for the determination of porosity in minerals and rocks.

If the fluid is confined in a planar, cylindrical or spherical cavity, the relaxation

can be written as [11]:

$$\frac{1}{T_{2,i}} = \frac{1}{T_{2,bulk}} + \rho(\frac{S}{V})_i$$
[3.5]

Here ρ is surface relaxivity. For the same water/oil system, ρ keeps constant.

$(S/V)_i$ is the surface to volume ratio of cavity i. For a sphere of radius a_i, Eq. [3.4]

becomes:

$$\frac{1}{T_{2,i}} = \frac{1}{T_{2,bulk}} + \rho\frac{3}{a_i}, \qquad a_i = 3\rho/(\frac{1}{T_{2,i}} - \frac{1}{T_{2,bulk}})$$
[3.6]

The number of protons present in a given volume of sample determines the

signal amplitude. For this reason, the fraction f_i that is associated to each $T_{2,i}$

value renders a direct measurement of the fraction of droplets with the radius a_i.

Drop size distribution of emulsions can be obtained from T_2 distribution. The

requirements for Eq. [3.5] are [5]:

1) Measurements are performed in the "fast diffusion" mode, that the

   characteristic time scale t_D for molecule diffusion should be much smaller

   than that of surface relaxation t_ρ. $\frac{t_D}{t_\rho} = \frac{a_i/D}{a_i^2/D} \ll 1$, $\Rightarrow \frac{\rho a_i}{D} \ll 1$. D is

   diffusivity of dispersed phase.

Chapter 3

2) The surface relaxivity (ρ) and the bulk relaxivity ($1/T_{2,\text{bulk}}$) of the drop phase are known. $T_{2,\text{bulk}}$ can be easily measured from a CPMG experiment on a bulk sample of the drop phase.

3) $T_{2,\text{bulk}}$ for the dispersed phase is indeed single-valued and not a distribution of characteristic bulk relaxation times.

4) Two independent sets of $T_{2,i}$ - f_i values can be resolved from the T_2 distribution of the emulsion for the oil and water phases, respectively.

The minimum and maximum drop sizes that can be determined via CPMG are, respectively [5]:

$$d_{\min} \approx 6\rho T_{2,\min} , \quad d_{\max} \approx \min\{D/2\rho, \ 2SNR\rho T_{2,bulk}/e\} \qquad [3.7]$$

Here $T_{2,\min}$ is the smallest T_2 of water drops measured by CMPG. *SNR* is signal to noise ratio of the measurement. D is diffusivity of dispersed phase.

Using the data reported in reference [5], the drop size range which can be measured by CPMG is 16 nm to 580 μm [5].

But in some cases, such as water in light oil emulsion, T_2 distribution of dispersed water phase is very close to that of continuous oil phase. Thus CPMG method is not appropriate because the T_2 distribution is not distinguishable. The alternative methods for estimating the water fraction and drop size distribution will be discussed in the following sections.

Chapter 3

3.3. Drop size distribution from NMR restricted diffusion measurement

3.3.1. Introduction

In the NMR restricted diffusion measurement, the pulsed magnetic field gradient spin-echo experiment (PGSE) was developed by Stejskal and Tanner [12]. The basic sequence consists of an *rf* 90° pulse, followed by a *rf* 180° pulse at time *τ*. As a result of this sequence, a spin-echo is collected at time 2*τ* (*echo spacing*), as shown in Figure 3.2 [5]. The *rf* 180° pulse is between two magnetic gradient pulses with strength *g* and duration *δ* that are separated by the diffusion time Δ.
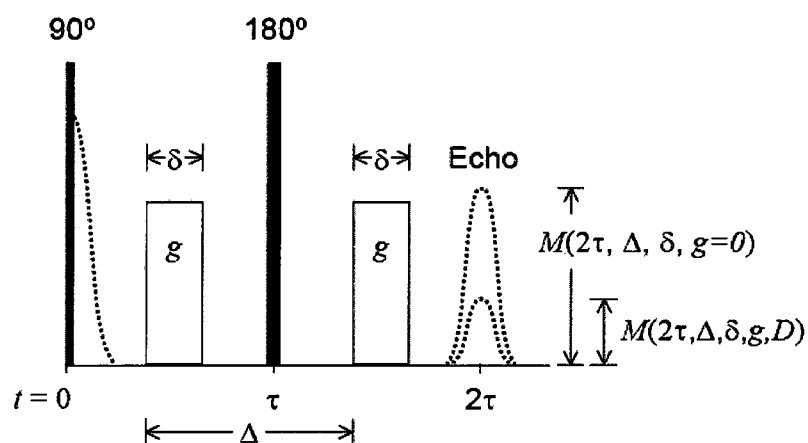
Figure 3.2 Basic sequence of PGSE measurement

The first pulse makes the spins with different frequencies dependent on their positions, encoding the phase of the spins. Then, after the 180° pulse inverts the precession, the second gradient pulse returns the spins to their original phase for measurement. However, some molecules diffuse and change their position during

the diffusion time. Those spins that have diffused are not decoded to their original phase and are no longer measured in the spin echo [12]. Hereby the amplitude of spin-echoes in the presence of gradient pulses is smaller than that in the absence of gradient pulses.

In the PGSE experiment, the amplitude ratio of spin-echoes in the presence and absence of gradient pulses ($g > 0$ and $g = 0$) R is measured.

$$R = \frac{M_{xy}(2\tau, g, \Delta, \delta, D)}{M_{xy}(2\tau, g = 0, \Delta, \delta, D)}, \quad 0 \leq R \leq 1 \qquad [3.8]$$

D is the fluid diffusivity. R is the spin-echo attenuation ratio. For isotropic bulk fluids in which molecules can diffuse freely (Fickian diffusion), the expression for R is [12]:

$$R_{bulk} = \exp[-\gamma^2 g^2 D \delta^2 (\Delta - \delta/3)] \qquad [3.9]$$

The constant γ is the gyromagnetic ratio of the nuclei ($\gamma = 2.67 \times 10^8$ rad.$T^{-1} \cdot s^{-1}$ for ^1H). This method can be used to measure self-diffusion coefficients.

In basic PGSE sequence, if T_2 of water droplets is small (due to small drop size or large surface relaxivity), spin echo amplitude becomes small because of transverse relaxation, which will reduce SNR and measurement accuracy. Eq. 3.10 shows the spin-echo signal amplitude as the function of echo spacing [6].

$$M_{xy}(2\tau) = M_z^0 \exp(-\frac{2\tau}{T_2}) \qquad [3.10]$$

Here $M_z{}^0$ is equilibrium magnetization in longitude direction. $M_{xy}(2\tau)$ is magnetization in longitude direction and transverse plane at time 2τ.

In this case, stimulated spin-echo PGSE sequence is used [13], as shown in Figure 3.3 [14]. The sequence is useful for systems with significantly different longitudinal (T_1) and transverse (T_2) relaxation times $(T_1 > T_2)$. This is often the case for systems with large interfacial area, such as emulsions.
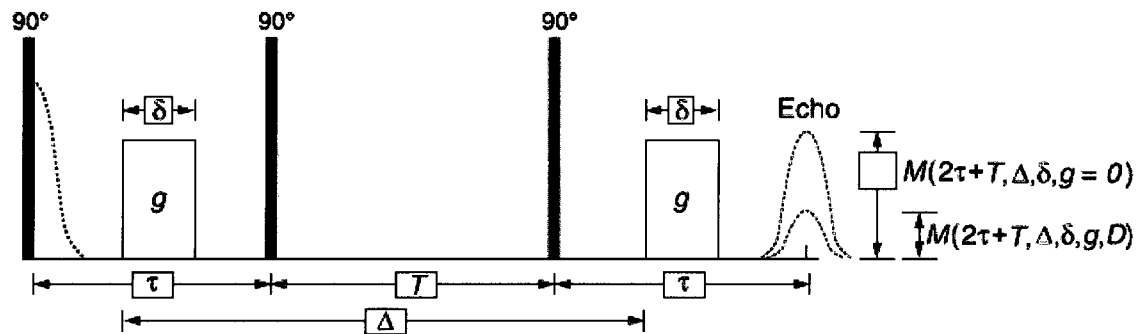
Figure 3.3 Sequence of stimulated spin-echo PGSE measurement

The sequence begins with a 90° rf pulse to be rotated to transverse plane, followed by a magnetic gradient pulse. The spins undergo transverse relaxation T_2. The second 90° rf pulse follows, moving the spins into the longitudinal direction, where they undergo longitudinal relaxation (T_1). The last 90° pulse moves the spins back to the transverse plane, followed by a second magnetic gradient pulse. The result is an echo, referred to as a *stimulated echo*. The spin-echo signal amplitude as the function of echo spacing is [6]:

$$M_{xy}(2\tau+T) = \frac{1}{2}M_z^0 \exp(-\frac{T}{T_1} - \frac{2\tau}{T_2})$$

[3.11]

This procedure allows increasing the diffusion time while reducing the effect of extended relaxation which will reduce the *SNR*. Eq. 3.8 can also be used to calculated spin echo signal attenuation for stimulated spin-echo PGSE sequence.

3.3.2. Drop size determination from PGSE measurement

Eq. [3.9] is limited to bulk fluids. But in many cases, the fluids are confined in small geometrics such as pores or droplets and cannot diffuse freely, which is referred as *restricted diffusion*. In these cases, Murday and Cotts [15] developed the equation for the PGSE sequence. For restricted diffusion within a sphere of radius *a*, the attenuation ratio R_{sp} is:

$$R_{sp} = \exp\left\{-2\gamma^2 g^2 \sum_{m=1}^{\infty} \frac{1}{\alpha_m^2(\alpha_m^2 a^2 - 2)}\left[\frac{2\delta}{\alpha_m^2 D} - \frac{\Psi}{(\alpha_m^2 D)}\right]\right\}$$

[3.12]

Here $\Psi = 2 + e^{-\alpha_m^2 D(\Delta-\delta)} - 2e^{-\alpha_m^2 D\Delta} - 2e^{-\alpha_m^2 D\delta} + e^{-\alpha_m^2 D(\Delta+\delta)}$

[3.13]

α_m is the mth positive root of the equation: $\alpha a \cdot J_{5/2}(\alpha a) - J_{3/2}(\alpha a) = 0$ [3.14]

J_k is the Bessel function of the first kind, order *k*.

If $\Delta \gg a^2/2D$, $\Delta \gg \delta$, Eq. [3.8] can be simplified as[1]:

$$R_{sp} = \exp(-\gamma^2 g^2 \delta^2 a^2 / 5)$$

[3.15]

Figure 3.4 shows the predicted attenuation of emulsified water droplets with different drop diameters from 5 to 50 μm. Here the diffusion time Δ is 500 ms,

gradient pulse duration δ is 3 ms, range of magnetic gradient is 0 - 40 G/cm. In the figure, water droplets with different drop diameters have different signal attenuation, which are the bases of getting drop size distribution from diffusion results. Droplets with diameter from 10 to 30 μm have the largest attenuation differences and most sensitive to the data fitting.
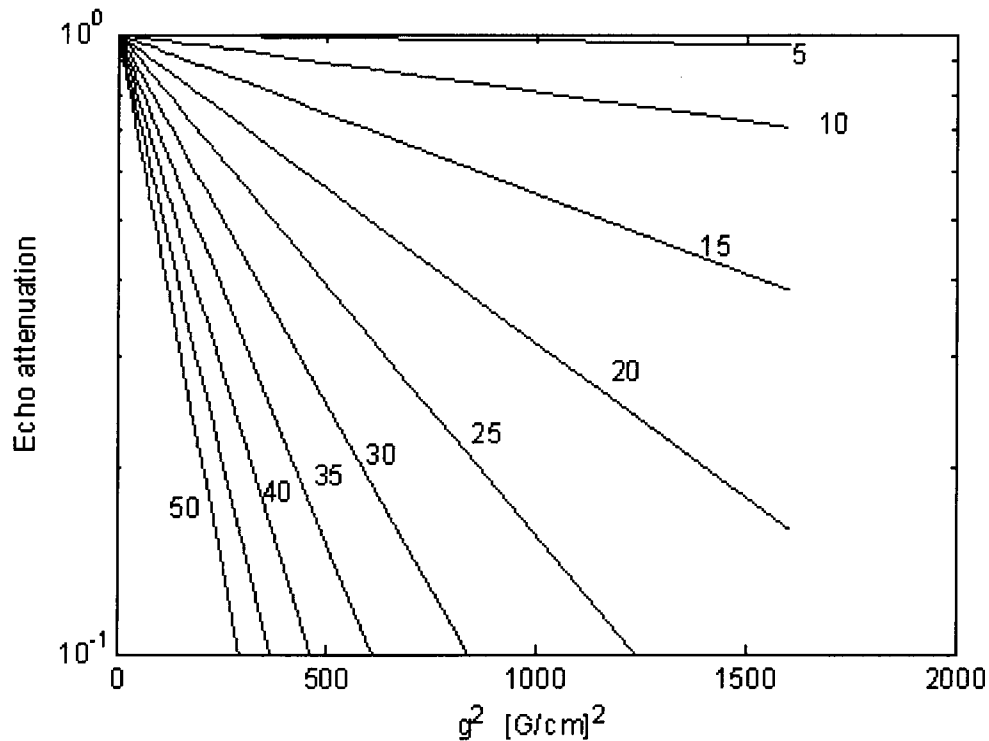
Figure 3.4 Predicted attenuation of water droplets with different drop diameters

For emulsions with a finite distribution of spherical droplet sizes, the attenuation ratio of the emulsified phase (R_{emul}) can be calculated as the sum of the attenuation ratios $R_{sp}(a)$, weighted by the probability of finding drops with such sizes in the dispersion [16]:

$$R_{emul} = \frac{\int_0^\infty p_v R_{sp}(a) da}{\int_0^\infty p_v da}$$ [3.16]

Here $p_v(a)$ is the volume-weighted distribution of sizes. $R_{sp}(a)$ is determined from Eq. [3.12].

The lognormal probability distribution function (p.d.f.), is the classic assumption for the drop size distribution in absence of additional information, because it is well known that sequential break-up processes yield such a distribution [17], [18].

$$p_v(d) = \frac{1}{\sqrt{2\pi} d\sigma} e^{-\frac{[\ln(d)-\ln(d_{gV})]^2}{2\sigma^2}}$$ [3.17]

d_{gV} and σ are the geometric volume-based mean diameter and the width or geometric standard deviation of the distribution, respectively.

For continuous oil phase, Eq. [3.9] is also valid. For an oil phase with the effective diffusivity distribution p (D_{CP}), the equation for the attenuation is [5]:

$$R_{oil} = \frac{\int_0^\infty p_D(D_{CP}) R_{bulk,CP}(D_{CP}) dD_{CP}}{\int_0^\infty p_D(D_{CP})(D_{CP}) dD_{CP}}$$ [3.18]

If the emulsion is partially separated, Eq. [3.9] can also be applied for separated bulk water, using bulk water diffusivity.

The maximum drop size that can be determined via PGSE is related to the one-dimension root-mean-square displacement of spins undergoing free (Fickian)

self-diffusion in isotropic, isothermal media during the diffusion time Δ [5]:

$$d_{\max} \approx \sqrt{2}\langle x^2 \rangle^{1/2} = 2\sqrt{D\Delta} \qquad [3.29]$$

Here $\langle x^2 \rangle^{1/2}$ is root-mean-square displacement. D is diffusivity.

The minimum drop size $d_{\min}$ that is measurable from PGSE data can be expressed as [5]:

$$d_{\min} = (175\lambda \frac{D}{\gamma^2 g^3 \delta_{\max}})^{1/4}, \quad \lambda = 1 - R_{sp}(a = d_{\min}/2, \delta = \delta_{\max}) \qquad [3.30]$$

Here $\delta_{\max}$ is the largest magnetic gradient duration can be used in the measurement (usually $\delta_{\max} = 0.2\Delta$). Plausible values for λ are $0.01 \leq \lambda \leq 0.05$.

3.3.3. Drop size determination of diluted bitumen emulsion

For diluted bitumen emulsion, the total attenuation for the emulsion can be written as:

$$R = \frac{M_{oil}(g>0) + M_{emul}(g>0) + M_{water}(g>0)}{M_{oil}(g=0) + M_{emul}(g=0) + M_{water}(g=0)} \qquad [3.19]$$

Subscripts *emul*, *oil* and *water* correspond to emulsified water, oil and bulk water phases.

$$R_{oil} = \frac{M_{oil}(g>0)}{M_{oil}(g=0)}, R_{emul} = \frac{M_{emul}(g>0)}{M_{emul}(g=0)}, R_{water} = \frac{M_{water}(g>0)}{M_{water}(g=0)} \qquad [3.20]$$

Substituting Eq. [3.20] in Eq. [3.19],

$$R = \frac{M_{oil}(g=0)R_{oil}}{[\sum M]_{g=0}} + \frac{M_{emul}(g=0)R_{emul}}{[\sum M]_{g=0}} + \frac{M_{water}(g=0)R_{water}}{[\sum M]_{g=0}} \qquad [3.21]$$

Here $\quad [\sum M]_{g=0} = M_{oil}(g=0) + M_{emul}(g=0) + M_{water}(g=0)$ [3.22]

Eq. [3.21] can be rewritten as:

$$R = \kappa_{emul} R_{emul} + \kappa_{oil} R_{oil} + \kappa_{water} R_{water}$$ [3.23]

Here κ is signal attenuation fraction of each phase.

$$\kappa_{oil} = \frac{M_{oil}(g=0)}{[\sum M]_{g=0}}, \ \kappa_{emul} = \frac{M_{emul}(g=0)}{[\sum M]_{g=0}}, \ \kappa_{water} = \frac{M_{water}(g=0)}{[\sum M]_{g=0}}$$ [3.24]

$M(t_E, g=0)$ in Eq. [3.22] is associated to the T_2 distribution of each phase. t_E is

echo spacing time, which is 2τ for basic PGSE sequence or $T+2\tau$ for stimulated

spin-echo PGSE sequence.

If T_2 distribution peaks for oil, emulsified water and bulk water are completely

separate, $M(t_E, g=0)$ can be expressed as:

$$M_{oil}(g=0) = M_z^0 \phi_{oil} HI_{oil} \sum_i x_i \exp(-\frac{t_E}{T_{2,i}})$$ [3.25]

$$M_{emul}(g=0) = M_z^0 \phi_{emul} \sum_i x_i \exp(-\frac{t_E}{T_{2,i}})$$ [3.26]

$$M_{water}(g=0) = M_z^0 \phi_{water} \sum_i x_i \exp(-\frac{t_E}{T_{2,i}})$$ [3.27]

HI is hydrogen index of fluid, which is 1 for water. Φ is component fraction of

oil, emulsified water or bulk water. x_i is normalized fraction of component with

relaxation time $T_{2,i}$ in T_2 distribution peak of oil, emulsified water or bulk water.

$$x_i = \frac{f_i(T_2 = T_{2,i})}{\sum f_i(T_2 = T_{2,i})}$$ [3.28]

Chapter 3

Figure 3.5 shows the schematic diffusion result of emulsion with oil as continuous phase, water as dispersed phase and separated bulk water. According to Eq. [3.23], the NMR signal attenuation of the emulsion is the combination of continuous oil phase, dispersed water phase and bulk water phase. For restricted diffusion, the apparent diffusivity of dispersed water phase is much smaller than the continuous oil or bulk water phase. Thus at initial time, most of the attenuation corresponds to continuous oil or bulk water phase; if the magnetic gradient is large enough, most of the signal attenuation corresponds to dispersed phase.
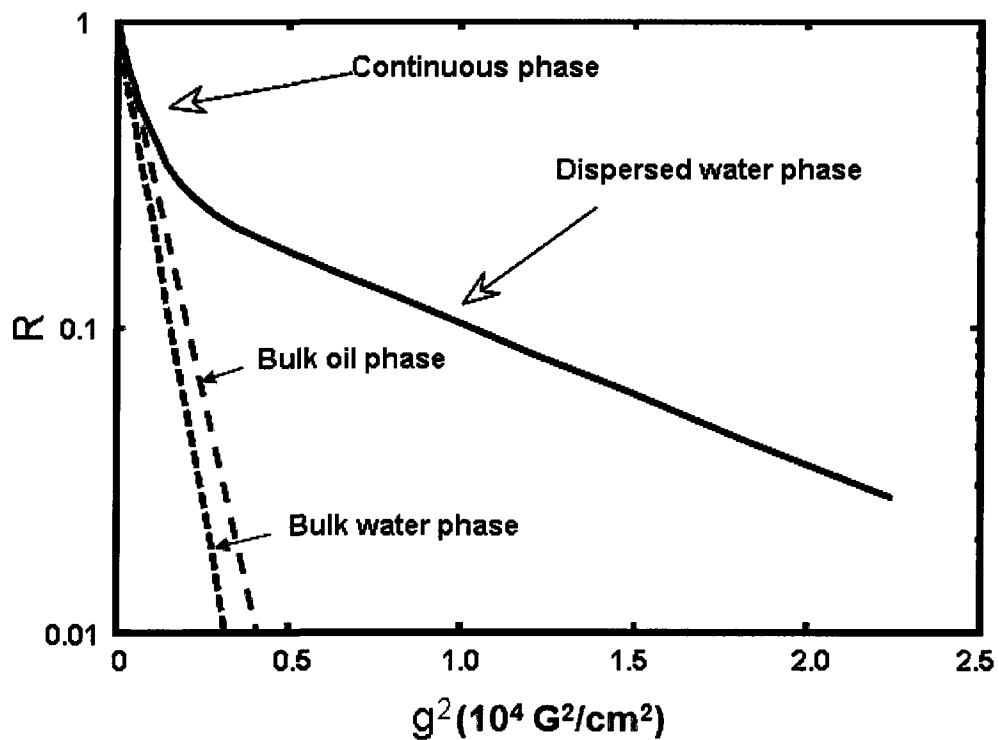
Figure 3.5 Schematic diffusion results of emulsion

The determination of the drop size distribution consists of performing a

Chapter 3

least-square fit of the experimental data for R, using d_{gV}, σ, D_{CP} and κ as fitting

parameters. Detailed procedure is as follows:

1) Estimating initial values of geometric volume-based mean diameter d_{gV}

   and geometric standard deviation σ; signal attenuation fraction κ_{oil}, κ_{emul}

   and κ_{water}; diffusivity of continuous oil phase D_{CP}.

2) Using Eq. [3.9] with D_{CP} and D_{water} to calculate attenuation R_{oil} and R_{water};

   using Eqs. [3.12], [3.16] and [3.17] to calculate attenuation R_{emul}; using Eq.

   [3.23] to calculate total attenuation of the emulsion R.

3) Performing least-square fitting of the experimental data R_{exp} for R until

   norm of the difference $||R_{exp}-R||$ is smaller than tolerance to get fitted

   values of all the parameters in step 1).

If combined with NMR CPMG T_2 distribution measurement, drop size

distribution and surface relaxivity of water in diluted bitumen ρ can be obtained [5].

In this case, fitting parameters are surface relaxivity ρ and phase signal

attenuation fraction κ. R_{emul} is calculated by drop size distribution, which is

obtained from T_2 distribution and surface relaxivity. Total signal attenuation of the

emulsion R is the weighted combination of phase signal attenuation with

attenuation fraction κ.   Detailed procedure is as follows:

1) Getting T_2 distribution of water drops via CPMG measurement; estimating

initial values of surface relaxivity ρ, phase signal attenuation fraction κ and diffusivity of continuous oil phase D_{CP}.

2) Using Eq. [3.6] with surface relaxivity ρ to calculate drop size distribution; Using Eq. [3.9] with D_{CP} and D_{water} to calculate attenuation R_{oil} and R_{water}; using Eqs. [3.12], [3.16] with drop size distribution to calculate attenuation R_{emul}; using Eq. [3.23] to calculate total attenuation of the emulsion R.

3) Performing least-square fitting of the experimental data R_{exp} for R until norm of the difference $\|R_{exp}\text{-}R\|$ is smaller than tolerance to get fitted values of all the parameters in step 1).

3.4. T_1 weighted one-dimensional (1-D) MRI profile measurement

3.4.1. Introduction

In T_1 weighted one-dimensional (1-D) MRI profile measurement, the sequence consists of an rf 90° pulse, followed by an rf 180° pulse at time τ. A spin-echo is collected at time t_E. The rf 180° pulse is between two magnetic field gradient pulses with strength g, as shown in Figure 3.6 [2]. The magnetic gradient is along the vertical direction z. The first magnetic gradient pulse is referred as *coding gradient*, which makes different spins along z direction have different *Larmor frequencies* and precede out of phase. The second magnetic gradient pulse is referred as *reading gradient*, which makes spins coherent and forms the

echo at time t_E. The measurement is repeated after time spacing t_R.
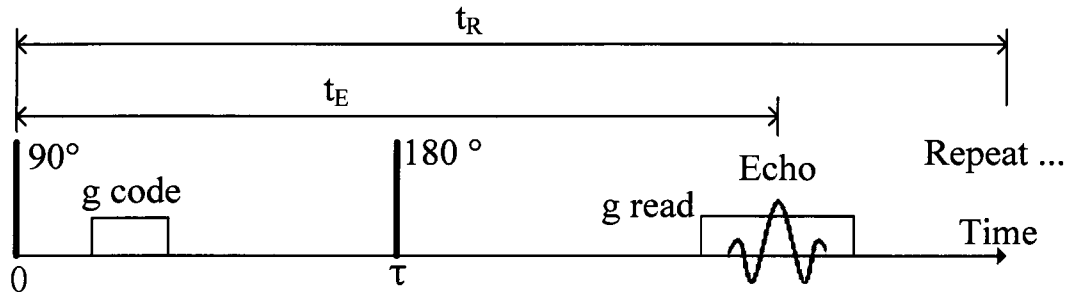
Figure 3.6 Sequence of MRI 1-D profile measurement

Magnetic gradient pulse is applied during echo signal collection. The total signal at the time of the echo is [2]:

$$S_z(t) = \int_{-\infty}^{+\infty} \rho(z) \cdot \exp[-i\gamma G_z(t - t_E)] \cdot dz \qquad [3.31]$$

A Fourier transform of $S_z(t)$ yields the spin density $\rho(z)$.

Signal amplitude at position z is proportional to spin density $\rho(z)$ and can be expressed as the function of T_1, T_2, t_R and t_E [2]:

$$A = A_0(1 - e^{-t_R/T_1})e^{-t_E/T_2} \qquad [3.32]$$

3.4.2. T_1 weighted 1-D MRI profile measurement

When the oil/water concentration is varying as a function of z, the contrast in the spin density is not large enough to give useful information of oil/ water distribution. This is the case for water-in-diluted bitumen emulsions in which large drops may accumulate at the bottom while small drops may stay at the top. To

Chapter 3

generate a contrast based on the relaxation time difference between oil and water, one solution is to perform a T_1 weighted spin density profile by stacking a certain number of scans repeated after a time t_R. Then, the amplitude at a given position z is given by:

$$A_T(z) = A_\infty [1 - \sum \varphi_i \exp(-t_w / T_{1,i})] \tag{3.33}$$

Here φ_i is the volume fraction for component i. $t_w = t_R - t_E \approx t_R$ is the waiting time. For water-in-oil emulsions, Eq. [3.19] can be written as:

$$A_T(z) = A_\infty [1 - \phi_{oil} \exp(\frac{-t_w}{T_{1,oil}}) - \phi_{water} \exp(\frac{-t_w}{T_{1,water}}) - \phi_{emul} \exp(\frac{-t_w}{T_{1,emul}})] \tag{3.34}$$

Here subscripts *oil*, *water* and *emul* correspond to continuous oil, bulk water and water droplets, respectively.

Figure 3.7 shows scheme of 1-D profile measurement for layered mixture of water and diluted bitumen. The left photograph shows layered mixture of water and diluted bitumen. The right part of the figure shows 1-D profile result of layered mixture. The *x* axis is signal amplitude of the sample, and the *y* axis position is the position measured from the middle of the sample. Signal amplitudes in oil layer and water layer have obvious difference. It is easy to find oil/ water interface from the step change of signal amplitude.
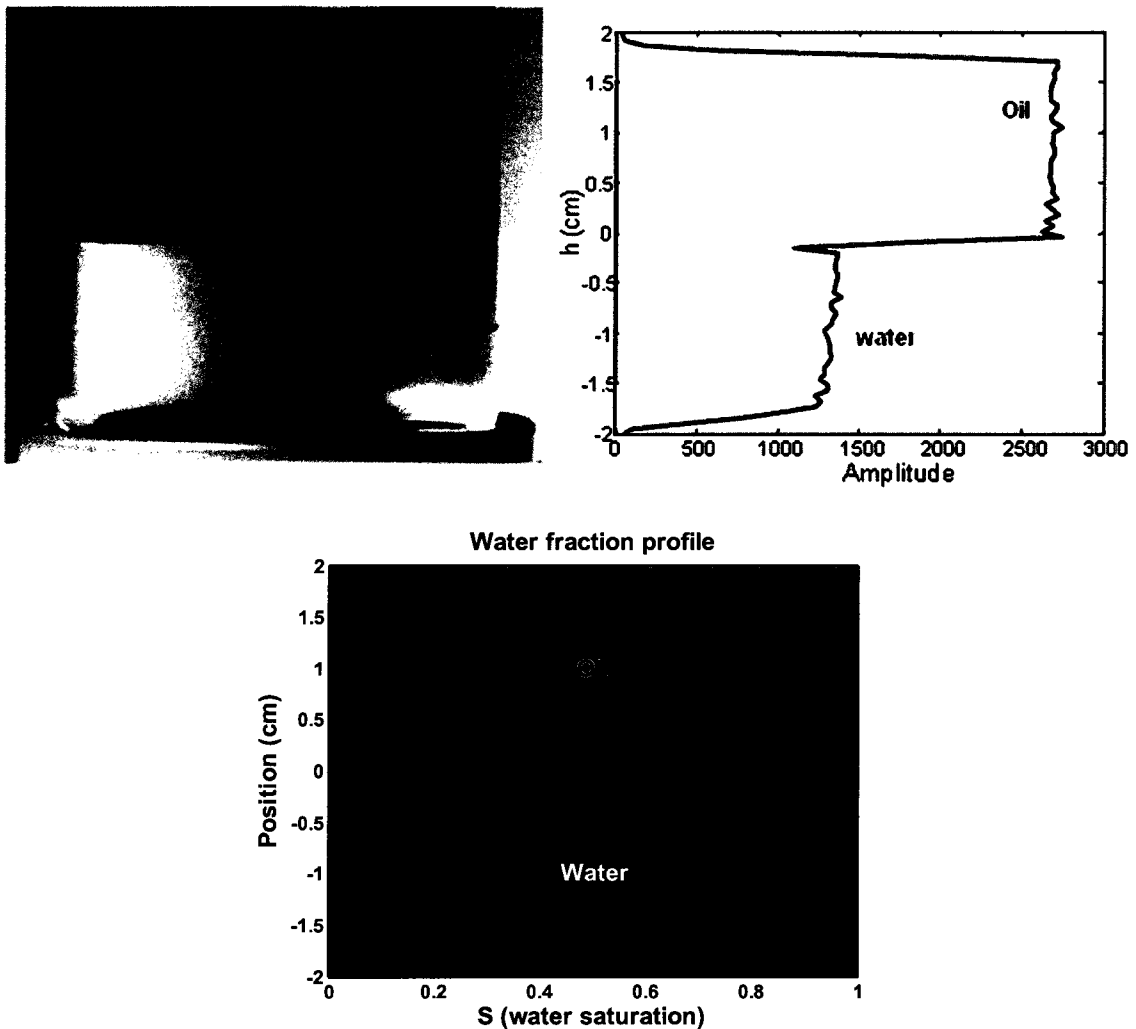
Figure 3.7 Scheme of 1-D profile measurement for layered mixture of water and diluted bitumen

The bottom part of the figure shows water/ oil fraction profiles of the sample. The red line shows water saturation/ fraction profile of layered mixture. On the top water fraction is zero, which reveals bulk oil layer (green part). Water fraction at the bottom is one, corresponding to bulk water layer (blue part).

Chapter 3

3.5. Materials and Methods

3.5.1. Materials

Samples of bitumen froth were received from Syncrude. Bitumen froth was diluted with naphtha. Dilution ratio (naphtha/ bitumen weight ratio, refer to as N/B ratio) is 2.4. The diluted bitumen contains about 1.0 $w.\%$ solids and less than 2.0 $w.\%$ water, which can be measured by centrifugation. Most of the clay solids in the sample are kaolinite and illite. Solids-free diluted bitumen was prepared by centrifuge with centrifugation acceleration 3500 g for 30 minutes. The aqueous phase used here is 1.0 $w.\%$ NaCl brine. All salts were from Fisher Scientific.

The bulk fluid properties are listed in Table 3.1. Viscosities were measured with a Brookfield DV-III + rheometer. A spindle (#18, viscosity range = 1.3 - 30,000 mPa·s) is immersed in a cylindrical cell containing approximately 7 ml of sample, and it is further set to rotate at a given angular velocity. T_2 and diffusivity were measured using MARAN II Spectrometer (2.2 MHz, Oxford Instruments).

When comparing the bulk properties of the diluted fluids, it is clear to see the difference between diluted bitumen with solids and solids-free diluted bitumen. The viscosity of diluted bitumen with solids is larger than that of diluted bitumen without solids, while the relaxation time and diffusivity are smaller. This is an indication of the effect of clay solids on the diluted bitumen.

Chapter 3

Table 3.1 Bulk fluid properties at 30°C

Bulk fluids	Density (g/ml)	Viscosity (cP)	T_{2peak} (s)	Diffusivity $(10^{-9} m^2/s)$
Brine	1.001	1.20	2.6	2.6
Diluted bitumen	0.815	2.12	0.413	1.0
Solids free diluted bitumen	0.814	2.05	0.556	1.3

Here the demulsifiers are polyoxyethylene (EO)/ polyoxypropylene (PO) alkylphenolformaldehyde resins (referred to as PR_X) provided by Nalco Chemical CO., with molecular weights around 3,500 Da and varying amounts of EO/PO groups in their structure (Table 3.2) [5] at constant EO/ PO ratio (3:1), which are used as coalescers for the emulsion. The solvent for the demulsifier is xylene. The demulsifier solution contains 10 $w.$% PR_X.

Table 3.2 EO/PO content of phenolic resins PR_X

Phenolic resin	PR_1	PR_2	PR_3	PR_4	PR_5	PR_6
EO/PO in molecule (wt. %)	25	33	41	46	54	66

3.5.2. Emulsion Preparation

Prior to emulsion preparation, different additives were added to aqueous phase. In the emulsion preparation, 60 ml emulsion (oil/water ratio 1.0, v/v) sample was prepared by mixing 30 ml 1.0 $w.$% NaCl brine and 30 ml diluted

bitumen (dilution ratio 2.4) in a flat-bottom glass tube (outer diameter 48 mm,

inner diameter 44 mm and length 230 mm) with a six-blade turbine [1] (Figure 3.8)

at ambient temperature. Stirring speed of the turbine is 3600 rpm and the mixing

time is 10 min.
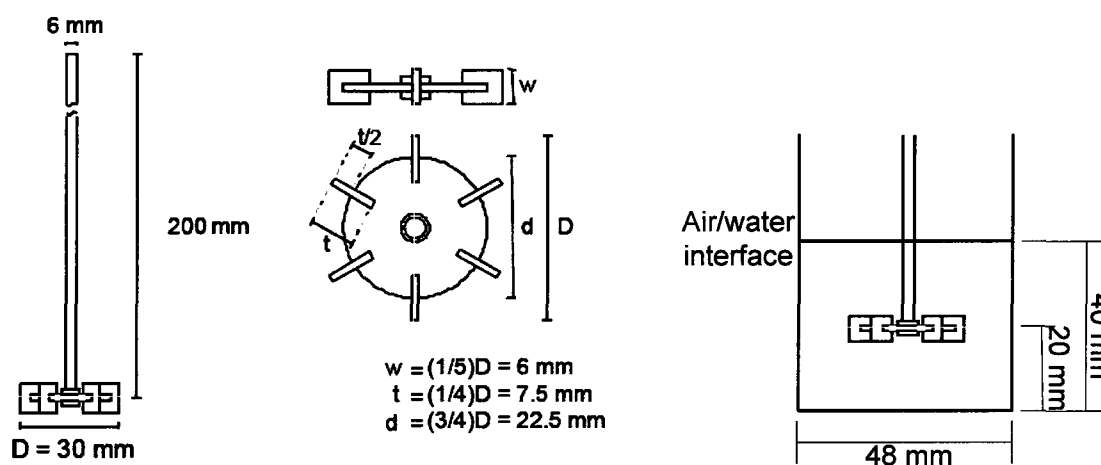
Figure 3.8 Sketch of the mixer and emulsion preparation

Different emulsion samples (samples 1 to 4) were prepared as comparison to

study the effects of demulsifier, clay solids and wettability agent, as described in

Table 3.3. Here 200 ppm optimal demulsifier PR$_5$ was used.

Table 3.3 Different emulsion samples for the measurement

Case	Emulsion with solids	Emulsion without solids
Without demulsifier	Sample1	Sample 3
With demulsifier	Sample 2	Sample 4

Study of the difference between samples 1 and 2, samples 3 and 4 can show

the effects of demulsifier; while difference between samples 1 and 3, samples 2 and 4 show the effects of clay solids.

3.5.3. Bottle test and demulsifier selection

Bottle tests were applied to find the optimal demulsifier for the emulsion sample. In the experiment, a batch of 25 ml fresh emulsions were added to the bottles (outer diameter 25 mm), then 200 ppm demulsifier (50 μl 10 % PR_x xylene solution for the 25 ml emulsion sample) was added to each emulsion sample. Afterwards, all the samples were shaken by hand for 1 minute and put into the oven at 30 °C.

3.5.4. NMR measurement of emulsion

Detailed procedure and parameters for NMR measurement of emulsion can be found in appendix A.

3.6. Results and Discussions

3.6.1. Demulsifier selection from bottle test

Figure 3.9 shows 24 hours emulsion samples (dilution ratio 2.4) with solids adding different demulsifiers PR_x at 30 °C. The first sample does not contain any demulsifiers as control. The other six samples contain 200 ppm demulsifiers PR_1 - PR_6, respectively. Samples with different demulsifiers have significantly different

separation results. Compared with other samples, emulsion sample adding PR_5

can get more separated oil and water and has the best separation. PR_5 is selected

as the optimal demulsifier.

Control PR_1 PR_2 PR_3 PR_4 PR_5 PR_6
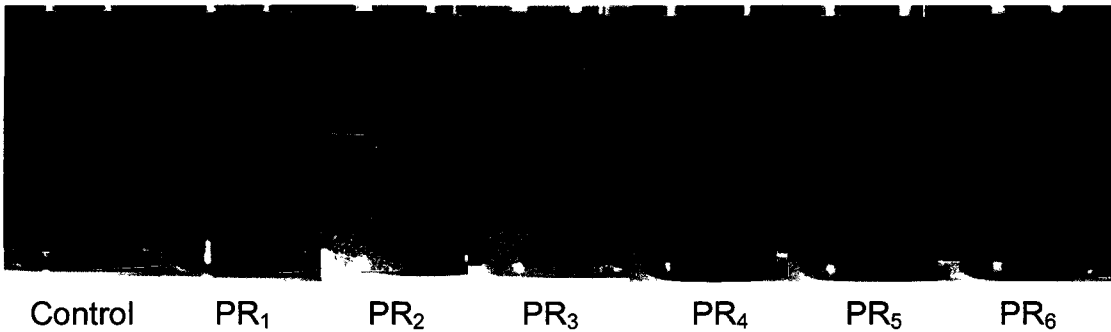
Figure 3.9 24 h emulsions with 200 ppm demulsifiers at 30 °C, N/B ratio 2.4

3.6.2. Emulsion characterized by CPMG T_2 distribution measurement

Figure 3.10 shows T_2 distribution of layered water/ diluted bitumen (sample 3,

dilution ratio 2.4, solids-free) mixture and water in diluted bitumen emulsion. The

red curve is T_2 distribution of layered water/ diluted bitumen mixture, the blue one

is that of water in diluted bitumen emulsion. For both curves, oil and water have

different T_2 distribution peaks, which are distinguishable. T_2 values of oil peak in

emulsion are smaller than those of bulk oil. This indicates surface relaxation

effects on the continuous oil phase. T_2 values of water drops in emulsion are

smaller than those of bulk water. The difference between the two peaks can be

used to calculate drop size distribution according to Eq. 3.6, if surface relaxivity ρ

is known. Combined with NMR restricted diffusion measurement, drop size

Chapter 3

distribution and surface relaxivity of water in diluted bitumen ρ can be obtained, as discussed in section 3.3.2.
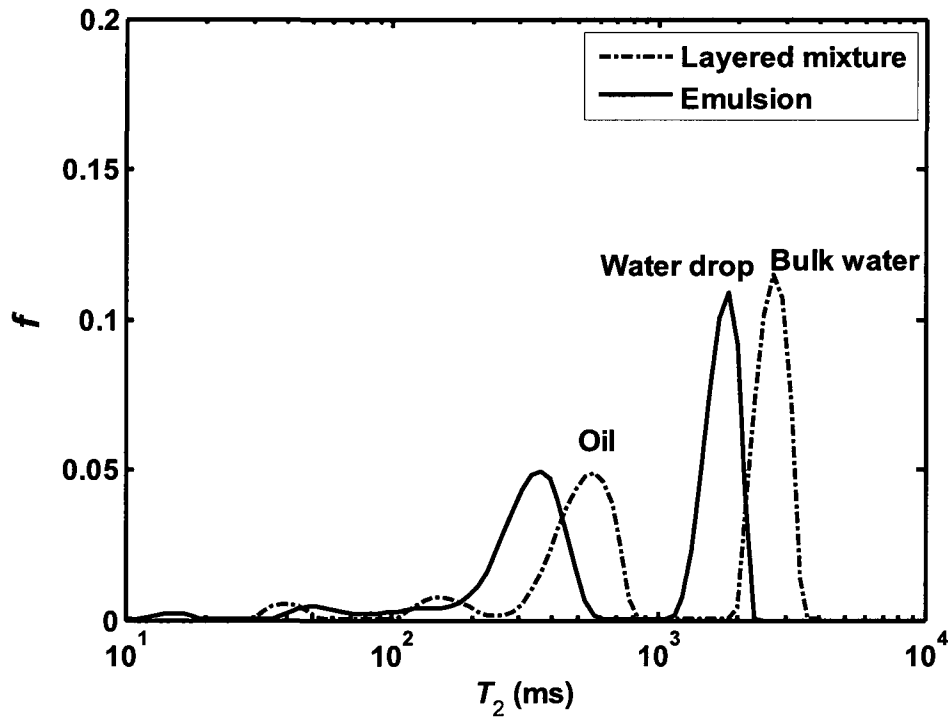
Figure 3.10 T_2 distribution of layered water/ oil mixture and water in oil emulsion

Figure 3.11 shows data fitting result of restricted diffusion measurement and drop size distribution of emulsion from T_2 distribution measurement. Surface relaxivity of water in diluted bitumen ρ is 0.6 μm/s based on the data fitting. This value can be applied for emulsions with same oil/ water system. With surface relaxivity known, drop size distribution can be calculated only from T_2 distribution of water drops. This is very convenient for the study of emulsion evolution since CPMG measurement only takes a few minutes to get the raw data.
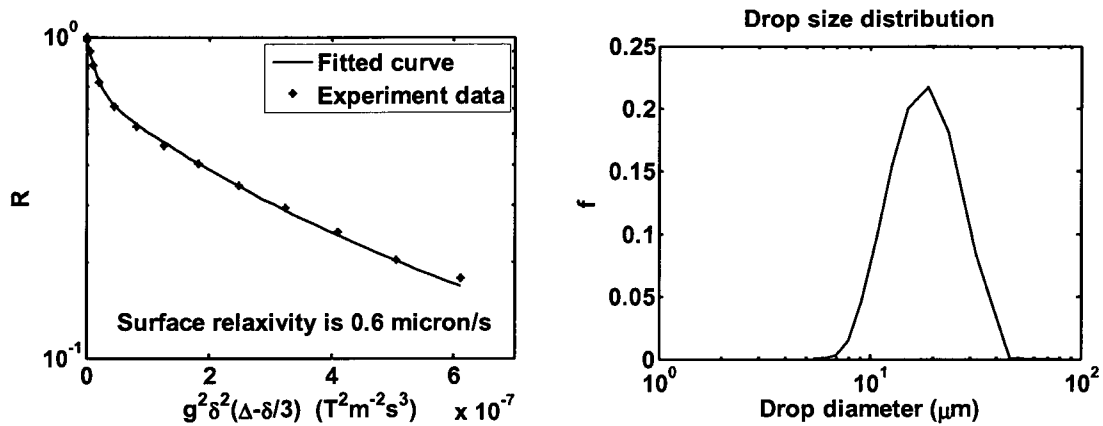
Figure 3.11 Restricted diffusion result and drop size distribution of emulsion

Figure 3.12 shows T_2 distribution of water in diluted bitumen (dilution ratio 2.4, solids-free) emulsion with 200 ppm demulsifier PR_5 and corresponding drop size distribution as the function of time.
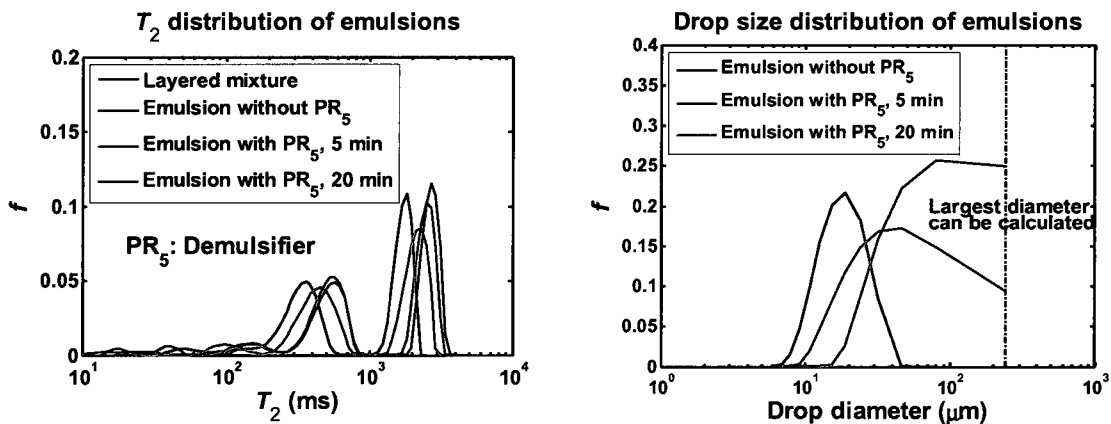
Figure 3.12 T_2 and drop size distribution of water in diluted bitumen emulsion adding 200 ppm demulsifier PR_5 as the function of time

After adding demulsifier PR_5, T_2 values of oil peak or emulsified water peak become larger and closer to those of bulk oil or water. After 20 minutes, T_2 distribution of water drops is very close to that of bulk water. Drop size of emulsion

Chapter 3

becomes larger as time increases and exceeds the largest drop size limit that can

be measured by CPMG method. This reveals that time evolution of emulsion

adding demulsifier can be characterized via CMPG T_2 distribution measurement.
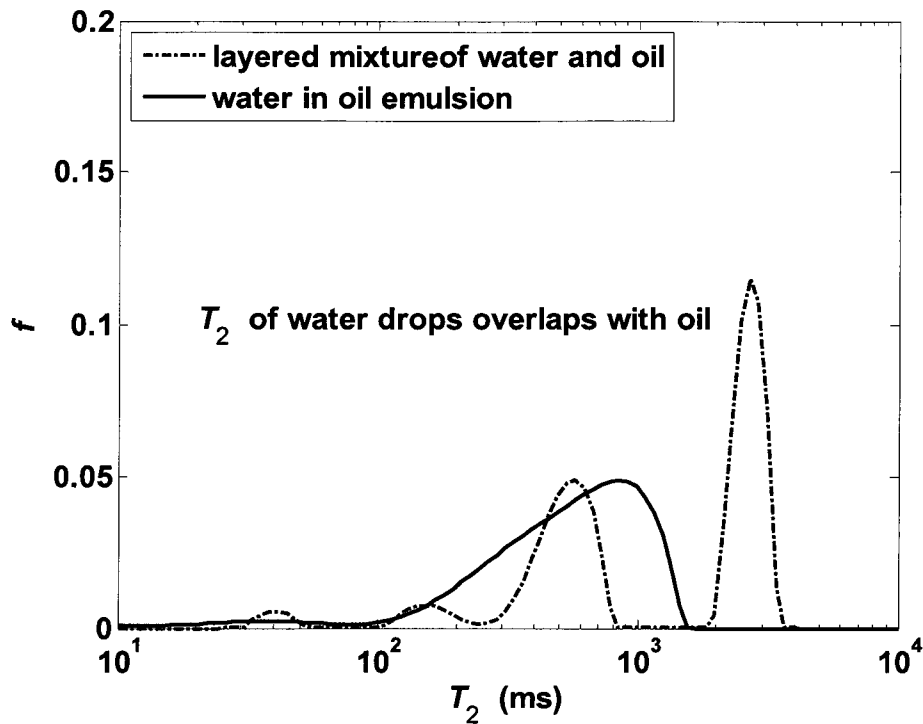
Figure 3.13 T_2 distribution of layered water/ oil mixture and water in oil emulsion

Figure 3.13 shows T_2 distribution of layered water/ diluted bitumen (dilution

ratio 2.4, solids-free) mixture and water in diluted bitumen (sample 1, dilution ratio

2.4, with clay solids) emulsion. In this case, T_2 distribution of water in diluted

bitumen emulsion has only one peak. T_2 distribution of water drops overlaps with

that of oil. T_2 distribution of water drops is not distinguishable and cannot be used

to calculate drop size distribution. To solve this problem, NMR PGSE restricted

diffusion measurement is required to get drop size distribution.

T_2 distribution evolutions of emulsion samples 1 - 4 (in Table 3.2) from CPMG measurement are shown in Figure 3.14. In the figures, T_2 distribution of layered mixture and picture of 12 h emulsion are also shown for reference.

Sample 1   Sample 2
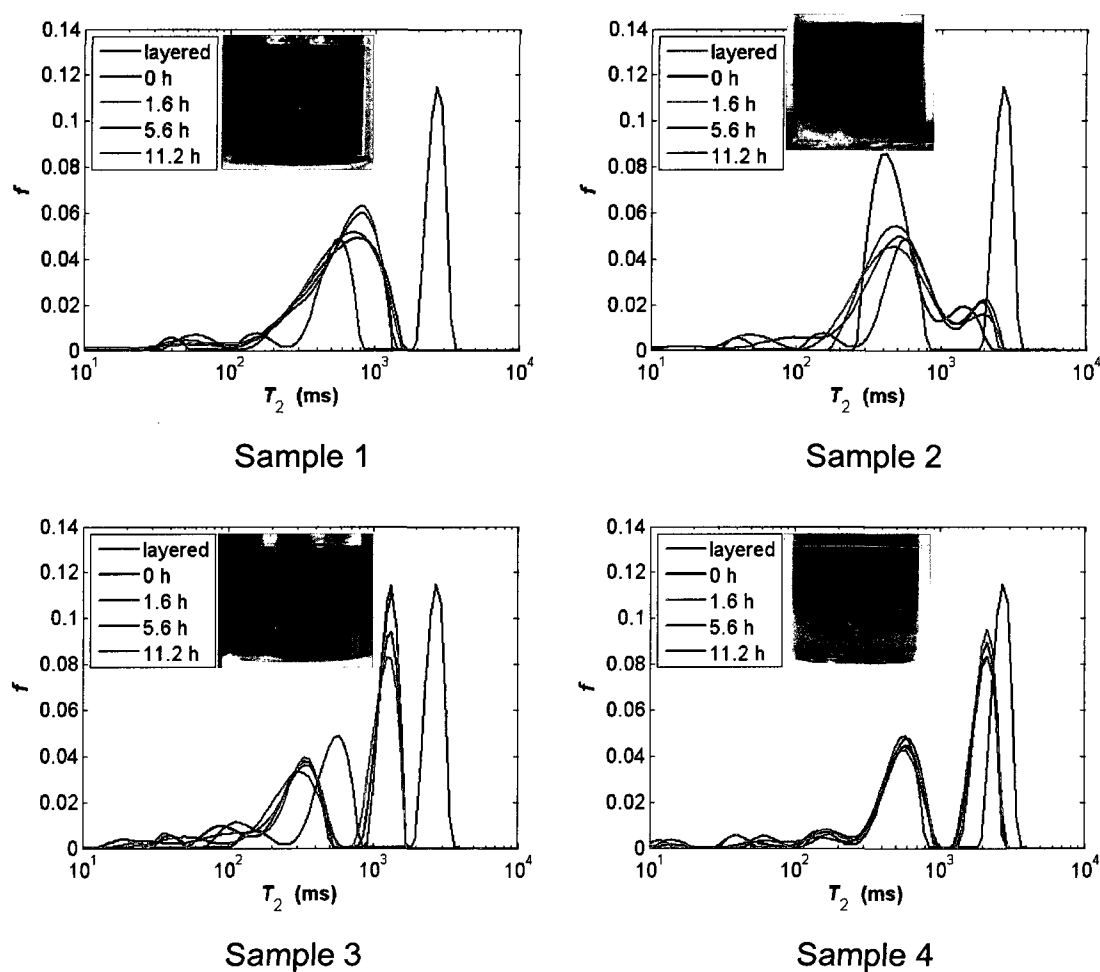
Sample 3   Sample 4

Figure 3.14 T_2 distribution of emulsion samples 1-4

In sample 2 and sample 4, 200 ppm demulsifier PR_5 (120 µl 10 % PR_5 in xylene solution for the 60 ml emulsion sample) was added to each emulsion

sample immediately after emulsion preparation. Afterwards, all the samples were shaken by hand during 1 minute.

In sample 1, unlike the layered mixture, T_2 distribution of emulsion has only one peak. Hence water content and drop size distribution of the emulsion cannot be obtained from CMPG measurement.

In sample 2, T_2 distribution of emulsion contains a larger peak for the W/O emulsion and a smaller peak for the separated bulk water. This is consistent with the observation in the experiment that free water forms at the bottom of the sample due to the emulsion coalescence.

In sample 3 and sample 4, T_2 distributions of emulsion contain two separate peaks. These are different from the two samples with solids. This difference may be due to the effect of the solids.

In sample 3, T_2 values of oil peak and water peak are smaller than those of bulk fluids. This implies the effect of surface relaxivity on the T_2 distribution.

In sample 4, T_2 distribution of oil peak is very close to that of bulk oil, which suggests the compete separation of the oil and water. This is consistent with the experiment at observation. T_2 distribution of water peak is smaller than that of bulk water. In sample 4, the water layer is yellowish, which suggests that the water is doped. Thereby the T_2 distribution of water peak is smaller.

Chapter 3

3.6.3. Drop size distribution from PGSE restricted diffusion measurement

Figure 3.15 shows NMR signal attenuation of water in diluted bitumen (sample 1, dilution ratio 2.4, with clay solids) emulsion and drop size distribution from data fitting.
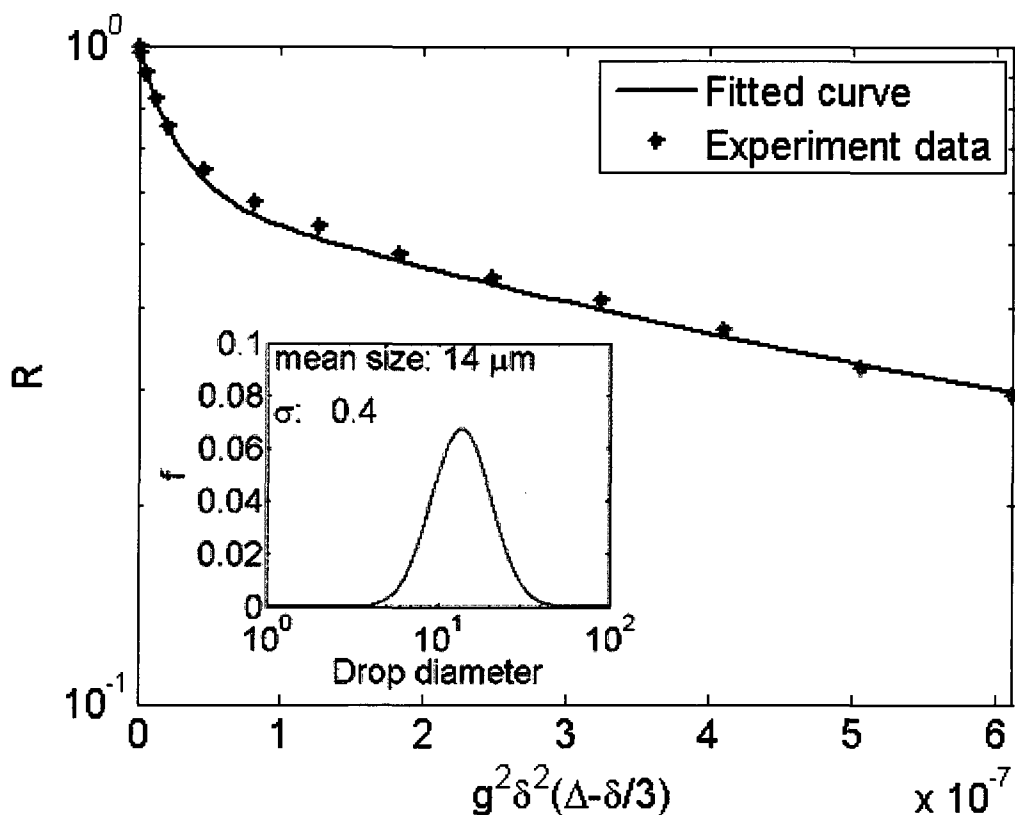
Figure 3.15 Fitting results of diffusion measurement for the emulsions (sample 1)

Here the diffusion time Δ is 500 ms, gradient pulse duration δ is 3 ms, range of magnetic gradient g is 0 - 40 G/cm. The sensitive range of drop size can be measured by the diffusion measurement is 6 - 72 μm. The determination of the drop size distribution consists of performing a least-square fit of the experimental

Chapter 3

data for R_{emul} as described in section 3.3.2, using d_{gV}, σ, D_{CP} and κ as fitting parameters. Based on data fitting, mean diameter d_{gV} and geometric standard deviation σ are 14 µm and 0.4. Signal attenuation fraction κ_{oil}, κ_{emul} and κ_{water} are 0.36, 0.02 and 0.62, respectively. Diffusivity of continuous oil phase D_{CP} is 5.7×10^{-10} m^2/s.

The time-dependent drop size distributions of different emulsion samples obtained from diffusion results are shown in Table 3.4.

In sample 4, after 3.2 hours, NMR signal attenuation is smaller than 0.01, which implies complete separation of the oil and the water. Thus a drop-size distribution of the emulsion cannot be obtained. Hence only first three results are listed.

For samples 1 and 3, the mean drop diameter, standard deviation σ, κ_{oil} and κ_{emul} do not change much with time, which suggests that the emulsions are stable; the κ_{water} values are very low, which shows that coalescence is very slow in the absence of demulsifier. In contrast, for samples 2 and 4, κ_{water} increases over time, which demonstrates that demulsifier PR$_5$ accelerates emulsion coalescence. The parameter κ_{emul} of sample 4 is much smaller than that in of sample 2, which indicates a lower emulsion content. Sample 2 has much more solids than sample 4; thus, the effect of solids is to make the emulsion more stable.

Chapter 3

Table 3.4 Time-dependent emulsion drop size distribution characterized by NMR restricted diffusion measurement of samples 1-4

Sample	Age (h)	Mean diameter (μm)	σ	K_{oil}	K_{water}	K_{emul}
1	0.8	15	0.40	0.37	0.02	0.61
	1.6	14	0.39	0.36	0.02	0.62
	3.2	12	0.41	0.39	0.04	0.57
	5.6	12	0.41	0.39	0.04	0.57
	11.2	11	0.42	0.41	0.05	0.54
2	0.8	17	0.50	0.49	0.05	0.51
	1.6	13	0.50	0.50	0.10	0.40
	3.2	14	0.52	0.44	0.13	0.43
	5.6	11	0.70	0.41	0.23	0.33
	11.2	11	0.62	0.40	0.30	0.30
3	0.8	11	0.33	0.31	0	0.69
	1.6	11	0.33	0.31	0	0.69
	3.2	11	0.34	0.32	0	0.68
	5.6	11	0.35	0.33	0	0.67
	11.2	12	0.36	0.32	0	0.68
4	0.8	20	0.70	0.54	0.30	0.16
	1.6	23	0.64	0.20	0.68	0.12
	3.2	27	0.57	0.20	0.70	0.10

3.6.4. Phase fraction profile from 1-D T_1 weighted MRI profile measurement

1-D T_1 weighted MRI profile measurement is based on the T_1 difference of different components. Figure 3.16 shows the profile measurement results of the

four emulsion samples described in Table 3.2. The waiting time t_w is 0.6 s. The imaging pulse field gradient is 0.8 G/cm. In Figure 3.16, x axis A is signal amplitude of the sample, y axis *position* is the position measured from the middle of the sample. It ranges from -2 cm to 2 cm; the total length is about 4 cm, which is equal to the height of the sample.
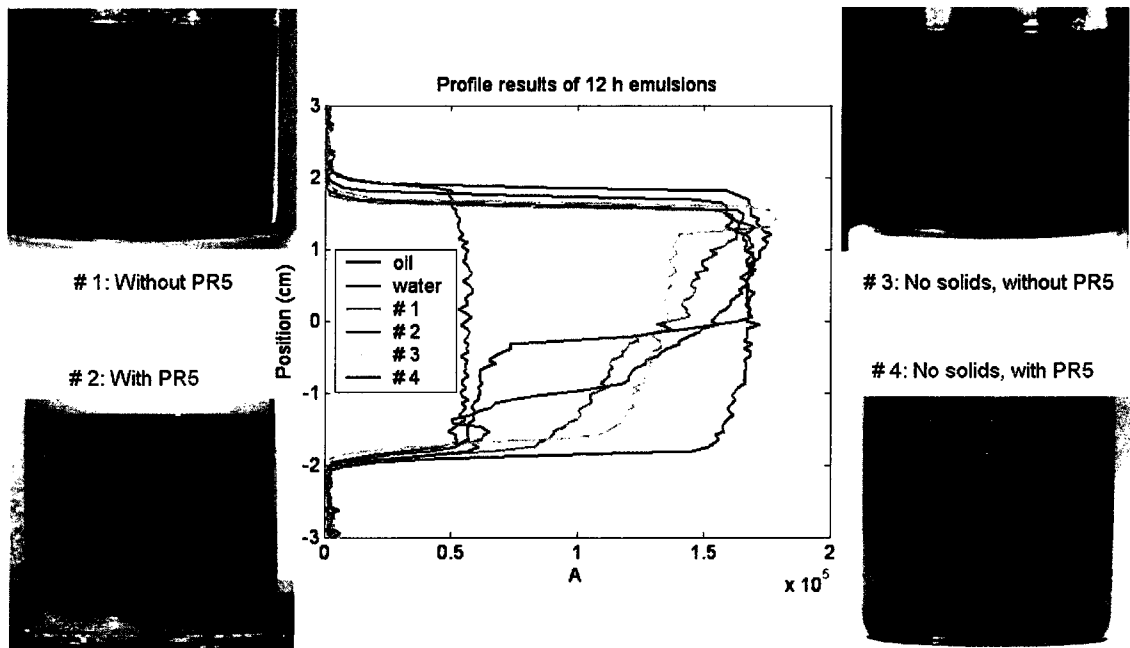
Figure 3.16 NMR 1-D T_1 weighted profile measurement of emulsion samples 1- 4

The T_1 value of water is greater than diluted bitumen, so the attenuation of water is smaller than diluted bitumen based on the Eq. [3.33]. Thereby in the profile results, the signal amplitude of water is smaller than that of oil. Based on the T_1 difference, the signal amplitudes of different phases in the emulsion become distinguishable.

Chapter 3

A comparison of samples 1 and 3 with samples 2 and 4 shows that coalescence is much more significant with added PR_5, which shows that PR_5 can accelerate emulsion coalescence. A comparison of samples 2 and 4 shows that the solids in sample 2 prohibit complete separation and form a middle rag layer, which is the focus of further studies.

If profile measurements are performed over time, the evolution of the emulsion such as the sedimentation and coalescence can be obtained from the results. From these profile results, water fraction profile can be obtained from the profile results if some simple assumptions are valid:

1) T_1 for oil, water droplet and bulk water can be considered as distinct single values. Thus Eq. [3.34] can be used for water fraction calculation.

2) The changes of T_1 during the time can be ignored. Thus the experiment data of fresh homogeneous emulsion can be used to calibrate for other emulsions.

3) In the samples without PR_5, emulsion coalescence is insignificant. These samples contain only water-in-oil emulsion. In the samples with PR_5, emulsified water coexists with either clean oil or free water, but not both. On the top is clean oil and emulsified water, at the bottom is W/O/W emulsion (microscopy observation is shown in section 2.6) and free water.

Calibration
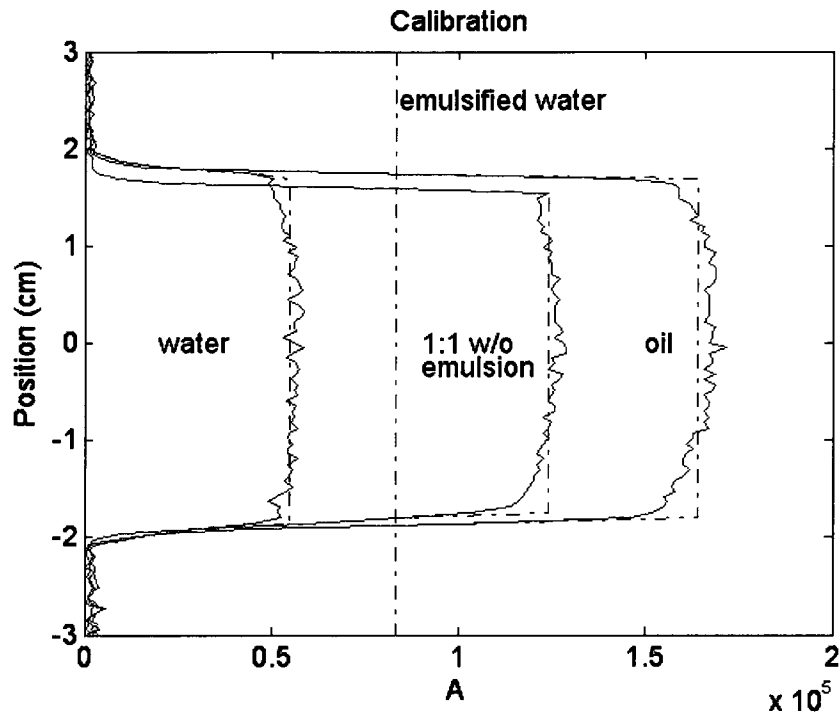
Figure 3.17 Calibration for calculation of water fraction (sample 1)

The calculation process is shown in Figure 3.17. First water amplitude A_{water}, $T_{1,water}$ 2.6 s, waiting time t_w 0.6 s, and Eq. [3.35] are used to calculate A_∞.

$$A_{water} = A_\infty \left[1 - \exp(-t_W / T_{1,water}) \right] \quad \Rightarrow \quad \text{Calculate } A_\infty \qquad [3.35]$$

The oil amplitude A_{oil} and Eq. [3.36] are used to calculate $T_{1,oil}$ for oil.

$$A_{oil} = A_\infty \left[1 - \exp(-t_W / T_{1,oil}) \right] \quad \Rightarrow \quad \text{Calculate } T_{1,oil} \qquad [3.36]$$

Fresh homogeneous emulsion amplitude, A_{emul} and Eq. [3.37] are used to calculate $T_{1,emul}$ for emulsified water.

$$A_{emul} = A_{\infty} \left[1 - \Phi_{emul} \exp(\frac{-t_W}{T_{1,emul}}) - (1 - \Phi_{emul}) \exp(\frac{-t_W}{T_{1,oil}}) \right] \Rightarrow \text{Calculate } T_{1,emul} \quad [3.37]$$

In Figure 3.17, the red dash-dotted line is the calculated amplitude value of emulsified water from calibration. This the lower bound of the amplitude for the system. Similarly, the pure oil amplitude is the upper bound of the amplitude for the system. Values below or above these bounds can be considered as fully saturated water or clean oil, respectively.

The parameters A_∞, $T_{1,water}$, $T_{1,oil}$, and $T_{1,emul}$ are known from calibration. T_1 values, emulsion data for A_{emul}, and Eq. [3.34] can be used to calculate the water fraction. Eq. [3.34] can be simplified as follows:

$$A_{emul}(z) = A_{\infty}[1 - \varphi_{oil}(z) \exp(\frac{-t_w}{T_{1,oil}}) - \varphi_{emul}(z) \exp(\frac{-t_w}{T_{1,emul}})]$$
$$\varphi_{oil}(z) + \varphi_{emul}(z) = 1 \quad\quad [3.38]$$

$$A_{emul}(z) = A_{\infty}[1 - \varphi_{water}(z) \exp(\frac{-t_w}{T_{1,water}}) - \varphi_{emul}(z) \exp(\frac{-t_w}{T_{1,emul}})]$$
$$\varphi_{water}(z) + \varphi_{emul}(z) = 1 \quad\quad [3.39]$$

In Eq. [3.38] and Eq. [3.39], A_{emul}, A_∞, t_w and T_1 values are known. Component fractions φ can be calculated from the equation.

As indicated previously, the samples without PR$_5$ contain only oil and emulsified water drops. Eq. [3.38] can be used to calculate water fraction. In the samples with PR$_5$, emulsified water coexists with clean oil at the top. Eq. [3.38]

can be used to calculate the emulsified water fraction. The bottom is free water and W/O/W emulsion, and Eq. [3.39] can be used to calculate free water fraction.

The profile results and calculated water fraction profiles of samples 1 - 4 are shown in Figures. 3.18 - 3.21. The red dashed lines in the figures represent the boundaries of the sample. The total height is a little less than 4 cm. x axis S is the emulsified or free water saturation of the sample, y axis *position* is the position measured from the middle of the sample. The waiting time t_w is 0.6 s. Total water content 0.50 is used for calibration of fresh emulsion. For other water fraction profile figures at later times, total water content φ obtained by integration over vertical position is listed to demonstrate consistency. For all four samples calculated and actual water contents were nearly equal at all times.

In the calculation of sample 1 (with solids, no PR_5, Figure 3.18), T_1 for bulk water, oil and emulsified water are 2.60 s, 0.63 s and 1.41 s, respectively. The first two of these, being bulk phase properties, are the same for all four samples. At initial time, the emulsion is homogeneous, and the water fraction is around 0.5. As time increases, the dispersed water fraction increases at the bottom and decreases on the top. This result is consistent with the visual observation of emulsion sedimentation.
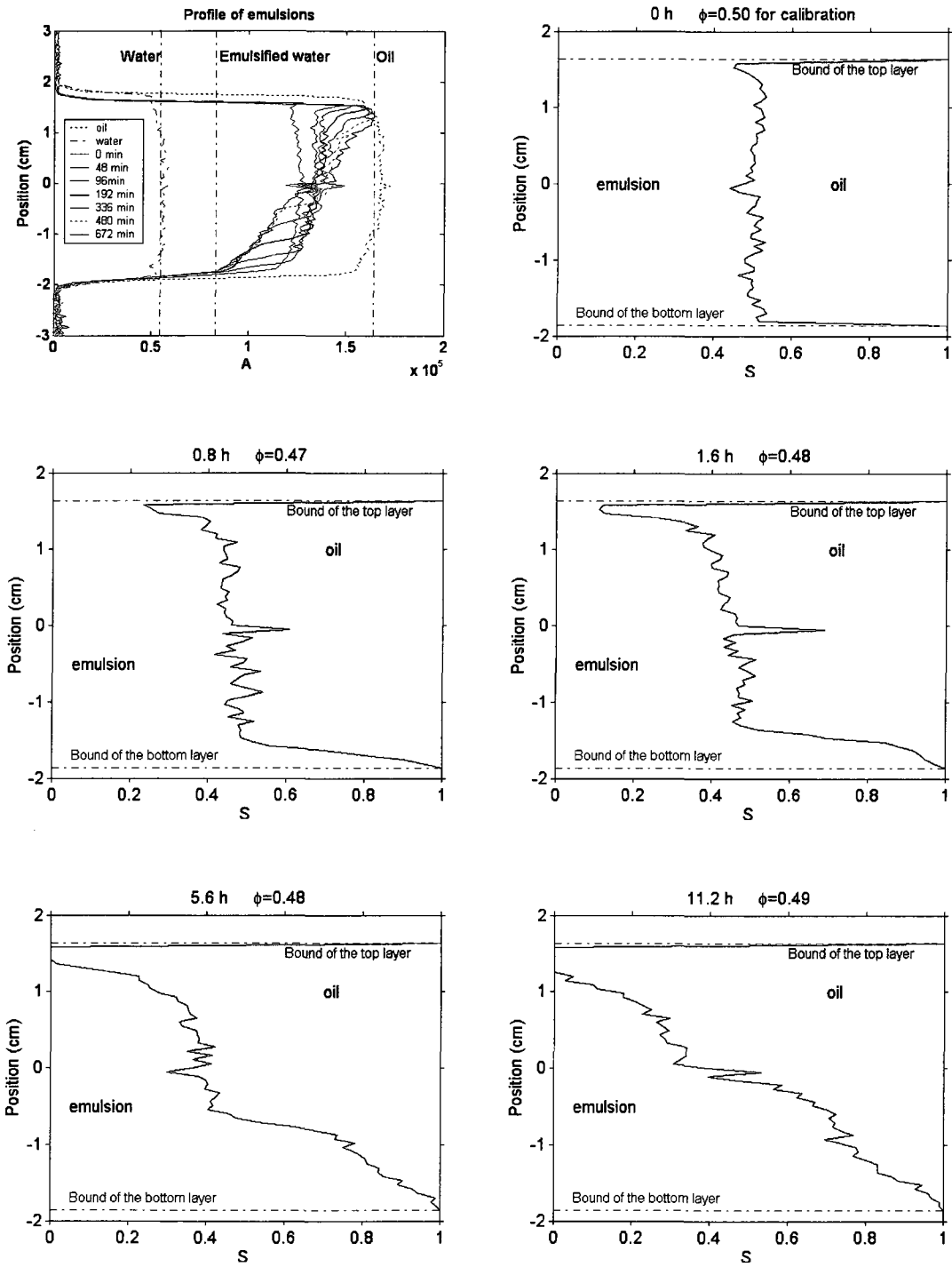
Figure 3.18 Profile results and water fractions of sample 1 (with solids, no PR₅)
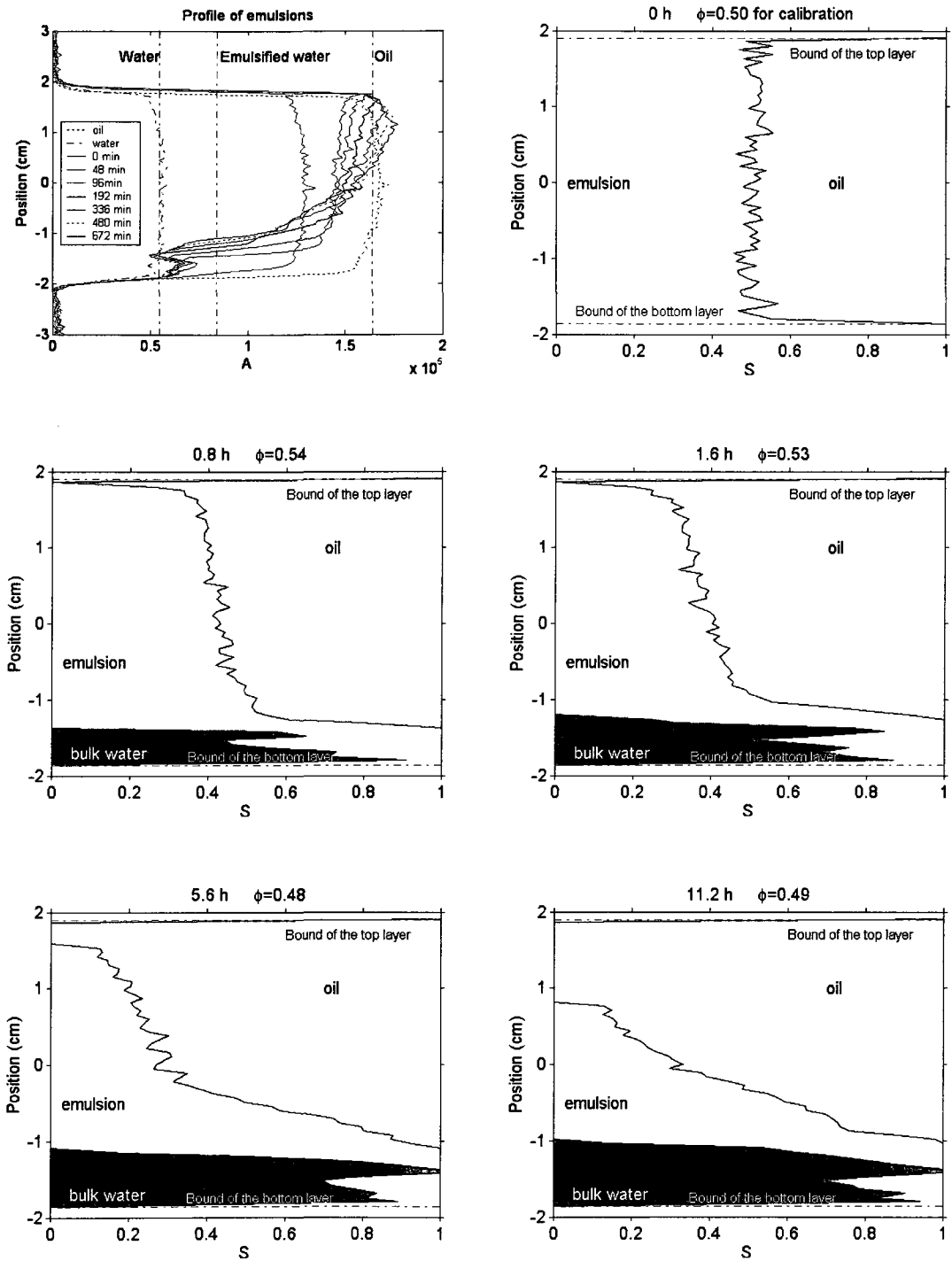
Figure 3.19 Profile results and water fractions of sample 2 (with solids and PR$_5$)
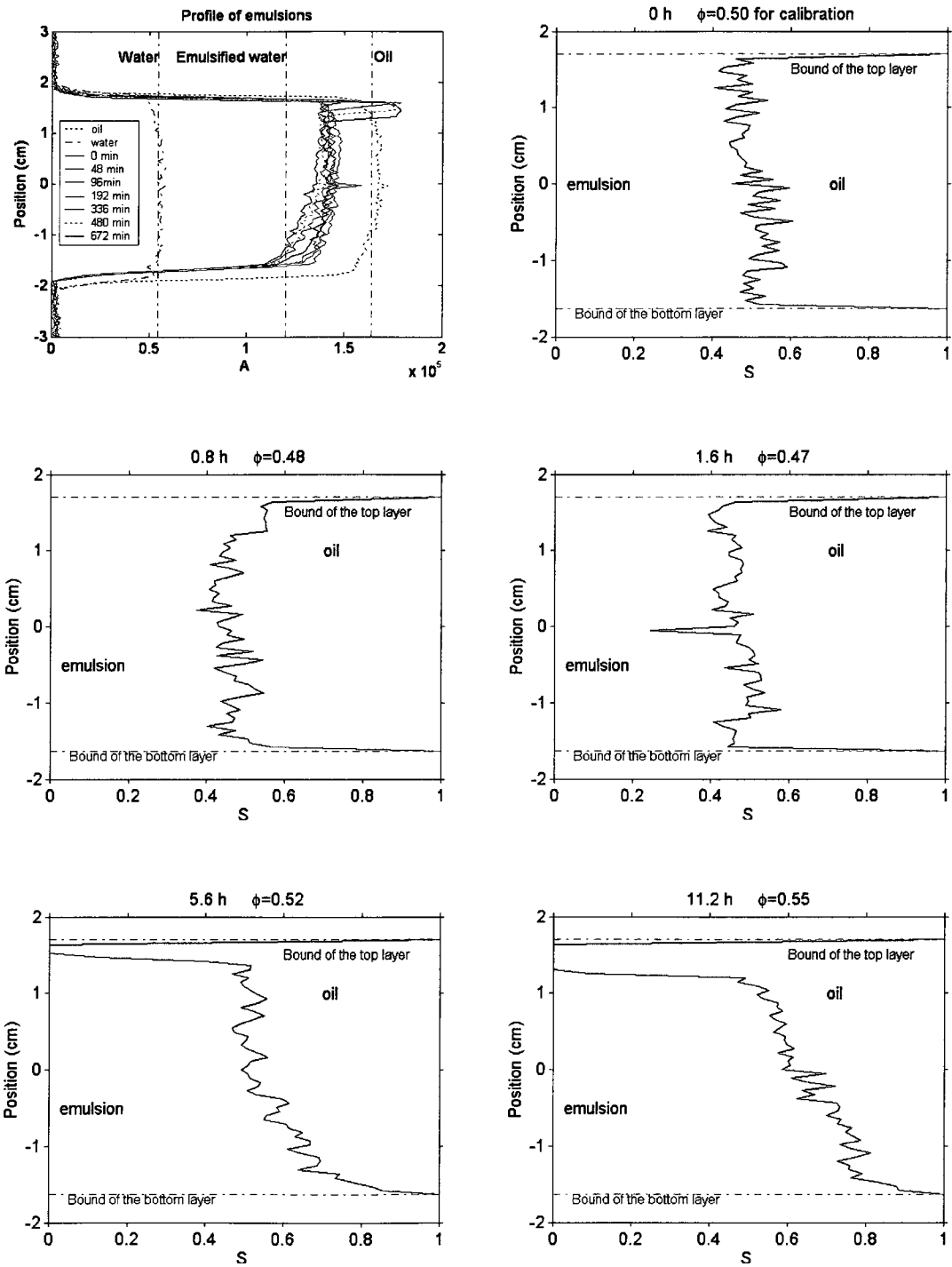
Figure 3.20 Profile results and water fractions of sample 3 (without solids or PR$_5$)
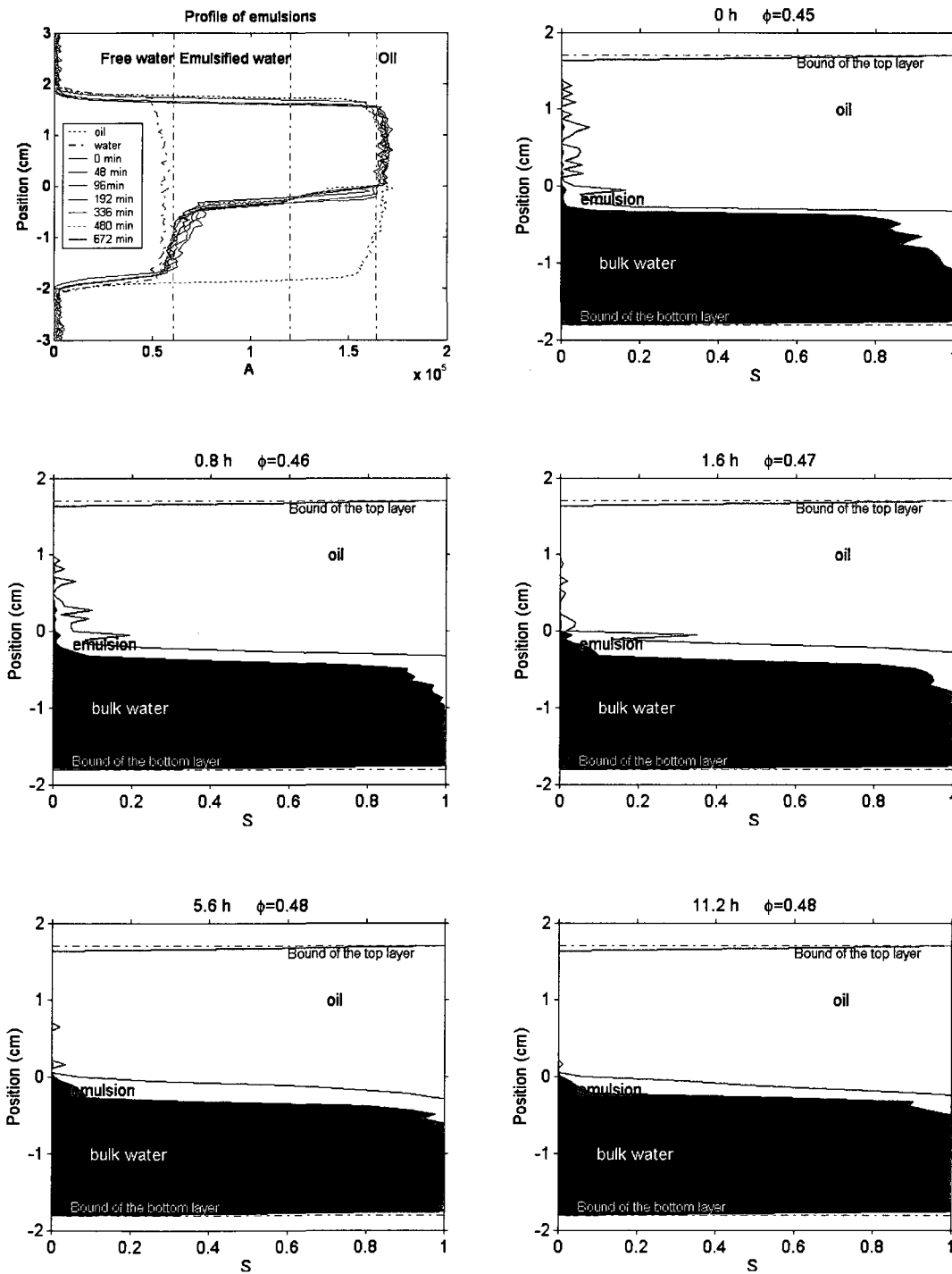
Figure 3.21 Profile results and water fractions of sample 4 (without solids, with PR$_5$)

From water fraction profiles, it is easy to see the sample has three layers. On the top, water fraction is zero, which corresponds to clean oil layer. In the middle, water fraction is around 0.5, which corresponds to a water-in-oil emulsion layer. At the bottom, water fraction is between 0.5 and 1.0, which corresponds to a concentrated water-in-oil emulsion layer. The step changes of the water fraction correspond to the fronts between layers.

In the calculation of sample 2 (with solids and PR_5, Figure 3.19), T_1 for bulk water, oil and emulsified water are 2.60 s, 0.63 s and 1.46 s, respectively. Besides sedimentation, coalescence occurs at the same time. The sample with PR_5 can achieve more complete separation than that without PR_5. Hence, on the top, the signal amplitude is close to that of pure oil, at the bottom the signal amplitude is close to that of bulk water. These results correspond to the results in Figure 3.15, in which on the top is pure oil, in the middle is an emulsion layer, and at the bottom is mostly separated free water. Emulsified water T_1 values of samples 1 and 2 are very similar, which shows consistency of the mixing process with given oil and water phases and indicates that the small amount of demulsifier in sample 2 does not significantly affect emulsified water T_1 values.

In the calculation of sample 3 (no solids, no PR_5, Figure 3.20), T_1 for bulk water, oil and emulsified water are 2.60 s, 0.63 s and 1.11 s, respectively. The

results of sample 3 are similar to those of sample 1. On the top, water fraction is zero, which corresponds to a clean oil layer. In the middle, water fraction is around 0.5, which corresponds to a water-in-oil emulsion layer. At the bottom, water fraction is close to 1.0, which corresponds to concentrated water-in-oil emulsion layer.

In the calculation of sample 4 (no solids, with PR_5, Figure 3.21), T_1 for bulk water, oil, emulsified water and separated free water are 2.60 s, 0.63 s, 1.11 s and 2.32 s, respectively. Here T_1 for emulsified water cannot be obtained from the calibration of sample 4, because at initial time sample 4 is not homogeneous, due to rapid coalescence. Thus here T_1 value for emulsified water is assumed to be that obtained from the calibration of sample 3. T_1 for separated free water (2.10 s) is also shorter than that of pure bulk water and is obtained from a separate NMR measurement.

For sample 4, from water fraction profiles the separation of oil and water is complete. On the top, water fraction is close to zero, which corresponds to clean oil layer. At the bottom, water fraction is 1.0, which corresponds to free water.

3.6.5. Sedimentation rate from 1- D T_1 MRI weighted profile measurement

In the profile results of samples 1 and 3, the step change of signal amplitude is a response to the sedimentation front (boundary between different layers).

Hence the velocity of the front can be obtained from profile measurement. As a result of emulsion sedimentation, clean oil layer resides on the top, emulsion layer is in the middle, and concentrated emulsion layer resides at the bottom.

Figure 3.22 shows the position of sedimentation front between concentrated emulsion layer and emulsion layer of sample 1 (with solids and no PR_5) as a function of time. At time zero, the sedimentation front starts from the bottom of the sample (-2 cm in Figure 3.16), and it moves upward with time. The front velocity (dh/dt) can be calculated by fitting the experimental data.
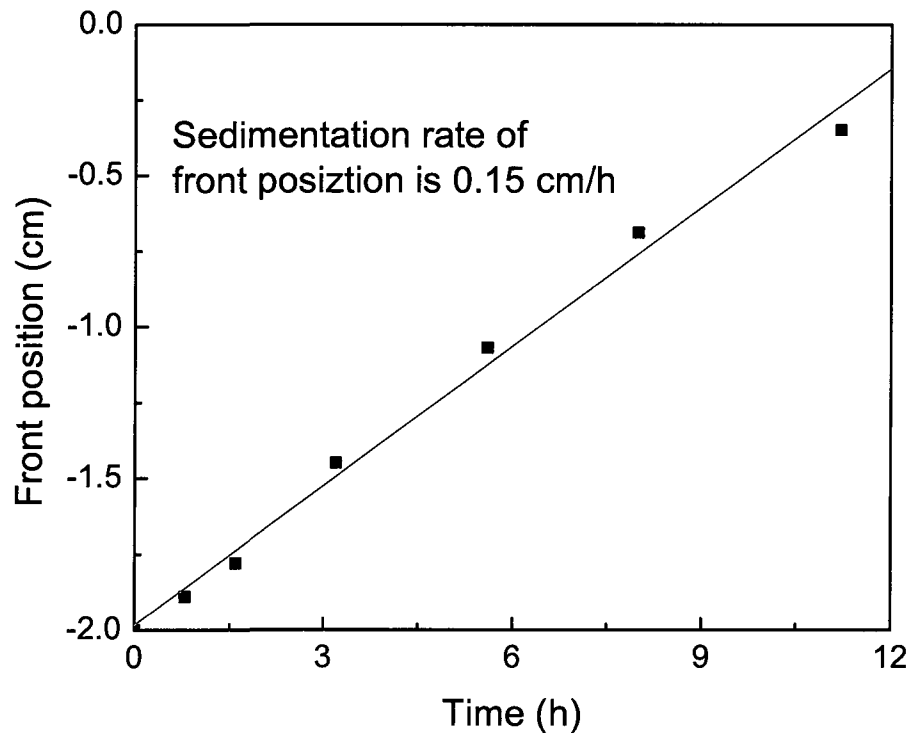
Figure 3.22 Front position sedimentation rate of emulsion sample 1

If we assume that the water fraction in each layer does not change during sedimentation, the sedimentation velocity within the emulsion can be obtained by applying a mass balance across the sedimentation front. If there is negligible sedimentation in the concentrated emulsion with volume fraction φ_{max}, the sedimentation velocity of water droplets in emulsion above the front is given by:

$$v_{lower} = \frac{\varphi_{max} - \varphi_e}{\varphi_e} \frac{dh}{dt} \qquad \text{(lower front)} \qquad [3.40]$$

In sample 3 (no solids, no PR$_5$, Figure 3.16) a sharp front moving upward from the bottom is less evident. However, a front moving downward from the top of sample 3 (though less clearly in sample 1) can be seen with nearly water-free oil above and emulsion below (Figure 3.23). A similar mass balance yields:

$$v_{upper} = \frac{\varphi_{min} - \varphi_e}{\varphi_e} \frac{dh}{dt} = -\frac{dh}{dt} \qquad \text{(upper front)} \qquad [3.41]$$

In these equations h is front position, v_{lower} and v_{upper} are the sedimentation velocity of water droplets in the emulsion, whose volume fraction φ_e is assumed as 0.50. The average water fraction in the concentrated emulsion layer 0.75 can be used as the φ_{max} value, and the average water fraction in the clean oil layer φ_{min} is close to zero.

The predicted sedimentation velocity of the emulsion can be calculated with the following equation, which is an empirical modification of Stokes Law: [19], [20]

Chapter 3

$$v = \frac{\Delta \rho g d^2}{18 \eta_C}(1 - \varphi_e)^n \qquad\qquad [3.42]$$

Here φ_e is again 0.50 and n is 8.6. $\Delta\rho$ 0.186 g/ml is the density difference

between water and oil; g is gravitational acceleration, d is the mean diameter of

water droplets, and η_C is the viscosity of oil phase.
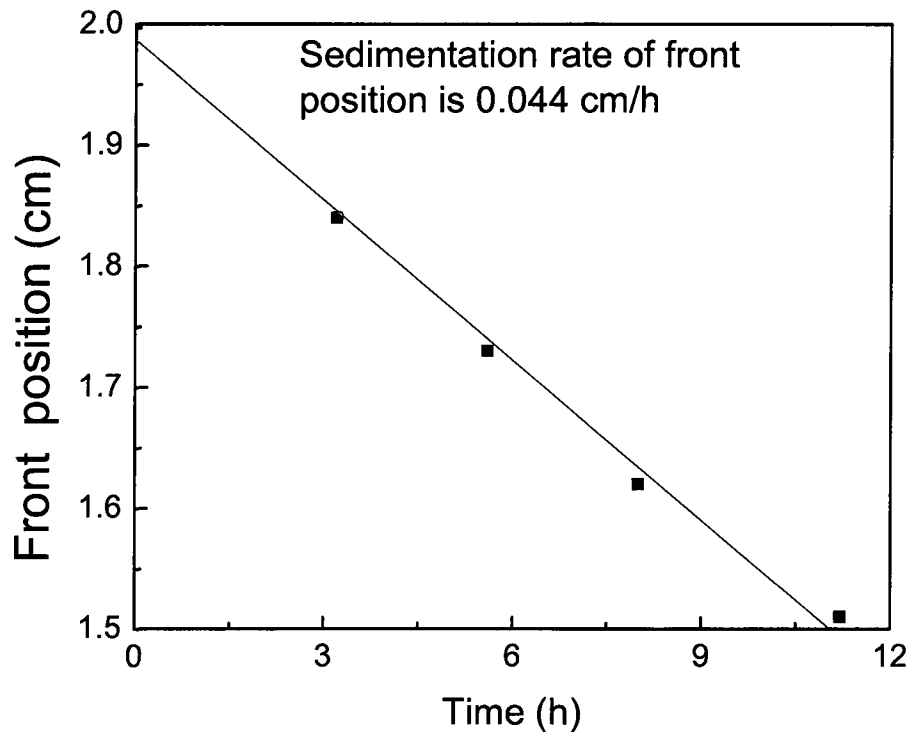
Figure 3.23 Front position sedimentation rate of emulsion sample 3

The experimental sedimentation velocity of water droplets for sample 1 with

Eq. [3.40] is 0.075 cm/h, while the predicted value from Eq. [3.42] is 0.0105 cm/h.

The larger experimental value implies that the water drops sediment with a larger

effective drop size. Thus the emulsion may be flocculated.

The same calculation procedure with Eq. [3.41] can be applied to upper front of sample 3 using the data of Figure 3.23. Here φ_e is 0.50. The experimental sedimentation velocity of water droplets is 0.044 cm/h, whereas the predicted value is 0.0103 cm/h. Their ratio is about 4:1, indicating that there likely some flocculation in this case as well. However, further investigation of flocculation in these emulsions is desirable.

3.7. Reference

[1]   B. Balinov, O. Söderman, Emulsions, the NMR perspective, Encyclopedic handbook of emulsion technology, J. Sjöblom, Editor. Marcel Dekker, Inc., New York, **2001**.

[2]   Z. Liang, P. C. Lauterbur, Principles of magnetic resonance, IEEE Press, **2005**.

[3]   H. Y. Carr, E. M. Purcell, Effects of diffusion on free precession in nuclear magnetic resonance experiments, *Phys. Rev.*, **1954**, 94, 630-638.

[4]   S. Meiboom, D. Gill, Modified spin-echo method for measuring nuclear relaxation times, *Rev. Sci. Instrum.*, **1959**, 29, 688-691.

[5]   A. Pena, G. Hirasaki, Enhanced characterization of oilfield emulsions via NMR diffusion and transverse relaxation experiments, *Adv. Colloid Interface Sci.*, **2003**, 105 103-150.

[6]   C. C. Huang, Estimation of rock properties by NMR relaxation methods, MS Thesis, Rice University, Houston, **1997**.

[7]   A. N. Tikhonov and V. Y. Arsenin, Solution of ill-posed problems, Winston & Sons, Washignton D.C., **1977**.

[8]   K. J. Dunn, G. A. LaTorraca, J. L. Warner, D. J. Bergman, On the calculation and interpretation of NMR relaxation times distribution, 69th ATCE, New

Orleans, **1994**, 25-28.

[9] G. A. LaTorraca, K. J. Dunn, P. R. Webber, and R. M. Carlson, Low-field NMR determinations of the properties of heavy oils and water-in-oil emulsions, *Magn. Reson. Imaging*, **1998**, 16, 659-662.

[10] K. Allsopp, I. Wright, D. Lastockin, K. Mirotchnik, A. Kantzas, Determination of oil and water compositions of oil/water emulsions using low field NMR relaxometry, *J. Can. Pet. Technol.*, **2001**, 40, 58-61.

[11] K. R. Brownstein and C. E. Tarr, Importance of classical diffusion in NMR studies of water in biological cells, *Phys. Rev. A*, **1979**, 19, 2446-2453.

[12] E.O. Stejskal and J. E. Tanner, Spin diffusion measurements: spin echoes in the presence of a time-dependent field gradient, *J. Chem. Phys.*, **1965**, 42, 288-292.

[13] E. Fukushima, S.B.W. Roeder, Experimental Pulse NMR, Perseus Books, **1981**.

[14] A. Pena, G. Hirasaki, NMR characterization of emulsions, Emulsions and emulsion stability, J. Sjöblom, Surfactant science series, CRC Press, **2006**.

[15] J. S. Murday and R.M. Cotts, Self-diffusion coefficient of liquid lithium, J. Chem. Phys., **1968**, 48, 4938-4945.

[16] K. J. Packer and C. Rees, Pulsed NMR studies of restricted diffusion. I. droplet size distribution in emulsions, *J. Colloid Interface Sci.*, **1972**, 40, 206-218.

[17] B. Epstein, Logaritmico-normal distribution in breakage of solids, *Ind. Eng. Chem.*, **1948**, 40, 2289-2290.

[18] J. L. Salager, M. Pérez-Sénchez, M. Ramírez-Gouveia, J. M. Andérez, M. I. Briceño-Rivas, Stirring-formulation coupling in emulsions, Récent Progrès en Génie des Procédés, **1997**, 11, 123-130.

[19] J.F. Richardson, W.N. Zaki, Sedimentation and fluidisation: Part I, *Trans. Inst. Chem. Eng.*, **1954**, 32, 35-53.

[20] G..K. Batchelor, Sedimentation in a dilute dispersion of spheres, *J. Fluid Mech.*, **1972**, 52, 245-268.

Chapter 4

4. Clay wettability and zeta potential characterization

This chapter mainly discusses clay wettability and its effect on rag layer. Zeta

potential measurement is used to characterize wettability change of clay.

4.1. Rag layer and clay wettability

Figure 4.1 shows 11.2 hours separation results of brine in diluted bitumen

(N/B 0.7) emulsions and 200 ppm demulsifier PR_5 at different pH, prepared at

30 °C as described in section 3.5.2.
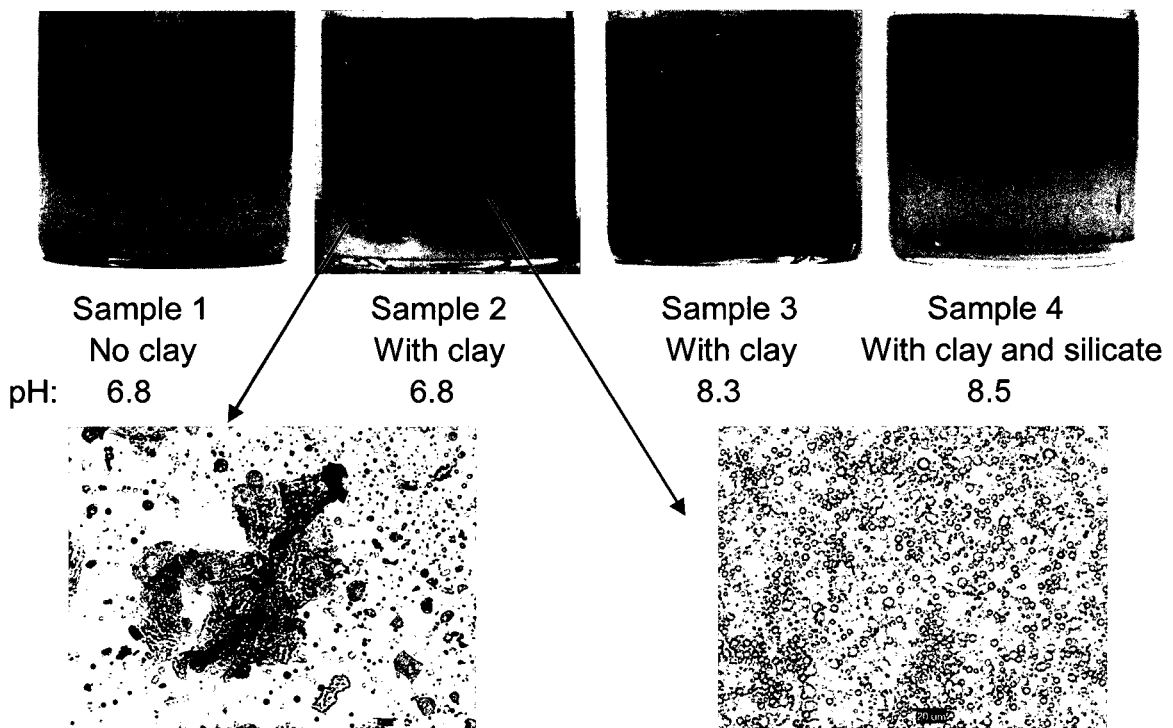
Figure 4.1 11.2 h diluted bitumen emulsions adding 200 ppm PR_5 at 30 °C

Sample1 is the emulsion without clay solids using 1.0 w.% NaCl brine at pH

6.8 (sample 4 in chapter 3). Sample 2 is the emulsion with clay solids using 1.0

w.% NaCl brine at pH 6.8 (sample 2 in chapter 3). Sample 3 is the emulsion with clay solids using diluted bitumen and synthetic brine (2.5×10^{-2} M NaCl, 1.5×10^{-2} M NaHCO$_3$, 2×10^{-3} M Na$_2$SO$_4$, 2×10^{-4} M CaCl$_2$ and 2×10^{-4} M MgCl$_2$) at pH 8.3. Sample 4 is the emulsion with clay solids using synthetic brine adding 1×10^{-4} M Na$_2$SiO$_3$ at pH 8.5.

In the absence of clay solids, the separation of the emulsion is almost complete after adding PR$_5$ at pH 6.8 (sample 1). If the emulsion contains clay solids (sample 2), addition of PR$_5$ results in coalescence of water drops, but the clay solids remain as rigid *skins* dispersed in water. The photomicrographs show that the bottom of oil-continuous phase is water-in-oil emulsion and the top of water-continuous phase contains clay solids skins. Instead of settling to the bottom, the clays, which are partially oil-wet, entrap oil to form skins with intermediate density, which stay in the middle between oil and water layers. Increase of pH from 6.8 (sample 2) to 8.3 (sample 3) can obtain better separation, but a rag layer still forms in the middle. Adding Na$_2$SiO$_3$ at pH 8.5 (sample 4) can get almost complete separation except for a thin rag layer in the middle.

Comparing samples 1 and 2, clay solids can make emulsion more stable and prevent the complete separation of oil and water. Comparing samples 2 and 3, increasing pH can enhance emulsion separation. Comparing samples 3 and 4,

adding silicate can yield even better separation and reduce the rag layer. The separation result of sample 4 is better than sample 2, but worse than sample 1. This indicates increasing pH and adding silicate can change the properties of clay solids, which will reduce the stabilization effects of clay solids on the emulsion.

Most of the clay solids in Athabasca bitumen are kaolinite and illite [1]. Kaolinite in clay solids has heterogeneous surface charge [2] and will present heterogeneous wettability when contacting with crude oil. This is very important to the emulsion stability. Kaolinite is finely divided crystalline aluminosilicate. The principal building elements of the clay minerals are two-dimensional arrays of silica layers and alumina layers. Sharing of oxygen atoms between silica and alumina layers results in two-layer mineral [2]. Kaolinite has permanent negative charge sites on the basal planes owing to the isomorphic substitution of the central Si and Al ions in the crystal lattice by lower positive valence ions [2]-[5]. Al–OH and Si–OH groups are exposed on hydroxyl-terminated planes. The amphoteric sites are conditionally charged, either positive or negative, depending on the pH. Positive charges can develop on the alumina faces and at the edges by direct H^+/OH^- transfer from aqueous phase [3], [4].

The point of zero charge (PZC) of amphoteric (mainly edge) sites, ranges from pH 5 to 9 depending on the kaolinite used [2]. PZC is determined by titration.

Chapter 4

It is not known which sites are responsible. The pH in oil sands operation process is around 8.5. At this pH, the basal surface of kaolinite is negatively-charged, while the edge surface of kaolinite is likely positively-charged.

Surface charge is important to kaolinite wettability. Takamura *et al.* found the carboxyl groups in bitumen can dissociate and form negatively charged sites on bitumen/ water interface [6]. The positively-charged edges of the kaolinite may adsorb negatively charged carboxylate components (i.e. naphthenates) of the oil and make that portion of clay solids partially oil-wet. The partially oil-wet clay solids can retard water-in-oil emulsion coalescence. They also entrap oil drops and form aggregates, which results in a rag layer in the middle of the sample.

If negatively charged carboxylate components can be replaced by other anions or can react with some cations, the surface of the solids can be made more hydrophilic. In this case, some of the adsorbed oil on the solid surface may be replaced by water, allowing the solid to settle to the bottom.

In clay wettability study, kaolinite is chosen as the model clay because it is a major ingredient of the clay solids and has heterogeneous wettability. Sodium naphthenate is used to modify kaolinite to be partially oil-wet. Different chemicals are applied to change the wettability of kaolinite from partially oil-wet to more water-wet.

Chapter 4

4.2. Wettability test of kaolinite

4.2.1. Materials and methods

Kaolinite ($Al_2Si_2O_5(OH)_4$) is obtained from Sigma-Aldrich (product #228834), with particle size 0.1 - 4 μm and specific surface area 17.44 m^2/g. All the salts in the synthetic brine were obtained from Fisher Scientific. Toluene used as oil phase is from Fisher Scientific.

Aqueous phase used here is synthetic brine with composition details shown in Table 4.1. The composition of synthetic brine is close to that present in industrial process water.

Table 4.1 Syncrude brine composition

Component	Concentration (mM)
NaCl	25.0
NaHCO$_3$	15.0
Na$_2$SO$_4$	2.0
*CaCl$_2$	0.3
*MgCl$_2$	0.3

* Absent in soft brine without Ca/Mg for zeta potential measurement in section 4.3.

Octyltrimethylammonium bromide (C$_8$TAB, M.W. 252.24) is from Lancaster Synthesis. Betaine samples are from Rhodia-McIntyre Group Ltd. Amine oxide samples are from Stepan Chemical Company. Sodium naphthenate is from Acros Organics.

Prior to sample preparation, 100 ppm (based on the total volume of the sample) sodium naphthenate and other additives were added to the synthetic brine. The equivalent naphthenic acid concentration is 2.25×10^{-5} M based on soap titration [7]. All samples of 1.0 *w.*% kaolinite in brine-toluene (1:1, *v*/*v*) were prepared by mixing 25 ml synthetic brine, 25 ml toluene and 0.50 g kaolinite in a flat-bottom glass bottle with a six-blade turbine, as shown in Figure 3.8. Stirring speed of turbine was 2000 rpm, and the mixing time was 5 minutes. After preparation, all the samples were left at ambient temperature for 24 hours to allow separation. After removing the top toluene layer, kaolinite in aqueous phase was collected by centrifugation at 5000 g for 30 minutes. This part of kaolinite is considered water-wet. Water-wet fraction of kaolinite is used to express the wettability of kaolinite.

4.2.2. Effect of naphthenate

Figure 4.2 shows the separation results of the samples with and without naphthenate. The first bottle is the sample without sodium naphthenate. This sample has almost complete separation of toluene, brine and kaolinite. Nearly all the kaolinite settles to the bottom of the aqueous phase. The second bottle is the sample with 100 ppm sodium naphthenate. The upper layer of the sample is oil-in-water emulsion with kaolinite. The lower layer is the aqueous phase with

kaolinite at the bottom. The third and fourth bottles are the samples with 100 ppm

sodium naphthenate adding 0.6 mM NaOH (24 ppm) or 0.3 mM Na$_2$SiO$_3$ (37 ppm),

respectively. These two samples have similar separation results to the second

sample. Comparing the first sample and other samples, adding naphthenate

changes the wettability of kaolinite to more oil-wet. In the last three samples,

some of the kaolinite becomes partially oil-wet and stays in the upper oil-in-water

emulsion layer.

	No Naphthenate	With Naphthenate	0.6 mM NaOH	0.3 mM Na$_2$SiO$_3$
pH	8.3	8.3	9.0	9.0
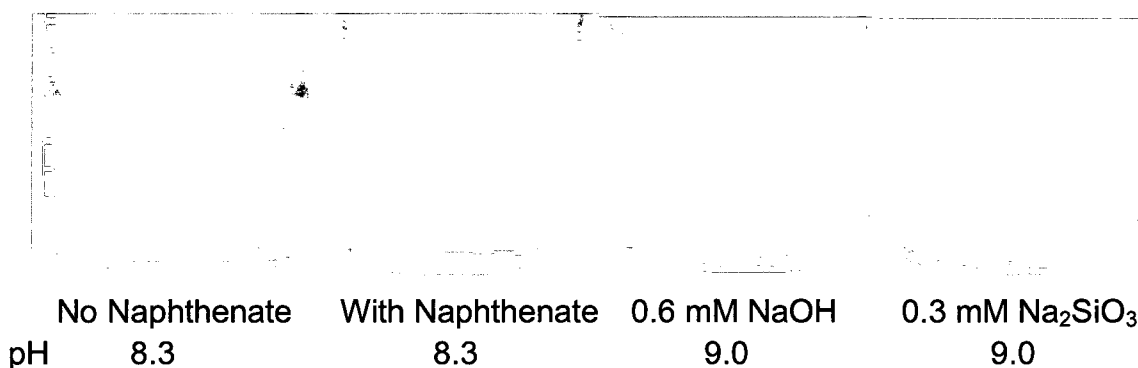
Figure 4.2 Separation of toluene-brine mixture with 1.0 % kaolinite

Figure 4.3 shows water-wet fraction of kaolinite in the samples with 1.0 *w.*%

kaolinite in toluene-brine mixture (1:1, *v/v*). The first bar is water-wet fraction (96%)

in the sample without sodium naphthenate at pH 8.3. Almost all the kaolinite is

water-wet in absence of naphthenate.

The second bar is water-wet fraction (18%) in the sample with 100 ppm

sodium naphthenate at pH 8.3. In this case, water-wet fraction is much lower with

the presence of naphthenate. This indicates naphthenate can change the

wettability of kaolinite from water-wet to more oil-wet. Kaolinite is partially

positively charged. The positively-charged sites can adsorb anionic naphthenate

and become oil-wet.
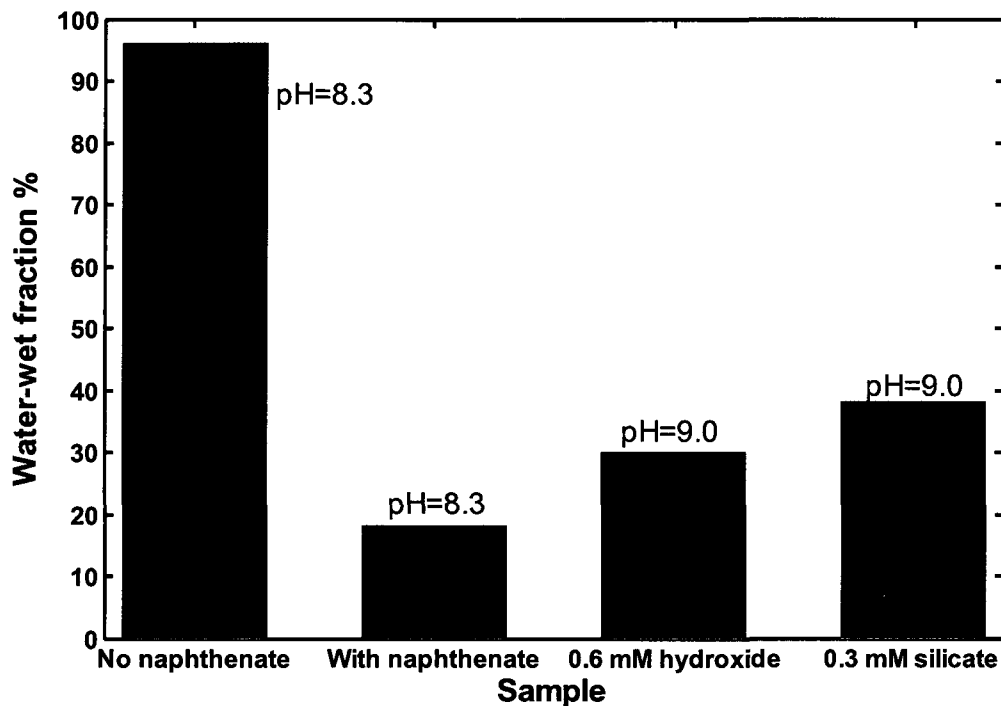
Figure 4.3 Water-wet fraction of kaolinite in toluene-brine mixture with 1.0 %
kaolinite

The third bar is water-wet fraction (30%) in the sample with 100 ppm sodium

naphthenate adding 0.6 mM NaOH at pH 9.0. Compared with the second bar,

water-wet fraction increases. Adding NaOH can convert some of the positively-

charged sites to negatively-charged sites. This can reduce the adsorption of

naphthenate on kaolinite surface and make kaolinite more water-wet.

The last bar is water-wet fraction (38%) in the sample with 100 ppm sodium

naphthenate adding 0.3 mM Na_2SiO_3 at pH 9.0. Compared with the second and third bars, water-wet fraction in the sample adding silicate is larger than adding NaOH. Silicate ion can adsorb on the positively-charged sites of kaolinite and reduce the adsorption of naphthenate on kaolinite surface, which can make kaolinite more water-wet. Compared with NaOH, silicate is more effective to change the wettability of kaolinite.

4.2.3. Effect of naphthenate concentration, NaOH and Na$_2$SiO$_3$

Figure 4.4 shows water-wet fraction of 1.0 *w.*% kaolinite in toluene-brine mixture (1:1, *v/v*) with naphthenate adding NaOH or Na_2SiO_3 at different pH 24 hours after preparation. The red and blue bars are water-wet fractions of kaolinite adding 100 ppm / 500 ppm naphthenate and hydroxide or silicate at different pH. The dashed line shows water-wet fractions of kaolinite without naphthenate as control, without NaOH or Na_2SiO_3 added.

At the same dosage of NaOH or silicate, kaolinite with 500 ppm naphthenate is less water-wet than that with 100 ppm naphthenate. Increase of naphthenate concentration makes naphthenate adsorption effect more significant and kaolinite is more oil-wet. For all the samples, kaolinite becomes more water-wet as pH increases. At higher pH, the surface of kaolinite is more negatively-charged. Hereby the effect of naphthenate adsorption on kaolinite wettability is less

significant at higher pH and kaolinite is more water-wet. At the same pH, adding

silicate can make kaolinite more water-wet than adding NaOH. NaOH only has

caustic effect to increase pH. For silicate, besides caustic effect, adsorption of

silicate ion on kaolinite positively-charged sites can make the surface of kaolinite

more negatively-charged and make kaolinite become more water-wet.
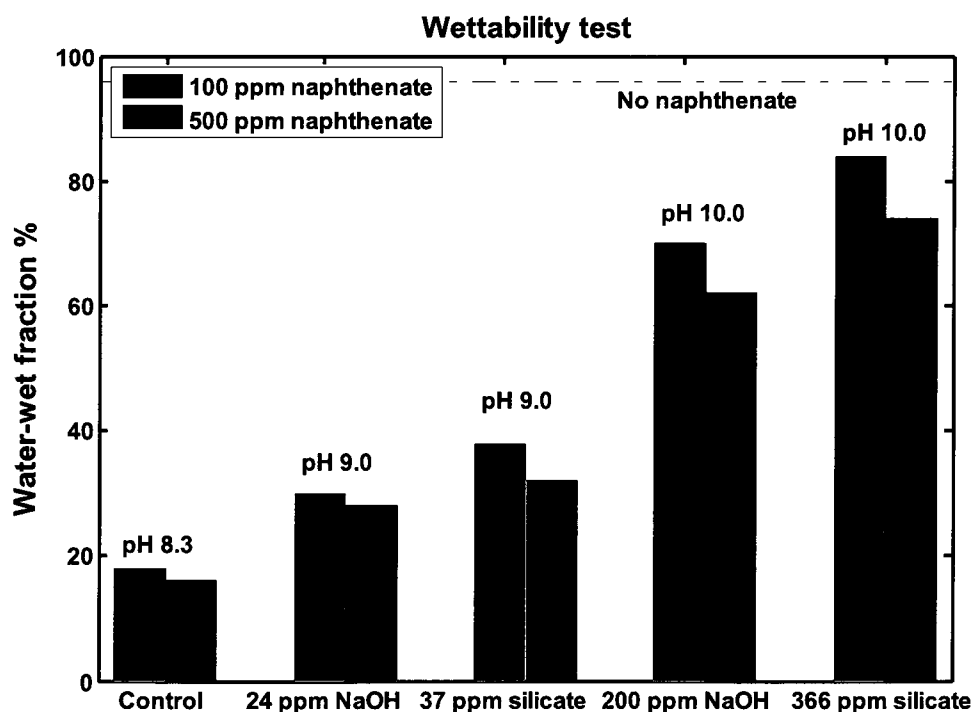
Figure 4.4 Water-wet fraction of kaolinite with different amount of naphthenate adding NaOH/ Na_2SiO_3 at different pH

Figure 4.5 shows water-wet fraction of 1.0 $w.\%$ kaolinite in toluene-brine

mixture (1:1, v/v) with 100 ppm naphthenate adding NaOH/ Na_2SiO_3 at different

pH 24 hours after preparation. Kaolinite becomes more water-wet as pH

increases. At the same pH, adding silicate can make kaolinite more water-wet than adding NaOH. Below pH 10.0, water-wet fraction of kaolinite increases rapidly as pH increases. At pH 10.0, water-wet fractions of kaolinite adding NaOH or Na_2SiO_3 are 70% and 84%, respectively. Above pH 10.0, water-wet fraction increases slowly as pH increases and reaches plateau. Water/ crude oil system with high pH will form O/W emulsion spontaneously, which should be avoided in emulsion separation process. Hence pH 10.0 is upper bound for employing wettability change using NaOH or Na_2SiO_3 in separation process.
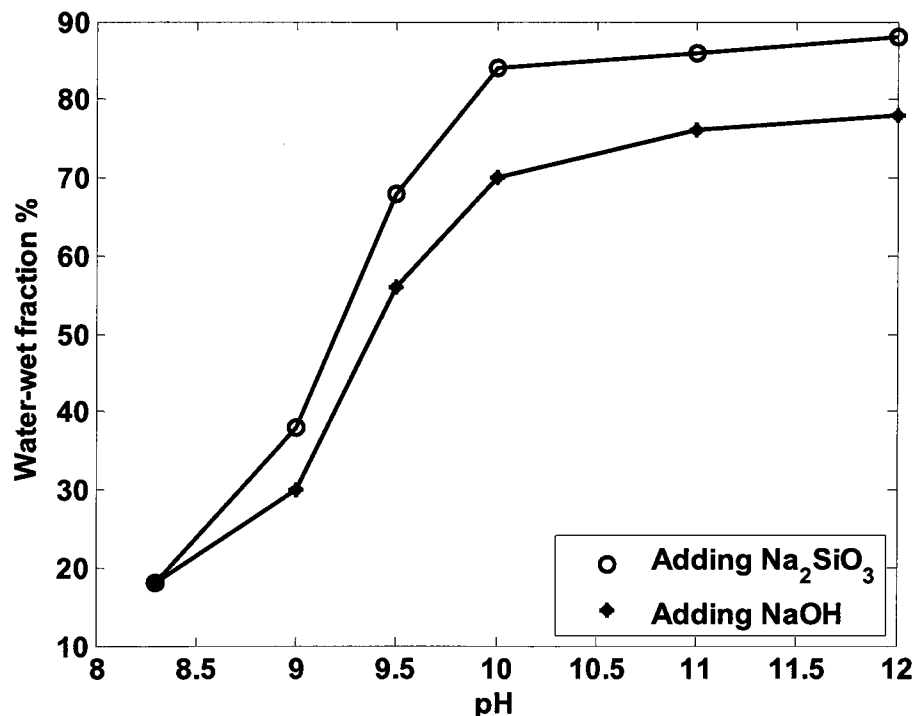
Figure 4.5 Water-wet fraction of kaolinite with 100 ppm naphthenate adding NaOH/ Na_2SiO_3 at different pH

Chapter 4

4.2.4. Effect of surfactant containing cationic groups

Cationic surfactants are used to change carbonate wettability via the mechanism forming ion pairs with carboxylates [8]-[10]. The authors proposed that carbonate surface can adsorb negatively-charged carboxylates and become oil-wet. Cationic surfactants can form ion pairs with carboxylates in aqueous solution and thereby displace carboxylates from carbonate surface to make carbonate more water-wet.

Table 4.2 Betaine samples used in wettability test

Product No.	Chemical name and Formula	Activity
3	Capryl/Capramidopropyl Betaine $C_8H_{17}/C_{10}H_{21}$-CO-NH-$(CH_2)_3$-$N^+(CH_3)_2$-CH_2-COO^-	33% - 38%
4	CoCo-Betaine $C_{12}H_{25}$-$N^+(CH_3)_2$-CH_2-COO^-	31%
5	Cocamidoprotyl Betaine in Isopropanol and Water $C_{11}H_{23}$-CO-NH-$(CH_2)_3$-$N^+(CH_3)_2$-CH_2-COO^-	43%
10	Octyl Betaine C_8H_{17}-$N^+(CH_3)_2$-CH_2-COO^-	50%
13	Caprylamidopropyl Betaine C_8H_{17}-CO-NH-$(CH_2)_3$-$N^+(CH_3)_2$-CH_2-COO^-	30%

Similar method can be used to change the wettability of kaolinite. Cationic surfactants can form ion pairs with anionic naphthenate and displace naphthenate

from kaolinite surface to make kaolinite more water-wet. Surfactants used here are octyltrimethylammonium bromide (C_8H_{17}-$\overset{+}{N}(CH_3)_2Br^-$, C_8TAB), betaine and amine oxide. C_8TAB is used here as a model cationic surfactant. The other two surfactants exhibit the equilibrium between zwitterionic and cationic forms, which depends on pH. The cationic form is dominant at lower pH. Tables 4.2 and 4.3 show betaine and amine oxide samples used in wettability test.

Table 4.3 Amine oxide samples used in wettability test

Commercial name	Formula	Activity
AMMONYX CDO Special	CH_3-$(CH_2)_x$-CO-NH-$(CH_2)_3$-$\overset{+}{N}(CH_3)_2$-O^- x=6 - 16	32.5%
AMMONYX DO	$C_{10}H_{21}$-$\overset{+}{N}(CH_3)_2$-O^-	30%
AMMONYX LO	$C_{12}H_{25}$-$\overset{+}{N}(CH_3)_2$-O^-	30%
AMMONYX MCO	C_xH_{2x+1}-$\overset{+}{N}(CH_3)_2$-O^- x=12 - 18	30%

4.2.4.1. Effect of C$_8$TAB

Figure 4.6 shows water-wet fraction of 1.0 w.% kaolinite in toluene-brine mixture (1:1, v/v) with 100 ppm / 200 ppm naphthenate adding different amounts of C_8TAB at pH 8.3 24 hours after preparation. The dashed lines show water-wet fractions of kaolinite with or without naphthenate as control, without C_8TAB added.

The blue and red dotted lines show 1:1 stoichiometry of C_8TAB with 100 ppm / 200 ppm naphthenate ($2.25×10^{-5}$ / $4.50×10^{-5}$ M). For both cases adding 100 ppm / 200 ppm naphthenate, as concentration of naphthenate increases, water-wet fraction of kaolinite increases to maximum and then decreases. The optimal concentration of C_8TAB (water-wet fraction of kaolinite reaches maximum) is close to the 1:1 stoichiometry value (equal molar concentration of C_8TAB and naphthenate) with 100 ppm / 200 ppm naphthenate. If the amount of naphthenate doubles, the optimal concentration of C_8TAB also doubles.

Figure 4.6 Water-wet fraction of kaolinite with 100/ 200 ppm naphthenate adding different amount of C_8TAB at pH 8.3
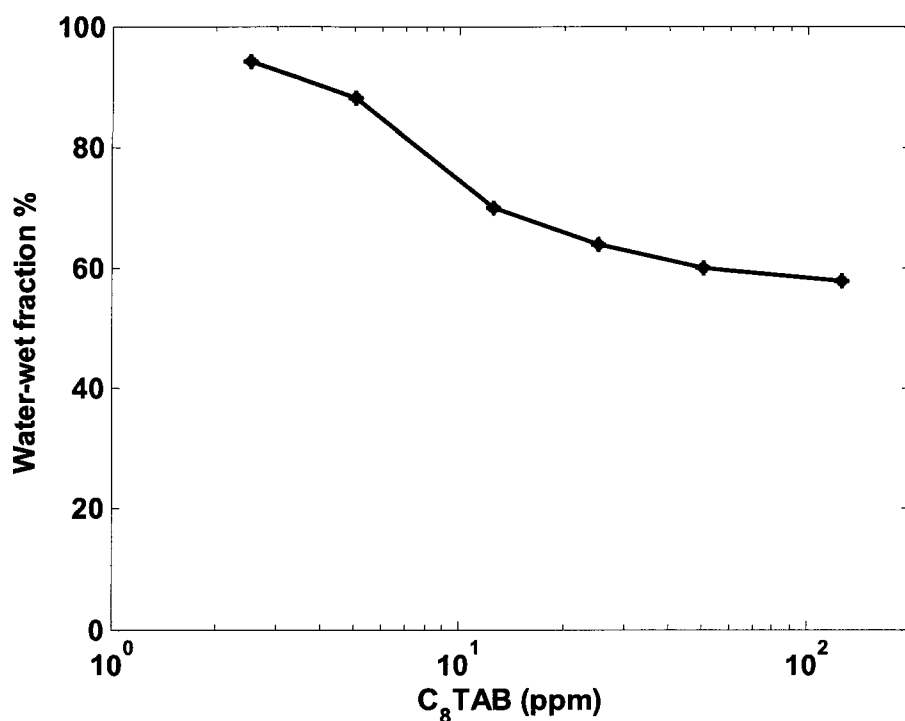
Figure 4.7 Water-wet fraction of kaolinite adding different amount of C_8TAB

Figure 4.7 shows water-wet fraction of 1.0 w.% kaolinite in toluene-brine

mixture (1:1, v/v) adding different amounts of C_8TAB at pH 8.3 24 hours after

preparation, without naphthenate added. In the figure, water-wet fraction of

kaolinite decreases as C_8TAB concentration increases. This reveals that adding

C_8TAB only makes kaolinite more oil-wet. Cationic surfactant C_8TAB can interact

with negatively-charged groups, for instance, negatively-charged sites on kaolinite

surface or with naphthenate. In the absence of naphthenate, C_8TAB will adsorb on

the surfaces of kaolinite with negatively-charged sites and make these surfaces

more oil-wet. If the system contains naphthenate, C_8TAB will interact preferentially

with naphthenate and form ion pairs. If naphthenate and C_8TAB are added in stoichiometric amounts, adsorbed naphthenate and C_8TAB are minimized. If C_8TAB is overdosed, the excess C_8TAB will adsorb on the negative surfaces of kaolinite and make them more oil-wet. Hence as C_8TAB concentration increases, water-wet fraction of kaolinite increases to maximum and then decreases.

4.2.4.2. Effect of betaine

Figure 4.8 shows water-wet fraction of 1.0 w.% kaolinite in toluene-brine mixture (1:1, v/v) with 100 ppm naphthenate adding 1000 ppm betaine (based on activity of betaine and total volume of the mixture) at pH 8.3 24 hours after preparation. The red and black dashed lines show water-wet fraction of kaolinite with/ without naphthenate as control, without betaine added. Comparison of all the results reveals that sample adding 1000 ppm betaine 13 has largest water-wet fraction of kaolinite (90%). Hence betaine 13 was used as optimal surfactant in the following wettability test to study the effect of dosage.

Figure 4.9 shows water-wet fraction of 1.0 w.% kaolinite in toluene-brine mixture (1:1, v/v) with 100 ppm naphthenate adding different amounts of betaine 13 at pH 8.3 24 hours after preparation. The two black dashed lines show water-wet fractions of kaolinite with or without naphthenate as control, without betaine added. The red dashed line shows 1:1 stoichiometry value of betaine 13

Chapter 4

with 100 ppm naphthenate (2.25×10^{-5} M). Water-wet fraction of kaolinite

increases from 50% to 88% when added betaine 13 increases from 100 ppm to

200 ppm. When added betaine 13 increases to 1000 ppm, water-wet fraction only

increases from 88% to 92%. If 200 ppm is chosen as optimal dosage of betaine

13, it is much larger than the 1:1 stoichiometry value with 100 ppm naphthenate.
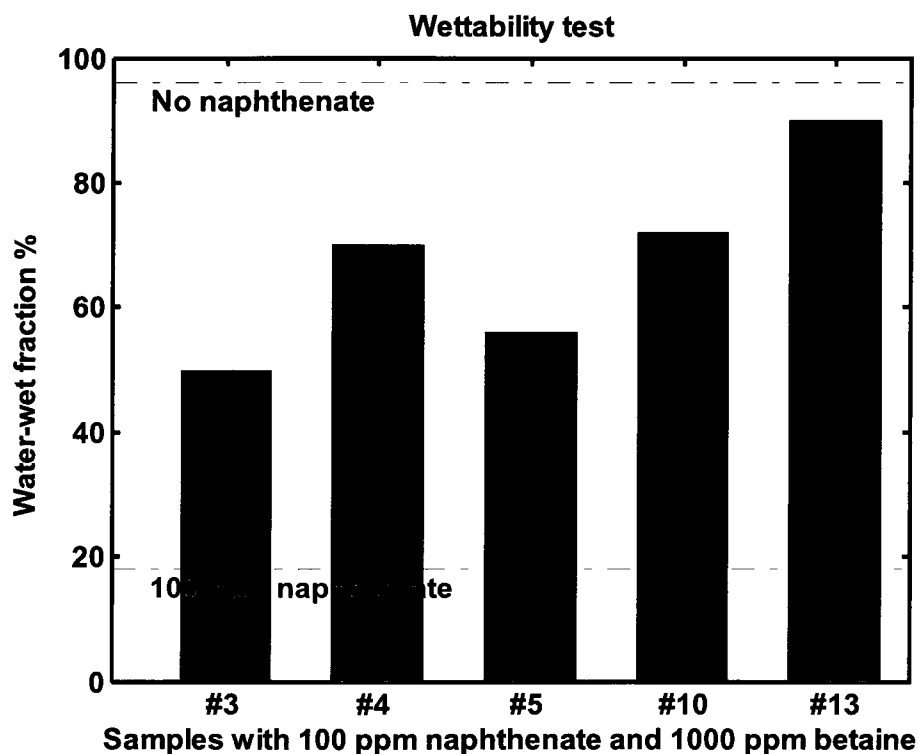
Figure 4.8 Water-wet fraction of kaolinite with 100 ppm naphthenate adding 1000 ppm betaine at pH 8.3

Betaine 13 is an electrically neutral chemical compound with a positively

charged cationic ammonium ion and a negatively charged functional carboxylate

group, which is referred to as a specific type of *zwitterion*. At a certain pH, betaine

can accept a hydrogen ion and becomes positively charged. The ratio of this type

of cation depends on the association equilibrium constants and pH. At pH 8.3,

only a small amount of betaine becomes positively charged and interacts with

naphthenate to form ion pairs. Hence the optimal dosage is larger than the 1:1

stoichiometry value.
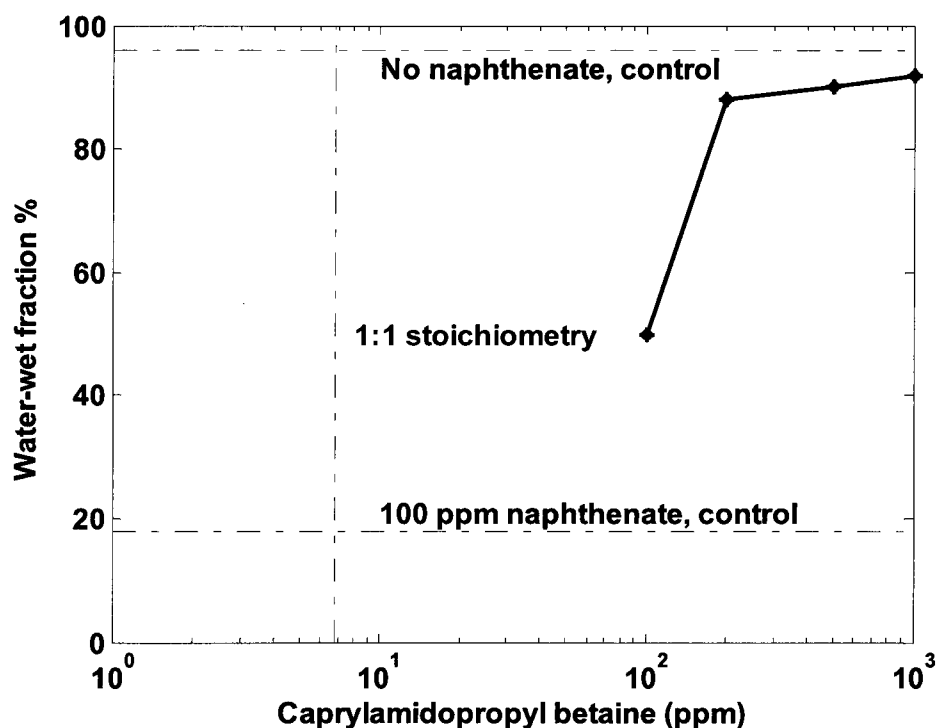
Figure 4.9 Water-wet fraction of kaolinite with 100 ppm naphthenate adding
different amount of betaine 13 at pH 8.3

Figure 4.10 shows water-wet fraction of 1.0 $w.\%$ kaolinite in toluene-brine

mixture (1:1, v/v) adding different amount of betaine 13 at pH 8.3 24 hours after

preparation, without naphthenate added. Similar to C_8TAB, water-wet fraction of

Chapter 4

kaolinite decreases as betaine 13 concentration increases. This indicates that adding betaine 13 only makes kaolinite more oil-wet. The decrease is slower than C_8TAB. Cationic ion of betaine 13 can interact with naphthenate. In the absence of naphthenate, betaine 13 will adsorb on the negative surfaces of kaolinite and make them more oil-wet. If the system contains naphthenate, cationic ion betaine 13 will interact with naphthenate and form ion pairs, which can make kaolinite more water-wet.
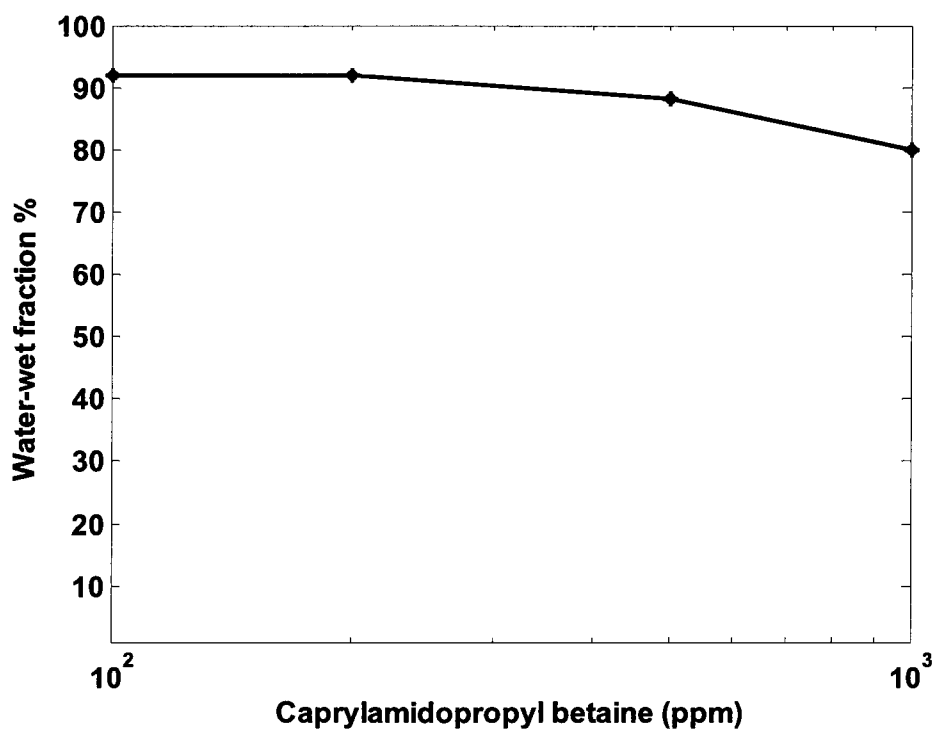
Figure 4.10 Water-wet fraction of kaolinite adding different amount of betaine 13 at pH 8.3

Chapter 4

4.2.4.3. Effect of amine oxide

Figure 4.11 shows water-wet fraction of 1.0 *w.*% kaolinite in toluene-brine mixture (1:1, *v/v*) with 100 ppm naphthenate adding 100 ppm / 1000 ppm amine oxide at pH 8.3 24 hours after preparation. The green and black dashed lines show water-wet fraction of kaolinite with or without naphthenate as control, without amine oxide added. Sample adding 100 ppm amine oxide DO has largest water-wet fraction of kaolinite (86%). Amine oxide DO was used as optimal surfactant to find the optimal dosage.
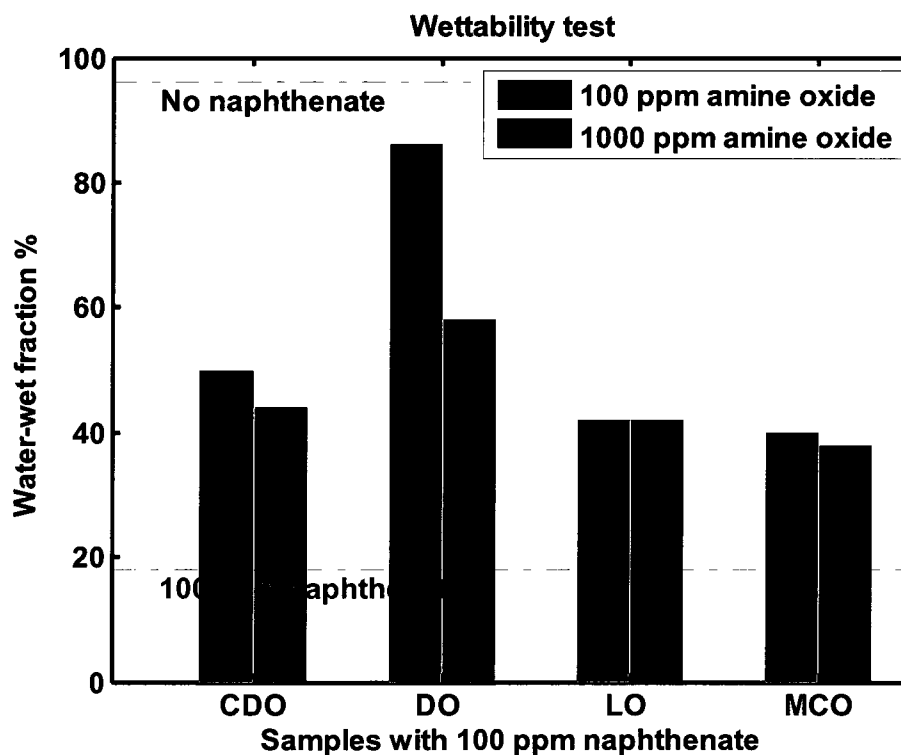
Figure 4.11 Water-wet fraction of kaolinite with 100 ppm naphthenate adding 100/ 1000 ppm amine oxide at pH 8.3

Figure 4.12 shows water-wet fraction of 1.0 *w*.% kaolinite in toluene-brine mixture (1:1, *v*/*v*) with 100 ppm naphthenate adding different amounts of amine oxide DO at pH 8.3 24 hours after preparation. The two black dashed lines show water-wet fractions of kaolinite with or without naphthenate as control, without amine oxide added. The red dashed line shows 1:1 stoichiometry value of amine oxide DO with 100 ppm naphthenate.
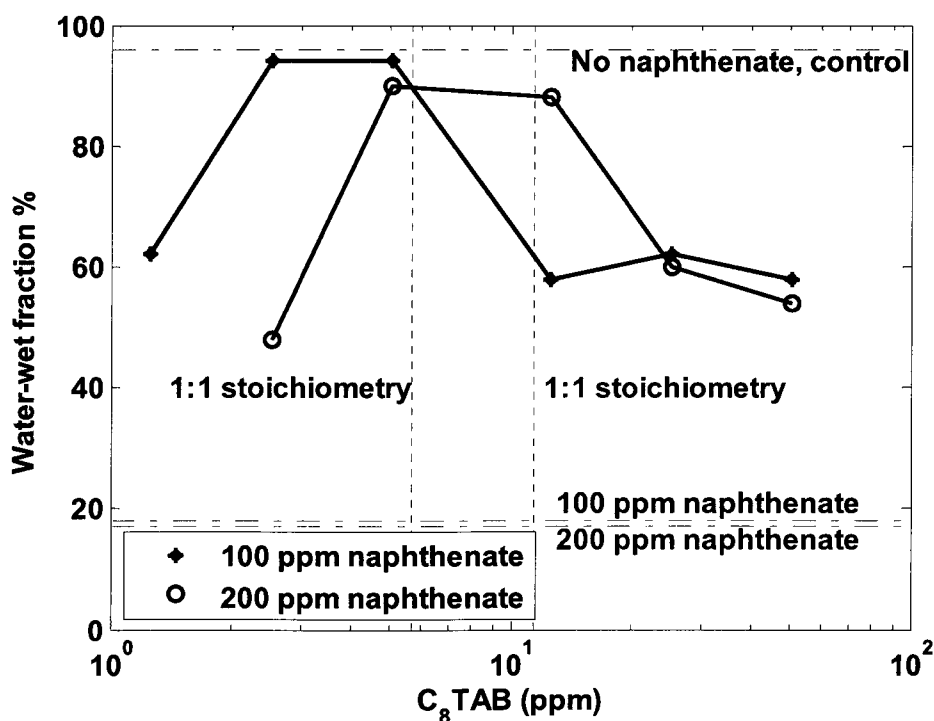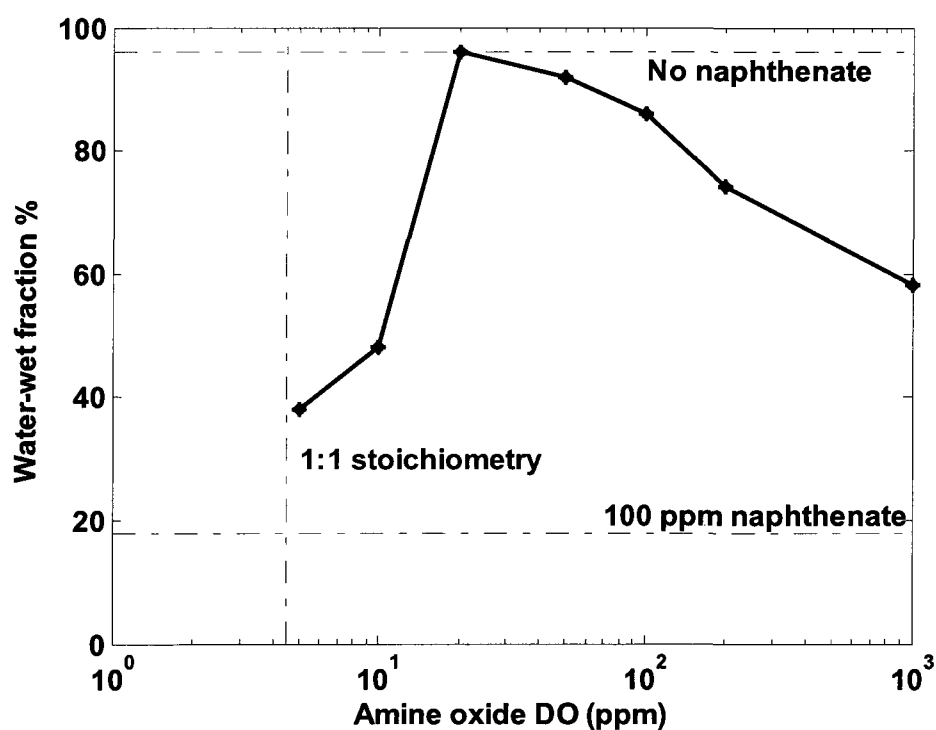

Figure 4.12 Water-wet fraction of kaolinite with 100 ppm naphthenate adding different amount of betaine 13 at pH 8.3

Water-wet fraction of kaolinite increases from 38% to 96% when added amine oxide DO increases from 5 ppm to 20 ppm. Then water-wet fraction of

kaolinite decreases as amine oxide DO concentration increases. Water-wet fraction of kaolinite at optimal dosage of amine oxide DO is the same as the sample without naphthenate. The optimal dosage of amine oxide DO is about 4.4 times the 1:1 stoichiometry value compared to 15 time for betaine 13 and equal amounts for C_8TAB.

Similar to betaine, amine oxide in chemistry is a neutral chemical compound with a positively charged cationic ammonium ion and a negatively charged functional carbonyl group. At pH 8.3, some of amine oxide becomes positively charged and interacts with naphthenate to form ion pairs. Hereby the optimal dosage is larger than the 1:1 stoichiometry value. If amine oxide is overdosed, the excess cationic type of amine oxide will adsorb on negative surfaces of kaolinite and make them more oil-wet. Hence as amine oxide concentration increases, water-wet fraction of kaolinite increases to maximum and then decreases.

Figure 4.13 shows water-wet fraction of 1.0 $w.\%$ kaolinite in toluene-brine mixture (1:1, v/v) with 100 ppm naphthenate adding C_8TAB, amine oxide DO or betaine 13 at pH 8.3 24 hours after preparation as comparison. The two black dashed lines show water-wet fractions of kaolinite with or without naphthenate as control. The blue, red or green dashed line shows 1:1 stoichiometry values C_8TAB, amine oxide DO or betaine 13 with 100 ppm naphthenate.
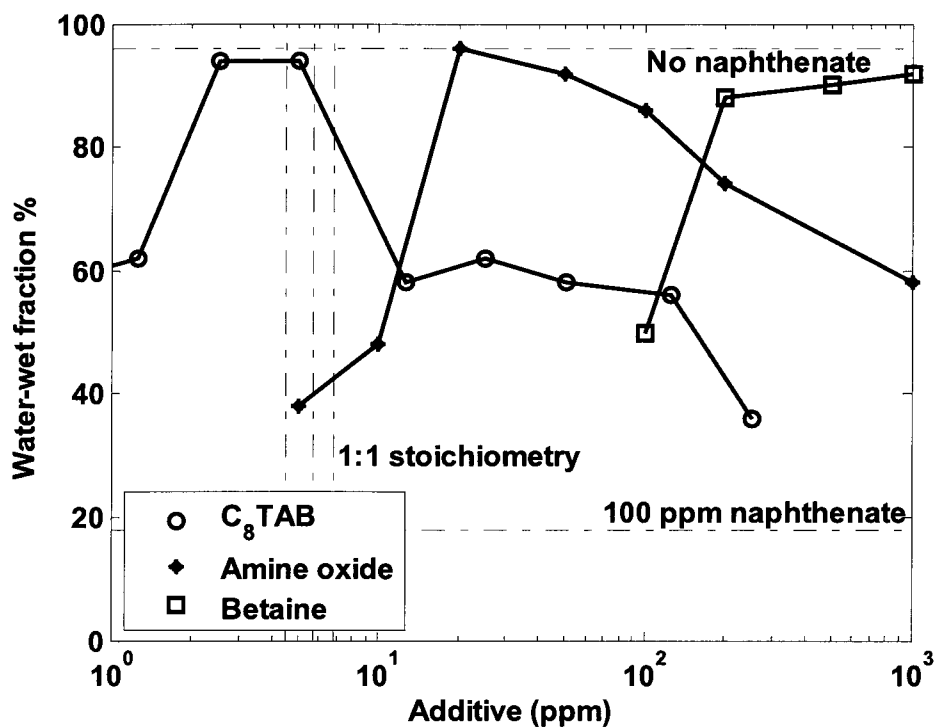
Figure 4.13 Water-wet fraction of kaolinite with 100 ppm naphthenate adding C_8TAB, betaine 13 or amine oxide DO at pH 8.3

Among three surfactants, the optimal dosages are as follows: C_8TAB < amine oxide DO < betaine 13. The sensitivity of overdosage has the opposite direction: C_8TAB > amine oxide DO > betaine 13. Smaller optimal dosage is better for wettability change. Based on this criterion, C_8TAB is the best. Lower sensitivity of overdosage is better. Otherwise water-wet fraction of kaolinite will decrease very fast if it is overdosed. If the exact concentration of naphthenate is unknown, amine oxide DO is better than the other two because it has intermediate optimal dosage and overdosage sensitivity.

Chapter 4

4.3. Wettability of kaolinite characterized by zeta potential

4.3.1. Introduction

Effect of NaOH and Na_2SiO_3 has been discussed in section 4.2.3. In this case, wettability of kaolinite depends on the surface charge change. Zeta potential can be used to characterize oxide surface charge [11], [12], which is related to wettability. Zeta potential of clay solids can also directly characterize the wettability change of clay solids. Liu *et al.* used zeta potential measurement to study the wettability of clay solids and the interactions between bitumen and clay [13], [14]. Wettability change may be important to the stability of water-in-bitumen emulsions.

To characterize the wettability change of kaolinite, zeta potentials of kaolinite in synthetic brine with different additives were measured. Sodium hydroxide (NaOH), sodium citrate ($Na_3C_6H_5O_7$), sodium meta-silicate (Na_2SiO_3), sodium ortho-silicate (Na_4SiO_4), and sodium carbonate (Na_2CO_3) were used to change surface charge and zeta potentials of kaolinite. In order to analyze and correlate the experimental zeta potential of kaolinite in synthetic brine, simplified Gouy-Stern-Grahame model was used [15].

4.3.2. Zeta potential model

In Gouy-Stern-Grahame model, the double layer can be divided into two regions: 1) the compact or Stern layer very near the solid surface in which the

charge and potential distribution are determined by the geometrical restrictions of ion and molecule size and interactions between ions and solid surface; 2) diffuse layer where the potential distribution can be predicted by Poisson-Boltzmann equation, as shown in Figure 4.14 [16].

The distance between solid surface and inner Helmholtz Plane is b. The distance between inner and outer Helmholtz Plane is d. Solid surface has surface charge density σ_s and potential ψ_s. The Inner Helmholtz Plane (IHP) has potential ψ_i. Stern layer has charge density σ_i. The Outer Helmholtz Plane (OHP) has surface potential ψ_d. Charge density of diffuse layer is σ_d.
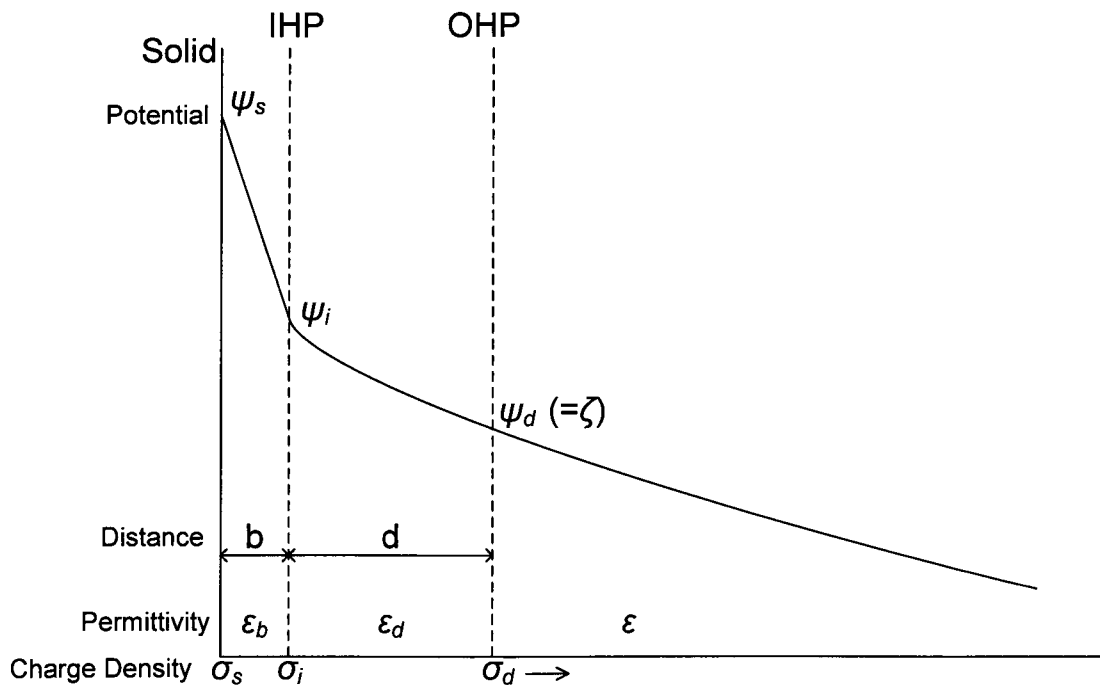
Figure 4.14 Gouy-Stern-Grahame model of double layer [16]

Chapter 4

The equations for Gouy-Stern-Grahame model are as follows: [16], [17]

$$\sigma_s + \sigma_i + \sigma_d = 0 \tag{4.1}$$

$$\psi_s - \psi_i = \frac{b\sigma_s}{\varepsilon_b} \tag{4.2}$$

$$\psi_i - \psi_d = \frac{-d\sigma_d}{\varepsilon_d} \tag{4.3}$$

$$\sigma_d = -\text{sign}(\sigma_d)\{2\varepsilon RT \sum_i c_i^0 [\exp(-z_i e\psi_d / kT) - 1]\}^{1/2} \tag{4.4}$$

b and d: thickness of compact layer and diffuse layer.

σ_s, σ_i and σ_d: charge density of solid surface, Stern layer and diffuse layer.

ψ_s, ψ_i and ψ_d: potential of solid surface, IHP and OHP.

ε_b and ε_d: permittivity in compact layer and diffuse layer.

z_i: valency of ion species.

ε: permittivity of bulk solution.

c_i^0: concentration of ion species i in the bulk.

Gouy-Stern-Grahame model can be simplified if making assumptions are made.

1) The shear surface coincides with the Outer Helmholtz Plane (OHP), thus zeta potential $\zeta = \psi_d$.

2) The charge of solids surface and Stern layer are combined into net surface charge. $\sigma_0 = \sigma_s + \sigma_i$.

Chapter 4

Figure 4.15 shows the simplified model of double layer.

Solid | IHP | OHP

Compact Layer

$\psi_d \ (=\zeta)$

Potential

Charge Density

$\sigma_0 = \sigma_s + \sigma_i$ $\sigma_d \rightarrow$
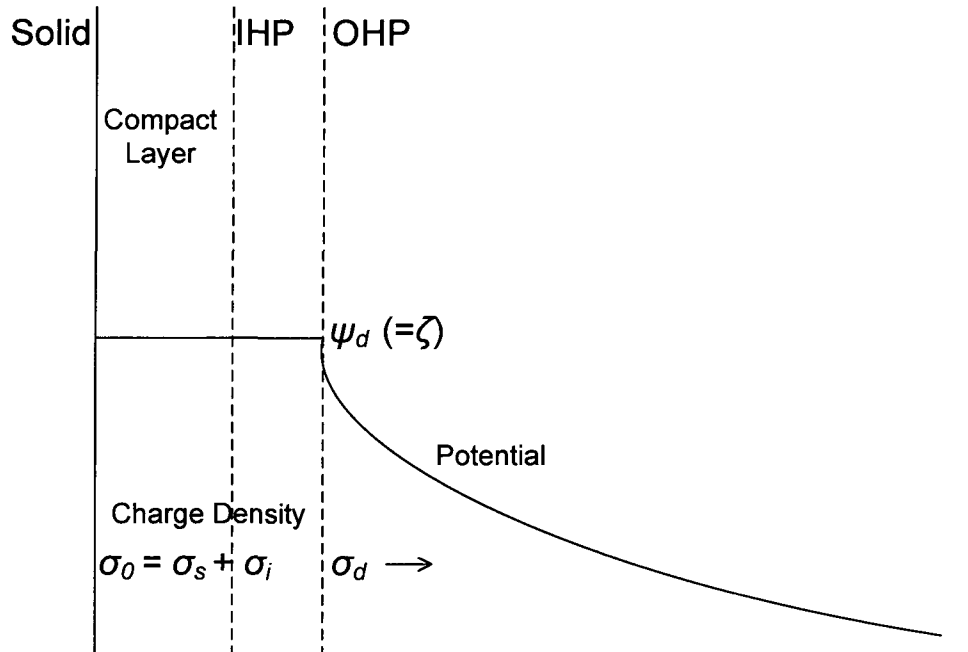
Figure 4.15 Simplified model of double layer

Eqs. [4.1] and [4.4] can be rewritten as:

$$\sigma_0 + \sigma_d = 0, \quad \sigma_0 = -\sigma_d \qquad [4.5]$$

$$\sigma_0 = -\text{sign}(\sigma_0)\{2\varepsilon RT \sum_i c_i^0 [\exp(-z_i e\zeta / kT) - 1]\}^{1/2} \qquad [4.6]$$

Near the charged surface, ion concentration is different from bulk solution due to the electrostatic attraction or repulsion. From Boltzmann equation, ion activity near kaolinite surface a_s is different from the bulk ion activity a_b,

$$a_s(M^{z_i}) = a_b(M^{z_i})\exp(-\frac{z_i e\zeta}{kT}) \qquad [4.7]$$

a_s and a_b: activity at surface and in the bulk.

M: ion species (cation or anion).

z_i: valency of ion species.

Simplified Gouy-Stern-Grahame model established the relationship between zeta potential and surface charge. To study the effects of pH and adsorption of counter ions, site-binding model of oxide/ water interface is widely used [18]-[23]. Surface charge of kaolinite can be explained by proton donor-acceptor reactions occurring simultaneously on alumina or silica sites of kaolinite [20], as expressed in Eqns. [4.8] and [4.9].

$$-AlOH_2^+ \rightleftharpoons -AlOH + H^+ \quad , \quad -AlOH \rightleftharpoons -AlO^- + H^+ \qquad [4.8]$$

$$-SiOH_2^+ \rightleftharpoons -SiOH + H^+ \quad , \quad -SiOH \rightleftharpoons -SiO^- + H^+ \qquad [4.9]$$
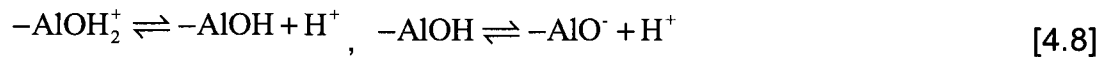
To apply the site-binding model the following assumptions are made:

1) The surface of kaolinite has amphoteric silica and alumina sites, which are pH-dependent. H^+ and OH^- will react with such surface sites. Permanent negatively charged sites $-B^-$ are inert sites, which are independent of pH.

2) The indifferent ions, such as Na^+ and Cl^-, will not specifically adsorb in the compact layer.

3) The specifically adsorbed ions, such as Ca^{2+}, Mg^{2+} and $HSiO_3^-$, will adsorb in the compact layer.

For counter ion adsorption, we consider kaolinite surface containing

amphoteric groups –AOH (A can be Al or Si) and permanent negatively charged sites –B⁻. Here silica sites and alumina sites are considered to have the same electrostatic interactions with counter ions. Amphoteric groups –AOH (–AlOH and –SiOH) are pH dependent, and can form either positively charged sites –AOH₂⁺, or negatively charged sites –AO⁻. Positively charged sites –AOH₂⁺ can adsorb anions. Negatively charged sites –AO⁻ can adsorb cations.

Eqs. [4.10] and [4.11] show the dissociation equilibrium of amphoteric groups –AOH and the equilibrium equation.

$$-\text{AOH} \rightleftharpoons -\text{AO}^- + \text{H}^+, \qquad \text{A: Al or Si} \tag{4.10}$$
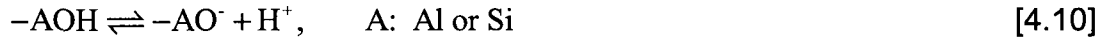
$$K = \frac{[\text{AO}^-]a_s(\text{H}^+)}{[\text{AOH}]} = \frac{[\text{AO}^-]a_b(\text{H}^+)\exp(-\frac{e\zeta}{kT})}{[\text{AOH}]} \tag{4.11}$$

K: surface reaction or surface adsorption equilibrium constants.

a_s and a_b: activity at surface and in the bulk.

Eq. [4.12] shows the surface adsorption equilibrium of Ca^{2+} on negatively charged groups –AO⁻. Eq. [4.13] shows the equilibrium equation.

$$-\text{AO}^- + \text{Ca}^{2+} \rightleftharpoons -\text{AOCa}^+, \qquad \text{A: Al or Si} \tag{4.12}$$
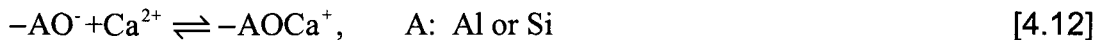
$$K_{\text{Ca}} = \frac{[\text{AOCa}^+]}{[\text{AO}^-]a_s(\text{Ca}^{2+})} = \frac{[\text{AOCa}^+]}{[\text{AO}^-]a_b(\text{Ca}^{2+})\exp(-\frac{2e\zeta}{kT})} \tag{4.13}$$

Table 4.4 shows equilibrium of different surface reactions.

Table 4.4 Equilibrium of surface reactions

Reaction	K
$-AlOH_2^+ \rightleftharpoons -AlOH + H^+$	$K_{Al+} = \dfrac{[AlOH]a_b(H^+)}{[AlOH_2^+]} e^{-\frac{e\zeta}{kT}}$
$-AlOH \rightleftharpoons -AlO^- + H^+$	$K_{Al-} = \dfrac{[AlO^-]a_b(H^+)}{[AlOH]} e^{-\frac{e\zeta}{kT}}$
$-SiOH_2^+ \rightleftharpoons -SiOH + H^+$	$K_{Si+} = \dfrac{[SiOH]a_b(H^+)}{[SiOH_2^+]} e^{-\frac{e\zeta}{kT}}$
$-SiOH \rightleftharpoons -SiO^- + H^+$	$K_{Si-} = \dfrac{[SiO^-]a_b(H^+)}{[SiOH]} e^{-\frac{e\zeta}{kT}}$
$-AO^- + Ca^{2+} \rightleftharpoons -AOCa^+,$ A: Al/ Si	$K_{Ca} = \dfrac{[AOCa^+]}{[AO^-]a_b(Ca^{2+})e^{-\frac{2e\zeta}{kT}}}$
$-AO^- + Mg^{2+} \rightleftharpoons -AOMg^+,$ A: Al/ Si	$K_{Mg} = \dfrac{[AOMg^+]}{[AO^-]a_b(Mg^{2+})e^{-\frac{2e\zeta}{kT}}}$
$-AOH_2^+ + HSiO_3^- \rightleftharpoons -AOH_2HSiO_3,$ A: Al/ Si	$K_{HSiO_3} = \dfrac{[AOH_2HSiO_3]}{[AOH_2^+]a_b(HSiO_3^-)e^{\frac{e\zeta}{kT}}}$
$-AOH_2^+ + H_3SiO_4^- \rightleftharpoons -AOH_2H_3SiO_4,$ A: Al/ Si	$K_{H_3SiO_4} = \dfrac{[AOH_2H_3SiO_4]}{[AOH_2^+]a_b(H_3SiO_4^-)e^{\frac{e\zeta}{kT}}}$
$-AOH_2^+ + HCO_3^- \rightleftharpoons -AOH_2HCO_3,$ A: Al/ Si	$K_{HCO_3} = \dfrac{[AOH_2HCO_3]}{[AOH_2^+]a_b(HCO_3^-)e^{\frac{e\zeta}{kT}}}$
$-AOH_2^+ + SO_4^{2-} \rightleftharpoons -AOH_2SO_4^-,$ A: Al/ Si	$K_{SO_4} = \dfrac{[AOH_2SO_4^-]}{[AOH_2^+]a_b(SO_4^{2-})e^{\frac{2e\zeta}{kT}}}$
$-AOH_2^+ + L^{3-} \rightleftharpoons -AOH_2L^{2-},$ A: Al/ Si, L:citrate	$K_L = \dfrac{[AOH_2L^{2-}]}{[AOH_2^+]a_b(L^{3-})e^{\frac{3e\zeta}{kT}}}$

Chapter 4

Table 4.5 Equilibrium constants of reactions in bulk solution [24], [25]

Reaction	K
$Ca^{2+} + C_6H_5O_7^{3-} \rightleftharpoons CaC_6H_5O_7^-$	7.9×10^4
$Mg^{2+} + C_6H_5O_7^{3-} \rightleftharpoons MgC_6H_5O_7^-$	2.2×10^3
$CaCO_3 \rightleftharpoons Ca^{2+} + CO_3^{2-}$	5.0×10^{-9}
$MgCO_3 \rightleftharpoons Mg^{2+} + CO_3^{2-}$	6.8×10^{-6}
$CaSiO_3 \rightleftharpoons Ca^{2+} + SiO_3^{2-}$	8.3×10^{-12}
$MgSiO_3 \rightleftharpoons Mg^{2+} + SiO_3^{2-}$	4.0×10^{-12}
$CO_2 + H_2O \rightleftharpoons H^+ + HCO_3^-$	4.3×10^{-7}
$HCO_3^- \rightleftharpoons H^+ + CO_3^{2-}$	4.0×10^{-11}
$H_4SiO_4 \rightleftharpoons H^+ + H_3SiO_4^-$	2.2×10^{-10}
$H_3SiO_4^- \rightleftharpoons H^+ + H_2SiO_4^{2-}$	2.0×10^{-12}
$H_2SiO_4^{2-} \rightleftharpoons H^+ + HSiO_4^{3-}$	1.0×10^{-12}
$HSiO_4^{3-} \rightleftharpoons H^+ + SiO_4^{4-}$	1.0×10^{-12}
$H_2SiO_3 \rightleftharpoons H^+ + HSiO_3^-$	2.0×10^{-10}
$HSiO_3^- \rightleftharpoons H^+ + SiO_3^{2-}$	1.0×10^{-12}
$H_3C_6H_5O_7 \rightleftharpoons H^+ + H_2C_6H_5O_7^-$	7.1×10^{-4}
$H_2C_6H_5O_7^- \rightleftharpoons H^+ + HC_6H_5O_7^{2-}$	1.7×10^{-5}
$HC_6H_5O_7^{2-} \rightleftharpoons H^+ + C_6H_5O_7^{3-}$	4.1×10^{-7}

Table 4.6 Effective diameter of the hydrated ions [26]

Ion	a (nm)	Ion	a (nm)
H^+	0.9	SiO_4^{4-}	0.4
OH^-	0.35	SO_4^{2-}	0.4
HCO_3^-	0.4	H_2L^-	0.35
CO_3^{2-}	0.45	HL^{2-}	0.45
*$HSiO_3^-$	0.4	L^{3-}	0.5
*SiO_3^{2-}	0.4	Ca^{2+}	0.6
$H_3SiO_4^-$	0.4	Mg^{2+}	0.8
$H_2SiO_4^{2-}$	0.4	**CaL^-	0.35
$HSiO_4^{3-}$	0.4	**MgL^-	0.35

*Data obtained by the estimation using carbonate and sulfate ions as reference.
** Data obtained by the estimation using H_2L^- ion as reference. L represents citrate.

Table 4.7 Calculated activity coefficients of ions in synthetic brine (I=0.0478 M)

Ions	γ	Ion	γ
H^+	0.935	SiO_4^{4-}	0.250
OH^-	0.915	SO_4^{2-}	0.707
HCO_3^-	0.917	H_2L^-	0.917
CO_3^{2-}	0.714	HL^{2-}	0.715
$HSiO_3^-$	0.917	L^{3-}	0.478
SiO_3^{2-}	0.707	Ca^{2+}	0.732
$H_3SiO_4^-$	0.917	Mg^{2+}	0.753
$H_2SiO_4^{2-}$	0.707	CaL^-	0.915
$HSiO_4^{3-}$	0.459	MgL^-	0.915

Both $-AlO^-$ and $-SiO^-$ sites can adsorb divalent cations. In the surface adsorption of divalent cations, these two sites are not distinguishable. In Eq. [4.13], $-AlO^-$ and $-SiO^-$ sites having the same equilibrium constant is assumed. For positively charged sites, $-AlOH_2^+$ and $-SiOH_2^+$ sites having the same equilibrium constant for adsorption of anions is also assumed.

Here the adsorption of $HSiO_3^-$ ion is considered instead of SiO_3^{2-} ion, because the concentration of $HSiO_3^-$ ion is much higher than SiO_3^{2-} ion in the brine. For the similar reason, $H_3SiO_4^-$ ion and $C_6H_5O_7^{3-}$ ion have the highest concentration and are considered in the adsorption. For weak electrolyte, such as SiO_3^{2-} ion, ion dissociation equilibrium needs to be considered.

$$H_2SiO_3 \rightleftharpoons H^+ + HSiO_3^- \qquad\qquad\qquad [4.14]$$

$$HSiO_3^- \rightleftharpoons H^+ + SiO_3^{2-} \qquad\qquad\qquad [4.15]$$
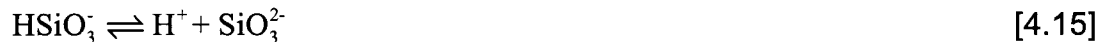
$$\frac{a_{H^+} a_{HSiO_3^-}}{a_{H_2SiO_3}} = K_{a1} \, , \quad \frac{a_{H^+} a_{SiO_3^{2-}}}{a_{HSiO_3^-}} = K_{a2} \qquad\qquad [4.16]$$

If more than one cation or anion adsorb on the surface, all the possible reactions need to be considered. Table 4.5 shows equilibrium constants of different species in bulk solution [24], [25].

The ionic strength of synthetic brine is 0.0478 M. For nonionic solute (e.g. H_2SiO_3), the concentration is low enough to consider the activity coefficient as 1.0. But for ions, the activity coefficients need to be calculated using extended

Chapter 4

Debye-Hückel equation (Eq. [4.17]) [26]. Table 4.6 shows the effective diameter of

the ions in the synthetic brine [26].

$$\log(\gamma_i) = -\frac{0.509 z_i^2 \sqrt{I}}{1 + 0.328 a_i \sqrt{I}} \qquad\qquad I = \frac{1}{2}\sum_i c_i z_i^2 \qquad\qquad [4.17]$$

γ_i: activity coefficient of ion species i.

z_i: valency of ion species i.

a_i: effective diameter of the hydrated ion species i, in units of Å.

I: ionic strength of the aqueous solution, in units of mol/kg.

c_i: concentration of ion species i, in units of mol/kg.

Table 4.7 shows the calculated activity coefficient of ions at the ionic strength

of synthetic brine.

4.3.3. Materials and methods

The aqueous phase used here is synthetic brine with pH 8.3, as introduced in

section 4.2.1. Kaolinite ($Al_2Si_2O_5(OH)_4$) is obtained from Sigma-Aldrich with

detailed information in section 4.2.1. Alumina (Al_2O_3) is obtained from

Sigma-Aldrich (product #19944-3), with particle size 150 mesh (104 μm), pore

size 5.8 nm and specific surface area 155 m²/g. All the salts in the synthetic brine

were obtained from Fisher Scientific.

All the samples of 50 ml 1.0 % (w/w) kaolinite or alumina suspension were

prepared in the brine with different additives. Branson Sonic Probe 450 was used for the sonication of the mixture (probe tip was placed about 1/2" into the solution, sonication rate at setting 4 for 1 minute). The mixture was left overnight. Before measurement the mixture was shaken and settled for 30 minutes to allow the sedimentation of larger particles and get stable suspension. Beckman Coulter Delsa 440 Doppler electrophoretic light scattering analyzer was used to measure zeta potential of kaolinite or alumina in the brine.

Standard mobility solution (conductivity 1000 mS/cm, mobility -4 $\mu m \cdot cm/V \cdot s$, Beckman Coulter, PN# 8301351) was measured at different position levels for calibration. The measured value at upper and lower stationary levels (84% and 16% of the depth) reflect the true mobility of the solution [17]. Kaolinite or alumina sample was measured at lower and upper stationary levels for three times respectively. The average value of zeta potentials of lower and upper stationary levels was chosen as the zeta potential value of the sample. Appendix B shows detailed procedure of zeta potential measurement.

4.3.4. Effects of additives on kaolinite zeta potential in synthetic brine

Kaolinite zeta potentials in synthetic brine with different additives were measured, as shown in Figure 4.16, to characterize wettability change of kaolinite. For all the samples, zeta potentials are more negative without Ca/ Mg ions

than with Ca/ Mg ions. The reason may be the adsorptions of Ca/ Mg ions on the

negatively charged surface sites of kaolinite. When Ca/ Mg ions adsorb on the

surface of kaolinite, the negatively-charged sites will become positively- charged.

Thus the net surface charge of kaolinite will become less negative. In the figure,

zeta potential will becomes more negative when adding sodium hydroxide,

sodium silicate, sodium citrate or sodium carbonate.
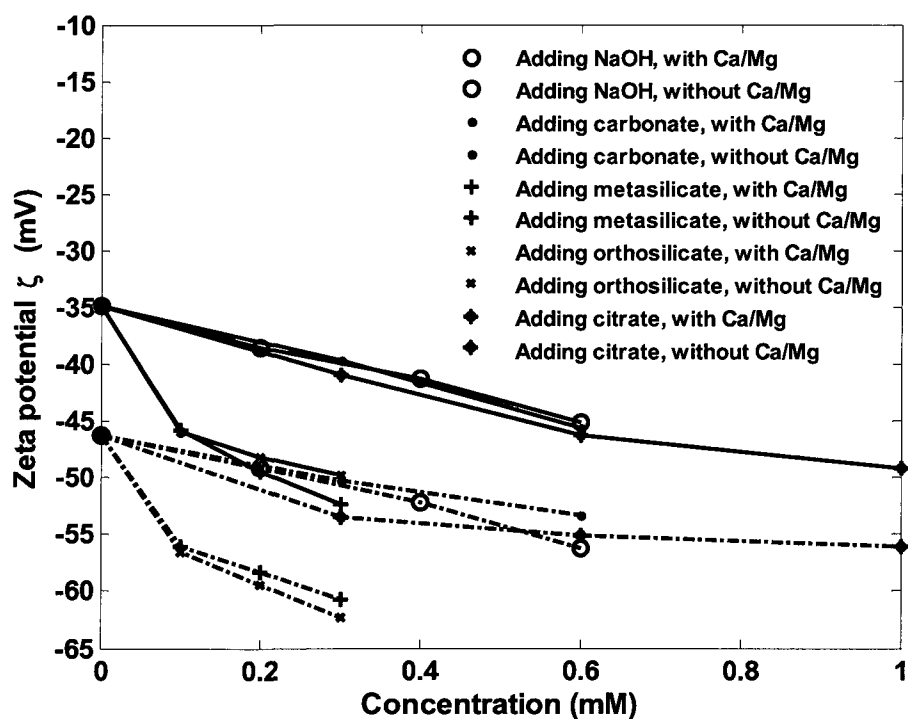
Figure 4.16 Zeta potentials of kaolinite in synthetic brine with different additives

Figure4.17 shows the zeta potential change (mV/mM) as the function of

additive concentration. Central difference method is used for calculation.

$$\frac{\Delta \zeta}{\Delta c}(\frac{c_1 + c_2}{2}) = \frac{\zeta(c_2) - \zeta(c_1)}{c_2 - c_1}$$

[4.18]

Here ζ is zeta potential and c is concentration of the additive.
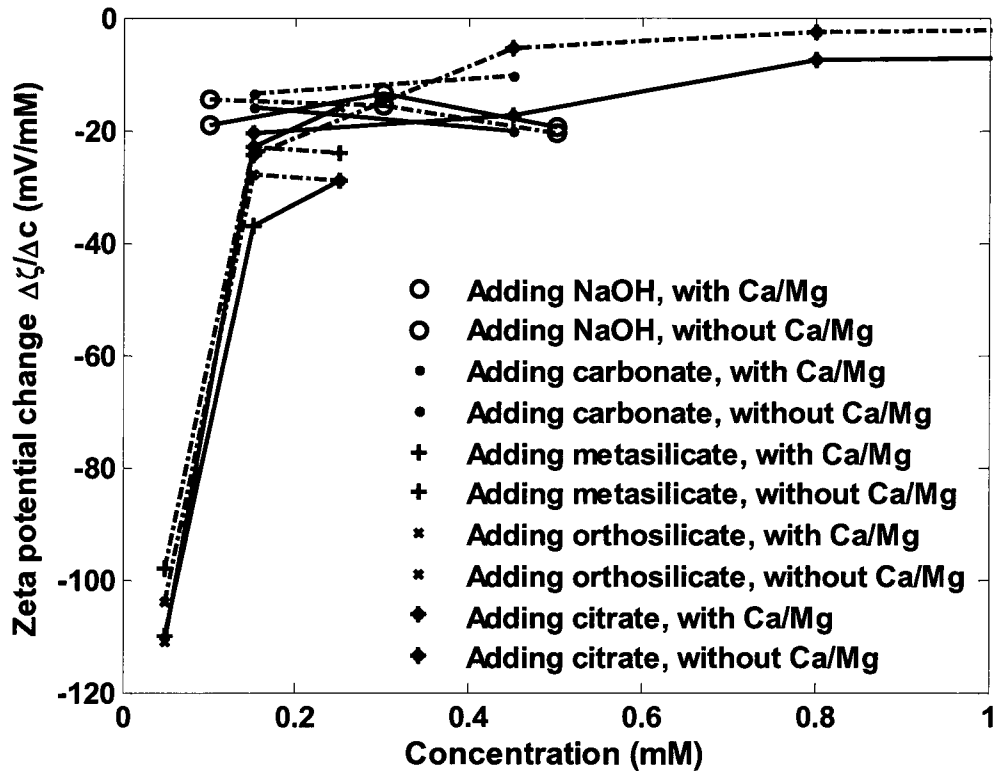
Figure 4.17 Zeta potentials change of kaolinite samples in synthetic brine

For hydroxide, citrate and carbonate, zeta potential change per unit additive concentration is around 15 - 25 mV/mM. But for meta- silicate or ortho-silicate, zeta potential change is much larger than other additives at low concentration ($<10^{-4}$ M). And zeta potential change decreases very fast with the increase of silicate concentration. Compare with other anions, silicate ions have the greatest effect per unit addition on changing zeta potential of kaolinite.

Chapter 4

4.3.5. Model parameters evaluation and experiment data correlation

In order to correlate zeta potentials of kaolinite in synthetic brine, parameter values in the model are required. In synthetic brine, the effects of pH, SO_4^{2-}, HCO_3^-, Ca^{2+} and Mg^{2+} need to be considered. Since Na^+ and Cl^- are indifferent ions, zeta potential measurements of kaolinite in NaCl brine or de-ionized water with different cations and anions are performed to obtain parameter values in the model.

4.3.5.1. Surface site density and dissociation constant

To get surface site density and dissociation constants, zeta potentials of kaolinite in 0.05 M NaCl brine (the ionic strength is close to that of synthetic brine) at different pH were measured. Here HCl and NaOH were used to adjust the pH. Equations for charge density and site dissociation equilibrium of kaolinite are:

$$\sigma_0 = e([AlOH_2^+]-[AlO^-]+[SiOH_2^+]-[SiO^-]-[B^-]) \tag{4.19}$$

$$[AlOH_2^+] = \frac{[AlOH]a_b(H^+)\exp(-\dfrac{e\zeta}{kT})}{K_{Al+}} \tag{4.20}$$

$$[AlOH] = \frac{[AlO^-]a_b(H^+)\exp(-\dfrac{e\zeta}{kT})}{K_{Al-}} \tag{4.21}$$

$$[SiOH_2^+] = \frac{[SiOH]a_b(H^+)\exp(-\dfrac{e\zeta}{kT})}{K_{Si+}} \tag{4.22}$$

$$[\text{SiOH}] = \frac{[\text{SiO}^-]a_b(\text{H}^+)\exp(-\frac{e\zeta}{kT})}{K_{\text{Si-}}}$$ [4.23]

$$[\text{AlO}^-] = \frac{N_{\text{Al}}}{1 + \frac{1}{K_{\text{Al-}}}a_b(\text{H}^+)\exp(-\frac{e\zeta}{kT}) + \frac{1}{K_{\text{Al+}}K_{\text{Al-}}}[a_b(\text{H}^+)\exp(-\frac{e\zeta}{kT})]^2}$$ [4.24]

$$[\text{AlOH}_2^+] = \frac{\frac{N_{\text{Al}}}{K_{\text{Al+}}K_{\text{Al-}}}[a_b(\text{H}^+)\exp(-\frac{e\zeta}{kT})]^2}{1 + \frac{1}{K_{\text{Al-}}}a_b(\text{H}^+)\exp(-\frac{e\zeta}{kT}) + \frac{1}{K_{\text{Al+}}K_{\text{Al-}}}[a_b(\text{H}^+)\exp(-\frac{e\zeta}{kT})]^2}$$ [4.25]

$$[\text{SiO}^-] = \frac{N_{\text{Si}}}{1 + \frac{1}{K_{\text{Si-}}}a_b(\text{H}^+)\exp(-\frac{e\zeta}{kT}) + \frac{1}{K_{\text{Si+}}K_{\text{Si-}}}[a_b(\text{H}^+)\exp(-\frac{e\zeta}{kT})]^2}$$ [4.26]

$$[\text{SiOH}_2^+] = \frac{\frac{N_{\text{Si}}}{K_{\text{Si+}}K_{\text{Si-}}}[a_b(\text{H}^+)\exp(-\frac{e\zeta}{kT})]^2}{1 + \frac{1}{K_{\text{Si-}}}a_b(\text{H}^+)\exp(-\frac{e\zeta}{kT}) + \frac{1}{K_{\text{Si+}}K_{\text{Si-}}}[a_b(\text{H}^+)\exp(-\frac{e\zeta}{kT})]^2}$$ [4.27]

Here K (K_{Al1}, K_{Al2}, K_{Si1} and K_{Si2}) N (N_{Al}, N_{Si} and N_{B}) are equilibrium constants

and surface sites densities, respectively, which can be obtained by fitting with the

experiment data. From Eqs. [4.19] - [4.27], zeta potential ζ_{cal} can be calculated

from the initial evaluates of K and N. Parameters estimation was done using

Matlab optimization toolbox. The object function to be determined is $\parallel \zeta_{\text{cal}} - \zeta_{\text{exp}} \parallel$.

Iteration terminates when $\parallel \zeta_{\text{cal}} - \zeta_{\text{exp}} \parallel <$ tolerance.

Figure 4.18 shows the experiment data and fitted curve of kaolinite zeta

potentials in 0.05 M NaCl brine at different pH. Zeta potential of kaolinite becomes

more negative with the increase of pH. Table 4.8 shows the calculated parameters from data fitting. The total amphoteric sites (N_{Al} + N_{Si}) have density 2.33 ×10^{-7} mol/m^2 (0.14 site/nm^2). Williams *et al.* used cation exchange capacity titration method to get amphoteric charge density [27]. The values are from -3 μC/cm^2 to -25 μC/cm^2 (site density 3.1×10^{-7} mol/m^2 - 2.6×10^{-6} mol/m^2). The fitted site density is close to the lower bound of literature value.
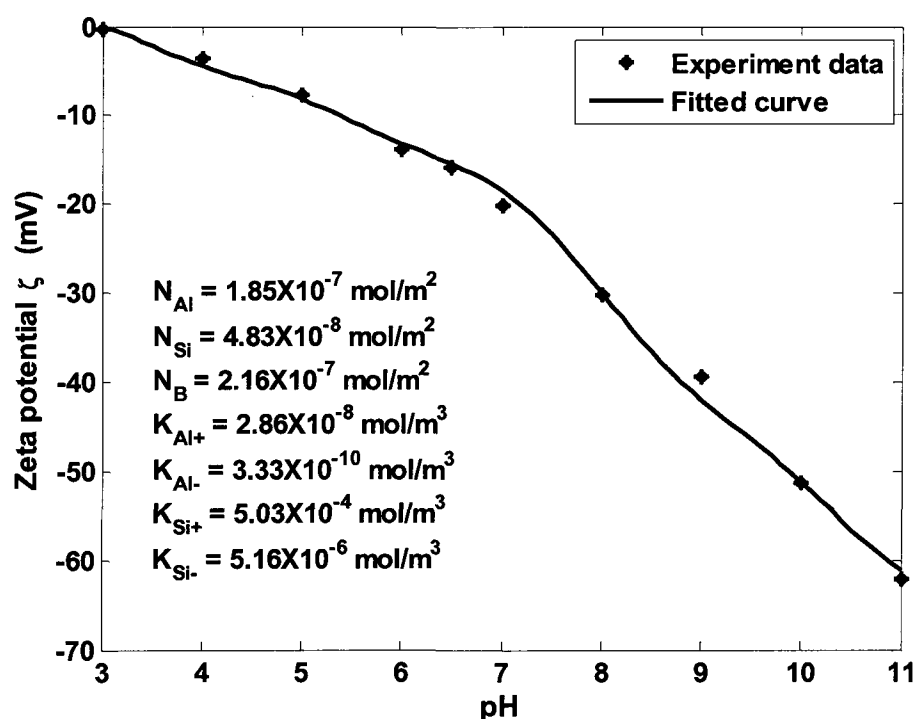
Figure 4.18 Zeta potential of kaolinite in 0.05 M NaCl brine at different pH

Figs. 4.19 and 4.20 show the sites fraction of –AOH, –AO⁻ and –AOH₂⁺ (A can be Al or Si) in –SiOH and –AlOH sites as the function of bulk pH in 0.05 M NaCl. As pH increases, the fraction of positively charged sites –AOH₂⁺ will

decrease; the fraction of negatively charged sites $-AO^-$ will increase. At pH 8 - 9, almost all silica sites are negatively charged; for alumina site, the fraction of positively charged site is higher than negatively charged site.

Table 4.8 Kaolinite surface site densities and dissociation constants

Reaction	K (mol/m^3)	N (10^{-8} mol/m^2)
$-AlOH_2^+ \rightleftharpoons -AlOH + H^+$	2.86×10^{-8}	18.5
$-AlOH \rightleftharpoons -AlO^- + H^+$	3.33×10^{-10}	
$-SiOH_2^+ \rightleftharpoons -SiOH + H^+$	5.03×10^{-4}	4.83
$-SiOH \rightleftharpoons -SiO^- + H^+$	5.16×10^{-6}	
Inert sites		21.6
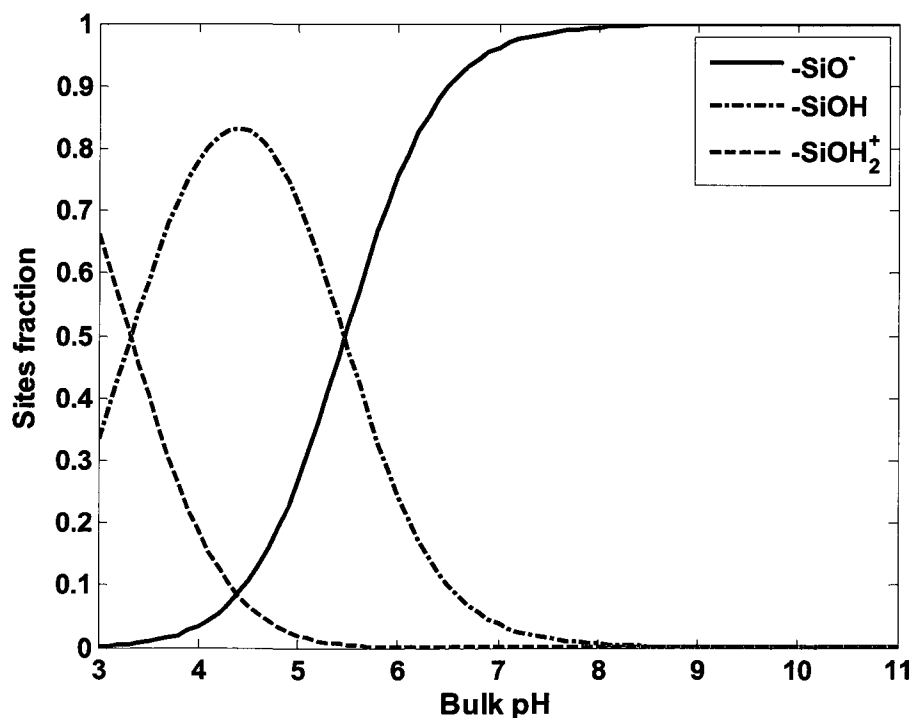
Figure 4.19 Silica sites fraction in kaolinite at different bulk pH in 0.05 M NaCl

Figure 4.20 Alumina sites fraction in kaolinite at different bulk pH in 0.05 M NaCl

In section 4.3.2, amphoteric silica and alumina sites on kaolinite surface is assumed. Based on the results of Figs. 4.19 and 4.20, above pH 8, silica sites are negatively charged, alumina sites are dependent of pH. To verify the assumption, zeta potentials of alumina in 0.05 M NaCl brine at different pH are measured. Equations for charge density and site dissociation equilibrium of alumina are:

$$\sigma_0 = e([AlOH_2^+] - [AlO^-]) \qquad [4.28]$$

$$[AlOH_2^+] = \frac{[AlOH]a_b(H^+)\exp(-\frac{e\zeta}{kT})}{K_{Al+}} \qquad [4.29]$$

$$[\text{AlOH}] = \frac{[\text{AlO}^-]a_b(\text{H}^+)\exp(-\frac{e\zeta}{kT})}{K_{\text{Al-}}}$$

[4.30]

Figure 4.21 shows the experiment data and fitted curve of alumina zeta potentials in 0.05 M NaCl brine at different pH. Zeta potential of alumina changes from positive to negative with the increase of pH. Dashed line shows zero zeta potential value as reference.
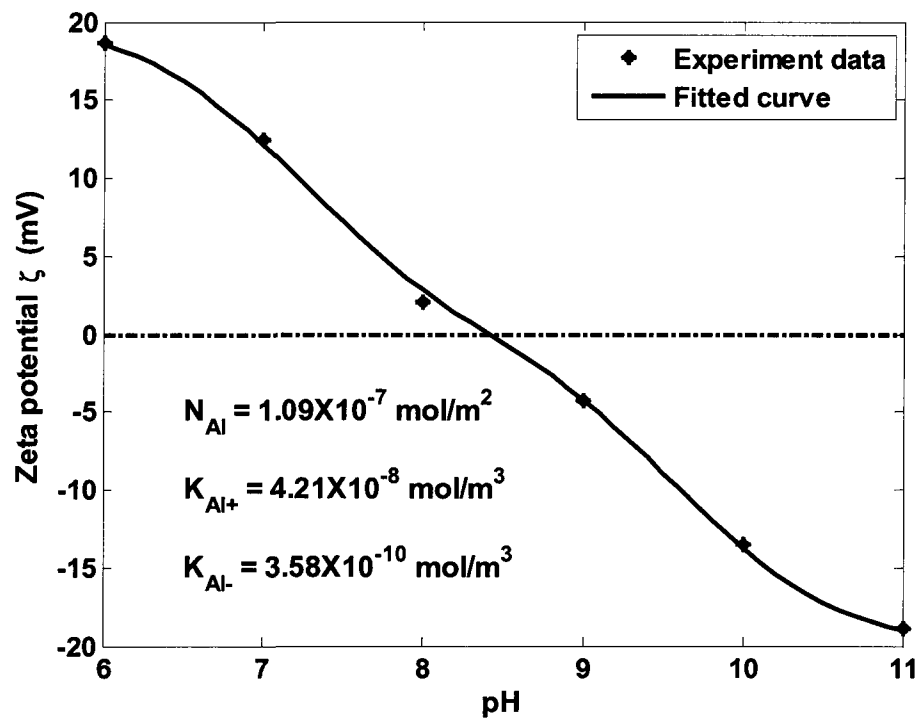
Figure 4.21 Zeta potential of alumina in 0.05 M NaCl brine at different pH

Table 4.9 shows the calculated parameters from data fitting. Dissociation equilibrium constants and site density of alumina are 4.21×10^{-8} mol/m^3, 3.58×10^{-10} mol/m^3 and 1.09×10^{-7} mol/m^2, respectively. For alumina sites on kaolinite, the

values are 2.86×10^{-8} mol/m^3, 3.33×10^{-10} mol/m^3 and 1.85×10^{-7} mol/m^2, respectively. For amphoteric alumina sites, kaolinite has the same magnitude of dissociation equilibrium constants and site density as alumina. This indicates kaolinite has similar amphoteric alumina sites to alumina and validates the assumption in section 4.3.2.

Table 4.9 Alumina site densities and dissociation constants

Reaction	K (mol/m^3)	N (10^{-8} mol/m^2)
$-AlOH_2^+ \rightleftharpoons -AlOH + H^+$	4.21×10^{-8}	10.9
$-AlOH \rightleftharpoons -AlO^- + H^+$	3.58×10^{-10}	
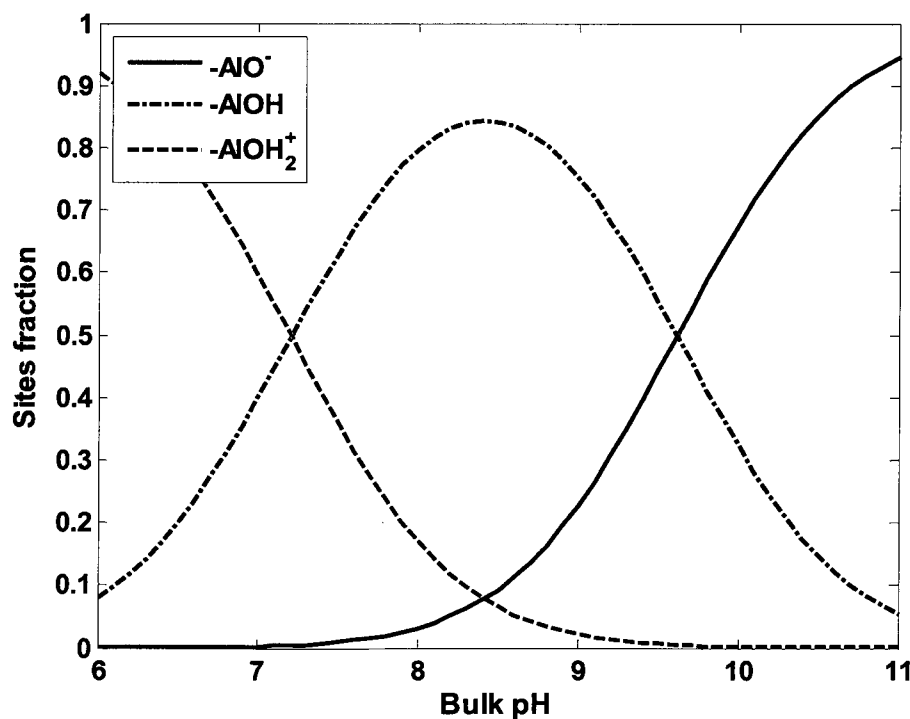
Figure 4.22 Alumina sites fraction at different bulk pH in 0.05 M NaCl

Chapter 4

Figure 4.22 shows the sites fraction of –AlOH, –AlO⁻ and –AlOH₂+ sites as the function of bulk pH in 0.05 M NaCl. As pH increases, the fraction of positively charged sites $-AlOH_2^+$ will decrease; the fraction of negatively charged sites –AlO⁻ will increase. This is similar to kaolinite in Figure 4.20.

4.3.5.2. Adsorption effect of anions SO_4^{2-} and HCO_3^-

Synthetic brine contains anions SO_4^{2-} and HCO_3^-. Zeta potentials of kaolinite in 0.05 M NaCl brine adding Na_2SO_4 at pH 6.5 were measured to study the effect of sulfate. In 0.05 M NaCl brine at pH 6.5, positively charged sites $-AOH_2^+$ (A can be Al or Si) can adsorb SO_4^{2-} ion and become negatively charged sites $-AOH_2SO_4^-$.

$$-AOH_2^+ + SO_4^{2-} \rightleftharpoons -AOH_2SO_4^- \qquad [4.31]$$

$$K_{SO_4} = \frac{[AOH_2SO_4^-]}{[AOH_2^+]a_s(SO_4^{2-})} = \frac{[AOH_2SO_4^-]}{[AOH_2^+]a_b(SO_4^{2-})\exp(\frac{2e\zeta}{kT})} \qquad [4.32]$$

$$\sigma_0 = e([AOH_2^+] - [AO^-] - [B^-] - [AOH_2SO_4^-]) \qquad [4.33]$$

Here K_{SO_4} is the adsorption equilibrium constant.

Using the similar method discussed in section 4.3.5.1, based on Eqs [4.6], [4.32] and [4.33], adsorption equilibrium constant can be calculated from experiment data. For the adsorption of other ions, similar method can be used to evaluate adsorption equilibrium constant. Figure 4.23 shows zeta potential of

kaolinite as the function of Na$_2$SO$_4$ concentration in 0.05 M NaCl brine at pH 6.5. The adsorption constant K_{SO4} is 0.195 m^3/mol.
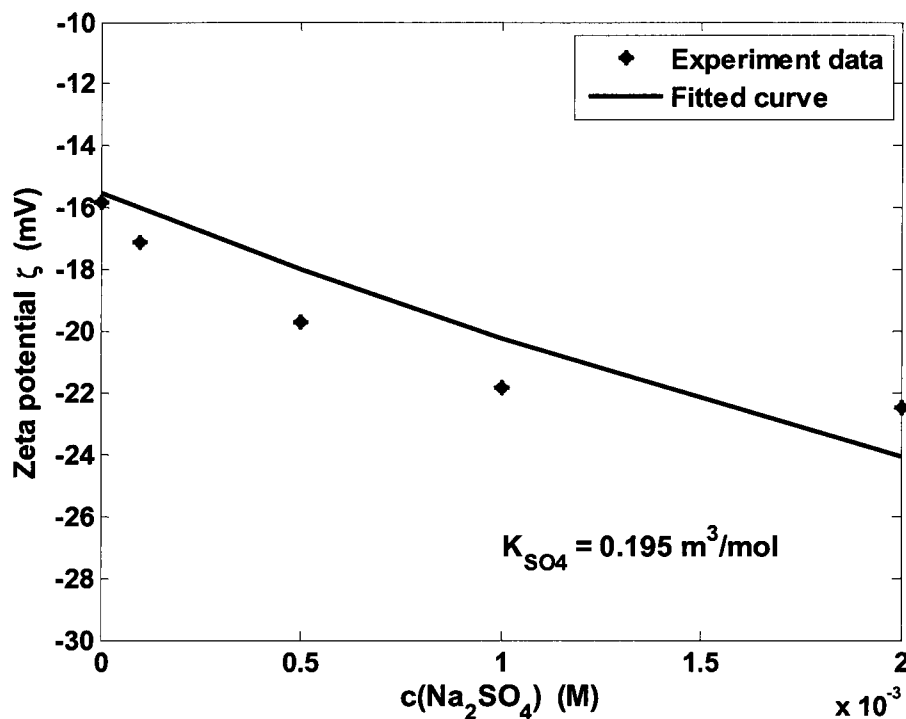
Figure 4.23 Kaolinite zeta potential in 0.05 M NaCl brine adding Na$_2$SO$_4$ at pH 6.5

In order to study the effect of bicarbonate, zeta potentials of kaolinite with different NaHCO$_3$ in de-ionized water at pH 8.3 were measured. In NaHCO$_3$ solution, positively charged sites –AOH$_2^+$ can adsorb HCO$_3^-$ ion and become neutral sites –AOH$_2$HCO$_3$.

$$-\text{AOH}_2^+ + \text{HCO}_3^- \rightleftharpoons -\text{AOH}_2\text{HCO}_3 \qquad [4.34]$$

$$K_{\text{HCO}_3} = \frac{[\text{AOH}_2\text{HCO}_3]}{[\text{AOH}_2^+]a_s(\text{HCO}_3^-)} = \frac{[\text{AOH}_2\text{HCO}_3]}{[\text{AOH}_2^+]a_b(\text{HCO}_3^-)\exp(\frac{e\zeta}{kT})} \qquad [4.35]$$

$$\sigma_0 = e([AOH_2^+]-[AO^-]-[B^-]) \qquad\qquad [4.36]$$

Here $KHCO_3$ is the adsorption equilibrium constant.
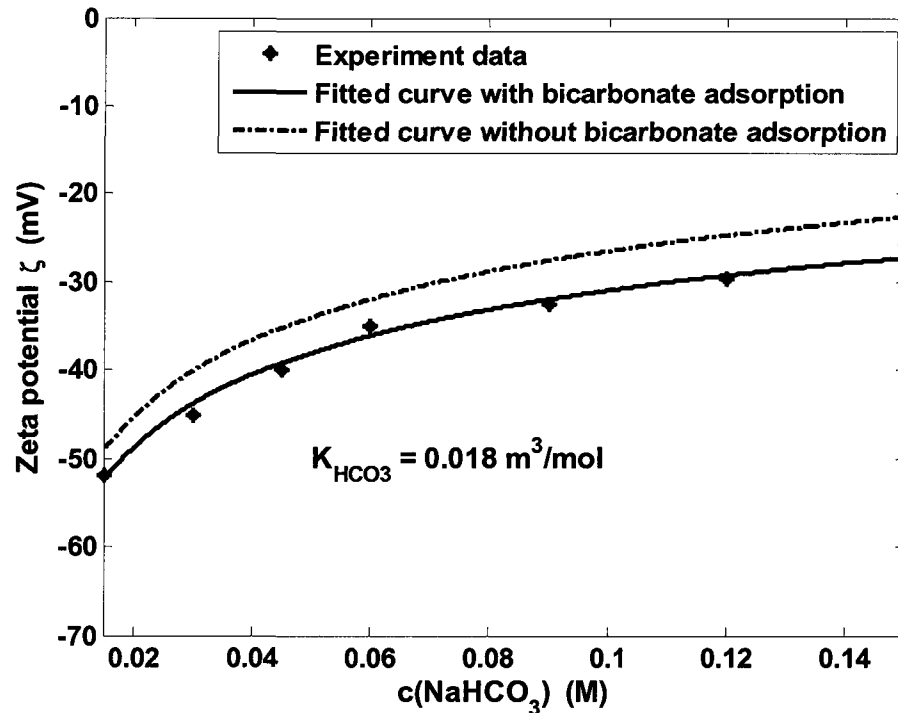
Figure 4.24 Kaolinite zeta potential adding $NaHCO_3$ in de-ionized water at pH 8.3

Figure 4.24 shows zeta potential of kaolinite as the function of $NaHCO_3$ concentration at bulk pH 8.3. With the increase concentration of $NaHCO_3$, zeta potential becomes less negative. This is due to the increase of ionic strength. The dashed curve shows the fitted results assuming no HCO_3^- ion adsorption. The deviation of experiment data and fitted result indicates the effect of HCO_3^- ion adsorption. The solid curve shows the fitted results assuming HCO_3^- ion adsorption and the adsorption constant K_{HCO3} is 0.018 m^3/mol. The fitted curve

assuming HCO_3^- ion adsorption is closer to the experiment data than the curve without assuming HCO_3^- ion adsorption.

From zeta potential result, anions SO_4^{2-} or HCO_3^- can adsorb on positively charged surface sites and make kaolinite zeta potential more negative.

4.3.5.3. Adsorption effect of cations Ca^{2+} and Mg^{2+}

Synthetic brine contains cations Ca^{2+} and Mg^{2+}. The negatively charged Al/ Si sites $-AO^-$ can adsorb Ca/ Mg ions and become positively charged.
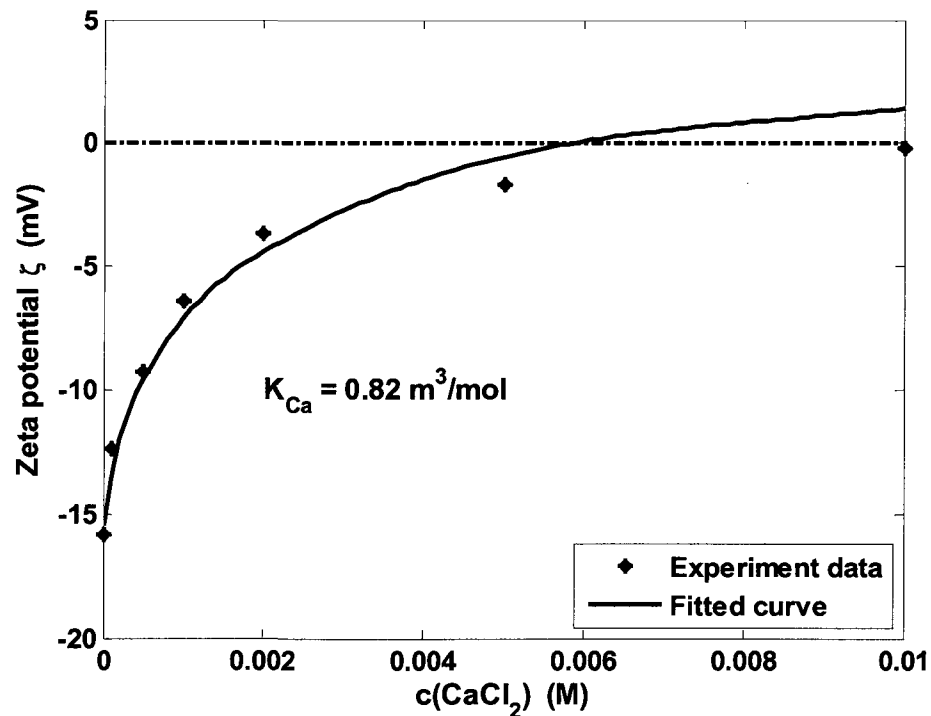
Figure 4.25 Kaolinite zeta potential in 0.05 M NaCl brine adding $CaCl_2$ at pH 6.5

In order to study the effect of Ca/ Mg ions, zeta potentials of kaolinite in 0.05

M NaCl brine adding $CaCl_2$ or $MgCl_2$ at pH 6.5 were measured.

$$-AO^- + Ca^{2+} \rightleftharpoons -AOCa^+, \quad -AO^- + Mg^{2+} \rightleftharpoons -AOMg^+ \qquad [4.37]$$
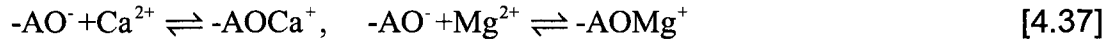
$$K_{Ca} = \frac{[AOCa^+]}{[AO^-]a_s(Ca^{2+})} = \frac{[AOCa^+]}{[AO^-]a_b(Ca^{2+})\exp(-\frac{2e\zeta}{kT})} \qquad [4.38]$$

$$K_{Mg} = \frac{[AOMg^+]}{[AO^-]a_s(Mg^{2+})} = \frac{[AOMg^+]}{[AO^-]a_b(Mg^{2+})\exp(-\frac{2e\zeta}{kT})} \qquad [4.39]$$

$$\sigma_0(Ca) = e([AOH_2^+]-[AO^-]-[B^-]+[AOCa^+]) \qquad [4.40]$$

$$\sigma_0(Mg) = e([AOH_2^+]-[AO^-]-[B^-]+[AOMg^+]) \qquad [4.41]$$

Here K_{Ca} and K_{Mg} are surface adsorption equilibrium constants.
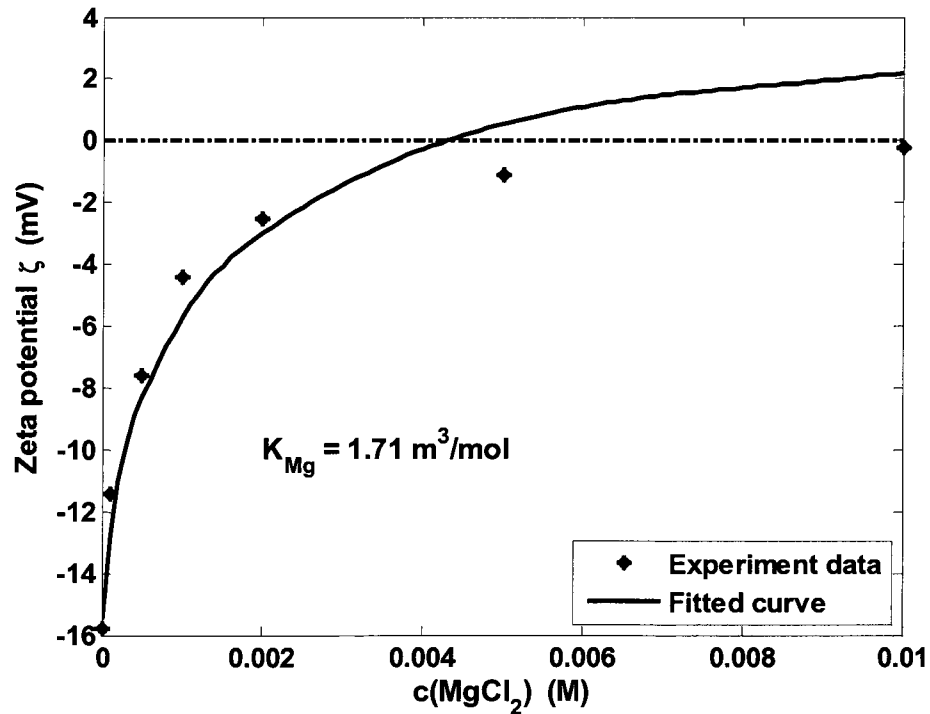
Figure 4.26 Kaolinite zeta potential in 0.05 M NaCl brine adding $MgCl_2$ at pH 6.5

Chapter 4

Using the similar method, adsorption equilibrium constants and surface sites density can be calculated from experiment data. Figs. 4.25 and 4.26 show kaolinite zeta potential as the function of $CaCl_2$ / $MgCl_2$ concentration in 0.05 M NaCl brine at pH 6.5. Dashed line shows zero zeta potential value as reference.

The equilibrium constant of Ca^{2+} ion K_{Ca} is 0.82 m^3/mol. The equilibrium constant of Mg^{2+} ion K_{Mg} is 1.71 m^3/mol. From zeta potential result, cations Ca^{2+} and Mg^{2+} can adsorb on negatively charged surface sites and make zeta potential of kaolinite less negative.

4.3.5.4. Effect of synthetic brine pH

Based on the site density and dissociation constant of kaolinite, zeta potential can be calculated at different pH. Figure 4.27 shows zeta potential of kaolinite in synthetic brine with or without Ca/ Mg ions adding NaOH at different pH.

In the brine with Ca/ Mg, based on the solubility product calculation, Ca^{2+} and CO_3^{2-} ions may form $CaCO_3$ precipitation, which will reduce the concentration of Ca^{2+}. The blue dashed curve shows the calculated zeta potential of kaolinite without Ca/ Mg. The red solid curve shows the calculated zeta potential of kaolinite with Ca/ Mg, with equilibrium Ca^{2+} concentration calculated from $CaCO_3$ solubility product. Increase of pH can make kaolinite zeta potential more negative. Adding NaOH, zeta potential change of kaolinite is around 15-20 mV/mM.

Increasing pH can enhance the dissociation of surface sites and make net surface charge more negative, hereby kaolinite zeta potential will become more negative.
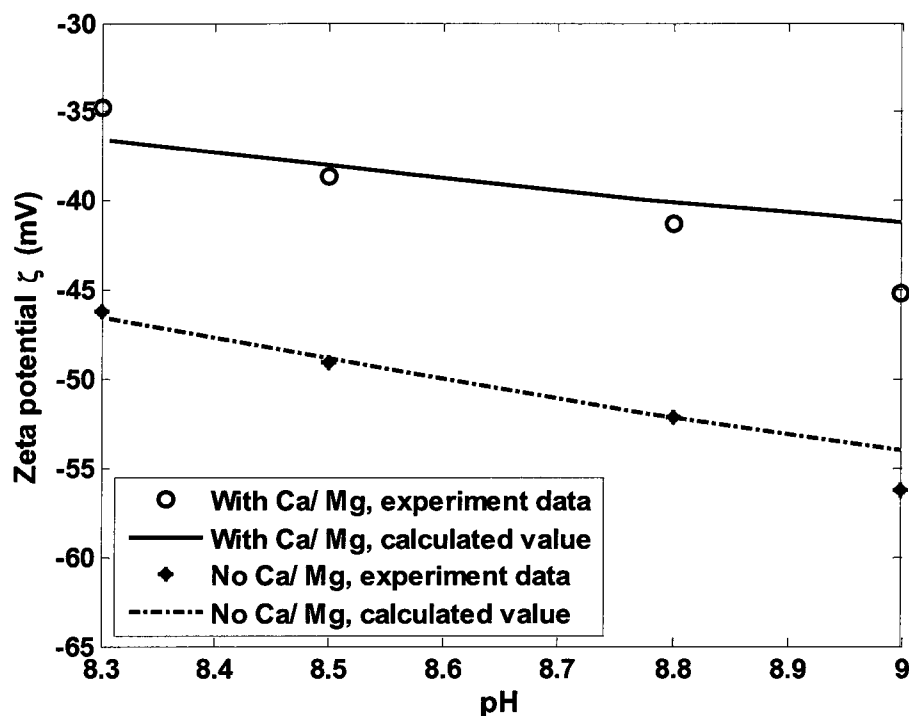
Figure 4.27 Kaolinite zeta potential in synthetic brine adding NaOH at different pH

4.3.5.5. Effect of carbonate

Carbonate has two effects on the zeta potential of kaolinite. Adding carbonate can increase pH and the concentration of HCO_3^- ion, which can make zeta potential of kaolinite more negative. Here only the adsorption of HCO_3^- ion is considered instead of CO_3^{2-} ion, because the concentration of HCO_3^- ion is much higher than CO_3^{2-} ion in the brine. Carbonate can also precipitate Ca^{2+} ion, which can also make zeta potential of kaolinite more negative.

Chapter 4

Figure 4.28 shows zeta potential of kaolinite in synthetic brine with or without Ca/ Mg adding Na_2CO_3. Adding 6.0×10^{-4} M Na_2CO_3, pH of the brine increases from 8.3 to 8.9. The blue dashed curve shows the calculated zeta potential of kaolinite without Ca/ Mg. The red solid curve shows the calculated zeta potential of kaolinite with Ca/ Mg, with equilibrium Ca^{2+} concentration calculated from $CaCO_3$ solubility product.
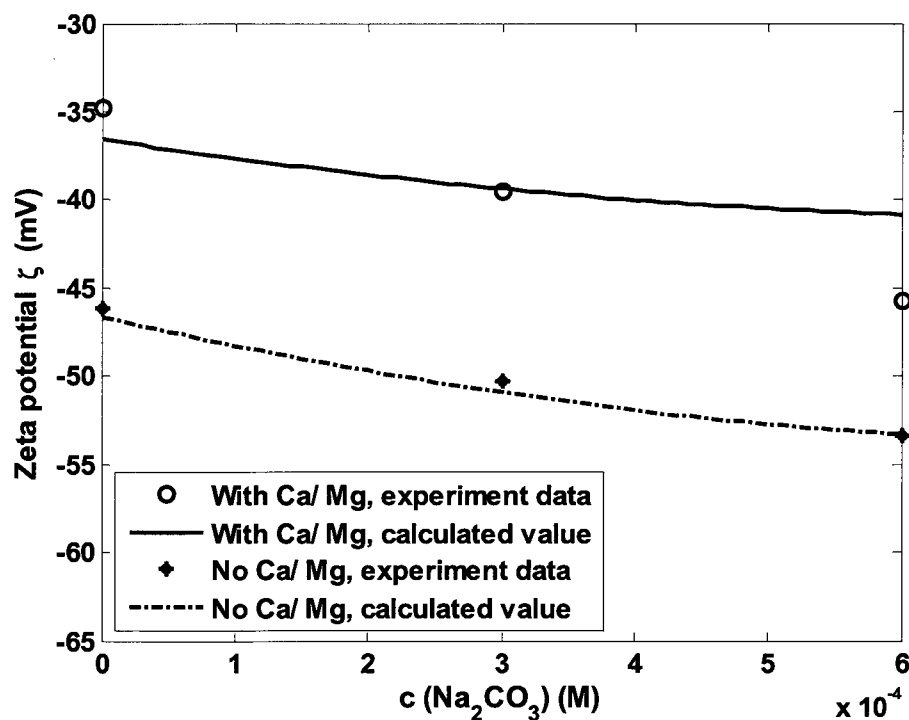
Figure 4.28 Kaolinite zeta potential in synthetic brine adding Na_2CO_3, pH 8.3 - 8.9

In the brine without Ca/ Mg, zeta potential change of kaolinite is around 15 mV/mM. In the brine with Ca/ Mg, zeta potential change of kaolinite is around 20 mV/mM. The precipitation of Ca^{2+} ion can make kaolinite zeta potential more

negative. Thus zeta potential change per unit addition in synthetic brine with Ca/ Mg (20 mV/mM) is greater than that in the brine without Ca/ Mg (15 mV/mM).

4.3.5.6. Effects of silicates

Silicate has two effects on the zeta potential of kaolinite. Adding silicate can increase the pH of the brine, which can make zeta potential of kaolinite more negative. Silicate can also adsorb on the positively charged sites $-AOH_2^+$, which can also make zeta potential of kaolinite more negative.

In synthetic brine, positively charged sites $-AOH_2^+$ can adsorb $HSiO_3^-$ or $H_3SiO_4^-$ ion and become neutral sites. Eqs. [4.42] - [4.47] give the surface reaction and equilibrium equation. Here only the adsorption of $HSiO_3^-$ or $H_3SiO_4^-$ ion is considered, because the concentration of monovalent ion is much higher than other silicate ions with higher valency.

$$-AOH_2^+ + HSiO_3^- \rightleftharpoons -AOH_2HSiO_3 \qquad [4.42]$$

$$K_{HSiO_3} = \frac{[AOH_2HSiO_3]}{[AOH_2^+]a_s(HSiO_3^-)} = \frac{[AOH_2HSiO_3]}{[AOH_2^+]a_b(HSiO_3^-)\exp(\frac{e\zeta}{kT})} \qquad [4.43]$$

$$\sigma_0 = e([AOH_2^+] - [AO^-] - [B^-]) \qquad [4.44]$$

$$-AOH_2^+ + H_3SiO_4^- \rightleftharpoons -AOH_2H_3SiO_4 \qquad [4.45]$$

$$K_{H_3SiO_4} = \frac{[AOH_2H_3SiO_4]}{[AOH_2^+]a_s(H_3SiO_4^-)} = \frac{[AOH_2H_3SiO_4]}{[AOH_2^+]a_b(H_3SiO_4^-)\exp(\frac{e\zeta}{kT})} \qquad [4.46]$$

$$\sigma_0 = e([AOH_2^+] - [AO^-] - [B^-]) \qquad [4.47]$$

Figs.4.29 and 4.30 show zeta potential of kaolinite in synthetic brine adding

Na_2SiO_3 or Na_4SiO_4. The blue dashed curve shows the fitted zeta potential of

kaolinite without Ca/ Mg. The red solid curve shows the fitted zeta potential of

kaolinite with Ca/ Mg.
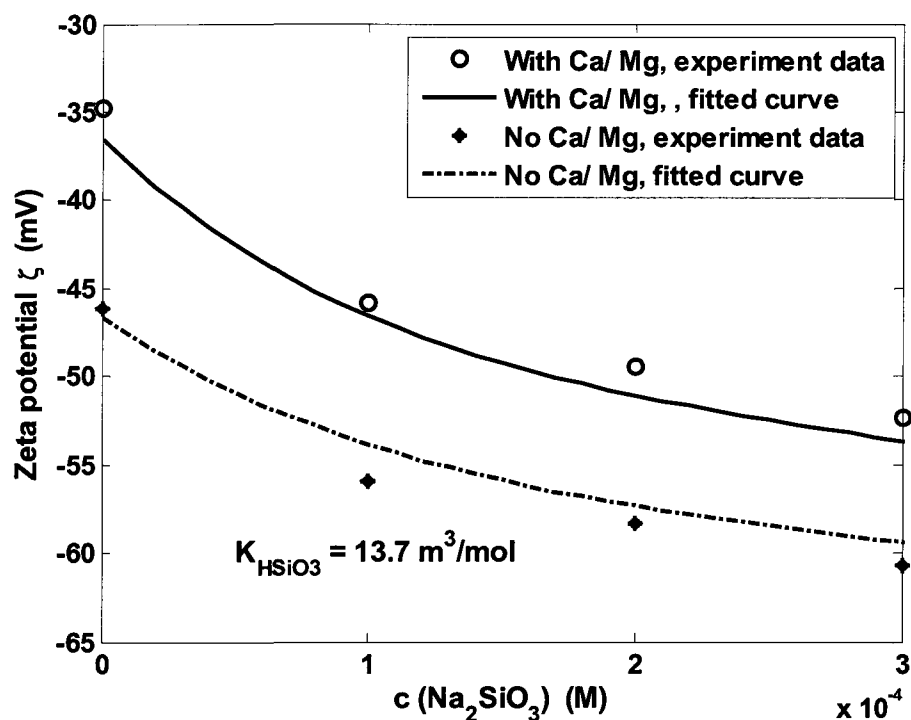
Figure 4.29 Kaolinite zeta potential in synthetic brine adding Na_2SiO_3, pH 8.3 - 9.0

At low concentration of silicate (0.05 mM), zeta potential change per unit

additive concentration is around 100 -110 mV/mM, which is about five times of

that adding sodium hydroxide (20 mV/mM). With the increase of silicate

concentration, zeta potential change per unit additive concentration decreases to

around 30 mV/mM. Meta-silicate and ortho-silicate have the similar effects on zeta

potential change of kaolinite. But adding meta-silicate has smaller effect on pH change than adding ortho-silicate. Adding 3.0×10^{-4} M Na_2SiO_3, pH of the brine increases from 8.3 to 9.0. Adding 3.0×10^{-4} M Na_4SiO_4, pH of the brine increases from 8.3 to 9.2. Equilibrium constants K_{HSiO3} and K_{H3SiO4} are 13.7 m^3/mol and 8.7 m^3/mol, respectively.
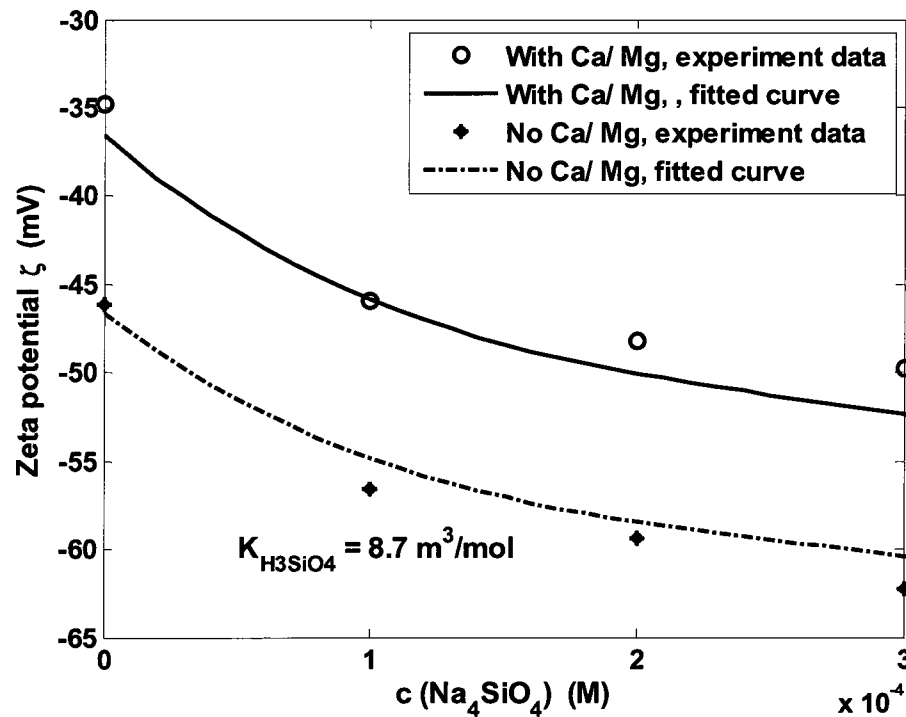
Figure 4.30 Kaolinite zeta potential in synthetic brine adding Na_4SiO_4, pH 8.3 - 9.2

4.3.5.7. Effects of citrate

Citrate can chelate Ca/ Mg ion (in Table 4.3), which can make zeta potential of kaolinite more negative. Citrate can also adsorb on the positively charged sites

$-AOH_2^+$, which can also make zeta potential of kaolinite more negative.

In synthetic brine, positively charged sites $-AOH_2^+$ can adsorb citrate ion $C_6H_5O_7^{3-}$ (L^{3-}) and become negatively charged sites $-AOH_2L^{2-}$. Here only the adsorption of L^{3-} ion is considered instead of other ions (HL^{2-} and H_2L^-) because in the brine the concentration of L^{3-} ion is much higher than other ions.

$$-AOH_2^+ + L^{3-} \rightleftharpoons -AOH_2L^{2-} \qquad [4.48]$$

$$K_L = \frac{[AOH_2L^{2-}]}{[AOH_2^+]a_s(L^{3-})} = \frac{[AOH_2L^{2-}]}{[AOH_2^+]a_b(L^{3-})\exp(\dfrac{3e\zeta}{kT})} \qquad [4.49]$$

$$\sigma_0 = e([AOH_2^+]-[AO^-]-[B^-]-2[AOH_2L^{2-}]) \qquad [4.50]$$

Figure 4.31 shows zeta potential of kaolinite in synthetic brine adding citrate. The blue dashed curve shows the fitted zeta potential of kaolinite without Ca/ Mg. The red solid curve shows the fitted zeta potential of kaolinite with Ca/ Mg. Adding citrate will not affect the pH of the brine. So the pH of synthetic brine stays 8.3 with different amount of citrate. With the increase of citrate concentration, zeta potential of kaolinite becomes more negative. At low citrate concentration (3×10^{-4} M), zeta potential change of kaolinite is around 20 mV/mM. But with the increase of citrate concentration, the decreasing tendency of zeta potential becomes saturated. Zeta potential change of kaolinite tends to zero. The equilibrium constant K_L is the 0.66 m^3/mol.
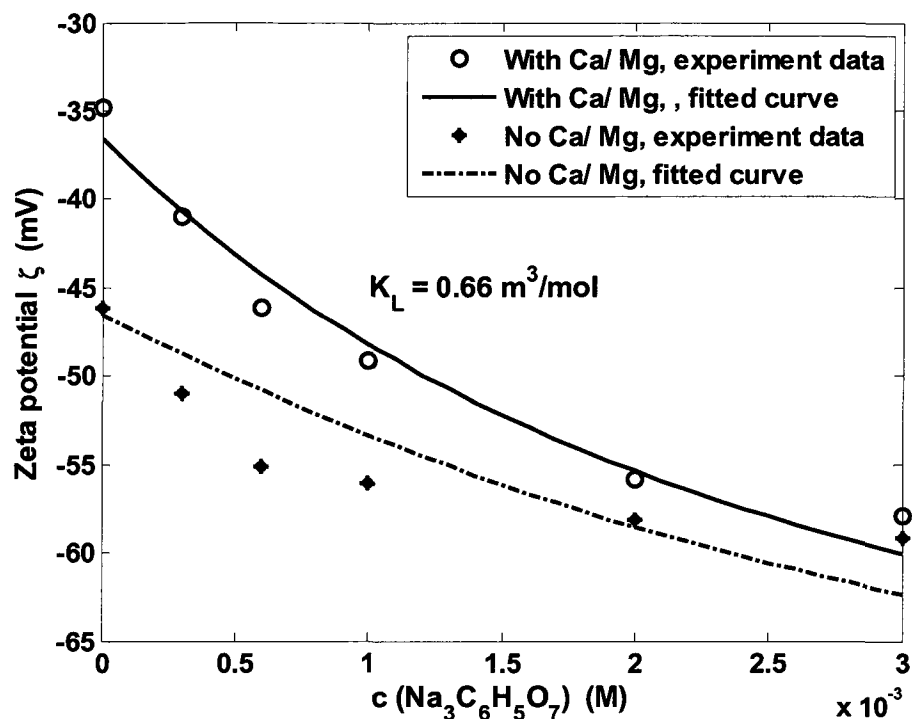
Figure 4.31 Kaolinite zeta potential in synthetic brine adding $Na_3C_6H_5O_7$, pH 8.3

Table 4.10 Adsorption equilibrium constants of surface reactions

Reaction	K (m^3/mol)
$-AO^- + Ca^{2+} \rightleftharpoons -AOCa^+$, A: Al/ Si	0.82
$-AO^- + Mg^{2+} \rightleftharpoons -AOMg^+$, A: Al/ Si	1.71
$-AOH_2^+ + HSiO_3^- \rightleftharpoons -AOH_2HSiO_3$, A: Al/ Si	13.7
$-AOH_2^+ + H_3SiO_4^- \rightleftharpoons -AOH_2H_3SiO_4$, A: Al/ Si	8.7
$-AOH_2^+ + HCO_3^- \rightleftharpoons -AOH_2HCO_3$, A: Al/ Si	0.018
$-AOH_2^+ + SO_4^{2-} \rightleftharpoons -AOH_2SO_4^-$, A: Al/ Si	0.195
$-AOH_2^+ + L^{3-} \rightleftharpoons -AOH_2L^{2-}$, A: Al/ Si, L:citrate	0.66

Chapter 4

Table 4.10 shows adsorption equilibrium constants of surface reactions with

different cations and anions. Based on the calculated equilibrium constants from

experiment data correlation, silicate has larger adsorption equilibrium constants

than other ions.

Figure 4.32 shows the bar diagram of zeta potential change per unit additives

of different anions based on Figure 4.17 in Section 4.3.4. The initial value is

calculated at lower additive concentration. The average value is the average zeta

potential change with different additive concentrations.
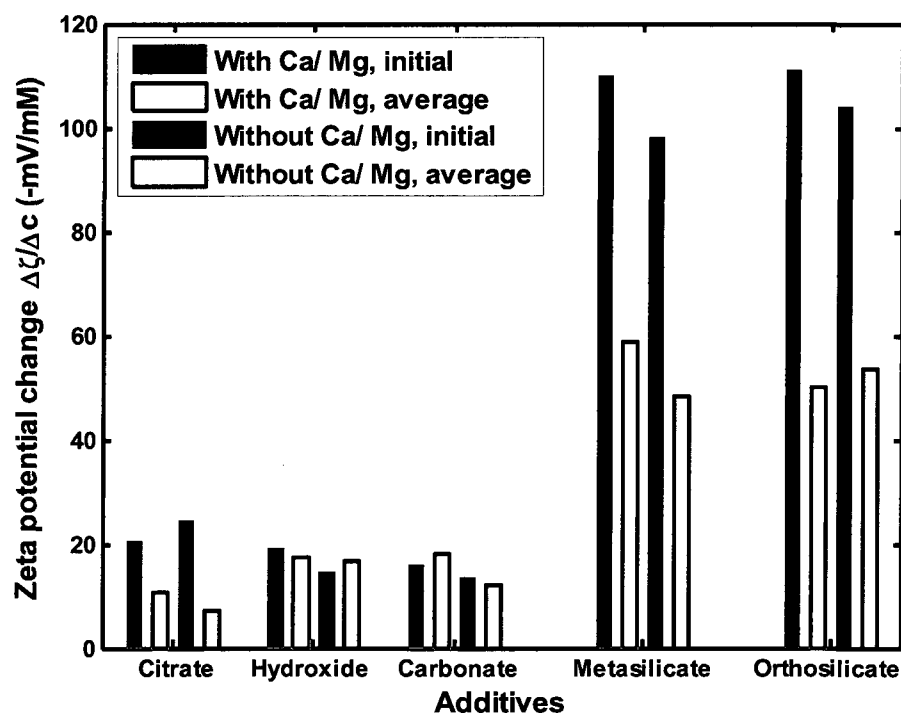
Figure 4.32 Zeta potential change with different additives in synthetic brine

Based on zeta potential results, increase of pH can make kaolinite zeta

potential more negative. Divalent cations (Ca^{2+} and Mg^{2+}) can make kaolinite zeta potential less negative; while some anions (HCO_3^-, CO_3^{2-}, $HSiO_3^-$, $H_3SiO_4^-$ and $C_6H_5O_7^-$) can make kaolinite zeta potential more negative. Silicate ions have the largest effect on kaolinite zeta potential change than other anions. This is consistent with the results in Table 4.10, in which silicate has larger adsorption equilibrium constants than other ions to make zeta potential of kaolinite more negative.

4.4. Reference

[1]   B. D. Sparksa, L. S.Kotlyara, J.B. O'Carrolla, K.H. Chung, Athabasca oil sands: effect of organic coated solids on bitumen recovery and quality, *J. Pet. Sci. Eng.*, **2003**, 39, 417-430.

[2]   E. Tombácz, M. Szekeres, Surface charge heterogeneity of kaolinite in aqueous suspension in comparison with montmorillonite, *Appl. Clay Sci.*, **2006**, 34, 105-124.

[3]   S. S. Lee, E. Matijevic, Surface and colloid chemistry of clays, *Chem. Rev.*, **1974**, 74, 385-400.

[4]   Van Olphen, H. An introduction to clay colloid chemistry. Interscience Publishes, New York, 1977.

[5]   Zhou, Z.; Gunter, W. D. The nature of the surface charge of kaolinite. Clays Clay Miner. 1992, 40 (3), 365-368.

[6]   Takamura, K.; Chow R. S. The electric properties of the bitumen/ water interface II. Application of the ionizable surface-group model. Colloids Surf. 1985, 15, 35-48.

[7]   S. Liu, Alkaline surfactant polymer enhanced oil recovery process, PhD thesis, Rice University, **2008**.

Chapter 4

[8] D. C. Standnes, T. Austad, Nontoxic low-cost amines as wettability alteration chemicals in carbonates, *J. Pet. Sci. Eng.*, **2003**, 39, 431-446.

[9] D. C. Standnes,T. Austad, Wettability alteration in chalk: 2. Mechanism for wettability alteration from oil-wet to water-wet using surfactants, . *J. Pet. Sci. Eng.*, **2000**, 28, 123-143.

[10] D. C. Standnes, T. Austad, Wettability alteration in carbonates: Interaction between cationic surfactant and carboxylates as a key factor in wettability alteration from oil-wet to water-wet conditions, *Colloids Surf. A,* **2003**, 216, 243-259.

[11] M. M. Sharma, J. F. Kuo, T. F. Yen, Further investigation of the surface charge properties of oxide surfaces in oil-bearing sands and sandstones, *J. Colloid Interface Sci.*, **1987**, 115, 9-16.

[12] R. Sprycha, Electrical double layer at alumina/ electrolyte interface, *J. Colloid Interface Sci.*, **1989**, 127, 1-11.

[13] J. Liu, Z. Zhou, Z. Xu, J. H. Masliyah, Bitumen-clay interactions in aqueous media studied by zeta potential distribution measurement, *J. Colloid Interface Sci.*, **2002**, 252, 409-418.

[14] J. Liu, Z. Zhou, Z. Xu, J. H. Masliyah, Interaction forces in bitumen extraction from oil sands, *J. Colloid Interface Sci.*, **2005**, 287, 507-520.

[15] D. C. Grahame, The electrical double layer and the theory of electrocapillarity, *Chem. Rev.*, **1947**, 41, 441-501.

[16] R. J. Hunter, H. J. L. Wright, The dependence of electrokinetic potential on concentration of electrolyte, *J. Colloid Interface Sci.*, **1971**, 37, 564-580.

[17] R. J. Hunter, Zeta potential in colloid science. Academic Press, **1988**.

[18] D. E. Yates, S. Levine, T. W. Healy, Site-binding model of the electrical double layer at the oxide/ water interface, *J. Chem. Soc., Faraday Trans. 1*, **1974**, 70, 1807-1818.

[19] J. A. Davis, R. James, J. Lekie, Surface ionization and complexation at the oxide/ water interface I. computation of electrical double layer properties in simple electrolytes, *J. Colloid Interface Sci.*, **1978**, 63, 480-499.

[20] J. A. Davis, J. Lekie, J.; Surface ionization and complexation at the oxide/ water interface II. surface properties of amorphous iron oxyhydroxide and adsorption of metal ions, *J. Colloid Interface Sci.*, **1978**, 67, 90-107.

Chapter 4

[21] J. A. Davis, J. Lekie, Computer simulation of the conductometric and potentiometric titrations of the surface groups on ionizable latexes, *J. Colloid Interface Sci.*, 1978, 65, 331-344.

[22] M. M. Sharma, T. F. Yen, Interfacial electrochemistry of oxide surfaces in oil-bearing sands and sandstones, *J. Colloid Interface Sci.*, **1984**, 98, 39-54.

[23] P. V. Bradey, R. T. Cygan, K. L. Nagy, Molecular controls on kaolinite surface charge, *J. Colloid Interface Sci.*, **1996**, 183, 356-364.

[24] D. R. Lide, Handbook of Chemistry and Physics. 71st Edition, CRC Press, Boston, **1990-1991**.

[25] L. G. Sillén, A. E. Martell, Stability Constants of Metal-Ion Complexes, Special Publication No.17, Chemical Society, London, **1971**.

[26] J. Kielland, Individual activity coefficient of ions in aqueous solutions. J. Am. Chem. Soc., **1937**, 59, 1675-1678.

[27] D. J. A. Williams, K. P. Williams, Electrophoresis and zeta potential of kaolinite. *J. Colloid Interface Sci.*, **1977**, 65, 79-87.

Chapter 5

5. Separation of diluted bitumen emulsion

This chapter mainly presents the methods and procedures that are focused on the brine in diluted bitumen emulsions with demulsifier, silicate and pH control.

5.1. Introduction

In chapter 3, PR_5 is chosen as optimal demulsifier for diluted bitumen emulsion. But a *rag layer* develops in the middle of the sample and prevents the complete separation of oil, water and clay solids. In the rag layer, clay solids are associated with oil components (e.g. asphaltenes) in diluted bitumen [1] - [5], which will stabilize water-in-oil emulsions [1] - [3]. To break the rag layer and get complete separation, associated oil should be separated from clay solids. Experiments show that a coated bitumen film can be separated from glass surface when contacting with water at high pH (pH 11) [6]. Contact angle of bitumen on glass surface increases with increase of pH, which reveals glass surface is more water-wet with increase of pH [6]. Sodium meta-silicate (Na_2SiO_3) can enhance the dispersion of clay solids and minimize bitumen-clay coagulation [7]. In chapter 4, increasing pH with silicate was shown to make kaolinite more water-wet. Increasing pH can also convert naphthenic acids in the oil to soaps, which can emulsify and separate oil from clay solids and form an oil-in-water emulsion. Hereby optimal demulsifier, silicate and pH control are used to break diluted

bitumen emulsion.

The separation procedure can be divided into three steps. The first step is emulsion coalescence and clean oil separation with PR_5 and silicate. The second step is clay solids separation from the rag layer by increasing pH and shaking. The last step is separation of the resulting oil-in-water emulsion by lowering the pH. Each step is studied to find optimal separation conditions.

5.2. Materials and emulsion preparation

Samples of Athabasca bitumen froth were provided by Syncrude Canada Ltd. Diluted bitumen samples were prepared by diluting with naphtha with dilution ratio 0.7. The density of diluted bitumen with dilution ratio 0.7 is 821 kg/ m^3 and the viscosity is 7.10×10^{-3} Pa·s (50 °C). The diluted bitumen contains 1.0 $w.\%$ solids and less than 2.0 $w.\%$ water, which can be measured by centrifugation. Most of the solids and water can be removed by centrifugation at 3500 g for 30 minutes.

Unless otherwise stated, the aqueous phase used here is synthetic brine with 2.5×10^{-2} M NaCl, 1.5×10^{-2} M $NaHCO_3$, 2×10^{-3} M Na_2SO_4, 2×10^{-4} M $CaCl_2$ and 2×10^{-4} M $MgCl_2$. The pH of synthetic brine is 8.3.

Different additives (e.g. Na_2SiO_3) were added the brine prior to emulsion preparation. Emulsion samples (60 ml) were prepared by mixing 30 ml brine and 30 ml diluted bitumen in a glass tube with a six-blade turbine (Figure 3.8). Stirring

speed of the turbine was 3600 rpm, and the mixing time was 10 min at desired temperature. The initial pH of brine was measured with a pH meter without contacting with diluted bitumen. The equilibrium pH of brine was measured with pH test paper when the brine reached equilibrium with diluted bitumen.

5.3. Emulsion coalescence and clean oil separation

5.3.1. Methods

To find optimal demulsifier, 200 ppm demulsifier PR_1 - PR_6 (based on the total volume of the emulsion sample) was added to the emulsion samples immediately after emulsion preparation. Afterwards, all the samples were shaken by hand at the same time for 1 minute and then stored at 50 °C. The photographs and photomicrographs of the samples were taken at ambient temperature shortly after removing samples from the oven. After photography, the samples were put back into the oven for storage.

To study the effect of pH and silicate, NaOH or Na_2SiO_3 was added to the aqueous phase to change the pH before emulsion preparation. 200 ppm optimal demulsifier is added to the emulsion samples immediately after emulsion preparation. Sample 1 was prepared as control without silicate. The initial pH (I. pH) of the brine measured by pH meter was 8.3. The equilibrium pH (E. pH) of the brine separated from the emulsion after addition of PR_5 was 8.0, which was

Chapter 5

measured by pH test paper. Sample 2 was prepared with $1.0x10^{-4}$ M silicate. The

initial pH of the brine was 8.5. The equilibrium pH of the brine was between 8.0

and 8.5. Other combinations of alkali and pH (samples 3 - 6) were tried as shown

in Table 5.1.

Table 5.1 Emulsion samples with different alkali at different pH

Sample	Na_2SiO_3	NaOH	*Initial pH	**Equilibrium pH
1	/	/	8.3	8.0
2	$1.0x10^{-4}$ M	/	8.5	8.0 – 8.5
3	/	$2.0x10^{-4}$ M	8.5	8.0 – 8.5
4	$2.0x10^{-4}$ M	/	8.8	8.5
5	/	$4.0x10^{-4}$ M	8.8	8.5
6	$1.0x10^{-4}$ M	$2.0x10^{-4}$ M	8.8	8.5

*The initial pH of brine was measured with a pH meter without contacting with diluted bitumen.
** The equilibrium pH of brine was measured with pH test paper when the brine reached equilibrium with diluted bitumen.

5.3.2. Results and discussions

Figure 5.1 shows 24 hours emulsion samples prepared with synthetic brine

and diluted bitumen with dilution ratio 0.7 at 50 °C, adding 200 ppm demulsifiers

PR_1 - PR_6 and $1.0x10^{-4}$ M Na_2SiO_3. Based on the results of bottle test, emulsion

adding PR_5 has the best separation and is chosen as the optimal demulsifier.

Figure 5.2 shows photographs of the six emulsion samples with 200 ppm

demulsifier PR_5 prepared as described in section 5.3.1. In the figure samples 2

and 3 have clearer aqueous phases than others. Sample 2 has more separated

free water and thinner rag layer. So sample 2 with silicate at initial pH 8.5 has the

best emulsion separation.

Control PR_1 PR_2 PR_3 PR_4 PR_5 PR_6
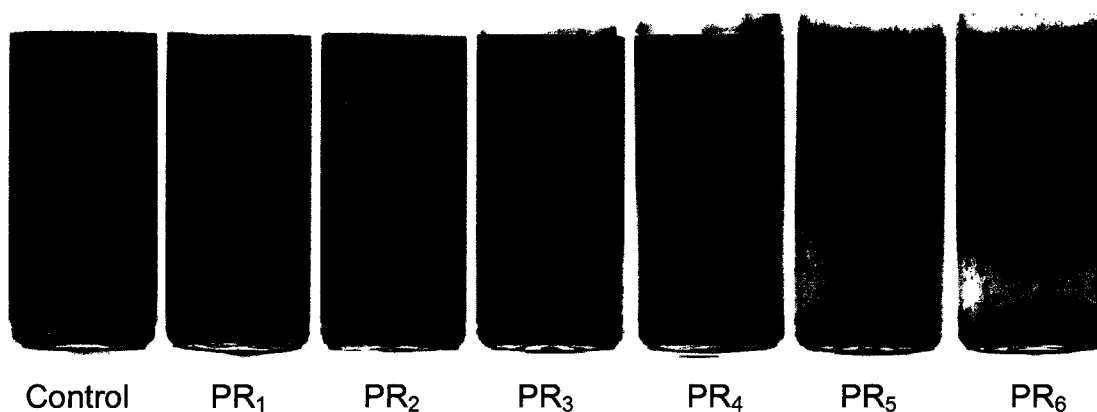
Figure 5.1 24 h emulsion adding 200 ppm demulsifier PR_1 - PR_6 at 50 °C
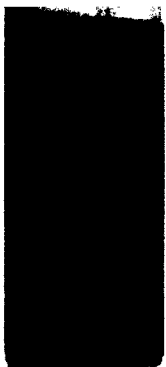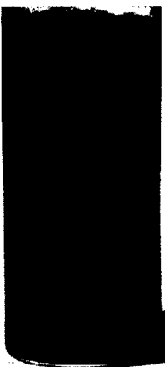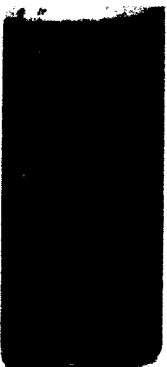
Sample:	1	2	3	4	5	6
Adding:		Na_2SiO_3	NaOH	Na_2SiO_3	NaOH	Na_2SiO_3&NaOH
I. pH:	8.3	8.5	8.5	8.8	8.8	8.8
E. pH:	8.0	8.0 - 8.5	8.0 - 8.5	8.5	8.5	8.5

Figure 5.2 Photographs of 24 h emulsion with 200 ppm PR_5 adding NaOH or Na_2SiO_3 at different pH

5.4. Clay solids separation from rag layer (effects of pH and shaking)

In this section we show that a second step of the separation involving increasing pH of the system can emulsify the oil to form an oil-in-water emulsion and separate oil from clay solids.

5.4.1. Methods

Emulsion samples were prepared with silicate at initial pH 8.5. 200 ppm demulsifier PR$_5$ was added to the emulsion samples immediately after preparation. Top clean oil layer was removed 24 hours after adding PR$_5$. After separating the clean oil layer, five samples were prepared then stored at 50 °C. Samples 7 -11 were prepared as shown in Table 5.2. Photographs were taken 24 hours later.

Table 5.2 Emulsion samples with 200 ppm PR$_5$ and different alkali at different pH after removing top clean oil layer

Sample	Na$_2$SiO$_3$	NaOH	Shaking	Initial pH	Equilibrium pH
7	/	/	without	8.5	8.0 – 8.5
8	/	2.0x10^{-4} M	without	8.8	8.5
9	/	/	with	8.5	8.0 – 8.5
10	/	2.0x10^{-4} M	with	8.8	8.5
11	1.0x10^{-4} M	/	with	8.8	8.5

Slides were prepared by sampling from different positions of emulsion samples for making microscopy observations. In the observation of clay solids

skins in the rag layer, slides were prepared by sampling from different positions of emulsion samples. The skins were observed for 10 minutes before adding NaOH. Then NaOH was added at time zero. The pH of the aqueous phase was increased from 8.5 to 9.5 by adding 0.1 M NaOH. Photomicrographs of clay solids skins were taken as the function of time.

5.4.2. Results and discussions

Figure 5.3 shows the photomicrographs of clay solids skins with time when increasing pH for 8.5 to 9.5 as described in section 5.4.1.

Before adding NaOH, the skins did not change in 10 minutes. After adding NaOH, the skins became smaller gradually and disappeared. Finally, only clay solids remained. Clay solids and the oil form rigid skins. Athabasca bitumen has a relatively high acid number (total acid number 3.3 mg KOH/ g oil) [8]. With an increase of pH, additional naphthenic acids in the oil form soaps and separate the oil from clay solids. So increasing pH can break the skins.

Based on the discussion in section 5.3.2, sample 2 with silicate at initial pH 8.5 has the best emulsion separation results. In the second step, emulsion samples were prepared starting with sample 2 of Table 5.1. After separating the clean oil layer, five samples were prepared as described in section 5.4.1.

Before adding NaOH (-10 min, pH 8.5)   Adding NaOH (0 min)

5 min after adding NaOH   10 min after adding NaOH

30 min after adding NaOH   60 min after adding NaOH (pH 9.5)

(The scale bar is 20 μm)
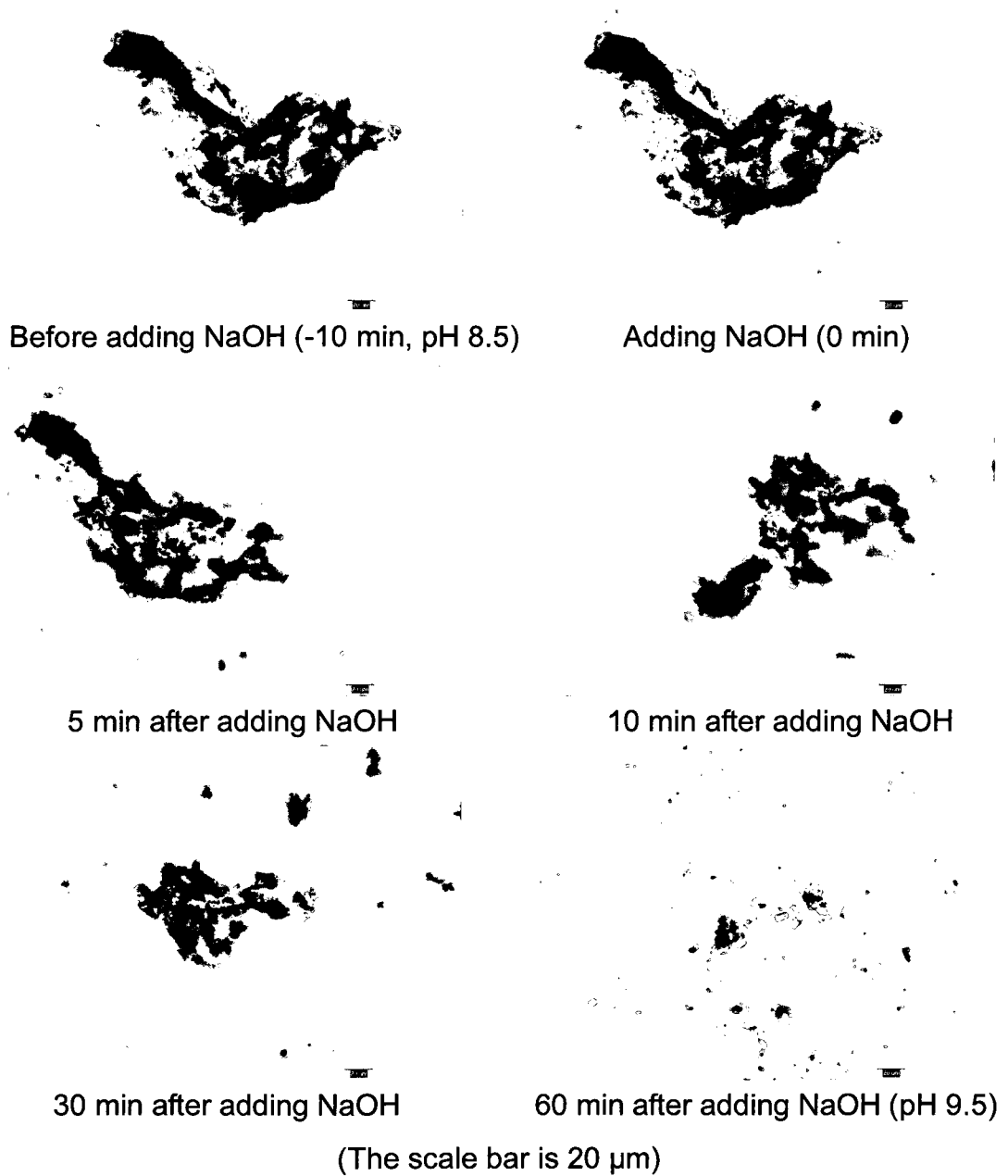
Figure 5.3 Clay solids skins with time when increasing pH from 8.5 to 9.5

Figure 5.4 shows photographs of the five samples after one day. All of them

have a layer containing oil on the top and a solids layer at the bottom. The

samples that were not shaken have loose solids layers. The samples that were

shaken have more compact solids layers.

Sample:	7	8	9	10	11
Adding:		NaOH		NaOH	Na$_2$SiO$_3$
			Shaking	Shaking	Shaking
I. pH:	8.5	8.8	8.5	8.8	8.8
E. pH:	8.0 - 8.5	8.5	8.0 - 8.5	8.5	8.5
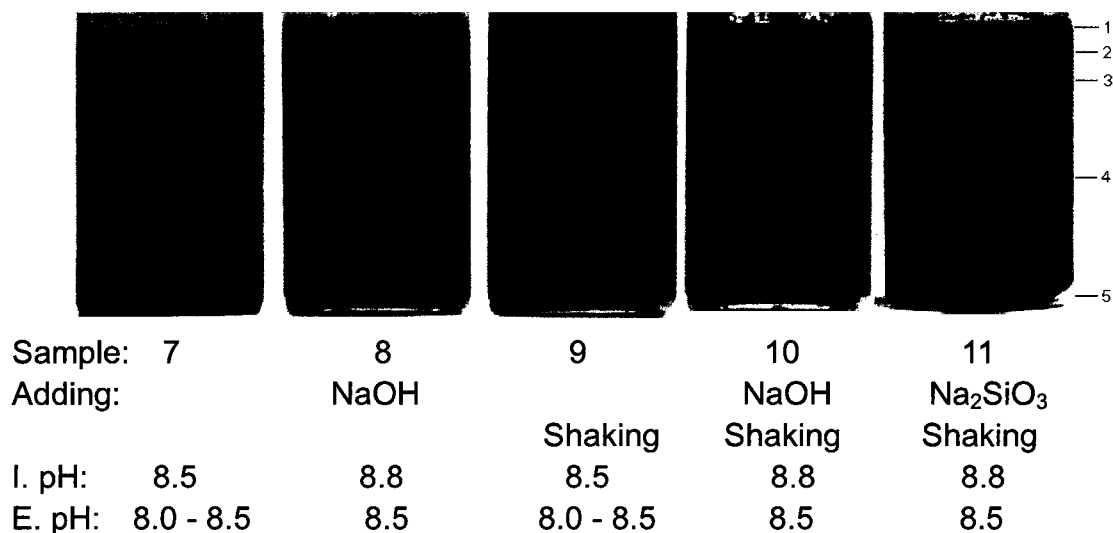
Figure 5.4 Photographs of 24 h emulsion with NaOH or Na$_2$SiO$_3$ at different pH

Figs. 5.5 – 5.7 show photomicrographs obtained by sampling from the five

different positions indicated on the right side in Figure 5.4. Sample 7, which is not

shaken, exhibits rigid skins in the rag layer (in Figure 5.5). Sample 8 has similar

results, though the pH was increased. In contrast, all three samples that are

shaken exhibit oil-in-water emulsions at the two highest sampling positions. A few

skins are seen in the lowest sampling position of sample 9, where nothing was

added and pH remained at 8.5 (Figure 5.6).   No skins are seen for samples 10,

where pH was raised to 8.8 (in Figure 5.7). Sample 11 has similar results to

Sample 10.
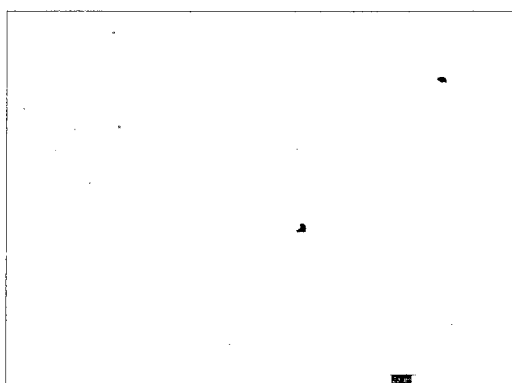
1. Top of the oil layer

2. Middle of the oil layer

3. Near oil/water interface
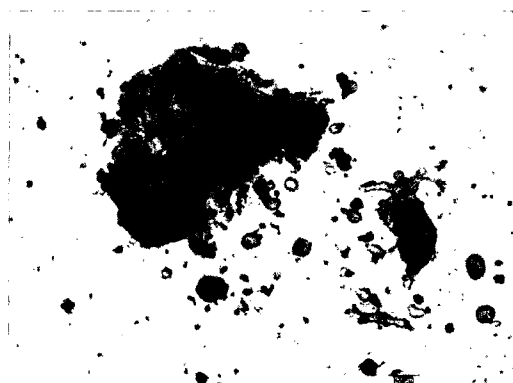
4. Water layer

5. Solids layer

(The scale bar is 20 μm)

(Equilibrium pH 8.0 – 8.5)

Figure 5.5 24 h emulsion without changing pH or shaking (Sample 7)
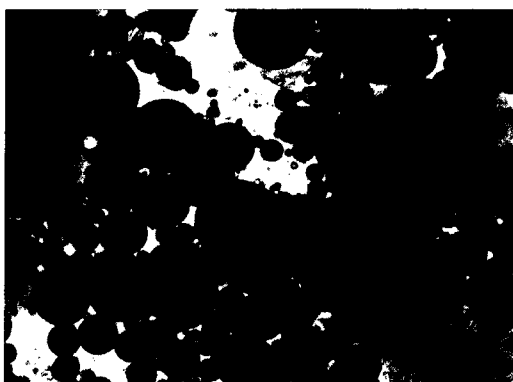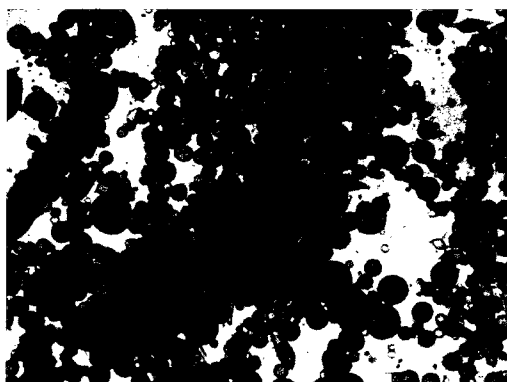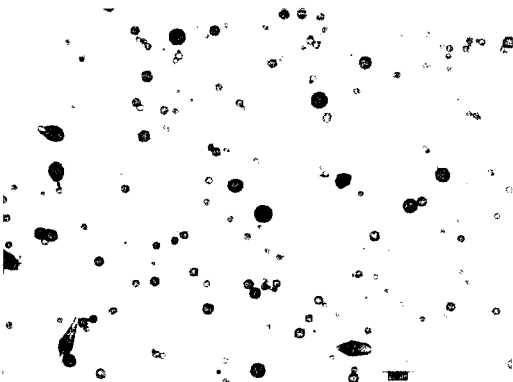
1. Top of the oil layer

2. Middle of the oil layer

3. Near oil/water interface
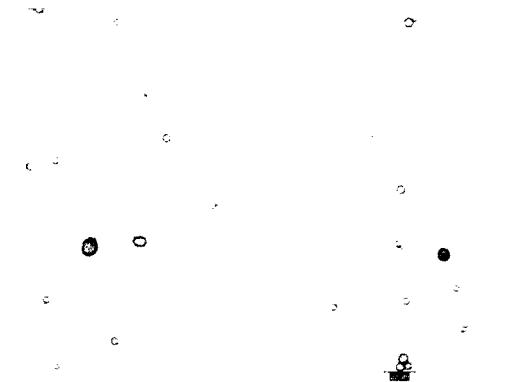
4. Water layer

5. Solids layer

(The scale bar is 20 μm)

(Equilibrium pH 8.0 – 8.5)

Figure 5.6 24 h emulsion with shaking, without adding NaOH (Sample 9)
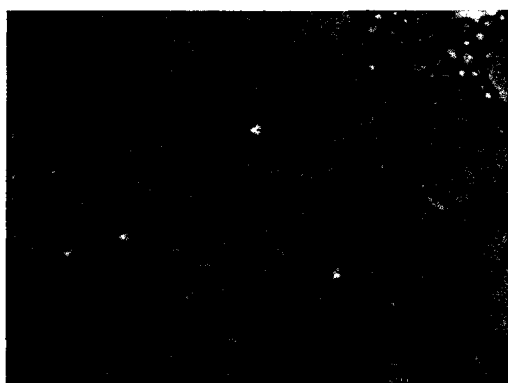
1. Top of the oil layer

2. Middle of the oil layer

3. Near oil/water interface
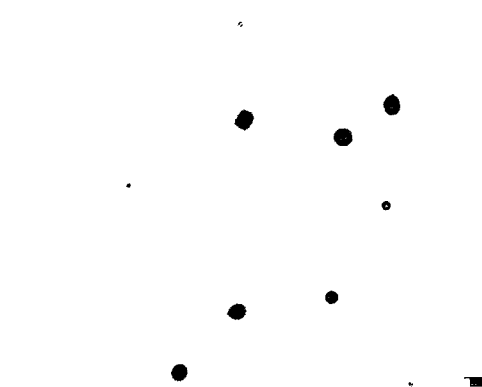
4. Water layer
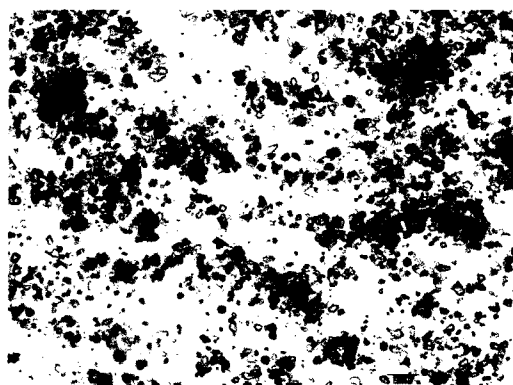
5. Solids layer

(The scale bar is 20 μm)

(Equilibrium pH 8.5)

Figure 5.7 24 h emulsion adding NaOH with shaking (Sample 10)

Based on comparison of the five samples, increasing pH only cannot separate oil from clay solids. Shaking only can offer external energy and separate part of the oil from clay solids, but the skins of clay solids do not completely disappear. A combination of increasing pH and shaking can separate the oil from clay solids and destroy all the skins. After removing top clean oil layer, increasing the pH of emulsion samples using NaOH or Na_2SiO_3 (samples 10 and 11) have similar separation results. So increasing the pH to 8.8 with shaking is a good method for the separation of clay solids.

5.5. Separation of oil-in-water emulsion (effects of pH)

5.5.1. Methods

30 ml of an oil-in-water diluted bitumen emulsion was prepared with 20 vol.% diluted bitumen and 80 vol.% synthetic brine. 200 ppm PR_5 was added to the diluted bitumen before emulsion preparation. 1×10^{-4} M silicate and 2×10^{-4} M NaOH were added to synthetic brine to increase the initial pH to 8.8. Then the emulsion sample was formed by shaking the bottle for 1 minute at ambient temperature. Several drops of 1.0 M HCl were added to the samples immediately after emulsion preparation. The samples were put into the oven at 50 °C. The pH was measured by pH paper when the system reached equilibrium.

Slides were prepared by sampling from different positions of emulsion

samples for making microscopy observations. In the microscopy observation of O/W emulsions, the pH of the aqueous phase was decreased from 8.8 to 4.5 by adding 0.1 M HCl. The O/W emulsion was observed for 10 min before adding HCl. Then HCl was added at time zero. Photomicrographs of clay solids skins were taken as the function of time.

5.5.2. Results and discussions

In the second step of the separation procedure described in section 5.4.2, increasing pH and shaking caused formation of an oil-in-water emulsion. In order to break this emulsion, the pH of the aqueous phase needs to be lowered in a third step. In this section, experiments are described in which hydrochloric acid (HCl) was used to find the optimal pH for demulsification.

Figure 5.8 shows the photomicrographs of o/w emulsions with time when lowering the pH from 8.8 to 4.5, as described in section 5.5.1.

Before adding HCl, the O/W emulsions did not coalesce in 10 min. After adding HCl, the O/W emulsions coalesced very fast and formed continuous oil phase finally. With the decrease of pH, soaps will form naphthenic acids and destabilize the O/W emulsions.

The following experiments were performed to find the optimal pH for oil-in-water emulsion coalescence, as described in section 5.5.1. Figure 5.9

shows photographs of three samples after 24 h having equilibrium pH values

ranging from 5.0 to 8.5. As pH decreases, the water layer becomes more

transparent.
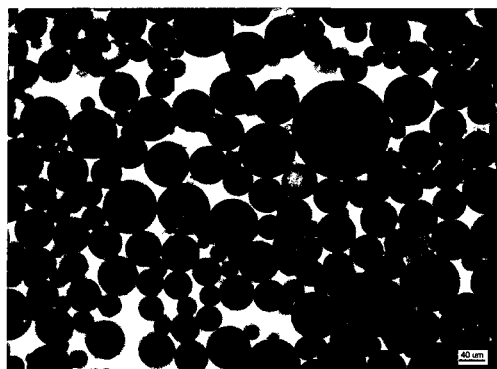
Before adding HCl (-10 min, pH 8.8)
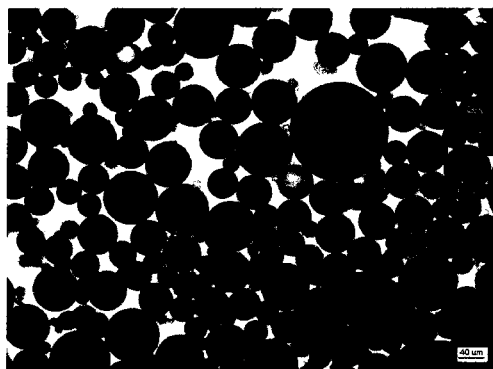
Adding HCl (0 min)

1 min after adding HCl
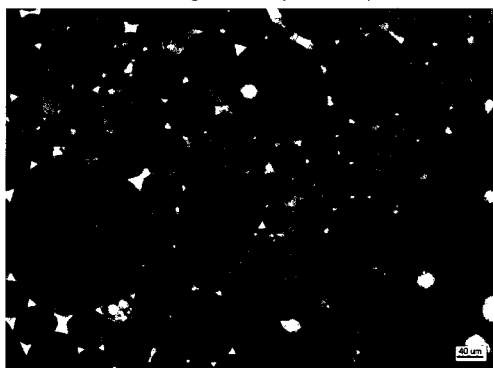
3 min after adding HCl
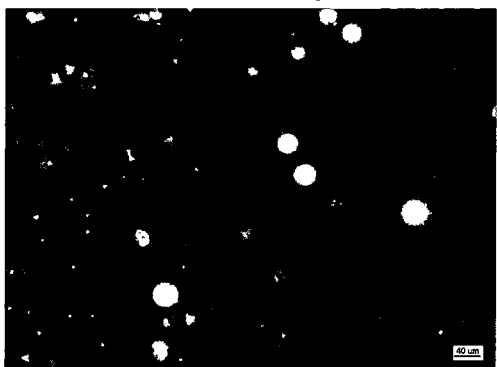
5 min after adding HCl
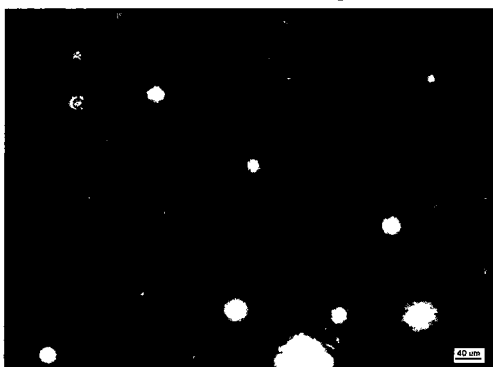
7 min after adding HCl (pH 4.5)

(The scale bar is 20 μm)

Figure 5.8 O/W emulsions with time when lowering pH from 8.8 to 4.5.
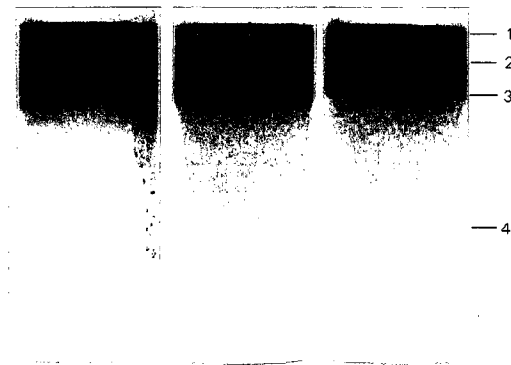
Equilibrium pH: 5.0   6.0   8.5

Figure 5.9 Photographs of 24 h emulsion samples adding HCl at different pH

1. Top of the oil layer

2. Middle of the oil layer

3. Near oil/water interface

4. Water layer
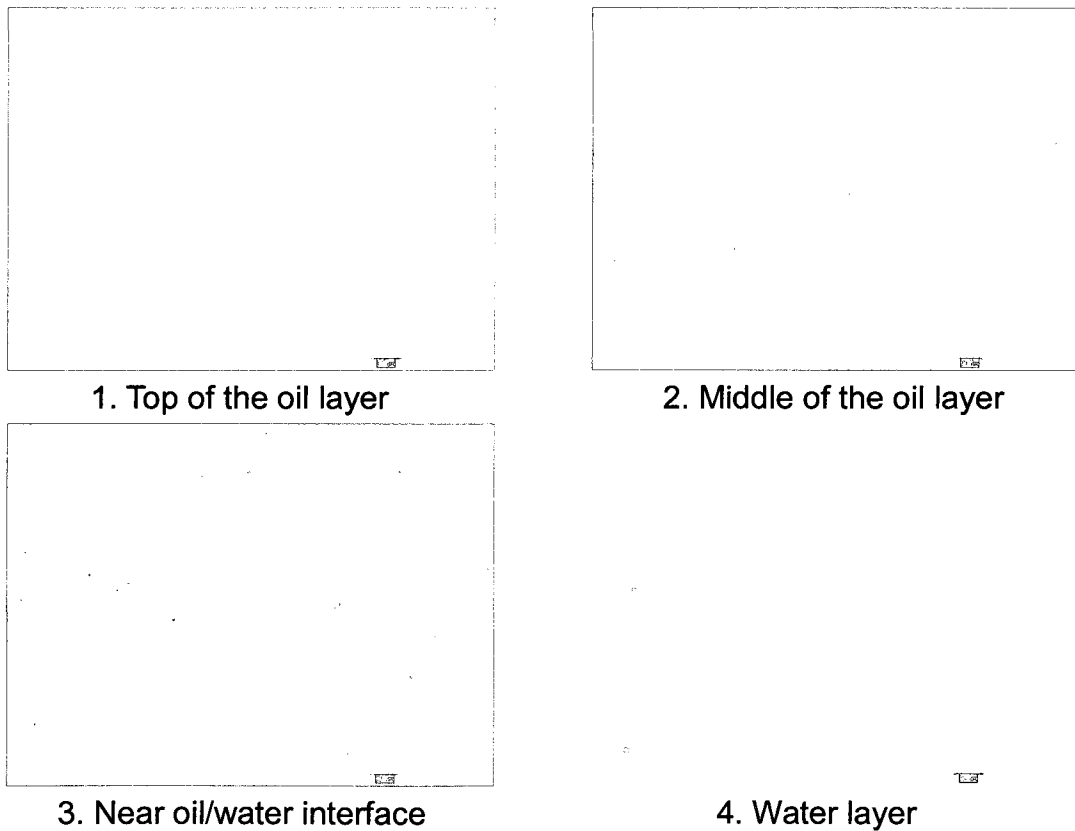
(The scale bar is 20 μm)

Figure 5.10 24 h emulsion adding HCl (equilibrium pH 5.0)

Figs. 5.10 - 5.11 show the photomicrographs of samples at equilibrium pH 5.0

and 6.0. At pH 6.0 (Figure 5.11), the top of the oil layer is clean oil. At the bottom of the oil layer is oil-in-water emulsion with relatively low oil concentration. At pH 8.5, the emulsion has similar result to that at pH 6.0. At pH 5.0 (Figure 5.10), the top of oil layer is clean oil, but in this case the bottom of the oil layer is oil with a few drops of dispersed water. The water layer is also almost clean. Emulsion samples at pH 5.0 and 6.0 have different emulsion type. Thus the original oil-in-water emulsion remains stable at pH 6.0, but not at pH 5.0.

1. Top of the oil layer

2. Middle of the oil layer

3. Near oil/water interface

4. Water layer

(The scale bar is 20 μm)
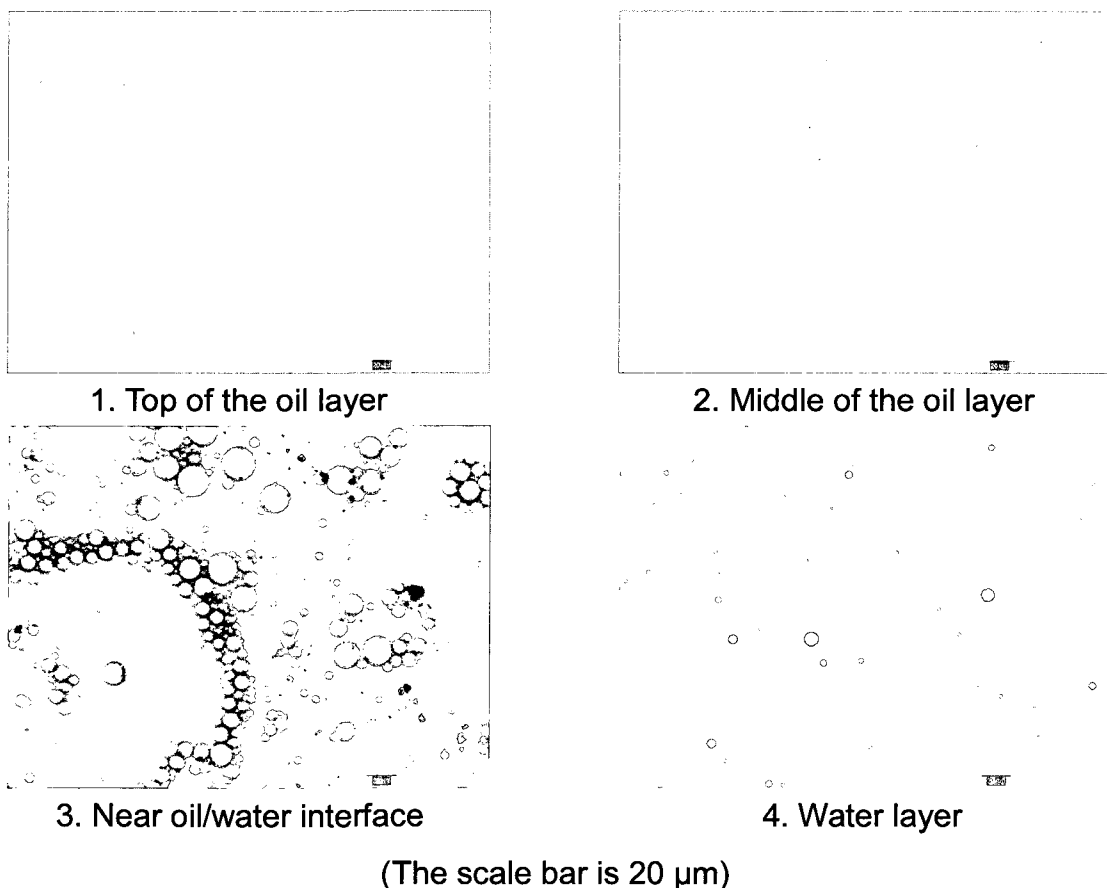
Figure 5.11 24 h emulsion sample adding HCl (equilibrium pH 6.0)

Chapter 5

This experiment shows that the oil-in-water emulsion can be broken at a low pH level, i.e. 5.0 or lower. Study of interfacial properties of emulsified bitumen droplets also shows that bitumen drops are unstable at low pH [9]. When the pH is low enough, all the soap will form naphthenic acid. The system will prefer to form a water-in-oil emulsion. But because the oil layer contains demulsifier PR_5, water-in-oil emulsions are not stable in the absence of clay solids. Thus clean oil and bulk water layers can be obtained.

5.6. Three-step separation of diluted bitumen emulsion

5.6.1. Methods

After finding the optimal separation conditions in each step (section 5.3 - 5.5), the entire three-step procedure was performed. 60 ml water-in-oil diluted bitumen emulsion was prepared with 50 vol.% diluted bitumen and 50 vol.% synthetic brine with 1×10^{-4} M silicate at 50 °C, as described in section 5.2. 200 ppm PR_5 was added to 30 ml emulsion sample immediately after preparation. The clean oil layer was removed 24 h after emulsion preparation. 2×10^{-4} M NaOH was added to aqueous phase to increase the initial pH to 8.8 with shaking. The emulsion layer and solids layer were separated 24 hours later. A total of 0.15ml 1.0 M HCl was added to the emulsion layer to lower the equilibrium pH to 5.0. Photographs of the separation were taken 24 hours later.

Chapter 5

5.6.2. Results and discussions

Figure 5.12 shows the photographs and photomicrographs for an experiment in which the entire three-step procedure was applied and photomicrographs at the seven different positions.
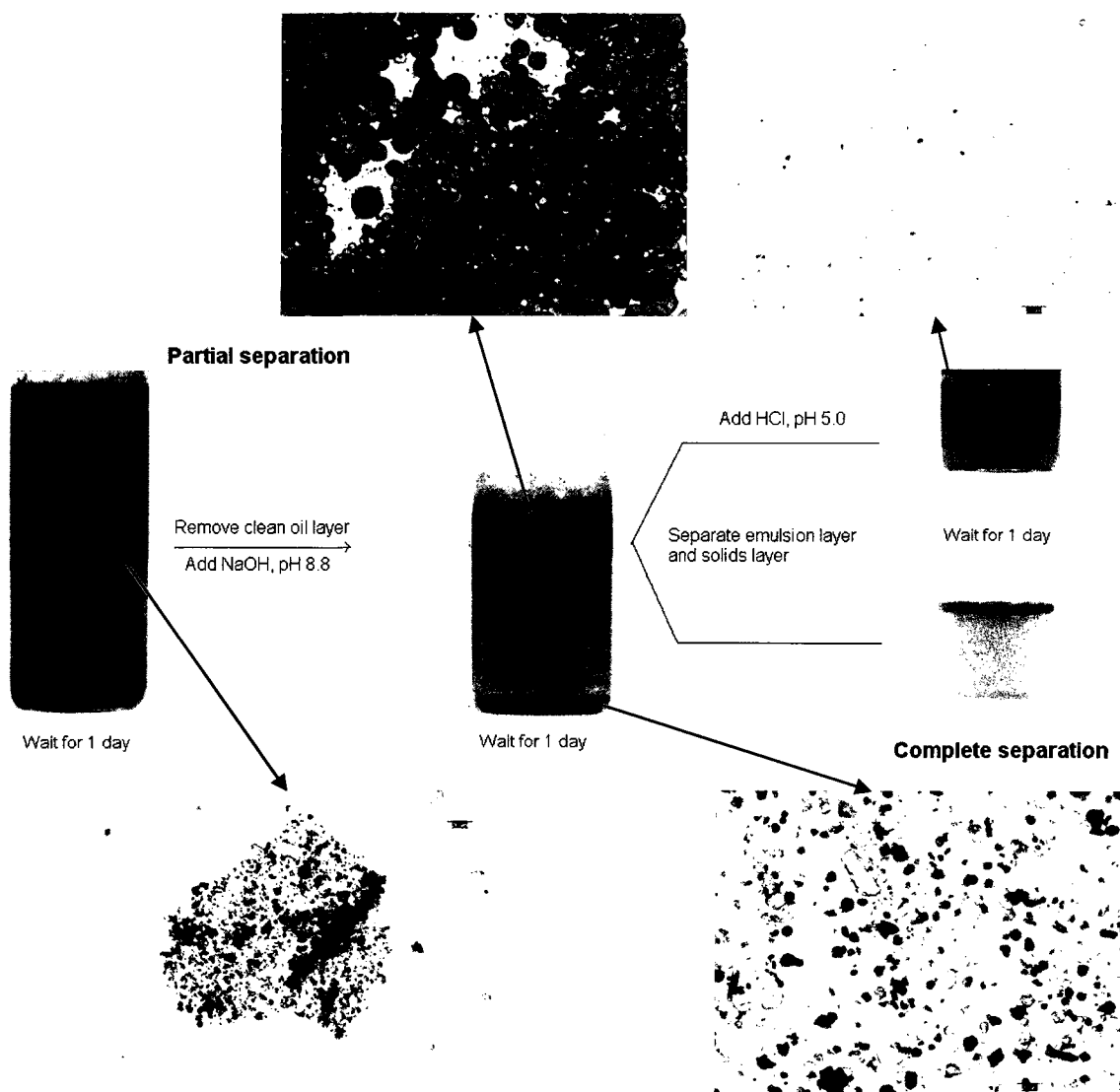
Figure 5.12 Photographs and photomicrographs of emulsion sample during the whole operation procedure

Based on the photomicrographs, the results after second and third steps are similar to those of Figs. 5.7 and 5.10 respectively, confirming that the same results are obtained when the steps are combined as when they are performed separately. The second step destroys the rag layer but forms an oil-in-water emulsion. The third step breaks the oil-in-water emulsion. After this three-step procedure, nearly all of the oil, water and clay solids can be separated.

5.7. Karl Fischer titration of water in diluted bitumen

5.7.1. Introduction

Karl Fischer (K-F) titration is a classic titration method in analytical chemistry that uses coulometric or volumetric titration to determine trace amounts of water in a sample. It was invented in 1935 by the German chemist Karl Fischer [10]. K-F reaction takes place in two steps:

$$H_2O+I_2+SO_2+3B \rightarrow 2BH^+I^-+BSO_3 \qquad [5.1]$$

$$BSO_3+ROH \rightarrow BH^+ROSO_3^- \qquad [5.2]$$

B: base (usually pyridine is used), ROH: Alcohol (usually methanol is used)

Usually the K-F reagent is the mixture of iodine, sulfur dioxide, pyridine and methanol. All the compounds are in excess amount except iodine. Based on the consumption of iodine water content can be calculated.

During the titration process, a constant voltage is applied between the two

platinum electrodes. Prior to equivalence point, the solution contains I^- but little I_2.

At the equivalence point, excess I_2 appears and an abrupt current increase marks

end point. K-F titration has nearly unlimited measuring range (1ppm to 100%) [11].

5.7.2. Materials and methods

5.7.2.1. Materials

K-F reagent is obtained from Sigma-Aldrich (Product# 36115-1L, around 5

mg water/ ml reagent, should be stored <15 °C). Methanol and toluene used as

titration solvents are from EMD Inc. Titration system is Metrohm KF-701 Titrino.

Samples of Athabasca bitumen were provided by Syncrude Canada Ltd.

Bitumen samples were diluted with naphtha with dilution ratio 0.7. Most of the

solids and water can be removed by centrifugation process, with a centrifugal

acceleration of 8000 g and a centrifugation time of 30 min.

5.7.2.2. Solubility test of diluted bitumen in toluene-methanol mixture solvent

Toluene-methanol mixture was prepared by mixing toluene and methanol

with different volume ratios. 1.0 ml diluted bitumen (dilution ratio N/B = 0.7) was

added to 25ml toluene-methanol mixture with electromagnetic stirring. After five

minutes, no precipitation indicates that the solvent can dissolve diluted bitumen

and can be used for titration.

5.7.2.3. Water content measurement K-F titration

A certain amount of sample was injected into the titration vessel with 25 ml solvent. Water content was measured by Metrohm K-F 701 titrator. Detailed procedure can be found in appendix C.

5.7.2.4. Titration calibration

In order to test the accuracy of K-F titration, emulsion samples of diluted bitumen (after centrifugation, dilution ratio N/B is 0.7) with different known water content were used for calibration. 30 ml emulsion samples were prepared by mixing different amount of de-ionized water and diluted bitumen (water content ranges from 10 mg/ml to 500 mg/ml) in a glass tube with a six-blade turbine. Stirring speed of the turbine was 3600 rpm, and the mixing time was 10 min at ambient temperature. K-F titration was performed to measure water content.

In order to test the lower limit of K-F titration, emulsion samples of diluted bitumen (after centrifugation, dilution ratio N/B is 0.7) were diluted with toluene at different ratio. K-F titration was performed to measure water content.

5.7.3. Results and discussions

5.7.3.1. Solvent selection for diluted bitumen

The default solvent for K-F titration is methanol, because methanol not only

takes part in the K-F reaction, but also is a good solvent for all the reagents including water. But methanol can't dissolve heavy oil components (e.g. asphaltenes). When diluted bitumen was added to methanol, asphaltenes precipitated immediately. The precipitation of asphaltenes on Pt electrodes will interfere with the titration and finally the titrator stops and shows system error "check electrode". In this case, the electrodes can be recovered by washing with toluene and methanol (first toluene then methanol) and restarting the titrator.

Asphaltenes have good solubility in toluene. But toluene itself can't be used as solvent for K-F titration (titrator shows system error "check electrode"). The mixture of methanol and toluene is a potential candidate for K-F titration. It needs to satisfy two criteria. First the mixture can dissolve diluted bitumen and no asphaltenes precipitate. Second the mixture will not affect the titration results. For pure water calibration, there should be no difference using methanol or the mixture as solvent.

Table 5.3 shows the solubility test of diluted bitumen in toluene-methanol mixture and also the titer calibration using the mixture. From the table, diluted bitumen can't dissolve in toluene-methanol mixture if toluene volume fraction is smaller than 75%. During titration, titrator shows system error "check electrode". If toluene volume fraction is above 75%, bitumen can dissolve in toluene-methanol

mixture. But if it is greater than 80%, titrator shows system error "check electrode".

In titer calibration, titer is 5.45 mg/ml using mixture with toluene volume fraction

75%; while titer is 11.88 mg/ml using mixture with toluene volume fraction 80%.

The titer value is 5.45 mg/ml using pure methanol. Using mixture with toluene

volume fraction 75% as solvent can get the same titer as using pure methanol; but

using mixture with toluene volume fraction 80% can't get the same titer. This

indicates toluene-methanol mixture with toluene volume fraction 75% is the

appropriate solvent for the titration of diluted bitumen.

Table 5.3 Solubility test and titer calibration using toluene-methanol mixture

Toluene ratio v. %	50	60	70	75	80	90	100
Soluble	No	No	No	Yes	Yes	Yes	Yes
Titer (mg/ml)	/	/	/	5.45	11.88	Error	Error

5.7.3.2. K-F titration calibration of water content in diluted bitumen

Table 5.4 shows water content in diluted bitumen (after centrifugation, dilution

ratio 0.7) with different water amount via K-F titration using toluene-methanol

mixture with toluene volume fraction 75%. Residual water content in diluted

bitumen after centrifugation is 0.26 w.% measured by K-F titration. The total water

content in diluted bitumen is the combination of added water amount plus residual

water content in diluted bitumen after centrifugation.

Chapter 5

Table 5.4 K-F titration calibration of water content in diluted bitumen

Water content (mg/ml)	Measured value (mg/ml)	Deviation %
12.1	11.5±0.3	4.6
52.0	50.6±0.6	2.7
101.9	106.9±4.4	4.9
201.7	205.6±2.9	1.9
501.1	508.3±10.1	1.4
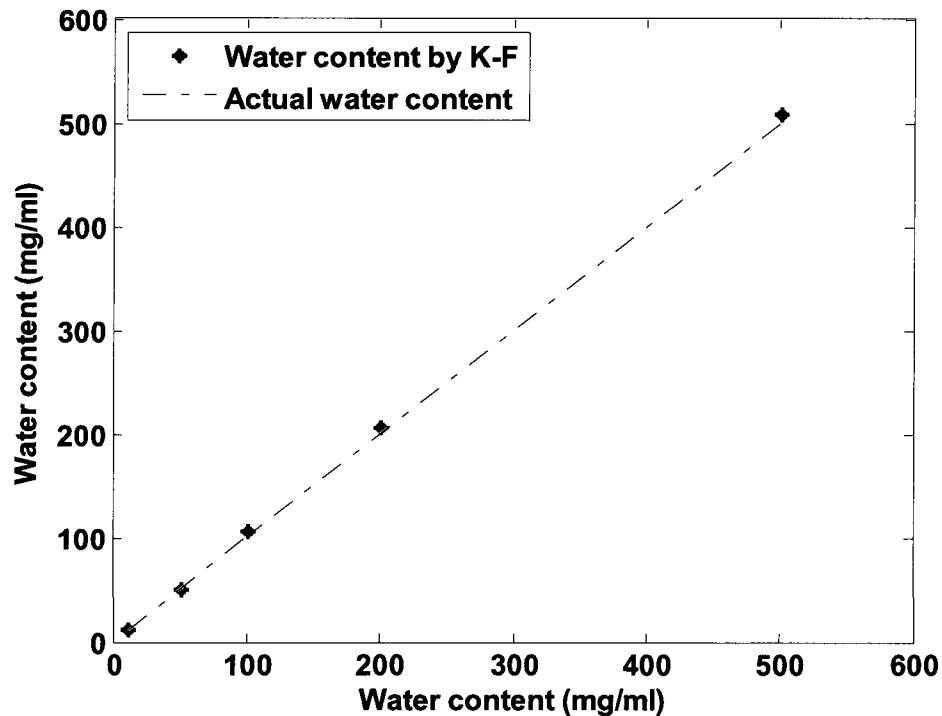
Figure 5.13 Measured water content by K-F as function of actual water content

Figure 5.13 shows measured water content by K-F method as function of actual water content. At different water amounts in diluted bitumen, measured water content values are close to the actual water content. The largest deviation between the measured water content and actual water content is less than 5 %.

Chapter 5

5.7.3.3. Lower limit of K-F titration

Table 5.5 shows water content in diluted bitumen (after centrifugation, dilution ratio 0.7) mixed with different amount of toluene. First column in the table is diluted bitumen content in diluted bitumen-toluene mixture. Second column in the table is measured water content in the mixture sample. Third column in the table is calculated water content in diluted bitumen.

Table 5.5 K-F titration of water content in diluted bitumen mixed with toluene

Diluted bitumen % in mixture	Water % in sample	Water % in diluted bitumen
100	0.27	0.27
50	0.15	0.31
25	0.04	0.17
10	0.02	0.23
5	0.02	0.43
1	0.02	1.98

As diluted bitumen content decreases, measured water content in the mixture sample reaches minimum 0.02 %. This is the lower limit of water content in diluted bitumen that can be measured by K-F titration.

Figure 5.14 shows measured water content by K-F method as function of diluted bitumen content in diluted bitumen-toluene mixture. When diluted bitumen content in diluted bitumen-toluene mixture is larger than 10 %, the variation is

Chapter 5

linear with correlation coefficient 0.987.
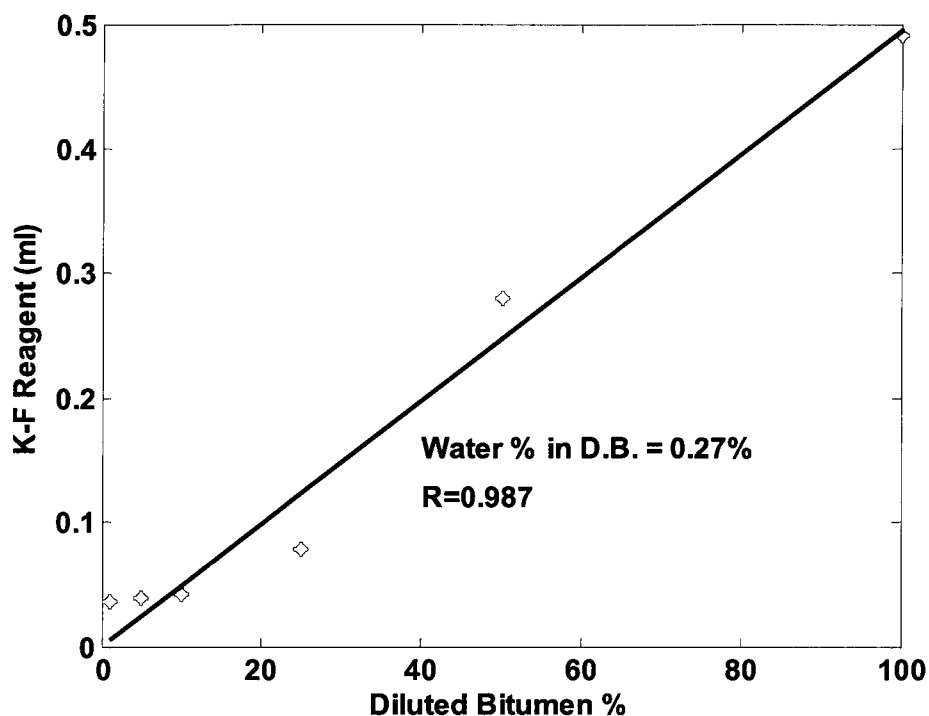
Figure 5.14 Measured water content by K-F as function of diluted bitumen content
in diluted bitumen-toluene mixture

5.7.3.4. Water content in oil layer after emulsion separation

Table 5.6 shows water content at different positions of oil layer (Figure 5.15

shows positions of sampling) in partially separated diluted bitumen emulsion with

200 ppm PR_5 and 1×10^{-4} M silicate (photograph of the sample is shown in

Figure5.1). From the result, water content in oil layer is not homogeneous. Water

content increases from the top to the bottom of oil layer after adding demulsifier

and silicate. This indicates the sedimentation effects by gravity.

Table 5.6 Water content at different position of oil layer in partially separated diluted bitumen emulsion with 200 ppm PR_5 and 1×10^{-4} M silicate

Position	Top of the oil layer	Middle of the oil layer	Bottom of the oil layer
Water %	1.77±0.14	3.86±0.15	7.30±0.45

5.8. Effects of solids, dilution ratio and silicate on emulsion stability

5.8.1. Materials and methods

5.8.1.1. Materials and emulsion preparation

Emulsion separation has been studied with N/B ratios 0.7 and 4.0 to find the effect of dilution ratio. Samples of Athabasca bitumen froth were provided by Syncrude Canada Ltd. Solids-free diluted bitumen was prepared by centrifugation (8000 g, 30 min). Diluted bitumen samples were prepared by diluting with naphtha with the ratios 4.0 and 0.7 (naphtha/bitumen, w/w). Diluted bitumen with dilution ratio N/B 0.7 has density 896 kg/ m^3, viscosity 4.84×10^{-3} Pa·s (80 °C) and contains 21.2 w.% water and 6.9 w.% solids. Diluted bitumen with dilution ratio N/B 4.0 has density 820 kg/ m^3, viscosity 8.1×10^{-4} Pa·s (80 °C) and contains 8.8 w.% water and 3.0 w.% solids, which was measured by centrifugation.

Aqueous phase used here is synthetic brine which contains 25 mM NaCl, 15 mM $NaHCO_3$, 2 mM Na_2SO_4, 0.3 mM $CaCl_2$ and 0.3 mM $MgCl_2$.

Emulsion preparation and bottle test are performed using synthetic brine at

Chapter 5

80 °C with similar procedure as described in sections 3.5.2 and 3.5.3. Water

content in oil layer is measured by K-F titration, as described in section 5.7.2.

5.8.1.2. Solid content and distribution by centrifugation

Solids in different layers of partially separated emulsion were collected by

centrifugation at 8000 g for 30 minutes. Here solid distribution in oil layer

(oil-continuous phase on the top with small amount of water and solid), rag layer

(water- continuous phase with oil and solid skins in the middle) and bottom layer

(water layer with solid sediments at the bottom) is studied. After centrifugation,

water and oil were removed and the open centrifuge tube was put in the oven (50

°C) overnight for drying. Weight of solid was measured and solid content in oil

layer was calculated based on original weight of oil layer. Solid distribution was

calculated based on solid in each layer and total weight of solid by centrifugation.

5.8.2. Results and discussions

5.8.2.1. Separation of solids-free emulsion

Figure 5.15 shows the photograph of brine in diluted bitumen with N/B ratios

0.7 and 4.0 24 h emulsion samples adding 200 ppm demulsifiers PR_1 to PR_6 at 80

°C. The first sample is emulsion without any demulsifier as control. The second to

the seventh are emulsion adding 200 ppm PR_1 to PR_6. The pH of the aqueous

phase is 8.3. Positions of sampling for residual water content measurement are

also shown in the figure.

N/B ratio 4.0
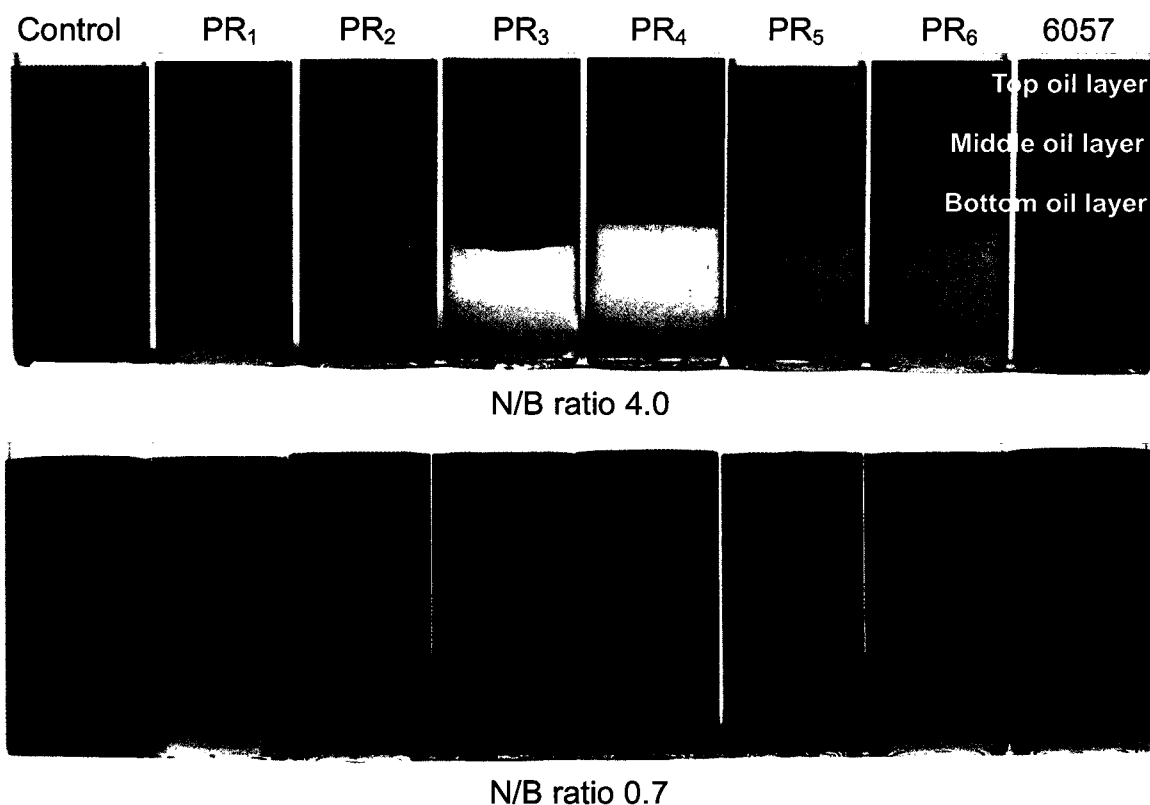
N/B ratio 0.7

Figure 5.15 24 h emulsion (solids-free) separation adding 200 ppm PR_1 to PR_6 at 80 °C, pH 8.3

Based on bottle test, almost complete separation of oil and water could be

achieved without solids in emulsion, and no rag layer formed. For N/B ratio 4.0,

emulsion adding 200 ppm PR_4 to PR_6 have better separation results than others;

for N/B ratio 0.7, emulsion adding 200 ppm PR_3 to PR_5 have better separation

results than others. Residual water content in oil layer was measured in these

samples, sampling from the positions indicated in Figure 5.15.

Chapter 5

Figure 5.16 shows bar diagrams of residual water content in oil layer using 200 ppm demulsifiers. The dashed line shows desired diluted bitumen residual water content criteria (2.0%). Residual water content in oil layer with N/B ratio 4.0 is lower than that with N/B ratio 0.7. At N/B ratio 4.0, residual water content in oil layer is close to desired diluted bitumen residual water content criteria (2.0%).

N/B ratio 4.0   N/B ratio 0.7
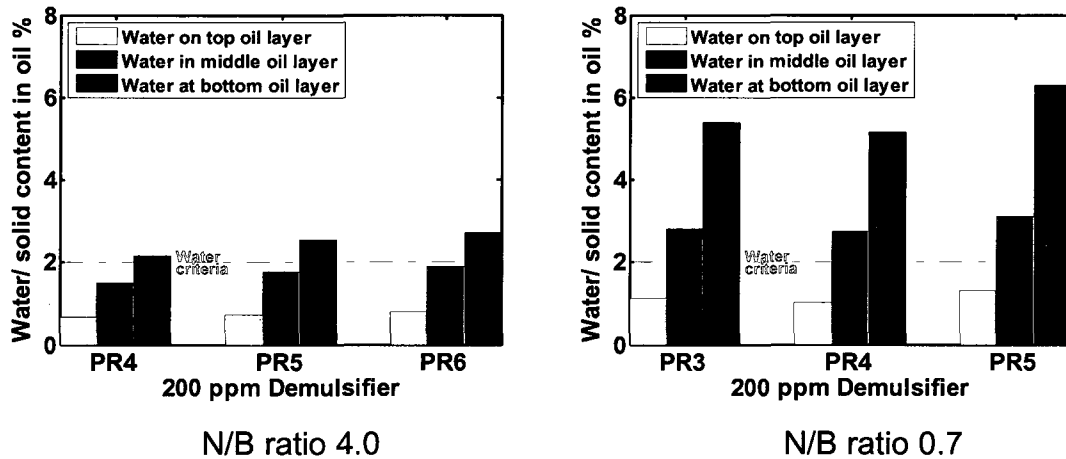
Figure 5.16 Water content in oil layer (solids-free) adding 200 ppm demulsifiers

Figure 5.17 shows the photographs of brine in diluted bitumen (dilution ratios 0.7 and 4.0) 24 h emulsion samples adding 200 ppm PR_1 to PR_6 at 80 °C. The first sample is emulsion without any demulsifier as control. The second to the seventh are emulsion adding 200 ppm PR_1 to PR_6. The pH of the brine is 8.3. The positions of sampling water/ solid conten and solid distribution measurement are also shown in the figure. Based on bottle test, for both dilution ratios 0.7 and 4.0, emulsion samples adding 200 ppm PR_3 to PR_6 have better separation results than

others. Separation results of samples with dilution ratio 4.0 are better than those

with dilution ratio 0.7. Emulsion samples with dilution ratio 4.0 adding 200 ppm

PR_3 to PR_6 have more separated oil on the top and more separated water at the

bottom, relatively thinner rag layer in the middle. The separation results of

emulsions with dilution ratio 0.7 are worse than the samples in Figure 5.1.

Comparison of the separation results will be discussed in section 5.10.
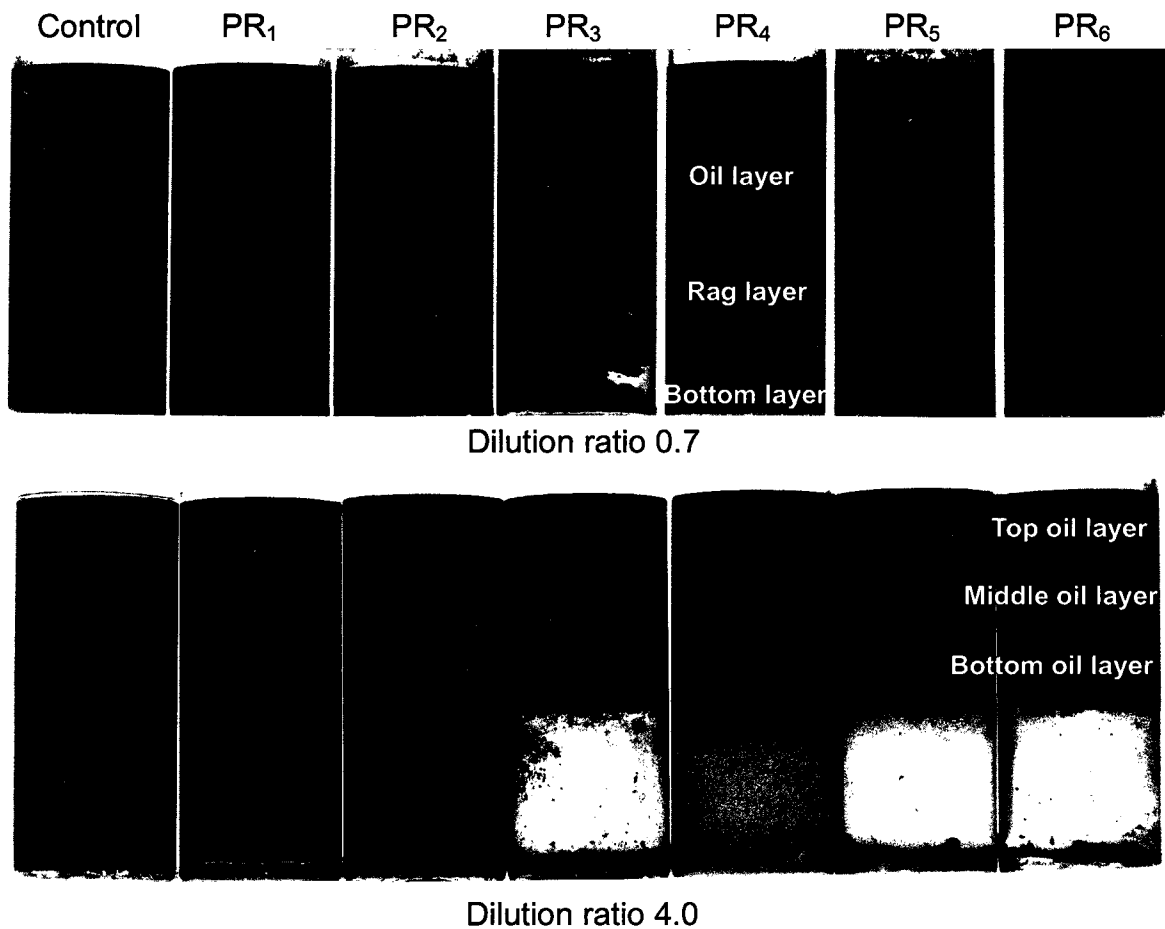
Figure 5.17 24 h emulsion separation adding 200 ppm PR_1 to PR_6 at 80 °C

Chapter 5

Figure 5.18 shows bar diagrams of residual water/ solid content in oil layer and solid distribution in different layers using 200 ppm demulsifiers PR_3 to PR_6. The red and black dashed lines show the desired residual water and solid content in oil (2.0% and 0.9%, respectively). For the sample with N/B ratio adding 200 ppm PR_4, rag layer is too thin that solid fraction in rag layer is considered as zero.
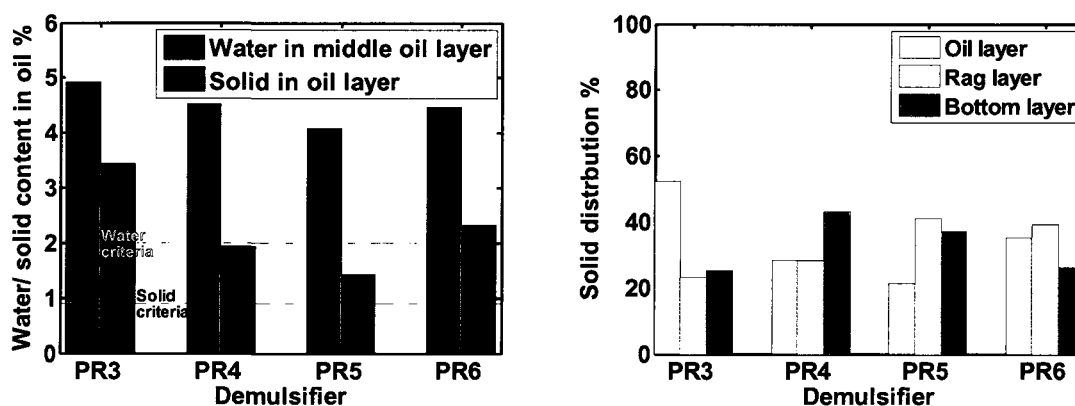
Dilution ratio 0.7
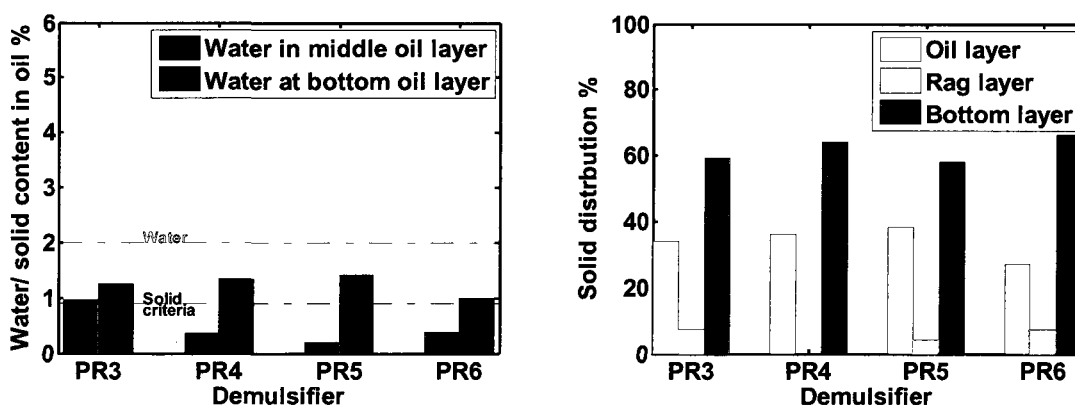
Dilution ratio 4.0

Figure 5.18 Water and solid content in oil layer and solid distribution in different layers adding 200 ppm demulsifiers PR_3 to PR_6

Chapter 5

In the middle of oil layer, samples with dilution ratio 0.7 all have water content greater than 4.0%; samples with dilution ratio 4.0 all have water content less than 1.0%. For both dilution ratios, emulsion samples adding PR_5 have lower water content than others. Samples with dilution ratio 0.7 have solid content in oil layer 2.0% - 4.5%. Emulsion samples have about 30% solid in oil and 30% solid at the bottom. Sample adding PR_5 has lowest solid content in oil layer. Samples with dilution ratio 4.0 have solid content in oil layer 1.0% - 1.5%. Emulsion samples have about 30% solid in oil and 60% solid at the bottom. Sample adding PR_6 has lowest solid content in oil layer.

Residual water and solid content in emulsion with N/B 0.7 are higher than that with 4.0. The reason could be the viscosity and density difference of diluted bitumen with N/B 0.7 and 4.0. At 80 °C, diluted bitumen after centrifugation with dilution ratio 0.7 has density 808 kg/ m^3 and viscosity 4.84×10^{-3} Pa·s; diluted bitumen with dilution ratio 4.0 has density 748 kg/ m^3, viscosity 8.1×10^{-4} Pa·s; density of brine is 975 kg/ m^3. Viscosity of diluted bitumen with dilution ratio 0.7 is about six times of that with dilution ratio 4.0. Diluted bitumen with dilution ratio 4.0 has 1.4 times the density difference between oil and water compared to that with dilution ratio 0.7. Higher viscosity of oil and lower density difference between oil and water can slow the sedimentation of water and solid in oil. Based on Stokes'

Law, sedimentation rate of water and solid in diluted bitumen with N/B ratio 4.0 is

8.1 times faster than that with N/B ratio 0.7.

5.8.2.2. Effects of silicate

Figure 5.19 shows the photographs of brine in diluted bitumen (dilution ratio

0.7) 24 h emulsion samples (pH 9.1) with 4×10^{-4} M silicate adding 200 ppm

demulsifiers PR_3 to PR_6 at 80 °C. The separation results are better than the

sample without silicate in Figure 5.17.

Control　　　PR_3　　　PR_4　　　PR_5　　　PR_6
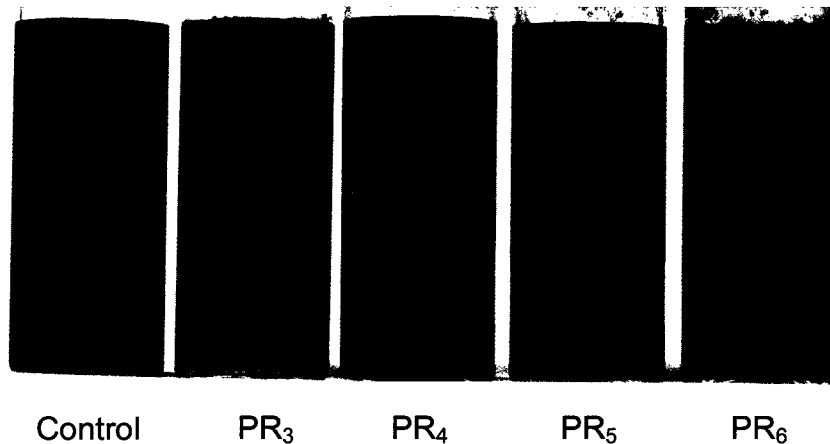
Figure 5.19 24 h emulsion (N/B 0.7) adding 200 ppm demulsifiers and 4×10^{-4} M
silicate at 80 °C, pH 9.1

Figure 5.20 shows bar diagrams of residual water/ solid content in oil layer

and solid distribution in different layers of 24 hours emulsion (dilution ratio 4.0)

adding 200 ppm demulsifiers PR_5 and PR_6 with different amounts of Na_2SiO_3. The

red and black dashed lines show the desired residual water and solid content in

oil (2.0% and 0.9%, respectively).

Chapter 5
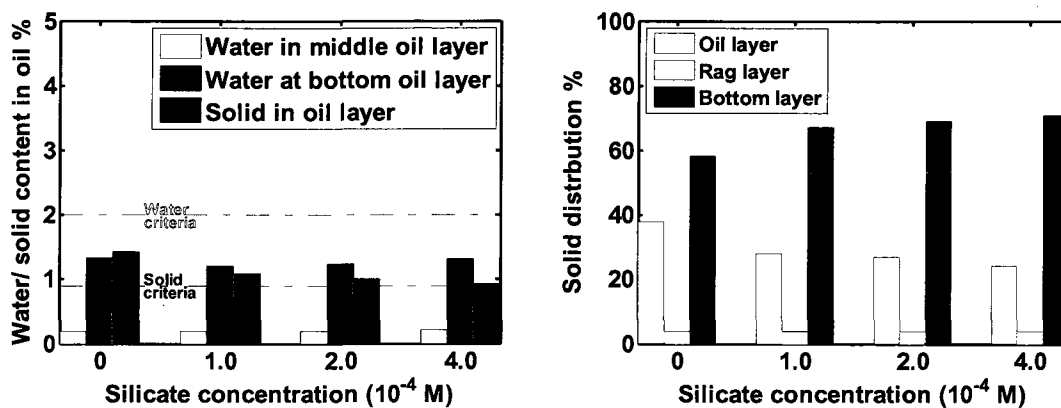
Adding 200 ppm PR$_5$

Adding 200 ppm PR$_6$

Figure 5.20 Water and solid content in oil layer and solid distribution in different layers adding 200 ppm PR$_5$ and PR$_6$ with different amount of silicate, N/B 4.0

Fig. 5.21 shows bar diagrams of residual water/ solid content in oil layer and solid distribution in different layers of 24 hours emulsion (dilution ratio 0.7) using 200 ppm demulsifiers PR$_3$ to PR$_6$ with and without Na$_2$SiO$_3$. The red and black dashed lines show the desired residual water and solid content in oil (2.0% and 0.9%, respectively).

Without silicate

With 4×10^{-4} M silicate

Figure 5.21 Water and solid content in oil layer and solid distribution in different layers adding 200 ppm PR$_3$ to PR$_6$ with and without silicate, N/B 0.7

In all the samples, residual water and solid content in oil with silicate are smaller than that without silicate. With silicate, less solids stay in the oil and more solids settle to the bottom.

Chapter 5

5.9. Asphaltene content of solid in different layers of emulsion

5.9.1. Materials and methods

Demulsifier 6057 was from Syncrude. Ltd. Solids in different layers emulsion were collected by centrifugation at 8000 g for 30 minutes. After centrifugation, oil and water were removed and the open centrifuge tube was put in the oven at 50 °C overnight until the weight did not change. Then the separated clay was treated with toluene several times until the supernatant toluene layer was colorless and transparent. Toluene was separated by centrifugation at 8000 g for 30 minutes. After drying, weight difference of solid before and after toluene treatment could be obtained. Asphaltene content in solid was calculated based on weight difference of solid and the total weight of solid before toluene treatment.

5.9.2. Results and discussions

Table 5.7 shows solid distribution and asphaltene content of solid in different layers of partially separated emulsions with 200 ppm 6057 24 hours after sample preparation at 80 °C. The pH of the aqueous phase without silicate is 8.3. The pH of the aqueous phase with 4×10^{-4} M silicate is 9.1.

From all the samples, clay solid has asphaltene content: in oil layer > in rag layer > at bottom layer. Clay solid in emulsion sample has oil-wet sequence: in oil layer > in rag layer > at bottom layer. The reason could be that solid with higher

asphaltene content is more oil-wet. At the same layer, sample with N/B ratio 0.7

has higher asphaltene content in solid than that with N/B ratio 4.0.

Table 5.7 Asphaltene content of solid in different layers of emulsion

Emulsion sample	Asphaltene % of solid		
	Oil layer	Rag layer	Bottom of water layer
N/B 4.0 and 200 ppm 6057	32	20	14
N/B 4.0, 200 ppm 6057 and 4×10^{-4} M silicate	29	20	15
N/B 0.7 and 200 ppm 6057	37	28	20

5.10. Remarks on emulsion separation

Based on bottle test, with demulsifier, almost complete separation of oil and

water could be achieved without solids in emulsion, and no rag layer formed. This

reveals that solid in bitumen froth has key effect on emulsion stability.

Comparison of separation results show that emulsion with dilution ratio 4.0 is

less stable than that with dilution ratio 0.7. In emulsion sample with dilution ratio

4.0, residual water and solid in oil are lower and the rag layer is almost eliminated.

The reason could be the viscosity and density difference of diluted bitumen with

N/B 0.7 and 4.0. Based on Stokes' Law, sedimentation rate of water in diluted

bitumen with N/B ratio 4.0 is 8.1 times faster than that with N/B ratio 0.7. It is

recommended to break the rag layer in emulsion at dilution ratio 4.0.

Based on the comparison of emulsion (dilution ratio 0.7) separation with 1%

solids (in Figure 5.1, at 50 °C) and 6.9% solids (in Figure 5.17, at 80 °C), the

emulsion with higher solid content is more stable. The rag layer in emulsion with

6.9% solids is thicker. The reason could be that more solids will adsorb or entrap

more oil and form a thicker rag layer.

Emulsion sample with silicate has better separation than that without silicate.

The residual water and solids content in oil layer of the sample with silicate is

smaller than that without silicate.

Treating rag layer in a separate stream can separate oil from solids and

break the rag layer. If the clean oil is removed after initial demulsification,

increasing pH with shaking can destroy the rag layer. A better separation would be

expected when this applying three-step separation.

5.11. Reference

[1] L. Kotlyar, B. Sparks, J. Woods, S. Raymond, Y. Le Page, W. Shelfantook, Distribution and Types of Solids Associated with Bitumen, *Pet. Sci. Technol.*, **1998**, 16, 1-19.

[2] X. Yang, S. Wang, Investigation and Characterization of Fine Solids Isolated From a Froth Treatment Plant, SPE/PS-CIM/CHOA 97788

[3] D. Sztukowski, H. Yarranton, Oilfield solids and water-in-oil emulsion stability, *J. Colloid Interface Sci.*, **2005**, 285, 821-833.

[4] B. Sparks, B L. Kotlyar, J. O'Carroll, K. Chung, Athabasca oil sands: effect of

organic coated solids on bitumen recovery and quality, *J. Pet. Sci. Eng.*, **2003**, 39, 417-430.

[5] Y. Tu, D. Kingston, J. Kung, L. Kotlyar, B. Sparks, Adsorption of Pentane Insoluble Organic Matter from Oilsands Bitumen onto Clay Surfaces, *Pet. Sci. Technol.*, **2006**, 24, 327-338.

[6] S. Basu, K. Nandakumar, J. Masliyah, On Bitumen Liberation from Oil Sands, *Can. J. Chem. Eng.*, **1997**, 75, 476-479.

[7] H. Li, Z. Zhou, Z. Xu, Masliyah J. Role of Acidified Sodium Silicate in Low Temperature Bitumen Extraction from Poor-Processing Oil Sand Ores, *Ind. Eng. Chem. Res.*, **2005**, 44, 4753-4761.

[8] B. Fuhr, B. Banjac, T. Blackmore, P. Rahimi, Applicability of Total Acid Number Analysis to Heavy Oils and Bitumens. *Energy & Fuels*, **2007**, 21, 1322-1324, 2007

[9] K. Moran, Roles of Interfacial Properties on the Stability of Emulsified Bitumen Droplet, *Langmuir*, **2007**, 23, 4167-4177.

[10] Fischer, K., Angew. Chemie, 48, 394, **1935**.

[11] Metrohm KF 701 Titrino manual, **1989**.

Chapter 6

6. Conclusions and future work

6.1. Conclusions

6.1.1. Emulsion characterization by NMR

Stable water in diluted bitumen emulsions persist in the absence of a demulsifier. The coalescence rate of the emulsion is very slow and is difficult to observe, even if most of the clay solids are removed by centrifuge before the emulsion preparation. The sedimentation rate is much faster compared with coalescence. Sedimentation rate of emulsion sample with solid is larger than that without solid.

PR_5 is an optimal demulsifier for the brine in diluted bitumen emulsions. For emulsion samples with and without solids, PR_5 can accelerate the coalescence rate. For the sample without solids, almost complete separation can be obtained; for the sample with solids, the separation is incomplete and a rag layer, which contains solids and has intermediate density, forms between the clean oil and free water layers. This rag layer prevents further coalescence and complete separation of the emulsified water.

NMR CPMG method can measure the T_2 distribution of water in diluted bitumen emulsions. But in emulsion sample with solids and no PR_5, T_2 distributions of dispersed water phase and continuous oil phase are not

distinguishable, which suggests drop size distribution of the emulsion can not obtained from CPMG measurement.

In this case, NMR restricted diffusion experiment (PGSE) can be used for the measurement of emulsion drop size distribution. In absence of demulsifier, experimental data from PGSE measurements shows the emulsion drop size does not change much during 11.2 hours. This is consistent with the observation that water in diluted bitumen emulsion is very stable without demulsifier.

NMR 1-D T_1 weighted profile measurement can distinguish the composition difference of the sample in vertical direction. Sedimentation rate of front position and water droplet sedimentation velocity can be obtained from profile results. Emulsion flocculation can be deduced by comparing the sedimentation velocity from experimental data and the calculated value from Stokes Law prediction. Coalescence can be detected from the time evolution of signal amplitude using pure oil and water as the references. Water fraction profile can be also calculated from the profile results.

6.1.2. Wettability test and zeta potential

Emulsion separation experiments show that clay wettability is important to emulsion stability. Emulsion separation is incomplete and a rag layer consisting of skins of solids, oil and emulsion forms near the interface between oil and water

layers when partially oil-wet clay solids are present. Increasing pH and adding silicate can make clay solids more water-wet and the volume of the rag layer smaller.

Kaolinite with 100 ppm sodium naphthenate in toluene-brine mixture is chosen as the model system for wettability test. Kaolinite is water-wet in toluene-brine mixtures. But when sodium naphthenate is added, most of kaolinite becomes oil-wet. It has been found that the higher the naphthenate concentration, the lower the water-wet fraction. Wettability of kaolinite can be altered by pH control, silicate and surfactant. NaOH and silicate can make kaolinite surface more negative, which results in kaolinite becoming more water-wet. But to reach water-wet fraction above 70% requires adding NaOH or silicate above pH 10.0. Adding 366 ppm silicate at pH 10 can get 80% of kaolinite water-wet. C_8TAB, amine oxide DO and betaine 13 with appropriate dosage (5 ppm, 20 ppm and 200 ppm) can make 90% kaolinite water-wet with 100 ppm naphthenate. Much less C_8TAB or amine oxide DO is required compared to betaine. Cationic groups of in these surfactants can interact with anionic naphthenate can form ion pairs, which can minimize the adsorption of C_8TAB and naphthenate and make kaolinite more water-wet. Wettability of kaolinite is sensitive to the dosage of C_8TAB and amine oxide. The adsorption of excess cationic groups on kaolinite surface makes

kaolinite more oil-wet. Wettability of kaolinite doesn't change much if betaine 13 is overdosed (200 - 1000 ppm).

Kaolinite in clay solids has heterogeneous surface charge, which affects its wettability. Zeta potential measurement is used to characterize wettability change of kaolinite. Calcium and magnesium ions in the aqueous solution can make the zeta potential of kaolinite in brine less negative. Adding NaOH, meta-silicate, ortho-silicate, citrate or carbonate can make the zeta potential of kaolinite in brine more negative. Compared with other anions, silicate ions have the greatest effect per unit addition on changing zeta potential of kaolinite.

Simplified Gouy-Stern-Grahame model and oxide site-binding model can be used to correlate the zeta potential of kaolinite in brine with different additives. Different additives have various surface reactions with kaolinite, which can change the zeta potential of kaolinite in brine. Adding NaOH can increase the pH; hydroxyl ion can react with the surface group of kaolinite, which will make zeta potential more negative. Sulfate ion and bicarbonate ion can adsorb on the surface of kaolinite and make zeta potential more negative. Calcium and magnesium ions can adsorb on the surface of kaolinite and make zeta potential less negative. Silicate can adsorb on the surface of kaolinite, in addition to raising the pH. Citrate ion can both adsorb on the surface of kaolinite and chelate with

Ca/ Mg ions, and has little effect on pH of synthetic brine. Carbonate ion can increase pH, bicarbonate ion concentration and precipitate Ca ions, which can make zeta potential more negative.

6.1.3. Diluted bitumen emulsion separation

At 50 °C, diluted bitumen emulsion with dilution ratio 0.7 adding demulsifier PR_5 produces incomplete separation with a rag layer between oil and water. When a small amount of silicate is present in the water drops, the solid particles are more water-wet and the volume of the rag layer is smaller. Optimal condition of aqueous phase for emulsion separation is adding 1×10^{-4} M sodium meta-silicate (Na_2SiO_3) at pH 8.5.

If the clean oil is removed after this initial demulsification step and sodium hydroxide is added to the remaining material with shaking to increase pH to 8.8, the skins making up the rag layer are destroyed, an O/W emulsion forms, and nearly all of the solids are released to the aqueous phase. Finally, adding hydrochloric acid to reduce pH to 5.0 breaks the O/W emulsion. This three-step procedure yields nearly complete separation of water, diluted bitumen and solids.

Karl Fischer titration can be used to measure water content in diluted bitumen. Toluene-methanol mixture with toluene volume ratio 75 % is the appropriate solvent for the titration of water in diluted bitumen. This method only needs small

sample quantities and the measurement itself is convenient. The lower limit of water content in diluted bitumen that can be measured by K-F titration is 0.02 %, which is not very easily measured by other methods. The titration results are consistent with different water amounts in diluted bitumen. The largest deviation between the measured water content and actual water content was less than 5% for the samples studied.

Dilution ratio of diluted bitumen has effect on emulsion stability. Residual water and solid contents in emulsion with N/B 0.7 are higher than that with 4.0. The reason could be the viscosity and density difference. Higher viscosity of oil and lower density difference between oil and water can slow the sedimentation of water and solid in oil. Based on Stokes' Law, sedimentation rate of water and solid in diluted bitumen with N/B ratio 4.0 is 8.1 times faster than that with N/B ratio 0.7.

With silicate, residual water and solid contents are lower and less solids stay in oil and more solids settle to the bottom. Emulsion with N/B 4.0 adding 200 ppm PR_6 meets desired residual water and solid criteria.

Clay solid has asphaltene content: in oil layer > in rag layer > at bottom layer. At the same layer, sample with N/B ratio 0.7 has higher asphaltene content in solid than that with N/B ratio 4.0.

Chapter 6

6.2. Future work

For diluted bitumen emulsion, NMR CPMG can not get useful information if T_2 distribution is not distinguishable for dispersed water and continuous oil phase; NMR PGSE restricted measurement can obtain drop size distribution, but can not get direct information of water/ oil fraction; 1-D MRI profile measurement can get water/ oil fraction profile, but needs total water/ oil fraction for calibration. Hence total water fraction can not be directly obtained from these measurements.

Profile diffusion editing measurement [1], which is the combination of these three methods, may be used in this case to solve the problem. This method can provide profile of 2-D T_2-D (diffusivity) or T_2-a (drop radius) map of the sample. If the parameters are appropriate, in T_2-D map, water and oil peaks can be separated by the diffusivity difference. Water fraction profile can be obtained by integrating the water and oil peaks separately of T_2-D map for each slice of the sample. Drop size distribution profile can be also obtained directly from T_2-a map.

The separation time (12 h - 24 h) is relatively long and the residual water and solid contents in oil are relatively high, which may not satisfy industrial requirements. To accelerate the aggregation and sedimentation of water and solid, appropriate flocculator needs to be used for emulsion to optimize the separation.

Wettability tests show that over 90 % of kaolinite becomes water-wet adding

C_8TAB, betaine 13 and amine oxide DO with optimal dosages. In future study, these surfactants can be considered as wettability agents for clay in diluted bitumen emulsion separation.

Water and solid contents in oil have been successfully measured by K-F titration and centrifuge. A proper procedure to characterize oil content in water layer and rag layer needs to be developed.

Temperature, water/ oil ratio and solid content also have effects on emulsion stability. In future work, the effects of these factors need to be evaluated.

6.3. Reference

[1] M. Rauschhuber, G. Hirasaki, Determination of saturation profiles via low-field NMR imaging, *International Symposium of the Society of Core Analysts*, Noordwijk, Netherlands, 27-30 September, **2009**.

Appendix A

Appendix A. NMR measurement parameters and procedures

NMR measurements are used to characterize emulsions by T_2 relaxation time distribution, restricted diffusion for drop size distribution, and vertical profile of oil, dispersed water, and free water.

A.1. Default parameter settings

Instruction Manual of MARAN shows basic commands (e.g. tuning, sequence loading and data saving) for NMR measurement. Default parameter settings for T_2 distribution, restricted diffusion and MRI profile measurements are shown in the script file *set_prarameters.ris*. All the script files can be found in the computer for MARAN at the directory C:\Program Files\Resonance\RiNMR\script.

Detailed instructions of parameters selection and data processing for T_2 measurement can be found in Huang's thesis (C. C. Huang, Estimation of rock properties by NMR relaxation methods, MS Thesis, Rice University, Houston, 1997). Here default parameters of T_2 measurement in script file were applied for all diluted bitumen emulsion samples.

A.2. Parameters for NMR restricted diffusion measurement

In NMR restricted diffusion measurement, sequence parameters are diffusion time Δ (D4 in script), duration of magnetic gradient pulse δ (D3 in script) and

Appendix A

amplitude of magnetic gradient pulse g (G1 in script).

For monodisperse emulsion with geometric mean drop size d_g and standard deviation σ_g, most of the droplets have sizes in the range of one standard deviation $[d_g/\exp(\sigma_g), d_g{}^*\exp(\sigma_g)]$, if lognormal distribution is assumed. For a set of parameters Δ, δ and g, the measurable minimum and maximum drop sizes in NMR restricted diffusion measurement can be calculated based on Eqs. [3.29] and [3.30]. Parameters for NMR restricted diffusion measurement are chosen that the drop size range $[d_g/\exp(\sigma_g), d_g{}^*\exp(\sigma_g)]$ is within the measurable drop size range $[d_{min}, d_{max}]$.

In NMR restricted diffusion measurement for all diluted bitumen samples, parameters are: diffusion time Δ 500 ms, gradient pulse duration δ 3 ms, range of magnetic gradient g 0 - 40 G/cm. The measurable drop size range is 4 μm - 72 μm. For instance, emulsion sample 1 in chapter 3 has geometric mean drop size 14 μm and standard deviation 0.4. Drop size in the range of one standard deviation is 9 μm - 21 μm, which is within the measurable drop size range 4 μm - 72 μm. Thereby correct drop size distribution can be obtained by NMR restricted diffusion measurement using above parameters.

If the emulsion is polydispersed, more than one set of parameters and multi-exponential data fitting are required. Details of parameters selection and data

processing can be found in Mark Flaum's thesis (Mark Flaum, Fluid and rock characterization using new NMR diffusion-editing pulse sequences and two dimensional diffusivity-T_2 map, PhD Thesis, Rice University, Houston, 2006).

A.3. Parameters for 1-D T_1 weighted MRI profile measurement

In 1-D T_1 weighted MRI profile measurement, waiting time t_w (RD in script) between successive scans is the key parameter. An appropriate value for waiting time t_w should be chosen to make profile amplitudes of emulsified water between that of bulk water and oil. If profile amplitudes of any two components are close each other, in water/ oil fraction calculation, these two components are not distinguishable, which will reduce the accuracy of the calculation.

Fig. A.1 (Fig. 3.17 in chapter 3) shows the amplitude profiles of bulk water, oil and emulsified water. T_1 for bulk water can be measured using INVREC sequence (details can be found in Instruction Manual of MARAN). Detailed calibration for T_1 values of oil and emulsified water are discussed in chapter 3. T_1 values for bulk water, oil and emulsified water are 2.60 s, 0.63 s and 1.41 s, respectively. Waiting time t_w is 0.60 s. In this case, amplitude profiles of bulk water, oil, emulsified water and fresh emulsion (1:1 w/o) are different each other and distinguishable.

Appendix A

Calibration
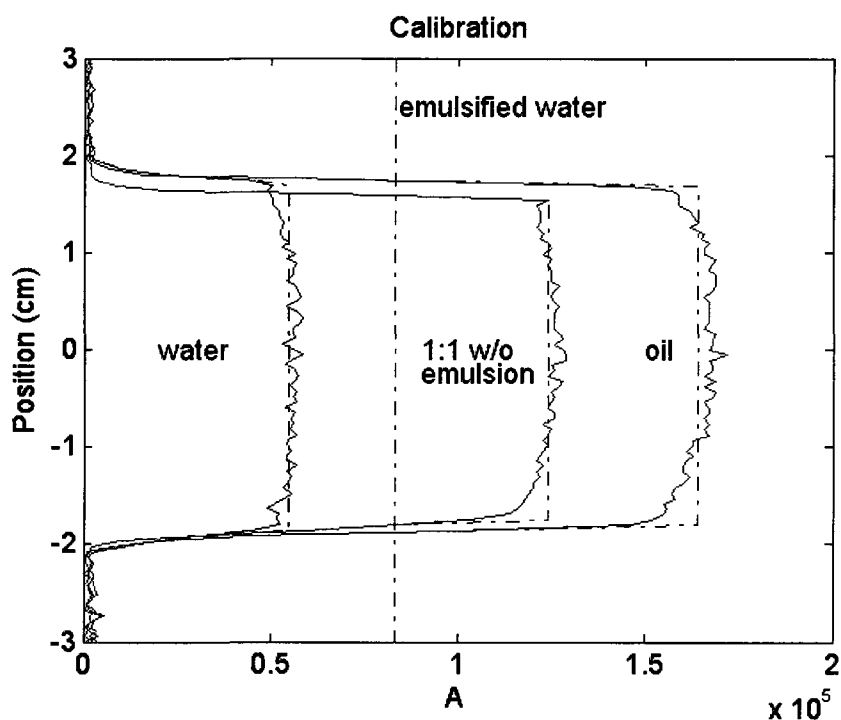
Figure A.1 Profile amplitudes of bulk water, oil and emulsified water

A.4. Procedure for T_2, restricted diffusion and profile measurements

Refer to Instruction Manual of MARAN.

1. Perform tuning for O1, 90° and 180° *rf* pulses.

2. Load script file *set_prarameters.ris* to set default parameters for all the measurement.

3. Load script file *t2_diff_profile.ris*, load file *G1_emul* for magnetic gradient *g* list (G1 in script) and file *OneD4_500ms* (for one-time measurement) or *RepeatD4_500ms* (for successive measurement as function of time) for

Appendix A

diffusion time Δ. Set the directory for data saving. Then T_2, profile and

restricted diffusion measurements will start one-by-one automatically.

4. After measurements, data will be saved to set directory automatically.

File *set_prarameters.ris*

Option Explicit

```
'*******************************************************

'* Script for setting default parameters of a diffusion sequence

'* Set the parameters for cpmg, profile and diffgp sequence

'*******************************************************


Sub Main()
'* General
      NMR.Execute("RFA0 100")

      NMR.Execute("DEAD1 60")

      NMR.Execute("DEAD2 20")


'* FID sequence
      NMR.Execute("~AMODE")

      NMR.Execute("LOAD FID")          ' load the sequence

      NMR.Execute("FW 100K")

      NMR.Execute("SI 1048")

      NMR.Execute("RG 20")

      NMR.Execute("DS 0")

      NMR.Execute("RG 5")

      NMR.Execute("RD 1S")


'* CPMG sequence
      NMR.Execute("~AMODE")

      NMR.Execute("LOAD CPMG")          ' load the sequence
```

Appendix A

NMR.Execute("TAU 300")

NMR.Execute("FW 100K")

NMR.Execute("SI 1")

NMR.Execute("RG 10")

NMR.Execute("DS 0")

NMR.Execute("RD 15S")

NMR.Execute("NECH 8000")

NMR.Execute("NS 16")

'* Profile sequence

NMR.Execute("~AMODE")

NMR.Execute("LOAD PROFILE")

NMR.Execute("RG 10")

NMR.Execute("FW 100K")

NMR.Execute("SI 64")

NMR.Execute("DW 40")

NMR.Execute("G1 500")

NMR.Execute("G2 500")

NMR.Execute("TAU 3000 ")

NMR.Execute("D1 100 ")

NMR.Execute("D2 1320 ")

NMR.Execute("D3 20 ")

NMR.Execute("RD 0.6s")

NMR.Execute("DS 4")

NMR.Execute("NS 64")

'* Diffgp sequence

NMR.Execute("~AMODE")

NMR.Execute("LOAD DIFFGP")   ' load the sequence

NMR.Execute("FW 100K")

NMR.Execute("RG 40")

NMR.Execute("GX 32767")

NMR.Execute("GY 32767")

Appendix A

```
        NMR.Execute("GZ 32767")

        NMR.Execute("DS 2")

        NMR.Execute("D1 200 ")

        NMR.Execute("D2 40000 ")

        NMR.Execute("D3 3000 ")

        NMR.Execute("D4 500000 ")

        NMR.Execute("D5 200 ")

        NMR.Execute("D6 1000")

        NMR.Execute("G2 500")

        NMR.Execute("RD 15S")

        NMR.Execute("SI 2048")

        NMR.Execute("DW 6")

        NMR.Execute("NS 16")

        NMR.StatusMessage("FID, CPMG, profile and Diffgp set ")


end sub
```

File *t2_diff_profie.ris*

```
Option Explicit

'******************************************************

'*    Script to perform diffusion for multiple D4 values

'*    g is varied according to the list and the range is decreased

'*    according to D4ref

'*    A CPMG and a profile is performed before each diffusion sequence

'*    a delay waittime can be inserted

'******************************************************

Dim ListName1        ' Name of list file 1

Dim ListName2        ' Name of list file 2

Dim DataName         ' Name of data file

'************************************************************************

Sub Main()


Dim r, q
```

Appendix A

```
Dim p

Dim s

Dim i

Dim NewO1

Dim Ext

Dim Current

Dim Size

Dim SaveSeq

Dim fso, aout, RepDel, NS

Dim D4ref, rfich, bruit, redg, waittime, choice


' to be set by the user

waittime=60          ' wait time between diffusion time

choice=1                    ' 1 for diffgp sequence

                     ' 2 for difgpcp sequence

' save before starting

D4ref=1000000

bruit=1                     ' no acquisition if signal too weak


If NoHardware Then

   ShowError("No hardware available")

   Exit Sub

End If


' Load G1 list


ListName1=GetListName(1)          ' Get list from command line; or prompt

If ListName1="" Then              ' Can not continue without a list

   Exit Sub

End If

If LoadList1(ListName1)=FALSE Then    ' Try to load list into memory

   Exit Sub

End If
```

Appendix A

```
' liste des valeurs de DELTA (D4)

ListName2=GetListName(2)              ' Get list from command line; or prompt

If ListName2="" Then                  ' Can not continue without a list

   Exit Sub

End If

If LoadList2(ListName2)=FALSE Then    ' Try to load list into memory

   Exit Sub

End If

DataName=GetDataName(3)                ' Get name from command line; or prompt

If DataName="" Then                    ' Empty string if <Cancel> pressed

   Exit Sub

End If


Current=NMR.GetParameter("%DATADIR")      ' Get current data directory

DeleteFile (Current & DataName & "?.*") ' Delete any existing files


NMR.Execute("~AMODE")

RepDel=NMR.GetParameter("RD")

NS=NMR.GetParameter("NS")

NMR.Execute("LOAD FID")

NMR.Execute("RD " & RepDel)

NMR.Execute("DS 0")

NMR.StatusMessage("RD set to " & RepDel)


''''''''''''''''''''''''''''''''''''''''''''''''''''''''''''''

i=0

' Load D4


   Do While NextList2(s)                  'get next value from list

      i=i+1

'    Reglage automatique de O1 avant chaque mesure de diffusion

         NewO1=DoAutoO1

'    Degauss de l'aimant
```

Appendix A

```
NMR.Execute("~AMODE")                          ' Change to Acquisition mode and
SaveSeq=NMR.GetParameter("%SEQFILE")     ' save current sequence
NMR.Execute("LOAD DEGAUSS")
NMR.Execute("GX 32767")
NMR.Execute("GY 32767")
NMR.Execute("GZ 32767")
NMR.Execute("NS 1")
NMR.Execute("DS 0")
NMR.GO
NMR.Execute("~AMODE")                          ' Change to Acquisition
NMR.Execute("LOAD CPMG")                       'perform cpmg before each diffusion
   NMR.StatusMessage("Perform CPMG   D4   = " & s )
NMR.GO
NMR.Execute("WR " & DataName & i & "T2" & "." & Ext & " Y")    ' save it
NMR.Execute("EX " & DataName & i & "T2" & "." & Ext & " T")    ' save it
NMR.Execute("~AMODE")
NMR.Execute("LOAD PROFILE")                    'perform profile before each diffusion
NMR.Execute("RD 0.6S")
NMR.StatusMessage("Perform Profile 3   D4   = " & s )
NMR.GO
NMR.Execute("~PMODE")                          ' Switch to Process
NMR.Execute("WR " & DataName & i & "prof" & "." & Ext & " Y")    ' save
NMR.Execute("EX " & DataName & i & "prof" & "." & Ext & " T")
NMR.Execute("FT")
NMR.Execute("MAG")
NMR.Execute("WR " & DataName & i & "prof_ft" & "." & Ext & " Y")    ' save
NMR.Execute("EX " & DataName & i & "prof_ft" & "." & Ext & " T")
NMR.Execute("~AMODE")
NMR.Execute("LOAD " & Chr(34) & SaveSeq & Chr(34)) ' mode and reload diffusion seq.
If LoadList1(ListName1)=FALSE Then   ' Try to load list into memory
    Exit Sub
End If
```

Appendix A

```
NMR.Execute("~PMODE")                    ' Switch to Process mode and
NMR.Execute("XY QUIT")                   ' Start XY display
NMR.Execute("XY")
NMR.Execute("~AMODE")                    ' Switch to Acquisition mode and
If (choice-1.5)< 0 Then
        NMR.Execute("LOAD DIFFGP")       ' and load the diffusion sequence
else
        NMR.Execute("LOAD DIFGPCP")          ' and load the diffusion sequence
End If
NMR.Execute("D4 " & s)               ' set D4
Ext=1                                ' Reset file extension
If (s-D4ref)>0        Then
        redg=sqr(s/D4ref)
else
        redg=1
End If
Set fso=CreateObject("Scripting.FileSystemObject")
  Set aout = fso.CreateTextFile(current & DataName & i & ".int",true)
    Do While NextList1(rfich)            ' Get next value from list
        NMR.Execute("~AMODE")                ' Go to Acquisition Mode
        r=rfich/redg
        'r=rfich
        NMR.Execute("G1 " & r)           ' set G1
          q=-r
        NMR.Execute("G3 " & q)           ' set G3
        NMR.StatusMessage("D4 = " & s )
        NMR.StatusMessage("G1 = " & r )
            NMR.Go
        If   (choice - 1.5) > 0 Then
            NMR.Execute("ROT")
        End If
    NMR.Execute("WR " & DataName & i & "." & Ext & " Y") ' save it
    Ext=Ext+1                            ' New extension
```

Appendix A

```
        NMR.Execute("SIZE 20")                    ' Get size of the echo and update XY

        Size=NMR.ReturnValue

        NMR.Execute("XY DATA " & r & Size)

        aout.WriteLine(r & Size)    ' store intensity into texte file

        If ( Size/NS )< bruit        Then

            Exit Do

        End If

    Loop

    aout.Close

    NMR.Execute("WAIT " & waittime)

  Loop

NMR.Execute("XY QUIT")

end sub
```

Appendix B

Appendix B. Methods for zeta potential measurement

B.1. Sample preparation

The aqueous phase used here is synthetic brine with pH 8.3, as introduced in section 4.2.1. Kaolinite ($Al_2Si_2O_5(OH)_4$) and alumina (Al_2O_3) are obtained from Sigma-Aldrich with detailed information in section 4.2.1. All the salts in the synthetic brine were obtained from Fisher Scientific.

All the samples of 50 ml 1.0 % (w/w) kaolinite or alumina suspension were prepared in the brine with different additives. Branson Sonic Probe 450 was used for the sonication of the mixture (probe tip was placed about 1/2" into the solution, sonication rate at setting 4 for 1 minute). The mixture was left overnight. Before measurement the mixture was shaken and settled for 30 minutes to allow the sedimentation of larger particles and get stable suspension. Beckman Coulter Delsa 440 Doppler electrophoretic light scattering analyzer was used to measure zeta potential of kaolinite or alumina in the brine.

B.2. Measurement Procedure

Refer to Coulter Delsa 440 Product Reference Manual, June 1988.

1. Prepare clay samples as described in section B.1.

2. Turn on the instrument for 1 h for warming up.

3. Perform position calibration of the sample. Inject clay dispersion into sample

cell and put sample cell into the instrument. Laser beam can be observed from microscope (along with the instrument). Move sample cell down until laser beam disappears, shift the micrometer to zero. This reveals laser beam reach the top edge of the sample. Then move sample cell up until laser beam disappears, shift the micrometer to 100. This reveals laser beam reach the bottom edge of the sample. Repeat several times until the top and bottom edges of the sample correspond to positions 0 and 100.

4. Use standard mobility solution (1000 mS/cm, mobility -4 μm·cm/V·s, Beckman Coulter, PN# 8301351) to perform the measurement at different position levels for calibration.

5. Perform zeta potential measurement for clay samples at lower and upper stationary levels (positions 84 and 16) for three times respectively. The average value of zeta potentials of lower and upper stationary levels was chosen as the zeta potential value of the sample.

6. Turn off the instrument after the measurement.

B.3. Results and discussions

Fig. B.1 shows the mobility profile of the standard mobility solution. The two ends of the blue line are mobility values at upper and lower stationary levels. The profile of standard mobility solution is symmetric. The measured mobility at

Appendix B

upper and lower stationary level (- 4.03 and -4.04 μm·cm/V·s) are almost the

same and very close to - 4 μm·cm/V·s, which is the reported mobility of standard

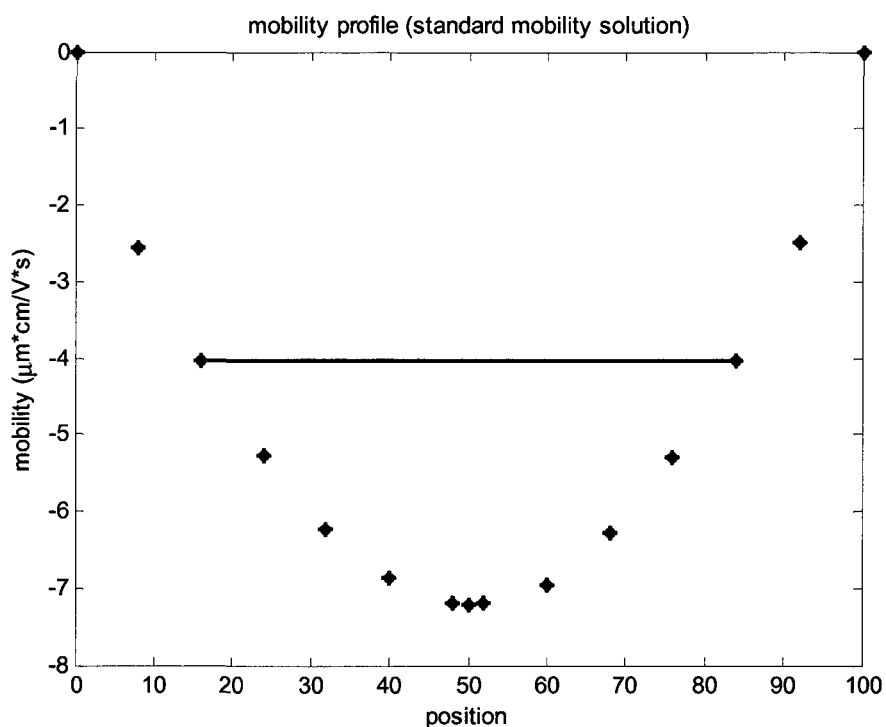mobility solution. This indicates the instrument and measurement are accurate.

Figure B.1 Mobility profile of standard mobility solution

Fig. B.2 shows the zeta potential profile of kaolinite sample in synthetic brine

(Conductivity 4040 mS/cm). The profiles of kaolinite sample are not symmetric.

Zeta potential values at upper and lower stationary level are not equal. The

reason may be that the kaolinite suspension is not homogeneous in the cell due to

the sedimentation. Thereby in the measurements, the sample was measured at

lower level and upper level for three times respectively. Table B.1 shows zeta

Appendix B

potential values of kaolinite in synthetic brine. Here the average value of zeta

potentials in upper and lower stationary levels is chosen as the zeta potential

value of the sample.

Table B.1 Zeta potential values of kaolinite sample in synthetic brine

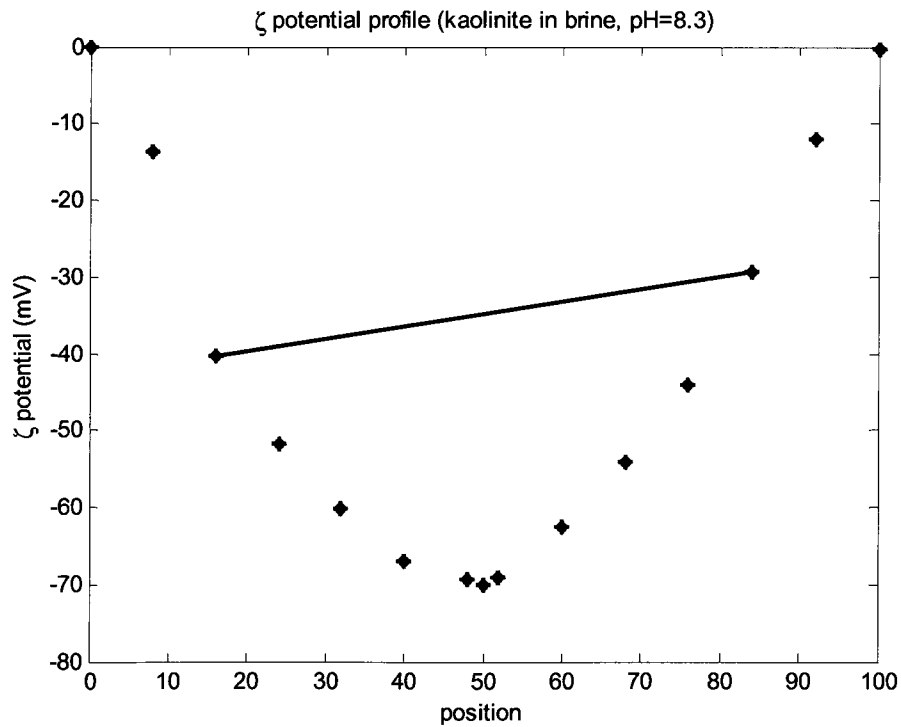| Measurements	ζ (upper, mV)	ζ (lower, mV)	ζ (mV)
1	-28.7	-39.3	-34.0
2	-27.6	-40.5	-34.1
3	-31.6	-41.1	-36.3
average	-29.3	-40.3	-34.8±1.8

Figure B.2 Zeta potential profile of kaolinite sample in synthetic brine

Appendix C

Appendix C. Karl-Fischer (K-F) titration procedure

Refer to Instruction Manual of K-F 701 Titrino, 1988.

C.1. Titer calibration

1. Add K-F reagent to the bottle on exchange unit. Connect the exchange unit and titration vessel via hose. Make sure the whole titration system is sealed except the connection to atmosphere through drying tube.

2. Turn on the power switch on the back of titrator. Press "Mode" key to select "Titer with H_2O or std.". Add 25 ml solvent to the titration vessel. Turn on the electromagnetic stirring.

3. Press "Start" key. The green indicator lamp "cond." on the titrator flashes. This means the titration cell is wet and being dried (conditioned). Wait until this lamp lights continuously which means the cell is dry and ready for titration.

4. Inject 25 µg pure de-ionized water into the titration vessel. Press "Start" key, enter the "smpl size" 25 µg. Press "Start" key again, titration starts.

5. When reached end point, the titrator stops automatically. The screen will show "KFR volume" and "Titer". Write down the titer for future titration measurement.

C.2. K-F titration for sample

1. Repeat step 1 in section 2.1.

Appendix C

2. Turn on the power switch on the back of titrator. Press "Mode" key to select "KFT". Add 25 ml solvent to the titration vessel.

3. Repeat step 3 in section C.1.

4. Inject a certain amount of sample into the titration vessel. Press "Start" key, enter the actual "smpl size". Press "Start" key again, titration starts.

5. When reached end point, the titrator stops automatically. The screen will show "KFR volume". Write down the results, combined with titer to calculate water content.

$$\text{Water content} = \frac{\text{KFR volume} \times \text{Titer}}{\text{Sample weight (g)}} \times 1000\%$$

Appendix D

Appendix D. Glass surface treatment of slides and cover slips

In microscopy observation of diluted bitumen emulsion, wettability of slides and cover slips are important. If the surface of slides and cover slips can be wetted by dispersed droplets (either water or oil), dispersed droplets will stick on the glass surface and coalesce. Thereby for water-in-oil emulsion, glass surface should be oil-wet; for oil-in-water emulsion, glass surface should be water-wet.

D.1. Methods to make glass surface hydrophilic

1. If glass surface is very clean and hydrophilic, no treatment needed.

2. If glass surface is not completely hydrophilic, put slides and cover slips into Nochromix cleaning solution (from Godax lab Inc.) for 1 h.

3. After that, put slides and cover slips into 0.1 M $NaHCO_3$ for 1 h to neutralize the residual acid.

4. Use de-ionized water to wash slides and cover slips.

5. Use tissue paper to wipe the residual water and the slides and cover slips are ready to use.

D.2. Methods to make glass surface hydrophobic

1. Put dry slides and cover slips into Silanization solution (From Fluka, dimethyl-dichlorosilane in heptane solution) for 1 min.

Appendix D

2. Use toluene then acetone to wash slides and cover slips.

3. Use tissue paper to wipe the residual acetone and the slides and cover slips are ready to use.